TULLY-FISHER DISTANCE MEASUREMENTS OF SPIRAL GALAXIES WITH WELL-OBSERVED TYPE Ia SUPERNOVAE

Thesis submitted by

Daryl Lee SEIBEL

BPA

MBA

MSc

07 November 2016

For the degree of

Doctor of Philosophy

in Astronomy

in the

Centre for Astronomy

James Cook University

Townsville QLD, Australia

STATEMENT OF ACCESS

I, Daryl L. Seibel, author of this work, understand that James Cook University will make this thesis available for use within the University Library and, via the Australian Digital Thesis network, for use elsewhere.

I understand that, as an unpublished work, a thesis has significant protection under the Copyright Act and I do not wish to place any further restriction on access to this work.

Daryl L. SEIBEL	07 November 2016
Signature	Date

STATEMENT OF SOURCES

I, Daryl L. Seibel, declare that this thesis is my own work and has not been submitted in any form for another degree or diploma at any university or other institution of tertiary education. Information derived from the published or unpublished work of others has been acknowledged in the text and a list of references is given.

Daryl L. SEIBEL — 07 November 2016

Signature — Date

STATEMENT OF ELECTRONIC COPY

I, Daryl L. Seibel, the author of this work, declare that the electronic copy of this thesis provided to the James Cook University Library is an accurate copy of the print thesis submitted, within the limits of the technology available.

Daryl L. SEIBEL — 07 November 2016

Signature — Date

STATEMENT OF CONTRIBUTION OF OTHERS

I, Daryl L. Seibel, author of this thesis acknowledge the contribution of John Danziger of Observatorio Astronomico di Trieste, as supervisor for this project, and David Blank of JCU as initial co-supervisor, for the editorial assistance of this paper. I acknowledge the contribution of Ray Cooke, Université Bordeaux for the editorial comments for the preliminary version of this paper. I acknowledge Lister Staveley-Smith, of the University of Western Australia for the contributory analysis and suggestions for the finalization of the thesis.

I acknowledge the contribution of Lister Staveley-Smith, of the University of Western Australia, and John Danziger for the observational supervision at the Parkes 64 m Radio Telescope and data reduction at CSIRO ATNF at Sydney, Australia for the Parkes sample.

I acknowledge the contribution of John Danziger for the initial collection of the Literature, Parkes, and the Parkes / NTT samples.

I acknowledge the contribution of Preben Grosbøl for the NIR observations at ESO La Silla, Chile for the Parkes / NTT sample.

I acknowledge the contribution of Lister Staveley-Smith and John Danziger for the 21 cm line width velocity measurements at the Parkes 64 m Radio Telescope and data reduction at CSIRO ATNF at Sydney, Australia for the 51-galaxy sub-sample of the Parkes / NTT sample set.

I acknowledge the contributions of Christina Magoulas for the assistance in using the Erdoğdu predictive peculiar velocity algorithm.

I declare that I made use of the advice of Lister Staveley-Smith of the University of Western Australia for the finalisation of this thesis.

I declare I did use the infrastructure of CSIRO ATNF for the use of the Parkes 64 m Radio Telescope for the observations in the course of the research for this thesis.

I declare I did use the infrastructure of ESO for the use of SOFI on the 3.5 m NTT, and TAROT at the La Silla Observatory, for the observations in the course of the research for this thesis.

I declare there were no other infrastructures external to JCU or external to an organisational unit within JCU used for this thesis.

I declare there were no other fees, stipend support, other supervision or collaborations, statistical support, editorial assistance, research assistance or other assistance.

Daryl L. SEIBEL	07 November 2016
Signature	Date

CONTENTS

ACKNOWLEDGMENT xvi

ABSTRACT 1

1 INTRODUCTION

1.1 Aim 3
1.2 Lambda-CDM 3
1.3 The Distance Ladder 4
1.4 The Tully-Fisher (TF) Relation: discovery 5
1.5 The Tully-Fisher Relation: refinement 6
1.6 Malmquist Bias 10
1.7 Type Ia Supernovae 11
1.8 The Hubble Constant 13
1.9 Peculiar Velocities 16
References 18

2 TULLY-FISHER AND SNe Ia TEMPLATES

2.1 Tully-Fisher Relation 22
2.2 SNe Ia Distance Scale 27
References 30

3 DATA FOR A LITERATURE-SAMPLE WITH WELL-OBSERVED SNe Ia

3.1 Sample Overview 32
3.2 Detailed Data 32
3.2.1 Apparent Magnitudes 34
3.2.2 Distance Moduli 36
3.3 Summary 37
References 64

4 PARKES OBSERVATIONS OF HOST GALAXIES WITH WELL-OBSERVED SNe Ia

4.1 The Joint Parkes and SNe Ia Sample (the Parkes Sample) 67
4.2 The Parkes Multibeam Receiver 67
4.2.1 Observations and Reduction 69
4.3 Parameterisation 70
4.4 Tabulation of the Parkes Data 79
4.5 Results 81
4.6 Summary 85
References 105

5 PARKES / NTT SAMPLE NEW NIR AND 21 CM LINE WIDTH VELOCITY MEASUREMENTS

5.1 The Parkes / NTT Sample 107
5.2 Light Curve of SN Ia 2012fr 108
5.3 The Tully-Fisher Relation Measurements 109
5.4 Calculations for the SNe Ia 111
5.5 Summary 112
References 142

6 DISCUSSION FOR THE THREE SAMPLE SETS

6.1 The Combined Data 143
6.2 The Hubble Constant 155
6.3 Galaxy Morphology and Bars 157
6.4 Malmquist Bias 157
6.5 Peculiar Velocities 161
6.5.1 Bulk Flow 161
6.5.2 Matter Density 165
References 171

7 CONCLUSION FOR THE THREE SAMPLE SETS

Conclusions 174
References 177

LIST OF TABLES

Table 1.1: Determinations of H_0 14

Table 2.1: k at Maximum Light 28

Table 3.1: The Literature Sample 44

Table 3.2: Apparent Magnitude B for the SNe Ia, Apparent Magnitude B_T, H^c, K_s and W_R^i for the Literature Sample 51

Table 3.3: Absolute Magnitude, Apparent Magnitude, and Distance Modulus for the Literature Sample 58

Table 4.1: Parkes 21 cm Multibeam receiver and correlator parameters 68

Table 4.2: Manually Measured Galaxies for the Parkes Sample 71

Table 4.3: Quality Categories Assigned to the Parkes Sample 79

Table 4.4: The Parkes Sample 90

Table 4.5: B-band photometry data for the SN Ia, and Galaxy Apparent Magnitudes B_T, H^c and K_s for the Parkes 46 galaxy sample 93

Table 4.6: New Uncorrected Observation Data for the Parkes Sample from Table 4.1 96

Table 4.7: Inclination and z Corrected to W_R^i Observation Data for the Parkes Sample from Table 4.6 99

Table 4.8: Absolute Magnitude, Apparent Magnitude, and Distance Modulus for the Parkes Sample 102

Table 5.1: Apparent Magnitude B_T, H^c and K_s for the Parkes / NTT Sample 123

Table 5.2: Apparent Magnitude B_T, H^c and K_s for the Parkes / NTT Sub-Sample 128

Table 5.3: The Parkes / NTT Sub-Sample Measurements 132

Table 5.4: SOFI - Absolute Magnitude, Apparent Magnitude and Distance Modulus for the Parkes / NTT Sub-Sample 136

Table 5.5: 2MASS - Absolute Magnitude, Apparent Magnitude and Distance Modulus for the Parkes / NTT Sub-Sample 139

Table 6.1: TF $\Delta\mu$ colour band comparative results 153

Table 6.2: H_0 measurements from this thesis 156

Table 6.3: H_0 measurements from the literature 156

Table 6.4: Mean difference and rms scatter for the TF and SNe Ia for the three sample sets 157
Table 6.5: Distribution of $\Delta\mu$ for spiral and barred spiral galaxies 157
Table 6.6: Bulk flow analysis for the TF and SNe Ia data 164
Table 6.7: Bulk flow of the local Universe 165
Table 6.8: β results for TF and SNe Ia peculiar velocities with the Erdoğdu, MAK and PSCz flow models 169
Table 6.9: β results from the literature 170
Table 6.10: Values for Ω_m from Planck, WMAP and this thesis 170

LIST OF FIGURES

Figure 1.1: Example NGC 706 7

Figure 1.2: SN Ia 2001el light curves for colour bands *B, V, R,* and *I* 12

Figure 3.1: Uncorrected Velocity width, W_{50} vs. Uncorrected Velocity width, W_{20} 33

Figure 3.2: Corrected Velocity width, W_{50}^{Ri} vs. Corrected Velocity width, W_{20}^{Ri} 34

Figure 3.3: Distance modulus, μ (TF W_R^i B_T) RC3 (mag) vs. Distance modulus, μ (TF W_R^i H^c) 2MASS (mag) 38

Figure 3.4: Distance modulus, μ (TF W_R^i B_T) RC3 (mag) vs. Distance modulus, μ (TF $W_R{}^i$ K_s) 2MASS (mag) 38

Figure 3.5: Distance modulus, μ (TF W_R^i H^c) 2MASS (mag) vs. Distance modulus, μ (TF $W_R{}^i$ K_s) 2MASS (mag) 39

Figure 3.6: Corrected Velocity width, log W_R^i vs. $M_{H\text{-}5 \log h}$ 2MASS (mag) 39

Figure 3.7: Corrected Velocity width, log W_R^i vs. $M_{K\text{-}5 \log h}$ 2MASS (mag) 40

Figure 3.8: Velocity, log *cz* (km s^{-1}) (CMB frame) vs. Distance modulus, μ (TF $W_R{}^i$ B_T) RC3 (mag) 40

Figure 3.9: Velocity, log *cz* (km s^{-1}) (CMB frame) vs. Distance modulus, μ (TF $W_R{}^i$ H^c) 2MASS (mag) 41

Figure 3.10: Velocity, log *cz* (km s^{-1}) (CMB frame) vs. Distance modulus, μ (TF $W_R{}^i$ K_s) 2MASS (mag) 41

Figure 3.11: Velocity, log *cz* (km s^{-1}) (CMB frame) vs. Distance modulus, μ (SNe Ia) (mag) 42

Figure 3.12: Distance modulus, μ (SNe Ia) (mag) vs. Distance modulus, μ (TF $W_R{}^i$ B_T) RC3 (mag) 42

Figure 3.13: Distance modulus, μ (SNe Ia) (mag) vs. Distance modulus, μ (TF $W_R{}^i$ H^c) 2MASS (mag) 43

Figure 3.14: Distance modulus, μ (SNe Ia) (mag) vs. Distance modulus, μ (TF $W_R{}^i$ K_s) 2MASS (mag) 43

Figure 4.1: Example NGC 1448 72

Figure 4.2: New 21 cm HI integrations 73

Figure 4.3: Uncorrected Velocity width, W_{50} vs. Uncorrected Velocity width, W_{20} 82

Figure 4.4: Corrected Velocity width, W_{50}^{Ri} vs. Corrected Velocity width, W_{20}^{Ri} 82

Figure 4.5: Distance modulus, μ (TF W_R^i B_T) RC3 (mag) vs. Distance modulus, μ (TF W_R^i H^c) 2MASS (mag)..... 83
Figure 4.6: Distance modulus, μ (TF W_R^i B_T) RC3 (mag) vs. Distance modulus, μ (TF $W_R{}^i$ K_s) 2MASS (mag)..... 83
Figure 4.7: Distance modulus, μ (TF W_R^i H^c) 2MASS (mag) vs. Distance modulus, μ (TF $W_R{}^i$ K_s) 2MASS (mag)..... 84
Figure 4.8: Corrected Velocity width, log W_R^i vs. $M_{H\text{-}5 \log h}$ 2MASS (mag) 85
Figure 4.9: Corrected Velocity width, log W_R^i vs. $M_{K\text{-}5 \log h}$ 2MASS (mag) 86
Figure 4.10: Velocity, log *cz* (km s^{-1}) (CMB frame) vs. Distance modulus, μ (TF $W_R{}^i$ B_T) RC3 (mag)..... 86
Figure 4.11: Velocity, log *cz* (km s^{-1}) (CMB frame) vs. Distance modulus, μ (TF $W_R{}^i$ H^c) 2MASS (mag)..... 87
Figure 4.12: Velocity, log *cz* (km s^{-1}) (CMB frame) vs. Distance modulus, μ (TF $W_R{}^i$ K_s) 2MASS (mag)..... 87
Figure 4.13: Velocity, log *cz* (km s^{-1}) (CMB frame) vs. Distance modulus, μ (SNe Ia) (mag) 88
Figure 4.14: Distance modulus, μ (SNe Ia) (mag) vs. Distance modulus, μ (TF $W_R{}^i$ B_T) RC3 (mag) 88
Figure 4.15: Distance modulus, μ (SNe Ia) (mag) vs. Distance modulus, μ (TF $W_R{}^i$ H^c) 2MASS (mag)..... 89
Figure 4.16: Distance modulus, μ (SNe Ia) (mag) vs. Distance modulus, μ (TF $W_R{}^i$ K_s) 2MASS (mag)..... 89
Figure 5.1: Light curve of SN Ia 2012fr..... 109
Figure 5.2: Uncorrected Velocity width, W_{50} vs. Uncorrected Velocity width, W_{20} ... 110
Figure 5.3: Corrected Velocity width, W_{50}^{Ri} vs. Corrected Velocity width, W_{20}^{Ri} 111
Figure 5.4: SOFI H^c -band (mag) vs. 2MASS H^c -band (mag)..... 113
Figure 5.5: SOFI K_s -band (mag) vs. 2MASS K_s -band (mag)..... 113
Figure 5.6: Distance modulus, μ (TF $W_R{}^i$ B_T) RC3 (mag) vs. Distance modulus, μ (TF $W_R{}^i$ H^c) SOFI (mag)..... 114
Figure 5.7: Distance modulus, μ (TF $W_R{}^i$ B_T) RC3 (mag) vs. Distance modulus, μ (TF $W_R{}^i$ K_s) SOFI (mag)..... 114

Figure 5.8: Distance modulus, μ (TF W_R^i H^c) SOFI (mag) vs. Distance modulus, μ (TF W_R^i K_s) SOFI (mag) 115
Figure 5.9: Distance modulus, μ (TF W_R^i B_T) RC3 (mag) vs. Distance modulus, μ (TF W_R^i H^c) 2MASS (mag) 115
Figure 5.10: Distance modulus, μ (TF W_R^i B_T) RC3 (mag) vs. Distance modulus, μ (TF W_R^i K_s) 2MASS (mag) 116
Figure 5.11: Distance modulus, μ (TF W_R^i H^c) 2MASS (mag) vs. Distance modulus, μ (TF W_R^i K_s) 2MASS (mag) 116
Figure 5.12: Corrected Velocity width, log W_R^i vs. $M_{H\text{-}5 \log h}$ SOFI / 2MASS (mag) 117
Figure 5.13: Corrected Velocity width, log W_R^i vs. $M_{K\text{-}5 \log h}$ SOFI / 2MASS (mag) 117
Figure 5.14: Velocity, log cz (km s^{-1}) (CMB frame) vs. Distance modulus, μ (TF W_R^i B_T) RC3 (mag) 118
Figure 5.15: Velocity, log cz (km s^{-1}) (CMB frame) vs. Distance modulus, μ (TF W_R^i H^c) SOFI / 2MASS (mag) 118
Figure 5.16: Velocity, log cz (km s^{-1}) (CMB frame) vs. Distance modulus, μ (TF W_R^i K_s) SOFI / 2MASS (mag) 119
Figure 5.17: Velocity, log cz (km s^{-1}) (CMB frame) vs. Distance modulus, μ (SNe Ia) (mag) 119
Figure 5.18: Distance modulus, μ (SNe Ia) (mag) vs. Distance modulus, μ (TF W_R^i B_T) RC3 (mag) 120
Figure 5.19: Distance modulus, μ (SNe Ia) (mag) vs. Distance modulus, μ (TF W_R^i H^c) SOFI (mag) 120
Figure 5.20: Distance modulus, μ (SNe Ia) (mag) vs. Distance modulus, μ (TF W_R^i K_s) SOFI (mag) 121
Figure 5.21: Distance modulus, μ (SNe Ia) (mag) vs. Distance modulus, μ (TF W_R^i H^c) 2MASS (mag) 121
Figure 5.22: Distance modulus, μ (SNe Ia) (mag) vs. Distance modulus, μ (TF W_R^i K_s) 2MASS (mag) 122
Figure 6.1: Uncorrected Velocity width, W_{50} vs. Uncorrected Velocity width, W_{20} ... 143
Figure 6.2: Corrected Velocity width, W_{50}^{Ri} vs. Corrected Velocity width, W_{20}^{Ri} 144
Figure 6.3: RC3 B_T-band b/a vs. 2MASS co-added IR bands of JHK b/a 145

Figure 6.4: K_s -band distance modulus vs. NED absolute magnitude 146
Figure 6.5: K_s -band distance modulus vs. EDD absolute magnitude 146
Figure 6.6: log(cosec(i)) from RC3 B_T -band vs. log(cosec(i)) from 2MASS co-added bands *JHK* 147
Figure 6.7: Distance modulus, μ (TF $W_R{}^i\, B_T$) RC3 (mag) vs. Distance modulus, μ (TF $W_R{}^i\, H^c$) mean of SOFI and 2MASS (mag) 148
Figure 6.8: Distance modulus, μ (TF $W_R{}^i\, B_T$) RC3 (mag) vs. Distance modulus, μ (TF $W_R{}^i\, K_s$) mean of SOFI and 2MASS (mag) 148
Figure 6.9: Distance modulus, μ (TF $W_R{}^i\, H^c$) mean of SOFI and 2MASS (mag) vs. Distance modulus, μ (TF $W_R{}^i\, K_s$) mean of SOFI and 2MASS (mag) 149
Figure 6.10: Corrected Velocity width, log W_R^i vs. Absolute H & K-band magnitude $M_{HK\text{-}5\log h}$ SOFI / 2MASS mean 149
Figure 6.11: Velocity, log cz (km s^{-1}) (CMB frame) vs. Distance modulus, μ (TF $W_R{}^i\, B_T$) RC3 (mag) 150
Figure 6.12: Velocity, log cz (km s^{-1}) (CMB frame) vs. Distance modulus, μ (TF $W_R{}^i$ in H^c and K_s) SOFI / 2MASS *mean* (mag) 151
Figure 6.13: Velocity, log cz (km s^{-1}) (CMB frame) vs. Distance modulus, μ (SNe Ia) 151
Figure 6.14: Distance modulus, μ (SNe Ia) (mag) vs. Distance modulus, μ (TF $W_R{}^i\, B_T$) RC3 (mag) 153
Figure 6.15: Distance modulus, μ (SNe Ia) (mag) vs. Distance modulus, μ (TF $W_R{}^i\, H^c$) SOFI / 2MASS mean (mag) 154
Figure 6.16: Distance modulus, μ (SNe Ia) (mag) vs. Distance modulus, μ (TF $W_R{}^i\, K_s$) SOFI / 2MASS mean (mag) 154
Figure 6.17: Velocity, log cz (km s^{-1}) (CMB frame) vs. TF H^c & K_s -band residuals $\Delta\mu$ (mag) 159
Figure 6.18: Velocity, log cz (km s^{-1}) (CMB frame) vs. SN Ia residuals $\Delta\mu$ (mag) ... 160
Figure 6.19: Velocity, log cz (km s^{-1}) (CMB frame) vs. Corrected $\log W_R^i$ 160
Figure 6.20: Sky coverage of the three samples, coordinates with an Aitoff projection 163
Figure 6.21: V_{pec}^{3KCMB} (TF) (km s^{-1}) vs. V_{pec}^{3KCMB} (SNe Ia) (km s^{-1}) 163
Figure 6.22: Cosine Apex Angle vs. Peculiar Velocity 164
Figure 6.23: PSCz vs. MAK, PSCz vs. Erdoğdu, and MAK vs. Erdoğdu 167

Figure 6.24: Growth parameter, β vs. χ^2 for Erdoğdu, MAK, and PSCz for TF and SN 169
Figure 6.25: Growth parameter, β vs. χ^2 for the combined Erdoğdu, MAK, and PSCz for TF and SN respectively 170

List of Appendices

Appendix: Definitions 179

TULLY-FISHER DISTANCE MEASUREMENTS OF SPIRAL GALAXIES WITH WELL-OBSERVED TYPE Ia SUPERNOVAE

Supervisors: Dr. John DANZIGER, Dr. Graeme WHITE, Dr. David BLANK, and Dr. Andrew WALSH

Advisor: Dr. Lister STAVELEY-SMITH

ACKNOWLEDGMENT

I thank Graeme White for his initial involvement and the opportunity for this project. My introduction to John Danziger, of Observatorio Astronomico di Trieste, for this project through Graeme has been most rewarding. John has provided a project that is relevant to the continued refinement of cosmology. This is a tremendous opportunity to compare two distance measurement methods for galaxy recession velocities $V < 6000$ km s^{-1}. This project, findings, and analysis are relevant to the much anticipated Square Kilometre Array (SKA). I thank John for the support, analyses, and mentoring for this project.

I thank Preben Grosbøl, introduced to the project by John Danziger, for the near-infrared images obtained for the Parkes / NTT sample. Preben's expertise in establishing the correct imaging methods, and advice on correction for instrumental effects and Galactic extinction resulting in accurate *H* and *K* band near-infrared photometry. The refined photometry provided more precise distance moduli values for the Parkes / NTT sample set.

I thank the Time Assignment Committee at CSIRO ATNF for the opportunity of observing time at the 64 m Radio Telescope in Parkes, Australia for this project titled P364. We observed the Parkes sample in two periods, April and October 2005, depending on the location of the objects. In addition, the ATNF Observatory and the 64 m Radio Telescope were utilised for the 21 cm observations for the 51-galaxy sample prior to my involvement in the project.

I appreciate all of the staff at Parkes for the welcome they extended to me as a novice in observational radio astronomy. I greatly appreciate Lewis Ball spending time at the end of his day for me to begin the observational program on the first evening. I arrived a day early to prepare for the following night's scheduled April observations. A cancellation occurred for that evening providing an extra ten hours of observation time. Fortunately, Lewis was willing to share his expertise that evening and had the foresight

to believe that I would succeed with that night's observations. Of the 17 galaxies scheduled for the night, I was able to obtain 16 integrations. Lewis's knowledge of the radio telescope and computer system, together with his presentation skills, allowed me to be fully functional for my observations. The remaining observations for the 29 objects in October were successful based on the thorough introduction.

John Reynolds was very helpful and informative during the observation sessions in April and October 2005. I thank John for his administrative, operational and observational knowledge. The collective efforts by the professional ATNF Parkes personnel provided me with an experience and training that will forever be etched in my mind.

I have had the great fortune of meeting and working with Lister Staveley-Smith of the University of Western Australia, and John Danziger supervising my 21 cm observations at the ATNF 64 m Radio Telescope at Parkes NSW, Australia for the Parkes sample. My gratitude goes to Lister for teaching the intricacies of 21 cm radio astronomy. Lister's patience and astrophysical expertise at the telescope, during the final data reduction in Sydney, and analysis at UWA are unparalleled. My inclusion in several meetings and presentations during my time in Sydney and at UWA was a tremendous bonus. I thank Lister Staveley-Smith and John Danziger for making the 21 cm observations for the Parkes / NTT sample prior to my introduction to the project. The continued expert input by Lister and John have been greatly appreciated in the evolution of the thesis project.

I am fortunate to have David Blank as a co-supervisor for the early stages of the project. David made significant suggestions and asked compelling questions, enhancing the scope of the study. I am grateful for Andrew Walsh as a co-supervisor and Director, Centre for Astronomy at James Cook University for assisting the completion of the project. Andrew has provided valuable recommendations for the successful outcome of the project. The continued efforts on behalf of Andrew, John and Lister for me to systematically assimilate, organise, and synthesise the data for the project is greatly appreciated.

I extend my gratitude to Alain Klotz, Professor at the Toulouse University in the IRAP (Institut de Recherche en Astrophysique et Planetologie) in Toulouse, France, and Michael Childress of RSAA (Research School of Astronomy & Astrophysics), Australian National University (ANU), for the light curve data of the most recent Type Ia Supernova, 2012fr in host galaxy NGC 1365 using TAROT.

This research made use of the ATNF Parkes 64 m Radio Telescope to make the new 21 cm observations. The Parkes Radio Telescope is part of Australia Telescope National Facility that is funded by the Commonwealth of Australia for operation as a National Facility managed by CSIRO. The new 21 cm observations were made for the Parkes sample, and the 51-galaxy sub-sample extracted from the Parkes / NTT sample with telescope time arranged by John Danziger.

This work is based on new NIR observations collected at the European Southern Observatory in Chile, corresponding to the observing proposal ESO No. 68.A0085(B) and No. 69.A0021(A). The infrared observations were made using SOFI infrared spectrograph and imaging camera on the 3.5 m NTT at the La Silla Observatory.

Observations of SN 2012fr in host galaxy NGC 1365 for *B, V,* and *R* band data were collected with TAROT located at the European Southern Observatory in La Silla, Chile. TAROT is the property of the French National Research Centre (CNRS).

This research makes use of the VizieR catalogue access tool, CDS Strasbourg, France.

This project makes use of the CfA Supernova Archive, that is funded in part by the National Science Foundation through grant AST 0606772.

The data contained within this paper makes use of the NASA / IPAC Extragalactic Database (NED). NED is operated by the Jet Propulsion Laboratory, California Institute of Technology, under contract with the National Aeronautics and Space Administration. This research makes use of the NASA / IPAC Infrared Science Archive, that is operated by the Jet Propulsion Laboratory, California Institute of Technology, under contract with the National Aeronautics and Space Administration.

This thesis makes use of data products from the Two Micron All Sky Survey (2MASS), that is a joint project of the University of Massachusetts and the Infrared Processing and Analyses Centre / California Institute of Technology, funded by the National Aeronautics and Space Administration and the National Science Foundation.

This thesis makes use of the Supernovae light curves from the Sternberg Astronomical Institute (SAI), Moscow University.

I acknowledge the usage of the HyperLeda database of the University of Lyon, France.

Daryl L. SEIBEL — 07 November 2016

Signature — Date

ABSTRACT

This thesis provides a comprehensive new set of distance measurements for nearby (cz < 6000 km s^{-1}) galaxies based on two of the best available distance indicators: the Tully-Fisher (TF) relation, and Type Ia Supernovae (SNe Ia). The Tully-Fisher relation relates absolute luminosity and rotation velocity, and is an excellent distance indicator for inclined spiral galaxies in the local Universe. SNe Ia are bright so-called 'standard candles' (albeit with a well-known dependences on colour and the decline rate of their light curves) that are used to measure distances to a range of host galaxies at large distances. Although generally more accurate than the former method, SNe Ia are relatively rare and distances can therefore only be measured to small samples of objects in the local Universe. This thesis provides new Tully-Fisher data for all southern hemisphere SN Ia host galaxies, thereby allowing a much better cross-comparison of the two methods than previously possible. Type Ia Supernova 2012fr is the latest SN Ia included in this thesis with a full light curve. Nevertheless, there are some SN Ia and host galaxy data that are incomplete. In many respects, this study is a pilot study for much larger samples that will be provided by the forthcoming SkyMapper supernova survey and the ASKAP WALLABY neutral hydrogen survey.

Measurements are presented for a total of 227 galaxies in the following three separate studies:

1. A sample of 130 galaxies for which homogenised optical and radio data is obtained from the literature, and are mainly in the northern hemisphere.
2. A sample of 46 galaxies with good existing photometry, but without prior radio data, were observed in 2005 with the ATNF Parkes 64 m Radio Telescope. This sample significantly adds to the available set of data for nearby southern galaxies.
3. New near-infrared imaging with the European Southern Observatory's New Technology Telescope (NTT), and the new 21 cm radio imaging with the Parkes 64 m telescope in 2004 is presented for a sample of 88 and 51 galaxies, respectively. This sample again significantly adds to the volume, and quality, of the available data.

For each of the above samples, SNe Ia distances are calculated using data published in the literature for optical photometry, namely peak brightness, colour and decay rate, where available. Tully-Fisher distances are calculated using neutral

hydrogen line width measurements and optical luminosities in the optical (B_T) and infrared (H^c and K_s) bands.

Although the total sample overlap between the SNe Ia and Tully-Fisher distances remains relatively small, no systematic significant differences are found. Nevertheless, the scatter is significant in our studies. Furthermore, compared with the SNe Ia distances, it is notable that there is significantly less dispersion in the distance moduli for the final Parkes / NTT sample, illustrating the value of the dedicated new observations presented here.

A comparison of our distance estimates with secondary calibration relations suggests higher values of the Hubble constant than previously measured: $H_0 = 76 \pm 4$ km s^{-1} Mpc^{-1} and $H_0 = 90 \pm 5$ km s^{-1} Mpc^{-1} for the Tully-Fisher and SNe Ia methods, respectively. The latter is significantly higher than the highly-accurate Planck result of $H_0 = 67 \pm 1$ km s^{-1} Mpc^{-1} suggesting that our samples are subject to selection effects, and are not volume-limited. We are biased by the exclusion of faint SNe Ia and possibly by faint SN Ia host galaxies due to radio sensitivity limits.

Peculiar velocities were calculated from the measured distances and redshifts. Of the 227 total galaxies in our sample sets, 177 galaxies have complete data for our study. An analysis of the bulk flow using the peculiar velocities in a combined sample of 177 SNe Ia and Tully-Fisher measurements shows that the sample is substantially at rest with respect to the rest frame defined by the Cosmic Microwave Background. The residual bulk flow of 208 ± 160 km s^{-1} is in agreement with the predictions of ΛCDM (Lambda-Cold Dark Matter) for a mean depth of 40 Mpc.

Finally, a comparison of our measured peculiar velocities with theoretical values reconstructed from models of the gravitational field deduced from redshift surveys has allowed us to investigate the relationship between gravity and the large-scale galaxy distribution. A value for the growth parameter of β = 0.37 ± 0.08 is measured, corresponding to a value for the dark matter density parameter at the present epoch of Ω_m = 0.16 ± 0.06, assuming a bias parameter b = 1; the latter not being measured in the thesis.

Future studies with SkyMapper and ASKAP will benefit greatly by having deeper, more numerous samples and will benefit from higher quality data. The existing data in the literature, particularly the photometry for historical SNe Ia, is of lower quality than newer data.

CHAPTER 1
INTRODUCTION

1.1 Aim

This thesis is an empirical study which compares two existing distance indicators for spiral galaxies: the luminosity-rotational line width relation referred to as the Tully-Fisher (TF; Tully & Fisher 1977) relation; and the Type Ia Supernovae (SNe Ia) 'standard candles'. The purpose of this study is to provide a quantitative comparison of the two methods for spiral galaxies in the field with recession velocities within $V < 6000$ km s^{-1} and to use the flow field to measure the Hubble constant and non-Hubble (peculiar) motions in the local Universe.

The importance of this study of observational cosmology is to evaluate the distribution of luminous matter in the local Universe, the predicted distance and peculiar velocity, and the relation of the estimates of the bulk flow as compared to ΛCDM (Lambda-Cold Dark Matter).

1.2 Lambda-CDM

Our study allows us to compare the results to determine if they are in agreement with the predictions of ΛCDM model that we work within. The ΛCDM model states that the Universe is comprised of three components: (1) ordinary matter (baryons); (2) dark matter (that has mass and interaction with gravity); and (3) dark energy (that accelerates the expansion of the Universe). The Friedmann equations in the context of general relativity, that support the ΛCDM model, begin with an initial premise that the universe is spatially homogeneous and isotropic. Lambda is the cosmological constant that is associated with dark energy used to explain the expansion of space against the effects of gravity. The cold dark matter accounts for the gravitational effects observed in very large-scale structures that cannot be accounted for by the quantity of the observed matter.

In the local Universe, homogenity of the expansion is not necessarily consistent with the ΛCDM and the Friedmann models. However, on a large scale, the distribution of the distant galaxies appears to be roughly uniform thoughout the Universe and is isotropic. There are three generalized Friedmann models: (1) the galactic density is high enough that the gravitational influence will eventually stop the expansion and the Universe will collapse – a finite Universe; (2) the Universe expands at a decreasing rate

where the density is equal to a critical value and the gravitational influence cannot overcome the velocity of the expansion – a flat Universe where the expansion eventually reaches zero; and (3) the galactic expansion is at a critical rate to avoid recollapse due to insufficient density for gravitational attraction – an infinite Universe. The Friedmann equations supporting the theorem where p is the total pressure (Xia & Wang 2016; NED):

$$H^2 = \left(\frac{a}{a}\right)^2 = \frac{8\pi G p}{3} - \frac{k}{a^2} + \frac{\Lambda}{3} \tag{1.1}$$

and

$$\frac{a}{a} = -\frac{4\pi G}{3}(p + 3p) + \frac{\Lambda}{3} \tag{1.2}$$

With the evolution of the Universe, it is conceivable that cold dark matter could be converted into dark energy. The current Dark Energy Survey (DES) is projected to characterise dark energy and dark matter, and the possible subsequent interaction. The DES survey shows that if the cosmological model is presumed to be ΛCDM, then the underlying physics can possibly be deduced from the DES probes (Abbott et al. 2016).

1.3 The Distance Ladder

There are several categories of distance measurement techniques. The so-called primary distance indicators allow the direct measurement of distance through, for example, a geometric technique such as Annual Parallax or main-sequence fitting. Secondary indicators rely on a primary technique to calibrate the distance of an 'archetype', but then extend measurement to larger distances. Notable examples are the Cepheid variable stars (Jacoby et al. 1992). Finally, tertiary distance indicators extend the measurement range even further by using secondary techniques for more distant objects. The TF and SNe Ia relations used in this thesis fall into the latter category. Newer SNe Ia observations now provide distance measurements accurate of 5% to 10% and the TF relation provides accuracies of 15% to 20% out to distances of 100 Mpc.

This 'distance ladder' has been discussed by many authors including Rowan-Robinson (1985), Jacoby et al (1992), Mould et al. (2000) and Reiss et al. (2009). Historically, the distance ladder has presented a number of problems. These arise from measurement error, compounding of errors, sample selection, intrinsic dispersion and

dependence on extra 'unknown' parameters. Until the early 1990's, this resulted in a factor-of-two uncertainty in the distances to nearby galaxies, and therefore a factor of two uncertainties in the Hubble time. Amongst other things, this uncertainty contributed to the delay in recognising the existence of dark energy. There were two independent projects in 1998 that suggested an acceleration in the expansion of the Universe using SNe Ia: Supernova Cosmology Project (Perlmutter et al. 1999), and the High-Z Supernovae Search Team (Riess et al. 1998), both of whom shared the 2011 Nobel Prize in physics. The accelerating Universe, attributed to dark energy or a cosmological constant, neatly reconciles the known ages of the oldest stars with that of the cosmologically-derived age of the Universe, as well as explaining the magnitude-redshift relation for distant supernovae.

1.4 The Tully-Fisher (TF) Relation: discovery

Hydrogen is the most abundant element in the interstellar medium (ISM). Neutral hydrogen (HI) atoms are abundant and ubiquitous in low-density regions of the ISM. They are detectable in the vacuum wavelength of $\lambda_0 = 21.1$ cm. There are two energy levels that result from the magnetic interaction between the quantized electron and proton spins. A photon is emitted when the relative spins change from parallel to antiparallel.

Tully and Fisher (1977) were the first to recognise the utility of the neutral hydrogen 21 cm line width - absolute luminosity relation. They used nearby galaxies with well-determined distances to demonstrate a power-law dependence between the two parameters. Therefore, distances to other galaxies could be calculated by simply measuring their *apparent* luminosities and *distance-independent* neutral hydrogen line widths, or rotation velocities. Their first calibrations were accomplished with the Local Group, and the M81 group that were previously measured using Cepheid variables by Sandage and Tammann (1974a, ST I; 1974b, ST II).

For their measurement in the Virgo Cluster, Tully & Fisher listed five requirements. The first was to study galaxies already measured photometrically by Holmberg (1958). The second was that the galaxies should lie within $6°$ of the centre of the cluster. The $6°$ radius of the region encloses the region they accepted as the Virgo Cluster, contending that the southern extension is physically not part of the Virgo Cluster. The third was to analyse the galaxy types Sb^+, Sc^-, and Sc^+ as described by

Holmberg (1958) (see appendix). The fourth was that the galaxies had to be inclined $45° < i < 85°$, using the axial ratios of Holmberg (1958), to avoid substantial inclination and internal absorption uncertainties. Knowing the inclinations to $\pm 5°$, the correction uncertainty was less than 2% - 3%. The final requirement was that the galaxies had to be sufficiently isolated to preclude any confusion in the HI profiles.

Measurements of the Virgo Cluster, and also the Ursa Major Cluster, showed a relationship between the distance modulus, line width and apparent magnitude of the form $\mu_0 = 3.5 + 6.25 \log \Delta V(0) + m_{pg}(0)$ for the magnitude relation with an uncertainty $\pm 0^m.6$ and for the diameter relation $\mu_0 = 25.6 + 3.7 \log \Delta V(0) - 5 \log a$. The accuracy determined was ± 15%.

1.5 The Tully-Fisher Relation: refinement

One of the key elements in the TF relation consists of the accurate measurement of the rotational line width. The 21 cm line width velocity measurement at 20% of peak intensity (W_{20}) and at 50% of peak intensity (W_{50}) have been used. Fisher and Tully (1981) considered that if widths are measured at a higher fraction of the peak, the measurement is sensitive to the exact form of the observed spectrum. If the line width intensity level is lower than 20%, there is too much sensitivity to noise.

Figure 1.1 is an example of the final data reduction of NGC 706 (Chapter 4 - new 21 cm line width observations) and the use of masking in order to fit a baseline and measure the profile width. A polynomial order of three was fitted. The two outer pairs of vertical dashed lines denote frequency ranges that were masked. The inner pair denotes the desired profile that was also excluded from the baseline fit. In the case of high S/N with low RFI, no masking was necessary. The plot also shows symbols that denote the 'width-maximised' (○), and width-minimised (×) values for W_{20} and W_{50}. The frequency of the peak profile emission is denoted ν_{Sp} (•) as in Meyer et al. (2004). The maximisation procedure starts at the position of the outer profile window and proceeds inward until reaching the required percentage of the peak flux density. The minimisation procedure starts at ν_{Sp} and searches outward.

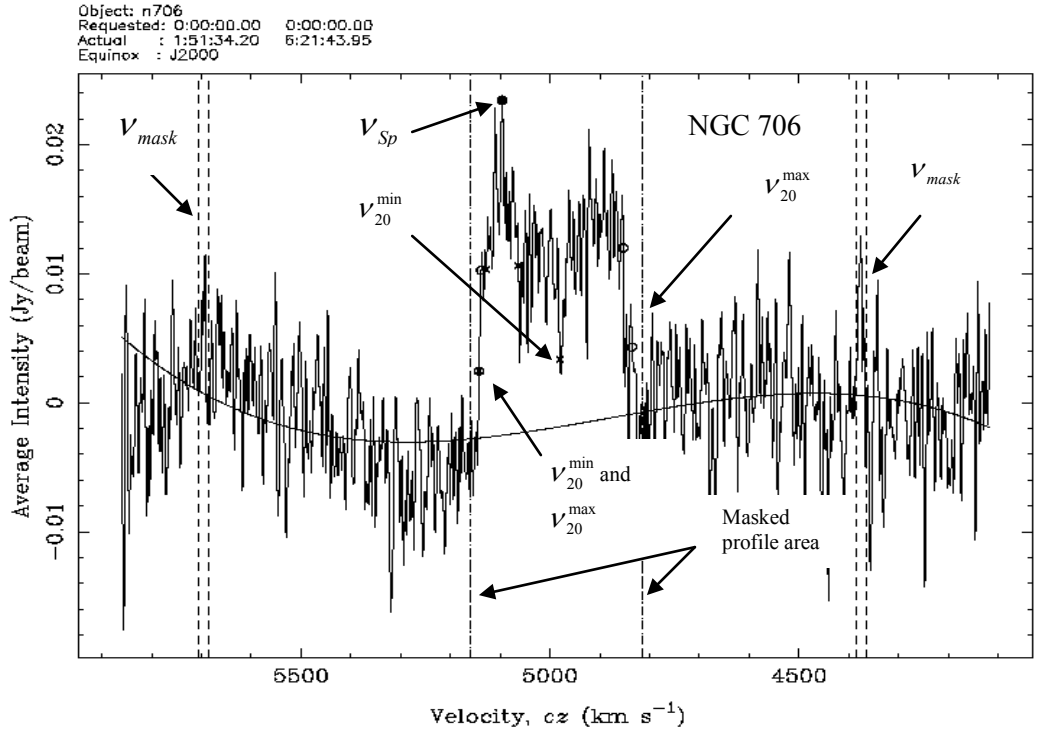

Figure 1.1: Example NGC 706

Bottinelli et al. (1983) proposed that the previous TF line width relation ignored the effects of the velocity dispersion in the gas. They reasoned that line width measures the combined effects of velocity dispersion and circular motion of the HI gas. Bottinelli et al. (1983) determined $W = 2(V_m \sin i + V_t)$ where $V_m \sin i$ is the projected maximum circular velocity, and V_t is the velocity dispersion. The systematic difference is less than $\pm$ 0.02 for 30° < i < 85° and 1.8 < log V_m < 2.5 for 80% to 90% of the sample. Bottinelli et al. (1983) concluded that any one of the three peak intensity levels, W_{20}, W_{40}, or W_{50} can be used. They stated that the TF relation $-M_T^0 = a(\log V_m - 2.2) + b$ is a function of the wavelength with values varying from $a(B) \cong 5$ in the blue wavelength to $a(H) \cong 10$ in the infrared. They posit the distance moduli will have greater errors using the *H*-band versus the *B*-band. Tully and Fouqué (1985) provide updated dispersion corrections to the line width measurements that apply to luminous and less-luminous systems.

Other studies were made to determine the best level of peak intensity by Tully and Fouqué (1985), and Giovanelli et al. (1997) who concluded that the W_{20} and the W_{50} level of peak intensity remain the preference.

Roth et al. (1994) and Donley et al. (2005) studied the effects of Signal / Noise (S/N) ratio on the errors of the HI line width velocity measurements. They concluded S/N < 5 becomes problematic owing to increased noise being introduced into the profile. The line widths are considered adequately measured only if the S/N at the emission line peak is ≥ 7. A steep sided profile with S/N > 10 provides a measurement of W_{20} with an accuracy of better than 10 km s^{-1}; profiles of $7 < S/N < 10$ have line width uncertainties of ~ 15 km s^{-1}.

The bandpass dependence of the TF relation is evident in the combined work of Tully and Fisher (1977), Bottinelli et al. (1983), Aaronson et al. (1979), Aaronson et al. (1980, Paper I and II), Aaronson et al. (1980, Paper III) and many others. The reason could be internal extinction or intrinsic wavelength-dependence. In either case, the *R* or *I* optical bands and the infrared bands are less affected by reddening and appear to offer the lowest scatter. For example, recent studies have tended to concentrate on the optical *I*-band or infrared *K*-band (Masters et al. 2006; Masters et al. 2008; Springob et al. 2007).

Longer wavelengths also lessen the effects of internal and Galactic extinction. Aaronson et al. (1980, Paper III) utilised the near-infrared (NIR) to make the first studies at longer wavelengths. The NIR bands are *J* $(1.11-1.36\mu m)$, *H* $(1.50-1.80\mu m)$, and *K* $(2.00-2.50\mu m)$. The *H*-band was used by Aaronson et al. (1980, Paper III) whereas the *K*-band is least affected by extinction (Jarrett et al. 2000) and is favoured by recent authors. Observations in the mid-infrared band at 3.6 μm have been used by Sorce et al. (2012), and 3.4 μm and 4.6 μm by Neill et al. (2014) and others.

Apparent magnitude corrections for Galactic absorption, inclination-dependent internal extinction, and *k*-correction (which accounts for redshift dependence) are necessary for the TF relation. These will be discussed further in Chapter 2. Tully et al. (2008) refined the absolute magnitude equations of Tully and Pierce (2000, Paper III) by correcting to the Cepheid zero point.

The inclination *(i)* of the plane of the galaxy with respect to the line-of-sight affects the determination of the true rotational velocity. There needs to be sufficient inclination to minimise errors in correcting the hydrogen profile for projection effects since this is probably the largest source of error in line widths. De-projected velocities are increasingly uncertain for galaxy observations approaching a face-on orientation.

The observed velocity width is smaller by a factor sin *(i)* than the intrinsic value, where *(i)* represents the galaxy inclination. Most studies use galaxies with an inclination $40° < i < 85°$, although Pierce (1994) included galaxies with an inclination $\geq 30°$ and Masters et al. (2008) accepted galaxies $\geq 25°$. Similar to these previous studies, we chose to include galaxies with inclinations $35° < i < 85°$ for our study. This removes galaxies with too much obscuration or inclination uncertainty. Finally, correction for cosmological broadening (due to universal expansion) must also be made, although these corrections are small over the redshift range considered.

Many other studies of the TF relation, other than those noted above, have been made using different samples of galaxies. Notable are studies by: Tully and Pierce (2000), Tully (2007 priv. comm.), Tully et al. (2008), Masters et al. (2006; 2008; 2014), Hong et al. (2014) and Springob et al. (2007). The latter were able to further refine the TF relation template by building samples of Spiral Cluster observations in the *I*-band (SCI) and Spiral Field observations in the *I*-band (SFI and SFI++). Although cluster samples are invaluable, their disadvantage is whether there may be intrinsic differences between galaxies in a cluster environment and those that are more isolated. For galaxy-group or galaxy-cluster studies, Aaronson and Mould (1986) proposed that when comparing such studies, possible disparities are the result of morphological type dependence. Moreover, using spirals from clusters is problematic for some studies owing to large peculiar motions.

The Jacoby et al. (1992) study suggested there is the possibility of less dependence when using the near-infrared (NIR). This thesis will use both the optical colour band *B* and the NIR bands *H* and *K*.

There are previous TF studies that incorporate supernova-derived distances: including those of Pierce (1994) who analysed 16 galaxies with a recession velocity $V < 2000$ km s^{-1}, and Shanks (1997) who compared the TF distance measurements for 11 spiral galaxies using the Hubble Space Telescope (HST) Cepheid distances and 12 spiral galaxies with SNe Ia distances for galaxies in the Leo Group, and in the galaxy clusters Virgo and Fornax. These studies contain relatively few data points, are from existing literature, and did not correct the SNe Ia for secondary parameter effects of progenitor and accretion rates, metallicity evolution, and the light curve variations in shape with the intrinsic, absolute brightness. Our study refines the comparison by utilising TF and SNe Ia distances for a larger sample.

1.6 Malmquist Bias

Malmquist bias (Malmquist, 1920; 1922) is important in a luminosity-based analyses owing to the potential of seeing only the brighter objects at the expense of the intrinsically fainter objects. The bias premise is that the more distant objects in a flux-limited sample are more likely to be the most luminous while the nearby objects are more likely to be the least luminous. Due to the finite scatter of the TF relation, this introduces a bias such that, even for a given line width, there will be an excess of galaxies whose luminosities are greater than predicted by a regression line fitted to a volume-limited sample. This can lead to spurious estimates of distances. The amplitude of the bias depends on the slope of the correlation and scatter of the relation.

Tammann (1978) argued to ignore field spiral galaxies because of Malmquist bias. The Aaronson et al. (1980, Paper III) study of galaxy clusters determined that the Malmquist effect and environmental effect were negligible because cluster members are at the same distance. Nevertheless, they noted the possible effect of low HI content of cluster galaxies. Nevertheless, our study is of field spiral galaxies with detectable SNe Ia and high HI mass for which some Malmquist bias does exist that will be identified in later chapters.

Hudson (1994) constructed a Hubble-law (velocity-versus-distance) diagram showing foreground and backside infall deviations from the linear Hubble law for the Great Attractor region. Similar deviations have been detected toward the Virgo Cluster. The Malmquist bias in this case, was found to artificially produce an apparent backside infall signal behind the galaxy cluster. This type of Malmquist bias produces spurious results where the distances in front of the concentration will be smaller and distances calculated for objects behind the concentration will be larger owing to the increasing distance and decreasing density.

Malmquist bias may be more prevalent in peculiar velocity studies where small distance errors result in large velocity differences. The 'homogenous' Malmquist bias factors in the non-flat luminosity function, with more galaxies at larger distances, and a varying selection function. 'Inhomogeneous' Malmquist bias is due to variations in large-scale structure along the line of sight (Springob et al. 2007).

Freudling et al. (1995) performed Monte Carlo simulations of maps of the peculiar velocity field that were derived from distance relations. The results varied from virtually free of biases, to results that were significantly biased. Other studies of Malmquist bias are by Hudson (1994), Willick (1994), Teerikorpi (1995; 1997; 2015),

Staveley-Smith and Davies (1989), Strauss & Willick (1995) and Butkevich et al. (2005).

1.7 Type Ia Supernovae

Due to their extreme brightness, SNe Ia are considered to be excellent standard candles (Jacoby et al. 1992). The progenitors for SNe Ia are either single or double-degenerate stars. One possibility is a binary star system in which one member is a red giant star that gradually expands and accretes matter from its outer layers onto the other member, a white dwarf star. When the Chandrasekhar limiting mass ($\sim 1.38\,M_{Sun}$) for the stability of an electron degenerate Carbon-Oxygen (C-O) object is reached, the degenerate electrons are not sufficient to counterbalance the gravity and the star begins to collapse. During the collapse, the density increases and when reaching $\sim 10^9\,gcm^{-3}$, the carbon ignites by nuclear fusion. In a highly degenerate object, the ignition occurs due to degeneracy pressure dependent only on the density and not on the temperature, resulting in a thermonuclear runaway.

A second possible progenitor involves the coalescence of two white dwarfs, therefore exceeding the Chandrasekhar mass limit and raising the ignition temperature past the nuclear fusion ignition point. It is the thermonuclear runaway fusion of C-O into iron, as in the single-degenerate scenario, that creates the energy that powers the SN Ia. The hot expanding electron gas in the supernova emits photons that are easily seen in the visible region. Spectral lines of Hydrogen and Helium are largely absent. The supernova remains visible until the density of the material and associated energy become low enough for it to become transparent.

The maximum brightness of Type Ia Supernovae are reasonably constant, which appears to reflect the constancy of the initial conditions. However, there is substantial dependence on post-maximum decline rate and colour. Empirically however, after these variables are taken into account, the corrected peak brightness is remarkably constant. It is the stability of the peak luminosity, modified by their decline rate that allows these explosions to be used as standard candles to measure the distance to their host galaxies.

All other types of SNe have a different mechanism for core collapse resulting in different spectral characteristics and a much wider range of intrinsic luminosity. By comparison, Type Ib/c Supernovae have a weak or no silicon absorption features and

Type II Supernovae show a hydrogen spectrum throughout. These supernovae can be luminous but do not have a consistent light curve or reach the same peak luminosity.

Type Ia Supernovae have a singly ionized silicon line at 615 nm near peak light and a characteristic light curve. Near the peak luminosity, the spectrum contains lines of intermediate-mass elements from oxygen to calcium. When the outer layers of the explosion have expanded to the point of transparency, the spectrum is dominated by light emitted by the material near the core of the star. As an example, the following Figure 1.2 taken from data in the literature contains the photometric light curves of *B, V, R*, and *I* passbands for SN Ia 2001el located in the host galaxy NGC 1448. This galaxy and SN Ia are part of the Parkes sample that will be discussed in Chapter 4. Figure 1.2 is presented to show the shape of the light curve prior to peak luminosity and then diminishing as time elapses after the peak.

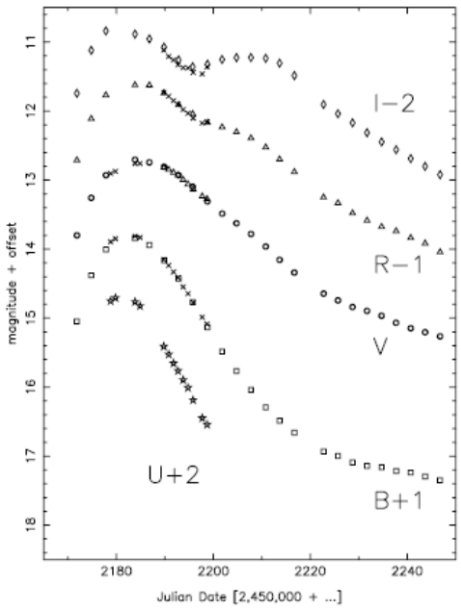

Figure 1.2: Optical photometry of SN Ia 2001el in the host galaxy NGC 1448 for *B*, *V*, *R*, and *I* colour bands. The Yale-AURA-Lisbon-Ohio (YALO) data are plotted as smaller open symbols. Data from the Cerro Tololo Inter-American Observatory (CTIO) 0.9 and 1.5 m telescopes are plotted as crosses (Krisciunas et al. 2003).

Hamuy (1996b) and Phillips (1999) were among the first to use the correlation between absolute magnitude and the initial rate of decline of the *B*-band light curve to improve distance accuracy for SNe Ia. Many others have since used this relation in more accurate studies of SNe Ia – for example Perlmutter et al. (1999), and Riess et al. (2005). The latter calibrated SNe Ia distance moduli using the Cepheid zero point based on HST/ACS observations of 64 Cepheid variables. It is important in such

studies to use only SNe Ia with as much light curve and photometric data as possible. Sparse data sets, even those without a measured peak magnitude, can be fit using the Multicolour Light Curve Shape (MLCS) method where the shape of the light curve is compared to parameterised light curves, or the Stretch method comparing to a template light curve. However, due to the inhomogeneous nature of the literature data available in this thesis, we will focus only using SNe Ia with complete light curve data, which requires the observations to have begun prior to peak luminosity and continuing beyond the peak.

Although fewer in number in the local Universe, the distances and peculiar velocities of the host galaxies of SNe Ia can be measured and used to study non-Hubble velocities. For example, Dai et al. (2011) found that for low redshift supernovae the bulk flow is consistent with previous determinations. The combination of accurate SN Ia distances, which can be as low as 5%, and the more numerous, but less accurate TF distances, is a powerful method for studying the local Universe.

Radburn-Smith et al. (2004) compared local SNe Ia with the IRAS PSC*z* (Infrared Astronomical Satellite Point Source Catalogue Redshift Survey) gravity field. They were able to measure an accurate value for the dimensionless growth parameter β (related to the matter density parameter Ω_m). Other more recent studies have been made by Pike & Hudson (2005), and Turnbull et al. (2012).

1.8 The Hubble Constant

The Hubble Law represents the relation between the recession velocity of a galaxy and its distance (Hubble 1929), where the Hubble Constant is defined $H_0 = V / d$ where V = velocity and d = distance. Although originally formulated for nearby galaxies, through the evolution of numerous studies since the initial 1929 Hubble premise, we now know that the Hubble constant varies with redshift and is dependent on the expansion rate at the redshift of the object in question. There have been many differing values derived for its current value H_0, depending on the type of object observed and the distance. TF-derived values, discussed later in this thesis, range from $53 < H_0 < 95$ km s^{-1} Mpc^{-1}. Values for the SNe Ia tend to be lower when compared to the TF-derived data. Tully et al. (2008) identified that variations in the determination of H_0 are expected and local results of $70 < H_0 < 80$ km s^{-1} Mpc^{-1} are reasonable. Samples limited to 3000 km s^{-1} may bias determinations due to the lack of

isotropic expansion for local galaxies – i.e., peculiar motions within a nearby sample are significant enough to affect the determination of H_0. There may also be differences due to systematic errors such as spectral and spatial resolution (ability to measure accurate linewidths or separate confused galaxies). There may be errors owing to non-linearities in the TF relationship. Aaronson et al. (1980, Paper III) determined a Hubble constant of $H_0 = 65$ km s^{-1} Mpc^{-1} within the Local Supercluster, $H_0 = 95$ km s^{-1} Mpc^{-1} outside the Local Supercluster.

Table 1.1 contains H_0 values from TF and SNe Ia distance determinations.

Table 1.1: Determinations of H_0

TF relation H_0		SNe Ia H_0	
km s^{-1} Mpc^{-1}	Ref	km s^{-1} Mpc^{-1}	Ref
75 ± …	1	63 ± 3 ± 3	9
95 ± …	2	65 ± 1± 6	10
73 ± 11	3	63 ± 2 ± 4	11
82 ± 16	4	68 ± 2 ± 5	12
80 ± …	5	64 ± 5 ± 5	13
77 ± 8	6	59 ± 6 ± …	14
71 ± 4 ± 7	7	73 ± 7 ± …	15
75.2 ± 3	8	74.4 ± 2.5	16

References

1-Tully and Fisher (1977)
2-Aaronson et al. (1980, Paper III)
3-Jacoby et al. (1992)
4-Tully (1998)
5-Tully et al. (1998)
6-Tully and Pierce (2000, Paper III)
7-Sakai et al. (2000)
8-Sorce et al. (2012)
9-Hamuy et al. (1996b)
10-Riess et al. (1998)
11-Phillips et al. (1999)
12-Gibson et al. (2000)
13-Jha (2002)
14-Saha et al. (2001)
15-Riess et al. (2005)
16-Riess et al. (2011)

Tully and Pierce (2000, Paper III) stated summarised H_0 values for the TF relation beginning in 1997 through 2000 ranging from $53 \pm 5 < H_0 < 71 \pm 4$ km s^{-1} Mpc^{-1}. They also measured $H_0 = 77 \pm 8 (95\%)$ km s^{-1} Mpc^{-1}. Sakai et al. (2000) summarised estimates of H_0 using the TF relation from 32 sources from 1976 to 1999 that ranged from $50 \pm 4 < H_0 < 92 \pm 19$ km s^{-1} Mpc^{-1}. The H_0 estimates are primarily from nearby galaxy clusters and groups.

Observations of the Cosmic Microwave Background (CMB) and Baryon Acoustic Oscillations (BAO) provide another path to the measurement of H_0. The 6dFGS (6 degree Field Galaxy Survey) BAO detection of Beutler et al. (2011) found $H_0 = 67 \pm 3.2$ km s^{-1} Mpc^{-1}. The Planck 2013 measurement (Planck Collaboration et al. 2013) is $H_0 = 67.3 \pm 1.2$ km s^{-1} Mpc^{-1}. Both studies are independent of the distance ladder, but the Planck measurement is a global observation under the assumption of flatness.

Recently, Bennett et al. (2014) compared the CMB, BAO, and cosmic distance ladder data sets for consistency at high and low redshifts. The combined analysis resulted in a best-fit Hubble constant of $H_0 = 69.6 \pm 0.7$ km s^{-1} Mpc^{-1}. The combined data constrains the Hubble constant to 1%.

For the galaxy samples presented in this thesis, we compare the distance moduli, μ predicted by the TF and SN Ia template relation with logarithmic redshift. An offset from the predicted straight line defined by $\mu = 25 + 5 \log(cz/H_0)$ may be due to an error in the adopted value of H_0. We use the mean of the *H* and *K* band TF relations that require suitable infrared photometry and 21 cm HI observations.

The remainder of this thesis presents 21 cm observations for 227 galaxies in the local Universe that have been hosts of SNe Ia. The goal of the observations is to compare SN Ia and TF distances for a test sample of objects. This will not only help produce a refined study of peculiar velocities in the local Universe, but will enable an improved calibration of both indicators and the measurement of possible dependence on other parameters. The three galaxy samples that will be discussed are:

1. A sample of 130 galaxies for which data is obtained from the literature. The data is carefully selected and corrected to ensure a set of data that is as homogeneous as possible.
2. New 21 cm observations are made for a sample of 46 galaxies, each with good existing photometry, using the ATNF Parkes 64 m Radio Telescope. This sample significantly adds to the available set of distance measurements for nearby southern galaxies.
3. New near-infrared imaging with the European Southern Observatory's New Technology Telescope (NTT) for 88 galaxies and the Parkes 64 m telescope

data is presented for 51 galaxies, respectively. This sample again significantly adds to the volume, and quality, of the available data.

1.9 Peculiar Velocities

There are two additional cosmological measurements that are well suited for our current data. Both of these rely on the measurement of peculiar velocity v_p, that is defined as the difference between redshift-distance *cz* and redshift-independent distance *D* expressed in units of velocity (see Davis & Scrimgeour 2014 for a more accurate form). Peculiar velocities represent deviations from the uniform Hubble flow due to gravitational perturbations from mass concentrations and are responsible for part of the scatter around the Hubble diagram. In standard theory, they represent motions arising from the growth of small density and velocity perturbations on the early Universe (Gorski 1988). The first measurement is that of bulk flow measured from the dipole anisotropy in the distribution of peculiar velocities to measure the mean motion of the local Universe with respect to the CMB (Cosmic Microwave Background) radiation. This flow is very sensitive to the large-scale matter distribution and homogeneity, and therefore the cosmological model (Li et al. 2012; Hong et al. 2014). The second measurement is the comparison of the individual peculiar velocities with those expected from the visible matter distribution. This is sensitive to cosmological parameters, in particular the matter density, and is a test of gravitational theory (Koda et al. 2014).

The shape of the power spectrum is dependent on total matter (Ω_m) content, Hubble constant (H_0), baryon content (Ω_b), and dark energy content (Ω_{DE}). In this study, we have a unique opportunity to study bulk flows using an *all-sky* sample with both TF and SNe Ia distances. Such a sample allows a better comparison of any systematic biases, if present, and a better quantification of errors.

Following this introductory chapter, Chapter 2 identifies the appropriate corrections and algorithms for this study. Chapter 3 examines the data existing in the literature for first sample of 130 galaxies. The data comprises new distance modulus computations for the TF relation and SNe Ia. Chapter 4 provides the details of new observations for the 21 cm HI line width velocity to determine the TF relation for the second sample of 46 galaxies. This particular study uses galaxy photometric and SNe Ia data in the literature. Finally, new NTT near-IR and Parkes 21 cm HI observations

are obtained for the third sample of galaxies and presented in Chapter 5. A discussion of the three sample sets is contained in Chapter 6, together with new cosmological measurements and the results of our study with respect to ΛCDM. Chapter 7 contains the conclusions.

REFERENCES

Aaronson, M., & Mould, J. 1986, ApJ, 303, 1

Aaronson, M., Mould, J., & Huchra, J. 1979, ApJ, 229, 1

Aaronson, M., Mould, J., & Huchra, J. 1980, ApJ, 237, 655 (Paper I)

Aaronson, M., Mould, J., & Huchra, J. 1980, ApJ, 238, 458 (Paper II)

Aaronson, M., Mould, J., Huchra, J., Sullivan, W. T., III, Schommer, R. A., & Bothun, G. D. 1980, ApJ, 239, 12 (Paper III)

Abbott, T., Abdalla, F. B., Aleksić, J., Allam, S., Amara, A., Bacon, D., Balbinot, E., Banerji, M., Bechtol, K., & 131 coauthors 2016, MNRAS, 460, 1270

Bennett, C. L., Larson, D., & Weiland, J. L. 2014, arXiv:1406.1718 [astro-ph.60]

Beutler, F., Blake, C., Colless, M., Jones, D. H., Staveley-Smith, L., Campbell, L., Parker, Q., & Saunders, W. 2011, MNRAS, 416, 3017

Bottinelli, L., Gouguenheim, L., Paturel, G., & de Vaucouleurs, G. 1983, A&A, 118, 4

Butkevich, A. G., Berdyugin, A. V., & Teerikorpi, P. 2005, MNRAS, 362, 321

Dai, D. C., Kinney, W. H., & Stojkovic, D. 2011, arXiv:1102.0800 [astro-ph.60]

Davis, T. M., & Scrimgeour, M. I. 2014, arXiv:1405.0105 [astro-ph.60]

Donley, J. L., Staveley-Smith, L., Kraan-Kerteweg, R. C., Islas-Islas, J. M., Schröder, A., Henning, P. A., Koribalski, B., Mader, S., & Stewart, I. 2005, AJ, 129, 220

Fisher, J. R., & Tully, R. B. 1981, ApJS, 47, 139

Freudling, W., da Costa, L. N., Wegner, G., Giovanelli, R., Haynes, M. P., & Salzer, J. J. 1995, AJ, 110, 920

Gibson, B. K., Stetson, P. B., Freedman, W. L., Mould, J. R., Kennicutt, R. C., Jr., Huchra, J. P., Sakai, S., Graham, J. A., Fassett, C. I., Kelson, D. D., Ferrarese, L., Hughes, S. M. G., Illingworth, G. D., Macri, L. M., Madore, B. F., Sebo, K. M., & Silbermann, N. A. 2000, ApJ 529, 723

Giovanelli, R., Haynes, M. P., Herter, T., Vogt, N. P., da Costa, L. N., Freudling, W., Salzer, J. J., & Wegner, G. 1997, AJ, 113, 53

Górski, K. 1988, ApJ, 332, 7

Hamuy, M., Phillips, M. M., Suntzeff, N. B., Schommer, R. A., Maza, J., & Avilés, R. 1996b, AJ, 112, 2398

Holmberg, E. B. 1958, MELu2, 136, 1

Hong, T., Springob, C. M., Staveley-Smith, L., Scromgeour, M. I. Masters, K. L., Macri, L. M., Koribalski, B. S., Jones, D. H., & Jarrett, T. H. 2014, MNRAS, 445, 402

Hubble, E. P. 1929, PNAS, 15, 168

Hudson, M. J. 1994, MNRAS, 266, 468

Li, M., Pan, J., Gao, L., Jing, Y., Yang, X., Chi, X., Feng, L., Kang, X., Lin, W., Shan, G., Wang, L., Zhao, D., & Zhang, P. 2012, ApJ, 761, 151

Jacoby, G. H., Branch, D., Ciardullo, R., Davies, R. L., Harris, W. E., Pierce, M. J., Pritchet, C. J., Tonry, J. L., & Welch, D. L. 1992, PASP, 104, 599

Jarrett, T. H., Chester, T., Cutri, R., Schneider, S., Skrutskie, M., & Hucra, J. P. 2000, AJ, 119, 2498

Jha, S. 2002, Exploding Stars, Near and Far, PhD Thesis (Cambridge: Harvard University)

Koda, J., Blake, C., Davis, T., Magoulas, C., Springob, C. M., Scrimgeour, M., Johnson, A., Poole, G. B., & Staveley-Smith, L. 2014, MNRAS, 445, 4267

Krisciunas, K., Suntzeff, N. B., Candia, P., Arenas, J., Espinoza, J., Gonzalez, D., Gonzalez, S., Hölfich, P. A., Landolt, A. U., Phillips, M. M., & Pizarro, S. 2003, AJ, 125, 166

Malmquist, K. G. 1920, Jour Medd. Lund Astron. Obs. Ser. II, 22, 1

Malmquist, K. G. 1922, Jour. Medd. Lund Astron. Obs. Ser. I, 100, 1

Masters, K. L., Crook, A., Hong, T., Jarrett, T. H., Koribalski, B. S., Macri, L., Springob, C. M., & Staveley-Smith, L. 2014, MNRAS, 443, 1044

Masters, K. L., Springob, C. M., Haynes, M. P., & Giovanelli, R. 2006, AJ, 653, 861

Masters, K. L., Springob, C. M., & Hucra, J. P. 2008, Erratum 2014, AJ, 135, 1738

Meyer, M. J., Zwaan, M. A., Webster, R. L., Staveley-Smith, L., Ryan-Weber, E., Drinkwater, M. J., Barnes, D. G., Howlett, M., Kilborn, V. A., Stevens, J., Waugh, M., Pierce, M. J., Bhatal, R., de Blok, W. J. G., Disney, M. J., Ekers, R. D., Freeman, K. C., Garcia, D. A., Gibson, B. K., Harnett, J., Henning, P. A., Jerjen, H., Kesteven, M. J., Knezek, P. M., Koribalski, B. S., Mader, S., Marquarding, M., Minchin, R. F., O'Brien, J., Oosterloo, T., Price, R. M., Putman, M. E., Ryder, S. D., Sadler, E. M., Stewart, I. M., Stootman, F., & Wright, A. E. 2004, MNRAS, 350, 1195

Mould, J. R., Huchra, J. P., Freedman, W. L., Kennicutt, R. C. Jr., Ferrarese, L., Ford, H. C., Gibson, B. K., Graham, J. A., Hughes, S. M. G., Illingworth, G. D., Kelson, D. D., Macri, L. M., Madore, B. F., Sakai, S., Sebo, K. M., Silbermann, N. A., & Stetson, P. B. 2000, ApJ, 545, 547

NED – NASA/IPAC Extragalactic Database – http://ned.ipac.caltech.edu/

Neill, J. D., Seibert, M., Tully, R. B., Courtois, H. M., Sorce, J. G., Jarrett, T. H., Scowcroft, V., & Masci, F. J. 2014, ApJ, 792,129

Perlmutter, S., Aldering, G., Goldhaber, G., Knop, R. A., Nugent, P., Castro, P. G., Deustua, S., Fabbro, S., Goobar, A., Groom, D. E., Hook, I. M., Kim, A. G., Kim, M, Y., Lee, J. C., Nunes, N. J., Pain, R., Pennypacker, C. R., Quimby, T., Lidman, C., Ellis, R. S., Irwin, M., McMahon, R. G., Ruis-Lapuente, P., Walton, N., Schaefer, B., Boyle, B. J., Filippenko, A. V., Matheson, T., Fruchter,A. S., Panagia, N., Newberg, H. J. M., & Couch, W. J. 1999, ApJ, 517, 565

Phillips, M. M., Lira, P., Suntzeff, N. B., Schommer, R. A., Hamuy, M., & Maza, J. 1999, AJ, 118, 1766

Pierce, M. 1994, ApJ, 430, 53

Pike, R. W., & Hudson, M. J. 2005, ApJ, 635, 11

Planck Collaboration; Abergel, A., Ade, P. A. R., Aghanim, N., Alina, D., Alves, M. I. R., Aniano, G., Armitage-Caplan, C., Arnaud, M.; Ashdown, M., & 238 co-authors 2013, arXiv:1303.5076 [astro-ph.60]

Radburn-Smith, D. J., Lucey, J. R., & Hudson, M. J. 2004, MNRAS, 355, 1378

Riess, A. G., Filippenko, A. V., Challis, P., Clocchiatti, A., Diercks, A., Garnavich, P. M., Gilliland, R, L., Hogan, C. J., Jha, S., Kirshner, R. P., Leibundgut, B., Phillips, M. M., Riess, D., Schmidt, B. P., Schommer, R. A., Smith, R. C., Spyromilio, J., Stubbs, C., Suntzeff, N. B., & Tonry, J 1998, AJ, 116, 1009

Riess, A. G., Li, W., Stetson, P. B., Filippenko, A. V., Jha, S., Kirshner, R. P., Challis, P. M., Garnavich, P. M., & Chornock, R. 2005, ApJ, 627, 579

Riess, A. 2009, APS, APR.J6001R

Riess, A. G., Macri, L., Casertano, S., Lampleitl, H., Ferguson, H. G., Filippenko, A. V., Jha, S. W., Li, W., & Chornock, R. 2011, ApJ, 730, 119

Riess, A. G., Nugent, P., Filippenko, A. V., Kirshner, R. P., & Perlmutter, S. 1998, ApJ, 504, 935

Roth, J., Mould, J., & Staveley-Smith, L. 1994 AJ, 108, 851

Rowan-Robinson, M. 1985, The Cosmological distance ladder: distance and time in the Universe (Chicago: Imported Publications)

Saha, A., Sandage, A., Tammann, G. A., Dolphin, A. E., Christensen, J., Panagia, N., & Macchetto, F. D. 2001, ApJ, 562, 314

Sakai, S., Mould, J. R., Hughes, S. M. G., Huchra, J. P., Macri, L. M., Kennicutt, R. C., Jr., Gibson, B, K., Ferrarese, L., Freedman, W. L., Han, M., Ford, H. C., Graham J. A., Illingworth, G. D., Kelson, D. D., Madore, B. F., Sebo, K., Silbermann, N. A., & Stetson, P. B. 2000, ApJ, 529. 698

Sandage, A., & Tammann, G. A. 1974a, ApJ, 190, 525 (ST I)

Sandage, A., & Tammann, G. A. 1974b, ApJ, 191, 603 (ST II)

Shanks, T. 1997, MNRAS, 290, 77

Sorce, J. G., Tully, R. B., & Courtois, H. M. 2012 ApJ, 758, 12

Springob, C. M., Masters, K. L., Haynes, M. P., Giovanelli, R., & Marinoni, C. 2007, AJSS, 172, 599

Staveley-Smith, L., & Davies, R. D. 1989, MNRAS, 241, 787

Strauss, M., & Willick, J. A. 1995, PhR, 261, 271

Tammann, G. A. 1978, Mem. Soc. Astr. Italy, 49, 315

Teerikorpi, P. 1995, ApL&C, 31, 263

Teerikorpi, P. 1997, ARA&A, 35, 101

Teerikorpi, P. 2015, A&A, 576, 75

Turnbull, S. J., Hudson, M. J., Feldman, H. A., Hicken, M., Kirshner, R. P., & Watkins, R. 2012, MNRAS, 420, 447

Tully, R. B. 1998, MmSAI, 69, 237

Tully, R. B. 2007, private communication (Honolulu: University of Hawaii)

Tully, R. B., & Fisher, J. R. 1977, A&A, 54, 661

Tully, R. B., & Fouqué, P. 1985, ApJS, 58, 67

Tully, R. B., & Pierce, M. J. 2000, ApJ, 533, 744 (Paper III)

Tully, R. B., Pierce, M. J., Huang, J. S., Suanders, W., Verheijen, M. A. W., & Witchalls, P. L. 1998, AJ, 115, 2264

Tully, R. B., Shaya, E. J., Karachentsev, I. D., Courtis, H. M., Kocekski, D. D., Rizzi. L., & Peel, A. 2008, ApJ, 676, 184

Willick, J. A. 1994, ApJSS, 92, 1

Xia, D.-M., & Wang, S. 2016, MNRAS, 463, 952

CHAPTER 2
TULLY-FISHER AND SNe Ia TEMPLATES

2.1 Tully-Fisher Relation

One of the main aspects of the TF relation is the determination of the neutral hydrogen (HI) line width of galaxies. The neutral hydrogen atom consists of a single nuclear proton and a single electron, each with a spin. The spin-parallel state is of higher energy than the spin's anti-parallel state. The energy difference of $6 \cdot 10^{-6} eV$ corresponds to a vacuum wavelength of $\lambda_0 = 21.1$ cm that is equivalent to a frequency $\nu_0 = 1420.406$ MHz. The hyperfine emission line is easily observed by radio telescopes owing to the total number of atoms of neutral hydrogen in the interstellar medium being very large. HI surveys provide a unique means to identify gas-rich galaxies since the HI is not affected by the dust in the Milky Way galaxy allowing observations of HI of distant galaxies.

The underlying physics to determine HI emission strength are based on the Einstein *A* coefficient. The coefficient describes the interaction of radiation with matter by the emission and absorption of radiation between two levels. The 21 cm line transition is a magnetic dipole corresponding to the Einstein *A* coefficient:

$$A_{mn} = \frac{64\pi^4}{3hc^3} \nu_{mn}^3 \left| \mu_{mn}^* \right|^2 \tag{2.1}$$

where μ_{mn}^* is the mean magnetic dipole moment of the oscillator. The value for the Einstein A coefficient is $A_{10} = 2.86888(7) \times 10^{-15} s^{-1}$, resulting in a rest frequency of $\nu_{10} = 1.402405751786(30) \times 10^9 Hz$.

The collision rate of interstellar hydrogen atoms in the interstellar medium results in a potential change of electron spin every ~400 years, which is sufficient to keep the level population in a Bolzmann distribution. This defines the excitation temperature, referred to as the spin temperature (T_s), expressed as:

$$\frac{N_1}{N_0} = \frac{g_1}{g_0} \exp\left(-\frac{h\nu_{10}}{kT_s} \right) \tag{2.2}$$

where

$$T_0 = \frac{h\nu_{10}}{k} = 0.682 \tag{2.3}$$

and

$$\frac{N_1}{N_0} = \frac{g_1}{g_0} = 3 \tag{2.4}$$

for $T_s >> T_0$ (Rohlfs & Wilson, 2006): N_1 = excited state, N_0 = ground state.

Many improvements to the TF relation have been suggested since the original paper of Tully & Fisher (1977). Aaronson et al. (1982) and later authors (e.g., Jacoby et al. 1992) concluded that *H*-band is a more accurate indicator over a greater range of morphological types of galaxies. Near infrared (NIR) light dominates the output of late-type galaxies and is less prone to internal and Galactic extinction. There are also improvements in inclination estimates due to the smoother nature of the galaxy disk compared to the long-used Holmberg (1958) optical approach using blue light. On the negative side, the sky background is higher in the infrared, making ground-based observations more difficult.

Tully (1998) later used even longer wavelength bands for his studies of 89 galaxies in three different clusters. The longest band considered, the K'-band (2.11 μm), has a shorter central wavelength than the *K*-band (2.20 μm) and was introduced by Wainscoat et al. (1992) to lessen the effects of atmospheric absorption and temperature-dependent thermal emission. The TF study has now been successfully extended to ~3.5 μm from Spitzer space telescope and 3.4 μm and 4.6 μm WISE (Wide-Field Infrared Survey Explorer).

Tully and Pierce (2000, Paper III) later showed that the intrinsic scatter is most significant for bands *B* and *K* and it is 20% better for the *R* and *I* bands. The *B*-band is sensitive to variations in recent star formation and variations in extinction and, as mentioned above, the rapidly increasing sky background toward longer wavelengths may contribute to increasingly large observational errors in the K'-band. Moreover, the slope of the TF relation steepens towards IR wavelengths, thus amplifying the effect of velocity width errors.

In their study, Tully and Pierce compared distances to the Ursa Major, Pisces and Coma clusters, showing that the SNe Ia observations provide distance measurements accurate of 5% to 10% and the TF relation provides accuracies of 15% to 20% out to distances $d > 100$ Mpc. They used Cepheid variables with zero point calibrators to resolve to a greater accuracy.

Galactic extinction is an important factor in distance accuracy. We adopt the results of the Schlegel et al. (1998) who used IRAS dust maps at 100 μm. Schlegel et al. (1998) used the dust maps for the reddening estimation and the Cosmic Microwave Background foregrounds. Schlafly & Finkbeiner (2011) used the SDSS (Sloan Digital Sky Survey) to derive reddening measurements. The total Galactic extinction for our study is calculated by using the following equation:

$$A_b^{\lambda} = R_{\lambda} E(B-V) \tag{2.5}$$

We adopt the Tully and Pierce (2000, Paper III) equation with the Schlegel et al. (1998) estimates: $R_{\lambda} = 4.32$ for $\lambda = B$ and 0.37 for $\lambda = K'$. For our study, $R_{\lambda} = 0.576$ for $\lambda = H^c$ from Schlegel et al. (1998) is used.

K-correction *(k)* is applied to the measured flux of an object with non-zero redshift and accounts for the change in response of the detector as the spectral energy distribution of the galaxy is shifted due to cosmological expansion. The size of the correction depends on the redshift and the nature of the spectrum. The *B*-band correction (Tully and Pierce 2000, Paper III) for *(k)* is $A_k^B = (3.6 - 0.36T)z$; Hubble stage *T* is the galaxy morphological type: 1, 3, 5, 7 = Sa, Sb, Sc, Sd. Tully and Pierce (2000, paper III) determined that the redshift effects *(k)* for the K'-band are negligible.

The following Tully and Pierce (2000, Paper III) axial ratio equation is used in our study to correct for inclination and galactic bulge:

$$\cos i = [(q^2 - q_0^2)/(1 - q_0^2)]^{1/2} \tag{2.6}$$

The ratio $q = b/a$ is the observed ratio of the minor to major axis and q_0 is the intrinsic axial ratio. This correction uses an assumption concerning the intrinsic thickness of the galaxy system. Early type galaxies have greater bulge components than later type disks. A flattening value $q_0 = 0.20$ was used by Tully and Pierce (2000, Paper III). As a galaxy orientation increases to face-on, the $1/\sin i$ deprojection correction becomes too uncertain. To avoid the errors of deprojection, the cut-off $i = 45°$ was used by them.

The RC3 axis ratios are based on the B_T-band data in the literature and were used for the B_T-band inclination data in the sample sets. We used the 2MASS (Two Micron All Sky Survey) co-added *JHK*-band axis ratio data to determine the inclination data for the near-infrared bands of *H* and K_s (K_s -band 2.15 μm).

Tully and Pierce (2000, Paper III) also used the correction for internal extinction and were used in our study: $A_i^\lambda = \gamma_\lambda \log(a/b)$ where a/b is the major to minor axis ratio and γ_λ is as follows:

$$\gamma_B = 1.57 + 2.75(\log W_R^i - 2.5)$$
$$\gamma_{K'} = 0.22 + 0.40(\log W_R^i - 2.5) \quad (2.7)$$

where W_R is defined below. Tully and Pierce (2000, paper III) did not include a formula for the *H*-band inclination-dependent internal extinction but Sakai et al. (2000) assumed $A_H = 0.5 A_I$.

The HI does not follow an exact circular orbit in the galactic disk. There is a degree of random motion superimposed. These random motions may broaden the line profile slightly. Tully and Fouqué (1985) corrected for random motion assuming a linear summation with rotation velocity above a transition width of $W_c = 120$ km s^{-1}. They assume the random motion is $W_t = 38$ km s^{-1}. The following formula for the rotation velocity W_R is adopted in our study (Tully and Fouqué 1985):

$$W_R^2 = W_{20}^2 + W_t^2 - 2W_{20}W_t\left[1 - \exp-(W_{20}/W_c)^2\right] - 2W_t^2 \exp-(W_{20}/W_c)^2 \quad (2.8)$$

There exists the possibility of random and systematic errors in the actual galaxy width and inclination angle. Lewis (1983) and Schneider et al. (1986) originally discussed errors in the TF line width algorithm. Roth et al (1994) perturbed the spectra of two intrinsically high S/N ratios using line widths obtained using outer threshold and Gaussian fit methods. Roth et al. (1994) determined that line widths are poorly reproduced for galaxy observations with S/N ≤ 5. Gaussian-fit widths are biased too low as S/N ratio decreases. Observations of galaxy with steep profiles are the most immune at the standard line width 20% and 50% levels.

The apparent magnitudes were subsequently corrected using the following: the H^c -band magnitudes were corrected for Galactic extinction and *k*-correction using the equation (2.5) and inclination extinction correction described, resulting in H^c. The *B*-band magnitudes were corrected for extinction using the equations defined previously to determine $B^{b,i,k} = B - A_B^b - A_B^{i-0} - A_B^k$. The Galactic extinction correction is A_B^b, A_B^{i-0} is the inclination correction to face-on and A_B^k is the *k*-correction. The K_s -band magnitudes were corrected for extinction using $K_s^{b,i} = K_s - A_K^b - A_K^{i-0}$.

The following are used for our study where Masters et al. (2008, Erratum 2014) corrected for inclination and absolute magnitudes for the TF relation using:

$$W_{corr} = \left(\frac{W_{F50} - \Delta_s}{1+z} - \Delta_t \right) \frac{1}{\sin i} \tag{2.9}$$

and

$$M_{corr} - 5\log h = m_X - A_X - I_X + k_X + T_X - 5\log v_{CMB} - 15 \tag{2.10}$$

where Δ_s corrects for instrumental resolution, Δ_t corrects for turbulent motions, $I_X = \gamma \log(a/b)$ is the internal obscuration correction, $k_H = -0.40z$ and $k_K = -1.52z$ are the *k*-corrections for the H^c and K_s bands respectively, and x = H or K. The morphological corrections for H^c-band are:

$$T_{Sa} = 0.24 - 3.60(\log W - 2.5) : T \le 2$$

$$T_{Sb} = 0.01 - 1.72(\log W - 2.5) : 3 \le T \le 4 \tag{2.11}$$

The morphological corrections for K_s -band are:

$$T_{Sa} = 0.27 - 3.73(\log W - 2.5) : T \le 2$$

$$T_{Sb} = 0.02 - 1.74\log W - 2.5) : 3 \le T \le 4 \tag{2.12}$$

Tully et al. (2008) refined the absolute magnitude equations for colour bands *B*, *R*, *I*, and *H* of Tully and Pierce (2000, Paper III) to be consistent with the zero point of the Hubble Space Telescope (HST) Cepheid Key Project (Freedman et al. 2001). The following are the absolute magnitude calibrations used for our study as defined by Tully et al. (2008) for the *B* and Masters et al. (2008, Erratum 2014) for *H*-band and *K* -band. Tully et al. (2008) used the Hubble constant $H_0 = 74$ km s^{-1} Mpc^{-1} to formulate the B_T expression, and Masters et al. (2008; Erratum 2014) used $H_0 = 72$ km s^{-1} Mpc^{-1}:

$$M_B - 5\log h = -19.99 - 7.27(\log W_R^i - 2.5)$$

$$M_H - 5\log h = -21.951 \pm 0.017 - (10.65 \pm 0.11)(\log W_R^i - 2.5)$$

$$M_K - 5\log h = -22.188 \pm 0.015 - (10.74 \pm 0.10)(\log W_R^i - 2.5) \tag{2.13}$$

Velocities are corrected to the centre of mass (barycentre) of the solar system. The correction accounts for the Earth's rotation of ~ 0.3 km s^{-1} and its orbit around the Sun of ~ 29.7 km s^{-1}. The Galactic Standard of Rest (GSR) and the 3K CMB frame are also calculated for our study using NASA / IPAC Extragalactic Database (NED) with the following equation:

$$V_{con} = V + V_{apex}[\sin(b)\sin(b_{apex}) + \cos(b)\cos(b_{apex})\cos(I - I_{apex})] \tag{2.14}$$

Corrections to the GSR use: $I_{apex} = 87.8°$, $b_{apex} = +1.7°$, and $V_{apex} = 232.3$ km s^{-1}. Corrections to the 3K CMB rest frame use: $I_{apex} = 264.14°$, $b_{apex} = +48.26°$, and $V_{apex} = 371.0$ km s^{-1} (Schmitz 2010 priv. comm.).

During the new 21 cm observations for the Parkes and Parkes / NTT samples, attempts were made to gather the W_{20}, W_{50}, and V_{50} data for as many galaxies as possible. Moreover, there were several galaxies where not all of the desired data could be collected or insufficient S/N ratio resulted. This is discussed in the following chapters.

2.2 SNe Ia Distance Scale

Phillips (1993) determined that although SN Ia on their own appeared to have reasonably constant luminosities, there was a high correlation between their peak luminosities and initial decline rates of the SNe. The slope of the correlation is steepest in *B* and progressively flattens in the *V* and *I* bands. SN Ia therefore became a much more powerful distance indicator.

In another influential study, Hamuy et al. (1995, 1996a) used a multi-dimensional fit to template light curves. Jha (2002) analysed 44 objects to establish a robust fit of *BVI* light curves for SNe Ia with the intent to determine the maximum light magnitudes and the parameter $\Delta m_{15}(B)$ for galaxies of all types ($\Delta m_{15}(B)$ is the 15-day decline rate of the observed magnitude). Jha (2002) used a parabolic fit to the *BVI* light curves to each set of templates and expanded the parameterisation to include the *UBV* templates developed by the Supernova Cosmology Project (Kim 1998). The findings showed the average template does not produce a consistent representation of the supernova light curve shape or luminosity. The typical SN Ia decline rate in *B*-band is ~ 1.10 mag over the first 15 days after maximum light. The *U*-band declines ~ 1.2 mag 15 days after *U*-band peak luminosity. The *V*-band declines ~ 0.5 mag 15 days after *B*-band max luminosity. The *U*-band peak luminosity occurs ~ 2.8 days prior to the maximum light in *B*-band.

Jha (2002) calculated the *k*-correction for the MLCS2k2 paper by adjusting the maximum light spectra to the redshift of the SN Ia using the CCM89 extinction law $R_V = 3.1$ (Cardelli et al. 1989). The intrinsic colours of the SN Ia can be determined at any epoch using the MLCS2k2 relations. Jha (2002) determined an estimate of the SN

Ia peak magnitude resulting in $M_V^0 = -19.31 \pm 0.10\,(\text{random}) \pm 0.20\,(\text{systematic})$ after correcting for the host galaxy extinction. The HST Key Project team (Gibson et al. 2000) determined an absolute peak magnitude of $M_V^0 = -19.00 \pm 0.07\,(\text{random}) \pm 0.20\,(\text{systematic})$. Hsiao et al. (2006) concluded the *k*-corrections for SNe Ia spectral features have a statistical error caused by the diverse spectral features to be 0.04 mag for a single observation.

In an updated study, Phillips et al. (1999), assuming a $H_0 = 65$ km s^{-1} Mpc^{-1}, determined the host galaxy reddening with the observed colour excess defined as:

$$(B_{\max} - V_{\max})_{corr} = (B_{\max} - V_{\max})_{obs} - E(B-V)_{Gal} - K_{B_{\max}-V_{\max}} \tag{2.15}$$

and $(B_{\max} - V_{\max})_{corr}$ was then adjusted for an unreddened SN Ia using:

$$E(B-V)_{host} = (B_{\max} - V_{\max})_{corr} - (B_{\max} - V_{\max})_0 \tag{2.16}$$

They determined that when the host galaxy reddening $E(B-V) < 0.8$, the variation of $K_{B_{\max}-V_{\max}}$ was less than the precision of the indicators and therefore the extinction is zero with no iteration. The observed colour excesses were then converted to true colour excesses for our study using:

$$E(B-V)_{true} = 0.981/[1/E(B-V)_{obs} - 0.050] \tag{2.17}$$

We adopted their use of the following equation to correct the observed maximum-light magnitudes for the reddening extinction:

$$A_B = [4.16 - 0.06E(B-V)_{true}]E(B-V)_{true} \tag{2.18}$$

Phillips et al. (1999) also used the Hamuy et al. (1993) *k*-correction *(k)*. In the *B*-band at $z = 0.005$ the correction is -0.005 and at $z = 0.02$ the correction is -0.013. The following data in Table 2.1 are interpolated from the Hamuy et al. (1993) determinations for *(k)*.

Table 2.1: *k* at Maximum Light

z	K_B	z	K_B
0.00500	0.005	0.01250	0.010
0.00625	0.006	0.01500	0.011
0.00750	0.007	0.01750	0.012
0.00875	0.008	0.02000	0.013
0.01000	0.009	0.02000	0.013

Phillips et al. (1999) convincingly showed that the $\Delta m_{15}(B)$ versus $M_{\max}$ relation decreases dispersion in the Hubble diagram. The host galaxy reddening corrections further decreases dispersion even though the Hubble constant is essentially

the same regardless of the correction. The extinction correction expression $R = A_B / E(B-V) = 4.1$ may amplify the photometric errors and any deviations due to intrinsic colour variations at maximum light or the photometric errors. The intrinsic colour at maximum light for SNe Ia occurring in late-type galaxies is $(B-V)_{\max} = 0.05$.

Riess et al. (2005) used four SNe Ia with highly calibrated Cepheid variables as a distance reference to establish a zero point for their SNe Ia distance calibration. Since Cepheid variables are considered one of the most accurate local distance secondary indicators, Riess et al. (2005) determined in accordance with the Cepheid analyses that a constant decrease of all SNe Ia distances by $M_V^0(t_0) - 19.44 = 0.27$ would bring the SNe Ia distance modulus in line with the known Cepheid zero point. This correction is adopted in this thesis.

There have been many studies, including by Jha (2002), Garnavich and Gallagher (2005), Hsiao et al. (2006), and Sullivan et al. (2006), that indicate how SNe Ia luminosity and $\Delta m_{15}(B)$ depend on galaxy type, active star formation and metallicity. The use of the methodologies and calibrations of Phillips (1993) and Phillips et al. (1999) assume that SNe Ia in spiral galaxies, although on average intrinsically brighter, follow the same behaviour as all others. Phillips et al. (2006) suggest this is a reasonable approach even if one identifies some SNe Ia that are not normal or canonical in their spectroscopic characteristics.

This chapter has provided a summary of the observables and literature-derived template relations required to derive TF and SN Ia distances. These relations are based on empirical determinations using Cepheid variables and galaxy clusters. The former provide a good absolute scale, whilst the latter provide a significant number of objects at constant distance. This calibration will be used in the following chapters for three different galaxy samples. Chapter 3 discusses a sample of galaxies from the literature; Chapter 4 discusses a new sample for which TF velocity widths were obtained from the Parkes 64 m radio telescope; and Chapter 5 discusses a new Parkes / NTT sample.

REFERENCES

Aaronson, M., Huchra, J., Mould, J. R., Tully, R. B., Fisher, J. R., van Woerden, H., Goss, W.M., Charmaraux, P., Mebold, U., Siegman, B., Berriman, G., & Persson, S. E. 1982, ApJS, 50, 241

Cardelli, J. A., Clayton, G. C., & Mathis, J. S. 1989, ApJ, 345, 245

Freedman, W. L., Madore, B. F., Gibson, B. K., Ferrarese, L., Kelson, D. D., Sakai, S., Mould, J. R., Kennicutt, Jr, R. C., Ford, H. C., Graham, J. A., Huchra, J. P., Hughes, S. M. G., Illingworth, G. D., Macri, L. M., & Stetson, P. B. 2001, ApJ, 553, 47

Garnavich, P. M., & Gallagher, J. 2005, ASPC, 342, 242

Gibson, B. K., Stetson, P. B., Freedman, W. L., Mould, J. R., Kennicutt, R. C., Jr., Huchra, J. P., Sakai, S., Graham, J. A., Fassett, C. I., Kelson, D. D., Ferrarese, L., Hughes, S. M. G., Illingworth, G. D., Macri, L. M., Madore, B. F., Sebo, K. M., & Silbermann, N. A. 2000, ApJ, 529, 723

Hamuy, M., Phillips, M. M., Maza, J., Suntzeft, N. B., Schommer, R. A., & Auilés, R. 1995, AJ, 109, 1

Hamuy, M., Phillips, M. M., Suntzeff, N. B., Schommer, R. A., Maza, J., & Avilés, R. 1996a, AJ, 112, 2391

Hamuy, M., Phillips, M. M., & Wells L. A. 1993, PASP, 105, 787

Holmberg, E. B. 1958, MELu2, 136, 1

Hsiao, E. Y., Pritchet, C. J., Howell, D. A., Conley, A., Sullivan, M., Carlberg, R. G., Nugent, P., & Phillips, M. M. 2006, AAS, 208, 1304

Jacoby, G. H., Branch, D., Ciardullo, R., Davies, R. L., Harris, W. E., Pierce, M. J., Pritchet, C. J., Tonry, J. L., & Welch, D. L. 1992, PASP, 104, 599

Jha, S. 2002, Exploding Stars, Near and Far, PhD Thesis (Cambridge: Harvard University)

Kim, A. G. 1998, arXiv:9805496 [astro-ph.60]

Lewis, B. M. 1983, AJ, 88, 962

Masters, K. L., Springob, C. M., & Hucra, J. P. 2008, Erratum 2014, AJ, 135, 1738

NED – NASA/IPAC Extragalactic Database – http://ned.ipac.caltech.edu/

Phillips, M. M. 1993, ApJ, 413L, 105

Phillips, M. M., Krisciunas, K., Suntzeff, N. B., Abraham, R. G., Beckett, M. G., Bonati, M., Candia, P., Corwin, T. M., Depoy, D. L., Espinoza, J., Firth, A. E., Freedman, W. L., Galaz, G., Germany, L., Gonzalez, D., Hamuy, M., Hastings, N. C., Hungerford, A. L., Ivanov, V. D., Labbé, E., Marzke, R. O., McCarthy, P. J., McMahon, R. G., McMillan, R., Muena, C., Persson, S. E., Roth, M., Ruiz, M. T., Smith, R. C., Smith, R., Strolger, L. G., & Stubbs C. 2006, AJ, 131, 2615

Phillips, M. M., Lira, P., Suntzeff, N. B., Schommer, R. A., Hamuy, M., & Maza, J. 1999, AJ, 118, 1766

Riess, A. G., Li, W., Stetson, P. B., Filippenko, A. V., Jha, S., Kirshner, R. P., Challis, P. M., Garnavich, P. M., & Chornock, R. 2005, ApJ, 627, 579

Rohlfs, K., & Wilson, T. L. 2006, Tools of Radio Astronomy (Berlin: Springer)

Roth, J., Mould, J., & Staveley-Smith, L. 1994 AJ, 108, 851

Sakai, S., Mould, J. R., Hughes, S. M. G., Huchra, J. P., Macri, L. M., Kennicutt, R. C., Jr., Gibson, B. K., Ferrarese, L., Freedman, W. L., Han, M., Ford, H. C., Graham, J. A., Illingworth, G. D., Kelson, D. D., Madore, B. F., Sebo, K., Silbermann, N. A., & Stetson, P. B., 2000, ApJ, 529, 698

Schlafly, E. F., & Finkbeiner, D. P. 2011, ApJ, 737, 103

Schlegel, D., Finkbeiner, D., & Davis, M. 1998, ApJ, 500, 525

Schneider, S. E., Helou, G., Salpeter, E. E., & Terzian, Y. 1986, AJ, 92, 742

Schmitz, M. 2010, private communication (NED)

Sullivan, M., Le Borgne, D., Pritchet, C. J., Hodsman, A., Neill, J. D., Howell, D. A., Carlberg, R. G., Astier, P., Aubourg, E., Balam, D., Basa, S., Conley, A., Fabbro, S., Fouchez, D., Guy, J., Hook, I., Pain, R., Palanque-Delabrouille, N., Perrett, K., Regnault, N., Rich, J., Taillet, R., Baumont, S., Bronder, J., Ellis, R. S., Filiol, M., Lusset, V., Perlmutter, S., Ripoche, P., & Tao, C. 2006, ApJS, 648, 868

Tully, R. B. 1998, MmSAI, 69, 237

Tully, R. B., & Fisher, J. R. 1977, A&A, 54, 661

Tully, R. B., & Fouqué, P. 1985, ApJS, 58, 67

Tully, R. B., & Pierce, M. J. 2000, ApJ, 533, 744 (Paper III)

Tully, R. B., Shaya, E. J., Karachentsev, I. D., Courtis, H. M., Kocekski, D. D., Rizzi. L., & Peel, A. 2008, ApJ, 676, 184

Wainscoat, R. J., & Lennox, L. C. 1992, AJ, 103, 332

CHAPTER 3
DATA FOR A LITERATURE-SAMPLE WITH WELL-OBSERVED SNe Ia

3.1 Sample Overview

The first sample of galaxies and supernovae in this thesis is derived from the literature. It consists of 130 spiral galaxy hosts of well-observed SNe Ia for the purpose of relating the distance scales obtained from the TF relation and the SN Ia standard candle relation. The well-observed SNe Ia provide complete light curve data as described in chapter 1. The sample is a compilation of objects in the field. Neither new 21 cm observations nor new photometric observations were made for this sample. Furthermore, the data is obtained from heterogeneous sources which limit the accuracy of the results compared with the later samples.

The input data for the sample of host galaxies and the associated SN Ia are compiled in Tables 3.1 through 3.3. The SNe Ia sample covers 67 years of observation from 1937C to 2004bd. Distance modulus calculations are consistently derived using the templates described in Chapter 2.

3.2 Detailed Data

Table 3.1 lists the galaxy, the associated SN Ia, and 21 cm line width measurements.

The 21cm data comes from several sources including the NRAO Green Bank 91 m and 43 m telescopes (Fisher and Tully 1981), the Bonn 100 m telescope and the Nancay telescope (Theureau et al. 1998). In the case of 20% velocity widths, W_{20} we use the data from the references noted at the end of the table. In the case of 50% velocity widths, W_{50} the homogenised HyperLeda database is preferred (Paturel et al. 2003).

A plot of the W_{50} values against W_{20} is shown in Figure 3.1. The mean difference is 55 km s^{-1} with an *rms* of 90 km s^{-1}. In Figure 3.2, the inclination-corrected values (see equation 2.6) have a smaller mean difference of 22 km s^{-1} and an *rms* scatter of 36 km s^{-1}. Many of the discrepant points in Figure 3.1 had axial ratios that were unsuitable for inclination-correction, so they do not contribute to the scatter in Figure 3.2.

The positions, galaxy types, redshifts and velocities in various reference frames in Table 3.1 are from the NASA Extragalactic Database (NED), which is again a compilation of various literature data sources. The recession velocities are the barycentric recession velocities corrected to the Galactic Standard of Rest, corrected for the Virgo infall, and corrected to the 3K CMB frame. Among the sample of 130 galaxies, 31 have a morphology defined as type S to Sdm, 32 are defined as type SA to SAdm, 34 are type SAB to SABd, and the remaining 33 galaxies are type SB to SBdm.

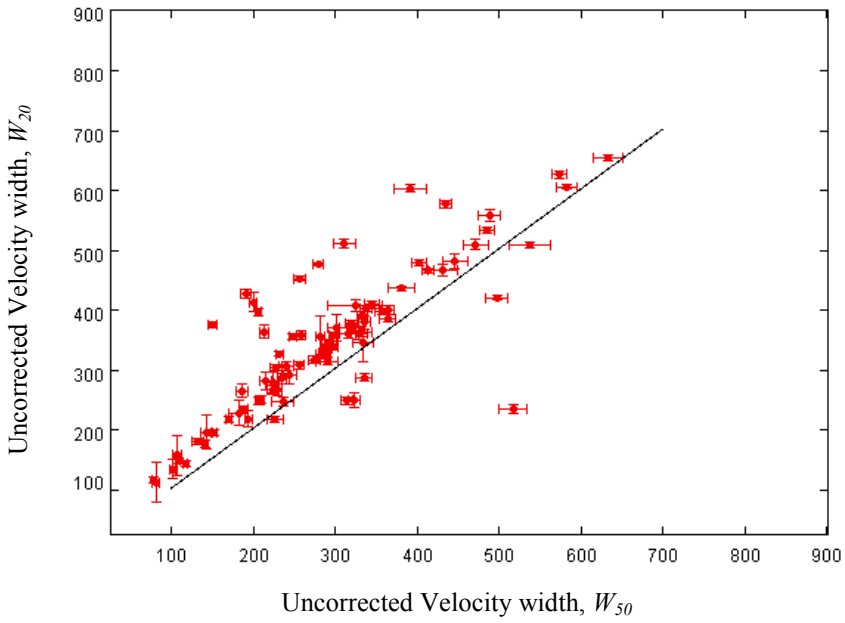

Figure 3.1: Literature sample velocity widths W_{50} plotted against W_{20}. No corrections for inclination are applied. The mean difference is 55 km s^{-1} with an *rms* scatter of 90 km s^{-1}.

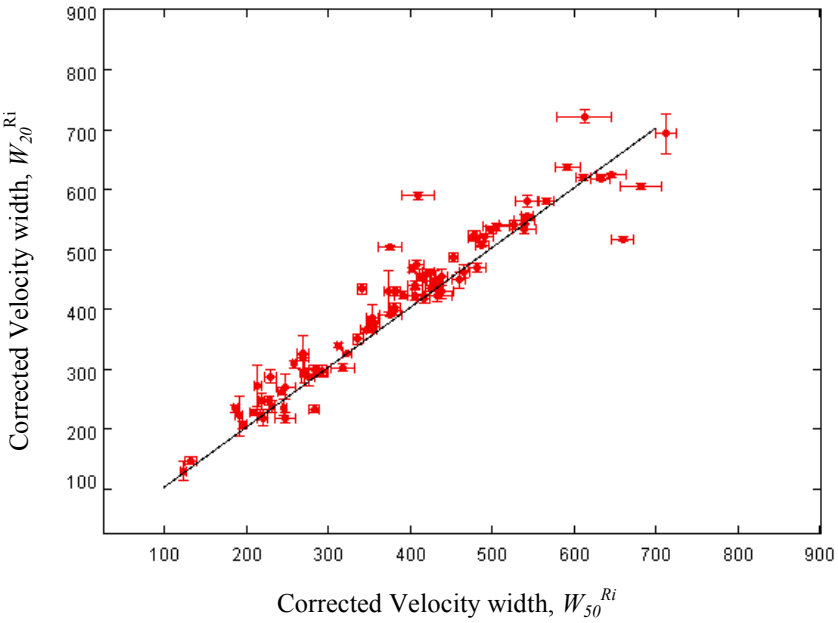

Figure 3.2: Literature sample using the RC3 data for the inclination-corrected velocity widths W_{50}^{Ri} plotted against W_{20}^{Ri}. The mean difference is 22 km s^{-1} with an *rms* scatter of 36 km s^{-1}.

3.2.1 Apparent Magnitudes

Table 3.2 contains the SNe Ia *B*-band apparent magnitude and $\Delta m_{15}(B)$ data from the multiple reference sources. The galaxy asymptotic total B_T -band apparent magnitudes are largely from RC3. These are generally photoelectric observations homogenised with standard templates and derived by extrapolation from data in multiple apertures and from surface photometry using a photoelectric zero point, B_T^S (de Vaucouleurs et al. 1991 RC3). The B_T -band apparent magnitude data in Table 3.1 were adjusted for Galactic extinction (Schlegel et al. 1998) and obscuration within the observed galaxy using the correction $B_T^{b,i} = B_T - A_B^b - A_B^{i-0}$ (de Vaucouleurs et al. 1991 RC3). The third Reference Catalogue of Bright Galaxies (RC3) is a reasonably homogenous listing of 23,010 large, bright galaxies imaged in the B_T-band (de Vaucouleurs et al. 1991 RC3).

The *H*-band and K_s (*K*-short) band NIR data are from 2MASS. The *H*-band filter has a central wavelength $1.65 \mu m$. The 2MASS NIR band window for K_s is $2.00 - 2.32 \mu m$ (Jarrett et al. 2000). The H^c and K_s bands in Table 3.2 are derived from elliptical aperture fitting to the isophotes. The two 1.3 m 2MASS telescopes instruments used for the NIR observations are located at Mt. Hopkins and CTIO, Chile. The Two Micron All Sky Survey (2MASS) covers 99.998% of the sky observed from

both the northern 2MASS facility at Mt. Hopkins, AZ and the southern 2MASS facility at Cerro Tololo, Chile, imaged in the *J, H,* K_s bands (2MASS). The number of galaxies in this chapter that have RC3 measurements is 72, whereas the number from 2MASS is 118.

Although the *K′*-band filter has been used previously (e.g., Tully 1998), data quality is improved using the K_s filter owing to less sensitivity to ambient temperature or variations of thermal emission at longer wavelengths, thus providing a better calibrated photometric survey (Carpenter 2001). The 2MASS catalogue provides both the total and isophotal magnitudes for the H^c and K_s band filters. The isophotal measurements are at the 20 mag per arcsec^2 isophote in K_s. This corresponds to ~1 sigma of the background *rms* using both circular and elliptically shaped apertures (Jarrett et al. 2000). The total aperture magnitude is obtained by integration of the surface brightness profile out to ~ 4 disk scale lengths.

There have been studies to determine whether the isophotal or the total photometric measurements are the most accurate representation. Karachentsev et al. (2002) used isophotal magnitudes in their 2MASS / TF relation study of flat edge-on galaxies. The uncertainty in the aperture correction for large galaxies diminishes S/N ratio. Isophotal magnitudes are also less affected by surface brightness fluctuations and stellar contamination than total magnitudes. In an examination of the K_s total and isophotal magnitudes, the K_s isophotal elliptical aperture photometry appears to provide the most precise measurement based on repeatability tests performed by Jarrett et al. (2000) on the 2MASS Extended Source Catalogue data. Masters et al 2008, Erratum 2014) and Said et al. (2015) used 2MASS Tully-Fisher Survey (2MTF) in the 2MASS Redshift Survey (2MRS) to measure TF distances to bright inclined spiral galaxies. They sought a universal calibration of the TF relation in the 2MASS *J, H, K* bands.

The optical and NIR images were manually measured to verify each galaxy's axial ratio in order to calculate the inclination using the equation (2.6). The *B*-band axis ratios are from the RC3 measurements of the major isophotal diameter, D_{25}, and the minor isophotal diameter, d_{25}, corresponding to the surface brightness level 25 mag arcsec^{-2}. The K_s-band axis ratio data are from the 2MASS K_s isophotal elliptical aperture photometry axis measurements at 20 mag arcsec^{-2}.

3.2.2 Distance Moduli

The 20% HI line width velocities W_{20} were firstly adjusted for cosmological redshift broadening using $W_R^c = W_R / 1+z$, followed by corrections for: (a) inclination using equation (2.6), and (b) random motions using equation (2.8). For W_{50}, the corresponding equation 2.9 was used (Masters et al. 2008, Erratum 2014). Although corrections for inclination and random motions are similar, it was prudent to follow the procedure appropriate to the template being used in order to compare derived Hubble constants in a meaningful manner. The corrected velocity width W_R^i therefore represents the 21 cm line width velocity corrected for broadening, inclination, and random motion. Template absolute magnitudes M_B, M_H, and M_K were calculated using equations (2.13) and corresponding distance moduli calculated using the extinction-corrected apparent magnitudes. Distances were also estimated using recession velocities. The heliocentric velocities were converted to the Galactic Standard of Rest (GSR) and 3K Cosmic Microwave Background radiation (CMB) using the equation (2.14).

The method for obtaining SN Ia distance moduli is summarised in §2.2. Extinction and host galaxy reddening were estimates using equations (2.15) to (2.17). The unreddened SNe Ia and absolute magnitudes were determined using the Phillips et al. (1999) correlation of the peak luminosity and $\Delta m_{15}(B)$. The SNe Ia *k*-corrections in *B*-band were made using the values listed in Table 2.1. The SNe Ia distance determinations were reduced using the Riess et al. (2005) 0.27 mag adjustment to the Cepheid zero point.

Table 3.3 lists the SN Ia and TF distance moduli calculated from the data in Tables 3.1 and 3.2. Figures 3.3 through 3.5 compare the TF distance moduli plots for the three colour bands B_T, H^c, and K_s for galaxies with an inclination $35° < i < 85°$. For the 47 galaxies plotted in Figures 3.3 and 3.4, the *rms* is around 0.55 and 0.61 mag respectively. However, the comparison of the 82 IR TF distance moduli in Figure 3.5 reveals a vastly smaller *rms* of 0.21 mag indicating more consistency between the closely spaced 2MASS bands than with the RC3 data. The 'median absolute deviation' (MAD), which is the median of the absolute value of the residuals is included in this chapter and will be included in the subsequent chapters for the distance modulus results. The H^c -band and K_s -band TF relation, where absolute magnitudes are used to estimate distance modulus, is shown in Figure 3.6 and 3.7 resulting in an *rms* of 0.99

mag and 1.06 mag respectively, around the template regression line. Figures 3.8, 3.9, 3.10 and 3.11 show the comparison of the redshift-distance with the Tully-Fisher and SNe Ia distance modulus, respectively. The respective *rms* scatter of 0.91, 1.11, 1.27 and 0.98 mag for B_T, H and K TF relations and the SNe Ia measurement, respectively, suggests similar distance accuracy for all of our indicators. The scatter and offset may be partly due to the inhomogeneity of data in the literature from multiple sources despite our efforts to standardise the data. Where the SNe Ia decline rate data was not complete, a template was used.

The SNe Ia distance modulus is plotted against the TF B_T-band distance modulus in Figure 3.12, and against the H^c and K_s TF distance modulus in Figure 3.13 and 3.14. The *rms* scatter in these three plots is 1.34, 1.50 mag and 1.42 mag, respectively.

3.3 Summary

This chapter provides new distance moduli for a sample of SN Ia and their host galaxies obtained purely from the literature, using the analysis techniques outlined in Chapter 2. The raw data were obtained from multiple authors and instruments; nevertheless, the data were reduced in a systematic manner. Dispersion about the distance relations appears to be substantial, indicating that observational errors are large. Nevertheless, the data presented in the chapter serves as a reference point for the next two samples of increased accuracy. A detailed comparative analyses is contained in chapter 6.

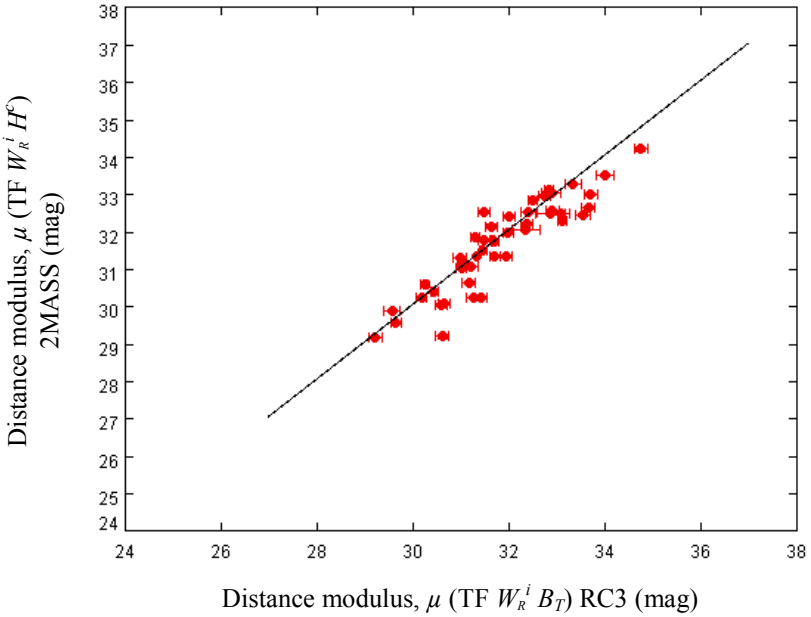

Figure 3.3: Comparison of RC3 B_T.-band based TF distance moduli and 2MASS H^c -band based distance moduli for 47 galaxies. The reference line is through the origin with a slope = 1.000. The mean difference is 0.20 mag, with an *rms* scatter of 0.55 mag and the Median Absolute Deviation (MAD) is 0.27 mag.

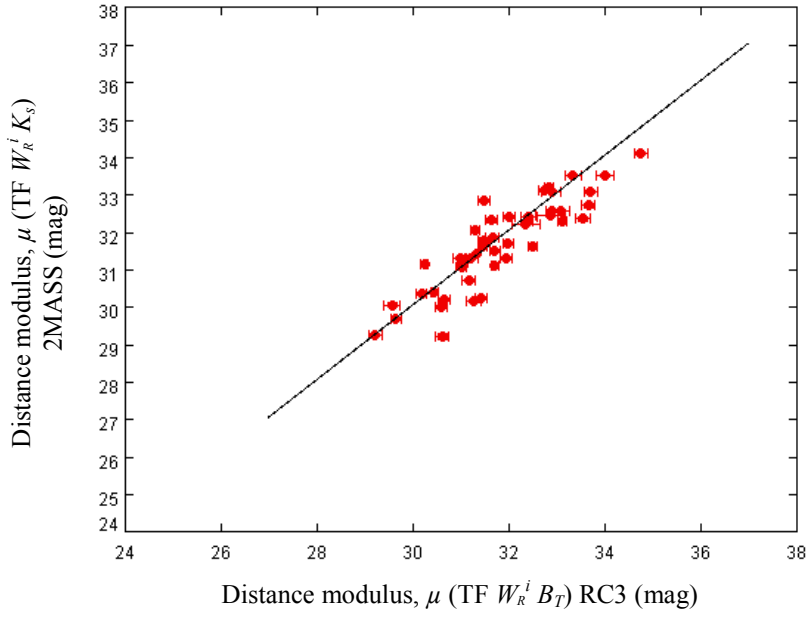

Figure 3.4: Comparison of RC3 B_T -band based TF distance moduli and 2MASS K_s -band based distance moduli for 47 galaxies. The reference line is through the origin with a slope = 1.000. The mean difference is 0.17 mag, with an *rms* scatter of 0.61 mag and the MAD is 0.25 mag.

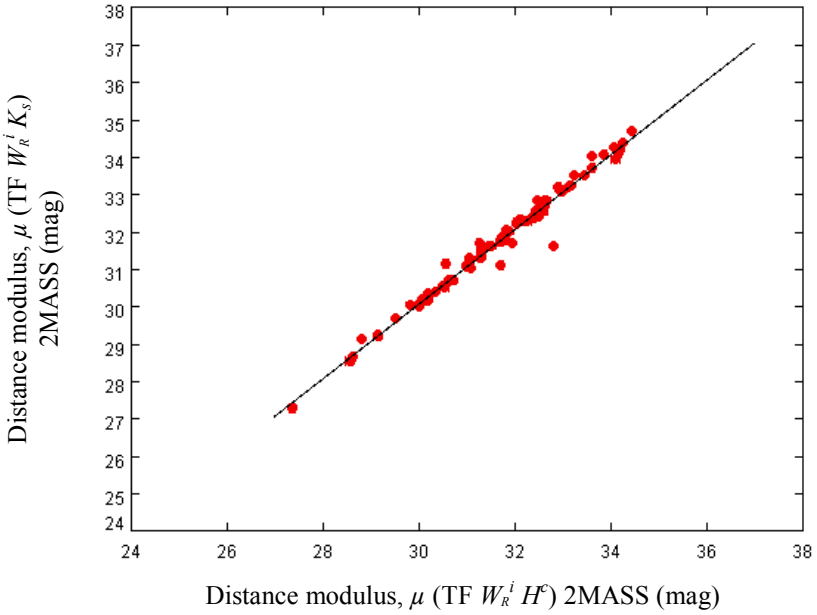

Figure 3.5: Comparison of 2MASS H^c -band based and 2MASS K_s -band based TF distance moduli for 82 galaxies. The reference line is through the origin with a slope = 1.000. The mean difference is -0.05 mag, with an *rms* scatter of 0.21 mag and the MAD is 0.03 mag.

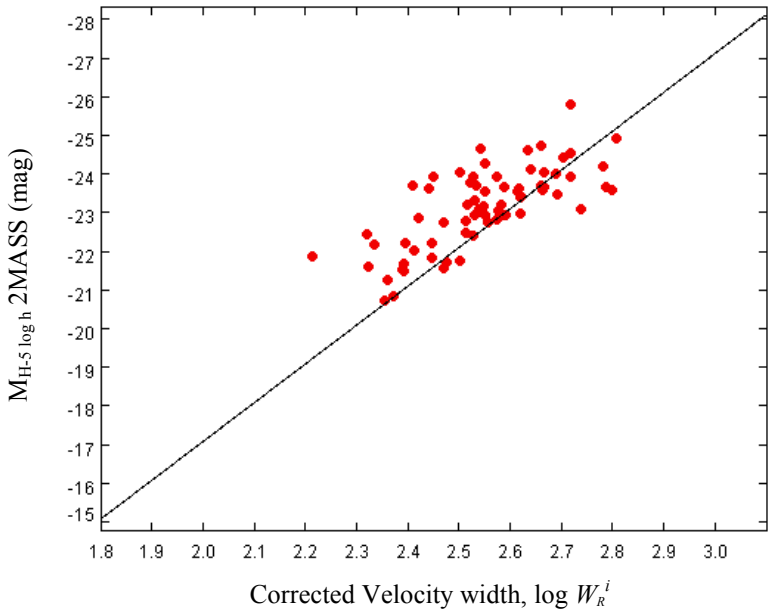

Figure 3.6: The 2MASS H^c -band based TF relation for 67 galaxies, where the absolute magnitude is estimated from redshift. The offset of 0.28 mag and the *rms* scatter of 0.99 mag.

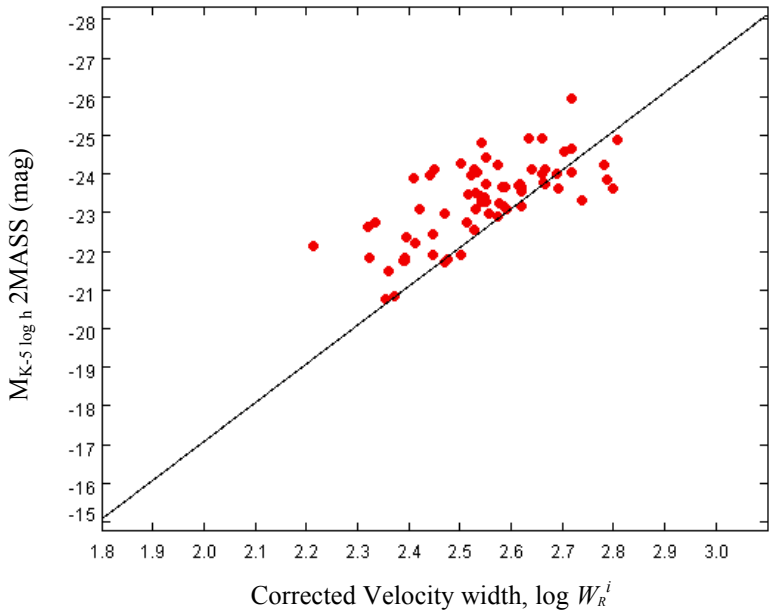

Figure 3.7: The 2MASS K_s -band based TF relation for 55 galaxies, where the absolute magnitude is estimated from redshift. The offset of 0.21 mag and the *rms* scatter of 1.06 mag.

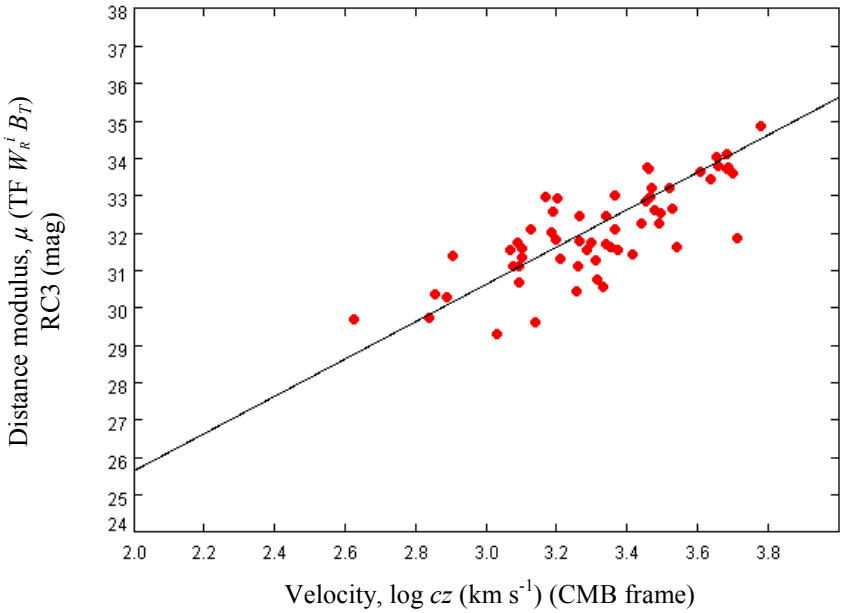

Figure 3.8: A comparison of redshift distance, log cz (CMB frame) with the RC3 B_T -band based TF distance modulus for 65 galaxies. The offset is -0.40 mag, with an *rms* scatter of 0.91 mag.

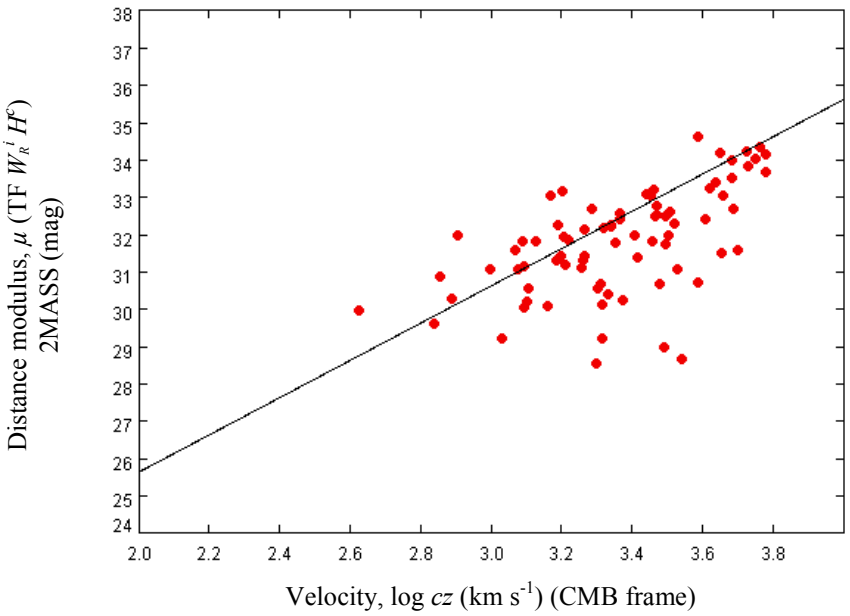

Figure 3.9: A comparison of redshift distance, log *cz* (CMB frame) with the 2MASS H^c -band based TF distance modulus for 58 galaxies. The offset is -0.49 mag, with an *rms* scatter of 1.11 mag.

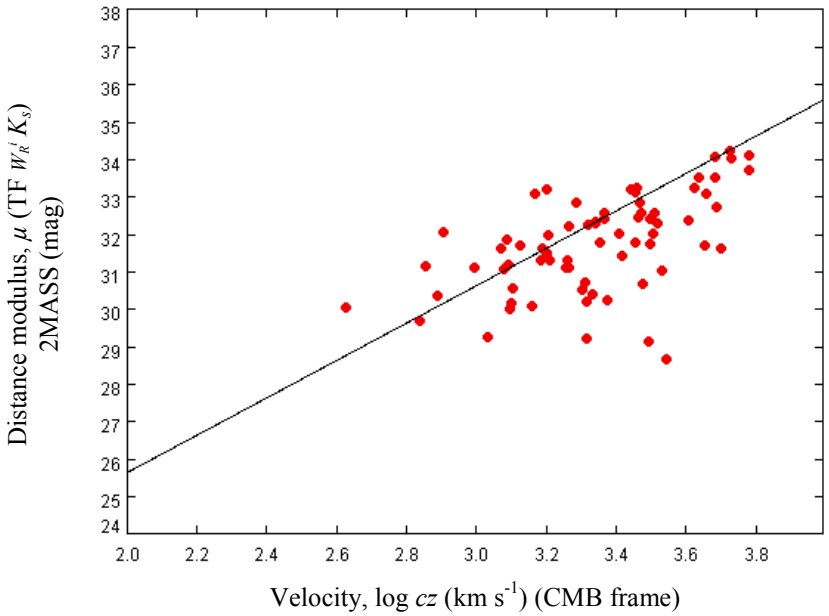

Figure 3.10: A comparison of redshift distance, log *cz* (CMB frame) with the 2MASS K_s -band based TF distance modulus for 58 galaxies. The offset is -0.37 mag, with an *rms* scatter of 1.27 mag.

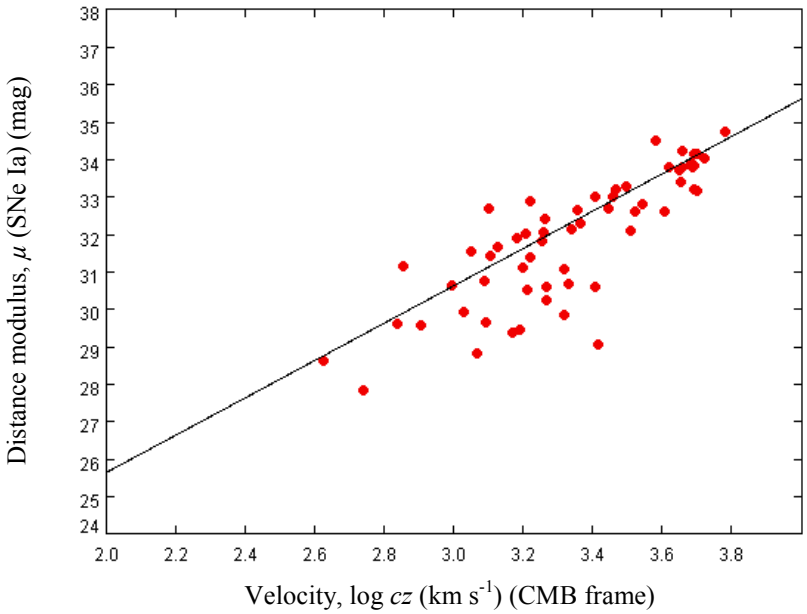

Figure 3.11: A comparison of redshift distance, log *cz* (CMB frame) with the SNe Ia distance modulus for 58 galaxies. The offset is -0.54 mag, with an *rms* scatter of 0.98 mag.

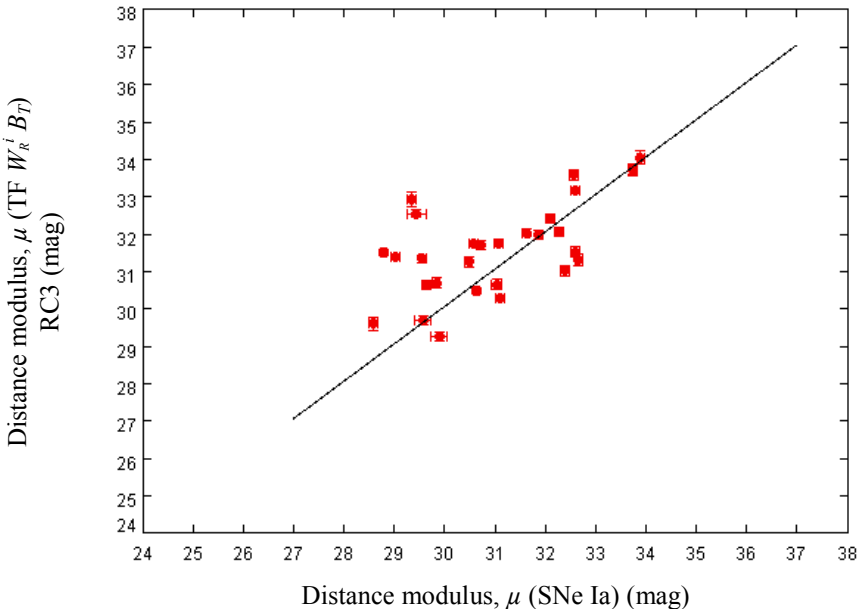

Figure 3.12: A direct comparison of SN Ia distance modulus versus the RC3 B_T-band based TF distance modulus for 29 galaxies. The reference line is through the origin with a slope = 1.000. The distance moduli have a mean offset of 0.54 mag, with an *rms* scatter of 1.34 mag and the MAD is 0.42 mag.

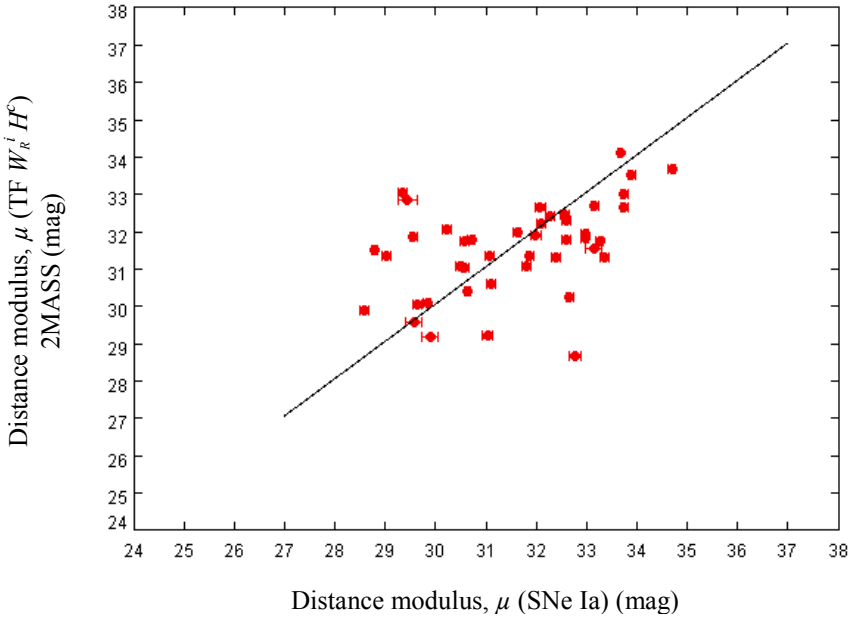

Figure 3.13: A direct comparison of SN Ia distance modulus versus the 2MASS H^c -band based TF distance modulus for 43 galaxies. The reference line is through the origin with a slope = 1.000. The distance moduli have a mean offset of -0.60 mag, with an *rms* scatter of 1.50 mag and the MAD is 0.45 mag.

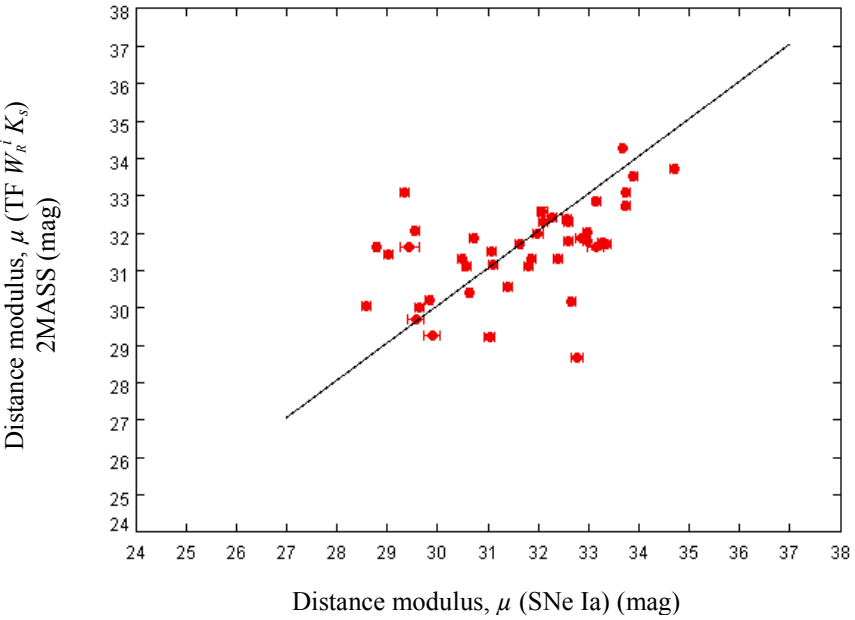

Figure 3.14: A direct comparison of SN Ia distance modulus versus the 2MASS K_s -band based TF distance modulus for 44 galaxies. The reference line is through the origin with a slope = 1.000. The distance moduli have a mean offset of -0.67 mag, with an *rms* scatter of 1.42 mag and the MAD is 0.43 mag.

Table 3.1: The Literature Sample

1	2	3	4	5	6	7	8	9	10	11	12	13	14	15	16	17	18	19
		Galaxy			SNe Ia		GSR		Virgo infall		3K CMB							
GALAXY		J2000 Epoch			J2000 Epoch		21 cm		velocity		velocity		z		W_{20}		W_{50}	
NAME	RA	DEC	TYPE		RA	DEC	km s^{-1}	σ	km s^{-1}	σ	km s^{-1}	σ	z	σ	km s^{-1}	σ	km s^{-1}	σ
IC 1151	15 58 32.2	17 26 30	SBc	1991M	15 58 34.8	17 27 29	2261	4	2479	14	2266	7	0.007235	0.000004	249	6	210	4
IC 1731	01 50 12.3	27 11 46	SABc	1983R	01 50 12.7	27 11 55	3621	5	3597	4	3230	20	0.011685	0.000003	217	14	194	5
IC 4182	13 05 49.5	37 36 18	SAm	1937C	13 05 52.4	37 37 08	369	2	314	4	550	16	0.001071	0.000013	54	3	…	…
IC 4221	13 18 30.3	-14 36 32	SAc	2002bs	13 18 30.3	-14 36 32	2784	5	2980	22	3204	22	0.009637	0.000017	217	5	226	10
MGC																		
-01-04-044	01 26 14.4	-06 05 39	SBc	1998dm	01 26 14.0	-06 06 14	2000	7	1923	13	1659	22	0.006535	0.000022	272	9	228	2
-02-16-002	06 04 34.9	-12 37 29	Sb	2003kf	06 04 35.4	-12 37 43	2066	8	2085	12	2306	8	0.007388	0.000017	280	14	215	7
-03-34-008	13 10 24.9	-16 55 58	S	1998dg	13 10 23.8	-16 56 08	2307	45	2523	51	2742	50	0.008159	0.000150	…	…	…	…
00-32-001	12 19 40.3	02 04 50	SBbc	1987D	12 19 41.0	02 04 26	2125	40	2424	48	2567	47	0.007395	0.000133	640	…	…	…
02-20-009	07 51 26.2	14 01 14	Sbc	1987O	07 51 28.5	14 01 19	4574	11	4670	15	4896	18	0.015604	0.000033	…	…	378	11
02-54-010	21 12 20.4	12 36 42	SBd	1990R	21 12 20.9	12 36 43	5047	12	5034	19	4536	24	0.016203	0.000032	…	…	96	5
05-29-024	12 09 09.6	29 16 24	SBb	1999gr	12 09 11.3	29 16 35	3922	10	4147	20	4217	23	0.013102	0.000033	…	…	…	…
06-06-062	02 35 37.3	37 38 21	SABd	1961P	02 35 35.7	37 37 28	3895	8	3904	14	3567	16	0.012605	0.000020	278	18	224	8
06-49-036	22 34 59.8	37 11 58	Sc	1978E	22 34 57.7	37 11 39	5073	13	5085	22	4539	24	0.016198	0.000033	…	…	153	8
07-16-008	07 37 37.1	41 56 49	SABbc	1988C	07 37 30.5	41 56 23	5903	6	6020	9	6029	11	0.019670	0.000020	360	11	329	11
08-17-043	09 09 32.9	50 16 55	Sb	2001G	09 09 33.2	50 16 51	5060	17	5225	20	5195	20	0.016770	0.000055	…	…	…	…
09-20-051	11 59 09.3	52 42 27	SBcd	1964E	11 59 01.6	52 41 34	1153	3	1456	21	1264	13	0.003609	0.000003	194	5	152	4
10-12-078	08 09 11.4	57 41 07	Sb	2003cp	08 09 11.1	57 41 14	5991	9	6132	13	6026	11	0.019770	0.000030	…	…	244	16
10-25-014	17 22 41.1	60 00 38	Scd	1999bv	17 22 40.7	60 00 13	5791	18	5942	23	5547	17	0.018663	0.000055	…	…	…	…
NGC 105	00 25 16.6	12 53 22	Sab	1997cw	00 25 17.3	12 53 06	5421	27	5348	31	4939	36	0.017646	0.000087	…	…	294	15
NGC 477	01 21 20.4	40 29 17	SABc	2002jy	01 21 16.3	40 29 55	6035	8	6032	18	5610	20	0.019600	0.000027	369	23	302	12
NGC 495	01 22 56.0	33 28 18	SB	1999ej	01 22 57.4	33 27 58	4260	11	4246	18	3831	22	0.013723	0.000033	…	…	…	…
NGC 523	01 25 20.8	34 01 29	Sb	2001en	01 25 22.9	34 01 31	4904	7	4888	16	4478	20	0.015871	0.000013	480	13	446	15
NGC 673	01 48 22.4	11 31 17	SABc	1996bo	01 48 22.8	11 31 15	5261	6	5186	14	4893	21	0.017285	0.000017	342	7	291	7
NGC 976	02 34 00.0	20 58 36	SAc	1999dq	02 33 59.7	20 58 30	4370	6	4332	12	4060	17	0.014327	0.000017	334	6	289	7

Table 3.1: Continued

1	2	3	4	5	6	7	8	9	10	11	12	13	14	15	16	17	18	19
		Galaxy			SNe Ia		GSR		Virgo infall		3K CMB							
GALAXY		J2000 Epoch			J2000 Epoch		21 cm		velocity		velocity		z		W_{20}		W_{50}	
NAME	RA	DEC	TYPE		RA	DEC	km s^{-1}	σ	km s^{-1}	σ	km s^{-1}	σ	z	σ	km s^{-1}	σ	km s^{-1}	σ
NGC 1003	02 39 16.9	40 52 20	SAcd	1937D	02 39 20.4	40 52 17	747	7	829	13	424	15	0.002088	0.000017	233	5	188	5
NGC 1084	02 45 59.9	-07 34 42	SAc	1963P	02 46 02.1	-07 34 50	1391	4	1342	7	1196	15	0.004693	0.000013	357	5	298	5
NGC 1164	03 01 59.8	42 35 06	SABab	1993ab	03 02 01.5	42 34 53	4288	12	4314	16	3999	17	0.013926	0.000037	…	…	283	14
NGC 1309	03 22 06.5	-15 24 00	SAbc	2002fk	03 22 05.7	-15 24 03	2073	5	2007	8	1984	11	0.007125	0.000013	142	4	117	2
NGC 1320	03 24 48.7	-03 02 32	Sa	1994aa	03 24 49.4	-03 02 33	2634	16	2577	17	2500	20	0.008883	0.000053	…	…	95	8
NGC 1640	04 42 14.5	-20 26 05	SBb	1990aj	04 42 15.3	-20 25 18	1478	6	1455	9	1575	4	0.005350	0.000013	158	14	…	…
NGC 1961	05 42 04.8	69 22 43	SABc	1998eb	05 42 12.0	69 22 26	4059	5	4185	12	3909	2	0.013122	0.000003	…	…	…	…
NGC 2268	07 14 17.4	84 22 56	SABbc	1982B	07 14 33.7	84 23 12	2380	9	2557	17	2196	7	0.007412	0.000023	401	5	337	7
NGC 2336	07 27 04.0	80 10 41	SABbc	1987L	07 27 26.4	80 09 31	2349	6	2529	15	2195	1	0.007352	0.000003	464	4	413	8
NGC 2441	07 51 54.7	73 00 56	SABb	1995E	07 51 56.7	73 00 35	3591	18	3752	21	3496	17	0.011575	0.000057	156	34	107	5
NGC 2487	07 58 20.4	25 08 57	SBc	1975O	07 58 21.1	25 08 06	4777	4	4892	10	5043	14	0.016148	0.000010	305	8	240	9
NGC 2595	08 27 42.0	21 28 51	SABc	1999aa	08 27 42.0	21 29 15	4249	5	4380	13	4572	17	0.014443	0.000013	376	4	320	7
NGC 2608	08 35 17.3	28 28 24	SBb	2001bg	08 35 18.8	28 28 06	2081	8	2273	17	2365	18	0.007122	0.000027	264	11	186	7
NGC 2748	09 13 43.0	76 28 31	SAbc	1985A	09 13 42.3	76 28 24	1607	6	1824	16	1507	3	0.004923	0.000007	…	…	258	7
NGC 2775	09 10 20.1	07 02 17	SAab	1993Z	09 10 19.6	07 01 40	1217	6	1424	21	1660	22	0.004503	0.000007	435	4	380	16
NGC 2841	09 22 02.6	50 58 35	SAb	1957A	09 21 50.4	50 59 43	674	3	841	12	809	12	0.002128	0.000010	604	4	582	12
NGC 2841	09 22 02.6	50 58 35	SAb	1999by	09 21 52.1	51 00 07	674	3	841	12	809	12	0.002128	0.000010	604	4	582	12
NGC 3021	09 50 57.1	33 33 13	SAbc	1995al	09 50 56.0	33 33 09	1510	4	1787	21	1804	19	0.005140	0.000013	302	5	228	7
NGC 3147	10 16 53.6	73 24 03	SAbc	1997bq	10 17 05.3	73 23 02	2925	5	3120	15	2861	04	0.009346	0.000003	345	34	334	12
NGC 3169	10 14 15.0	03 27 58	SAa	2003cg	10 14 16.0	03 28 02	1102	7	1340	24	1591	25	0.004130	0.000013	508	5	537	25
NGC 3190	10 18 05.6	21 49 56	SAa	2002bo	10 18 06.5	21 49 42	1200	14	1502	28	1587	26	0.004240	0.000047	601	6	392	20
NGC 3190	10 18 05.6	21 49 56	SAa	2002cv	10 18 03.7	21 50 06	1200	14	1502	28	1587	26	0.004240	0.000047	601	6	392	20
NGC 3227	10 23 30.6	19 51 54	SAB	1983U	10 23 29.3	19 51 55	1079	4	1352	23	1480	23	0.003859	0.000010	419	4	497	13
NGC 3251	10 29 16.8	26 05 57	SBbc	1999gj	10 29 19.2	26 06 20	5033	9	5216	18	5391	23	0.016965	0.000030	465	9	431	18
NGC 3294	10 36 16.2	37 19 29	SAc	1992G	10 36 18.6	37 19 16	1578	6	1886	24	1848	19	0.005290	0.000020	399	7	364	8

Table 3.1: Continued

1	2	3	4	5	6	7	8	9	10	11	12	13	14	15	16	17	18	19
		Galaxy			SNe Ia		GSR		Virgo infall		3K CMB							
GALAXY		J2000 Epoch			J2000 Epoch		21 cm		velocity		velocity		z		W_{20}		W_{50}	
NAME	RA	DEC	TYPE		RA	DEC	km s^{-1}	σ	km s^{-1}	σ	km s^{-1}	σ	z	σ	km s^{-1}	σ	km s^{-1}	σ
NGC 3367	10 46 34.9	13 45 03	SBc	1986A	10 46 36.5	13 45 01	2947	8	3168	22	3385	25	0.010142	0.000024	247	6	206	4
NGC 3367	10 46 34.9	13 45 03	SBc	2003aa	10 46 36.8	13 45 32	2947	8	3168	22	3385	25	0.010142	0.000024	247	6	206	8
NGC 3368	10 46 45.7	11 49 12	SABab	1998bu	10 46 46.0	11 50 07	797	6	800	11	1246	25	0.002992	0.000013	354	4	314	5
NGC 3370	10 47 04.0	17 16 25	SAc	1994ae	10 47 01.9	17 16 31	1198	5	1551	29	1615	24	0.004266	0.000013	284	9	248	6
NGC 3389	10 48 27.9	12 31 59	SAc	1967C	10 48 25.2	12 32 40	1211	7	1565	30	1656	25	0.004364	0.000019	277	9	235	14
NGC 3435	10 54 48.3	61 17 24	Sb	1999bh	10 54 47.0	61 17 20	5244	10	5428	16	5295	13	0.017205	0.000030	362	11	336	6
NGC 3625	11 20 31.3	57 46 53	SABb	1983W	11 20 32.2	57 47 00	2019	5	2279	18	2098	12	0.006471	0.000013	248	13	213	7
NGC 3627	11 20 14.9	12 59 30	SABb	1989B	11 20 13.9	13 00 19	643	5	447	13	1075	25	0.002425	0.000010	374	4	323	5
NGC 3687	11 28 00.6	29 30 40	SABbc	1989A	11 27 58.1	29 30 35	2485	6	2756	22	2804	22	0.008362	0.000020	187	4	150	11
NGC 3735	11 35 57.3	70 32 08	SAc	1998cn	11 35 54.4	70 32 10	2819	8	3030	17	2776	9	0.008993	0.000023	509	8	481	14
NGC 3786	11 39 42.5	31 54 33	SABa	2004bd	11 39 42.2	31 54 32	2669	6	2932	21	2965	21	0.008933	0.000020	451	4	311	7
NGC 3811	11 41 16.6	47 41 27	SBcd	1969C	11 41 17.0	47 41 40	3154	6	3389	18	3317	16	0.010357	0.000020	286	8	256	…
NGC 3913	11 50 38.9	55 21 14	SAd	1963J	11 50 38.3	55 21 01	1032	5	1308	20	1123	12	0.003182	0.000013	54	3	…	…
NGC 3913	11 50 38.9	55 21 14	SAd	1979B	11 50 43.4	55 21 39	1032	5	1308	20	1123	12	0.003182	0.000013	54	3	…	…
NGC 3953	11 53 48.9	52 19 36	SBbc	2001dp	11 53 45.2	52 20 57	1121	3	1419	21	1238	13	0.003510	0.000007	425	7	382	6
NGC 3982	11 56 28.1	55 07 31	SABb	1998aq	11 56 25.9	55 07 43	1187	7	1485	22	1279	13	0.003699	0.000020	234	7	191	17
NGC 3987	11 57 20.9	25 11 43	Sb	2001V	11 57 24.9	25 12 09	4477	5	4689	18	4810	22	0.015018	0.000017	575	7	517	7
NGC 3992	11 57 36.0	53 22 28	SBbc	1956A	11 57 43.1	53 22 27	1121	3	1417	21	1227	13	0.003496	0.000004	475	3	434	6
NGC 4045	12 02 42.2	01 58 36	SABa	1985B	12 02 44.0	01 58 45	1875	5	2212	30	2333	25	0.006591	0.000010	324	7	279	9
NGC 4096	12 06 01.1	47 28 42	SABc	1960H	12 06 07.5	47 30 38	622	4	693	7	775	15	0.001888	0.000013	325	4	285	4
NGC 4178	12 12 46.4	10 51 57	SBdm	1963I	12 12 45.6	10 51 31	307	3	182	9	715	24	0.001248	0.000002	286	6	232	10
NGC 4185	12 13 22.2	28 30 40	Sbc	1982C	12 13 23.7	28 29 32	3897	5	4123	19	4194	21	0.013022	0.000017	384	6	335	10
NGC 4414	12 26 27.1	31 13 25	SAc	1974G	12 26 28.3	31 12 22	724	6	603	9	991	20	0.002388	0.000020	411	16	364	5
NGC 4419	12 26 56.4	15 02 51	SBa	1984A	12 26 55.7	15 03 17	-307	5	-301	8	64	23	-0.000871	0.000017	286	5	200	11
NGC 4495	12 31 22.9	29 08 11	Sab	1994S	12 31 21.8	29 08 04	4554	6	4770	18	4831	21	0.015177	0.000020	395	6	332	4

Table 3.1: Continued

1	2	3	4	5	6	7	8	9	10	11	12	13	14	15	16	17	18	19
		Galaxy			SNe Ia		GSR		Virgo infall		3K CMB							
GALAXY		J2000 Epoch			J2000 Epoch		21 cm		velocity		velocity		z		W_{20}		W_{50}	
NAME	RA	DEC	TYPE		RA	DEC	km s^{-1}	σ	km s^{-1}	σ	km s^{-1}	σ	z	σ	km s^{-1}	σ	km s^{-1}	σ
NGC 4496A	12 31 39.2	03 56 22	SB	1960F	12 31 42.0	03 56 48	1650	4	…	…	2072	24	0.005771	0.000010	175	7	141	3
NGC 4501	12 31 59.1	14 25 13	SAb	1999cl	12 31 56.0	14 25 35	2235	4	…	…	2605	23	0.007609	0.000010	532	5	485	9
NGC 4527	12 34 08.5	02 39 13	SABbc	1991T	12 34 10.2	02 39 56	1654	3	…	…	2079	24	0.005791	0.000003	388	4	333	7
NGC 4536	12 34 27.1	02 11 17	SABbc	1981B	12 34 29.5	02 11 59	1725	3	2110	33	2151	24	0.006031	0.000003	336	3	297	6
NGC 4579	12 37 43.6	11 49 05	SABb	1989M	12 37 40.7	11 49 25	1466	2	…	…	1843	23	0.005060	0.000020	362	9	332	12
NGC 4639	12 42 52.4	13 15 27	SABbc	1990N	12 42 56.7	13 15 23	974	6	…	…	1338	23	0.003395	0.000018	356	8	258	5
NGC 4675	12 45 31.9	54 44 15	SBb	1997Y	12 45 31.4	54 44 17	4849	37	5054	40	4915	39	0.015866	0.000124	…	…	334	23
NGC 4902	13 00 59.7	-14 30 49	SBb	1991X	13 01 01.4	-14 30 28	2557	7	2767	23	3001	24	0.008756	0.000017	265	7	224	7
NGC 4948	13 04 55.9	-07 56 52	SBdm	1994U	13 04 56.1	-07 56 52	1027	7	1243	24	1451	24	0.003746	0.000021	…	…	139	8
NGC 4981	13 08 48.7	-06 46 39	SABc	1968I	13 08 49.3	-06 46 40	1590	5	1940	31	2005	23	0.005604	0.000013	265	9	229	6
NGC 5005	13 10 56.2	37 03 33	SABbc	1996ai	13 10 58.1	37 03 35	995	5	1284	22	1174	17	0.003156	0.000017	556	10	488	14
NGC 5054	13 16 58.5	-16 38 05	SAbc	2004ab	13 16 58.2	-16 37 53	1629	7	1904	28	2056	23	0.005807	0.000020	340	7	296	6
NGC 5055	13 15 49.3	42 01 45	SAbc	1971I	13 15 49.6	41 59 32	550	3	554	4	688	14	0.001614	0.000003	396	4	357	8
NGC 5378	13 56 51.0	37 47 50	SBa	1991ak	13 56 48.6	37 47 31	3116	25	3360	31	3233	28	0.010470	0.000083	…	…	419	25
NGC 5426	14 03 24.8	-06 04 09	SAc	1991B	14 03 24.4	-06 04 21	2519	6	2742	22	2845	20	0.008579	0.000010	408	6	344	9
NGC 5427	14 03 26.0	-06 01 51	SAc	1976D	14 03 28.2	-06 01 19	2565	4	2786	21	2891	19	0.008733	0.000017	405	10	324	33
NGC 5440	14 03 01.0	34 45 28	Sa	1998D	14 02 59.3	34 44 54	3758	7	3985	18	3885	15	0.012305	0.000020	624	5	574	9
NGC 5468	14 06 34.9	-05 27 11	SABcd	1999cp	14 06 31.3	-05 26 49	2793	4	3003	20	3112	19	0.009480	0.000013	147	5	109	2
NGC 5468	14 06 34.9	-05 27 11	SABcd	2002cr	14 06 37.6	-05 26 22	2793	4	3003	20	3112	19	0.009480	0.000013	147	5	109	2
NGC 5668	14 33 24.3	04 27 02	SAd	1954B	14 33 24.1	04 26 42	1580	5	1889	25	1813	17	0.005277	0.000017	115	6	79	2
NGC 5708	14 38 16.3	40 27 24	Sdm	2002jo	14 38 16.4	40 27 14	2854	18	3095	25	2896	20	0.009176	0.000057	…	…	145	11
NGC 5746	14 44 55.9	01 57 18	SABb	1983P	14 44 56.0	01 57 12	1723	10	2000	25	1943	18	0.005751	0.000033	652	4	633	18
NGC 6063	16 07 13.0	07 58 44	Scd	1999ac	16 07 15.0	07 58 20	2919	6	3098	15	2944	8	0.009500	0.000017	289	15	244	8
NGC 6384	17 32 24.3	07 03 37	SABbc	1971L	17 32 26.1	07 04 02	1784	5	1938	13	1627	3	0.005554	0.000004	378	11	336	7
NGC 6616	18 17 41.1	22 14 18	Sab	2002dk	18 17 43.5	22 14 53	5733	40	5828	41	5443	40	0.018533	0.000130	…	…	…	…

Table 3.1: Continued

1	2	3	4	5	6	7	8	9	10	11	12	13	14	15	16	17	18	19
	Galaxy			SNe Ia			GSR		Virgo infall		3K CMB							
GALAXY	J2000 Epoch			J2000 Epoch			21 cm		velocity		velocity		z		W_{20}		W_{50}	
NAME	RA	DEC	TYPE		RA	DEC	km s^{-1}	σ	km s^{-1}	σ	km s^{-1}	σ	z	σ	km s^{-1}	σ	km s^{-1}	σ
NGC 6627	18 22 38.9	15 41 53	SBb	1998V	18 22 37.4	15 42 08	5437	10	5521	14	5152	11	0.017586	0.000025	111	34	81	4
NGC 6636	18 22 03.5	66 37 13	Sc	1989P	18 22 01.8	66 36 12	4202	38	4351	41	3910	37	0.013326	0.000123	560	26	419	20
NGC 6835	19 54 32.9	-12 34 03	SBa	1962J	19 54 30.9	-12 34 28	1720	10	1746	12	1387	18	0.005374	0.000030	179	6	132	7
NGC 6916	20 23 33.1	58 20 39	SBbc	2002cd	20 23 34.4	58 20 47	3329	11	3445	20	2919	14	0.010344	0.000023	360	9	315	10
NGC 6951	20 37 14.1	66 06 20	SABbc	2000E	20 37 13.8	66 05 50	1644	9	1803	19	1266	11	0.004750	0.000005	328	6	286	6
NGC 7253B	22 19 30.1	29 23 16	Sc	2002jg	22 19 28.8	29 23 04	4704	13	4704	21	4158	25	0.014987	0.000033	…	…	219	10
NGC 7448	23 00 03.6	15 58 49	SAbc	1997dt	23 00 02.9	15 58 51	2370	7	2347	17	1828	26	0.007318	0.000003	306	7	256	6
NGC 7495	23 08 57.2	12 02 53	SABc	1973N	23 08 49.4	12 02 57	5050	8	4991	18	4517	26	0.016301	0.000013	216	4	170	4
NGC 7541	23 14 43.9	04 32 04	SBbc	1998dh	23 14 40.3	04 32 14	2830	8	2772	17	2318	26	0.008969	0.000018	477	4	402	9
NGC 7606	23 19 04.8	-08 29 06	SAb	1987N	23 19 03.3	-08 28 37	2331	6	2256	14	1874	26	0.007442	0.000017	526	9	…	…
NGC 7678	23 28 27.9	22 25 16	SABc	2002dp	23 28 30.4	22 25 44	3668	9	3639	19	3133	25	0.011639	0.000017	315	6	274	7
NGC 7723	23 38 57.1	-12 57 40	SBb	1975N	23 38 54.8	-12 57 09	1951	9	1874	14	1529	26	0.006254	0.000027	354	34	282	5
NGC 7742	23 44 15.7	10 46 01	SAb	1993R	23 44 16.4	10 46 09	1809	6	1775	16	1296	26	0.005547	0.000003	87	4	65	2
UGC 646	01 03 26.4	32 14 14	SB	1998ef	01 03 26.9	32 14 12	5473	11	5448	19	5019	23	0.017742	0.000030	…	…	348	12
UGC 1087	01 31 26.6	14 16 39	SAc	1999dk	01 31 26.9	14 17 06	4582	4	4516	14	4181	21	0.014960	0.000003	…	…	119	4
UGC 3261	05 11 32.4	17 03 22	Sdm	2003F	05 11 33.0	17 03 28	5136	5	5143	5	5155	5	0.017242	0.000017	…	…	232	6
UGC 3329	05 36 32.6	16 38 56	Sbc	1999ek	05 36 31.6	16 38 18	5206	10	5224	10	5278	10	0.017522	0.000033	…	…	450	12
UGC 3336	05 55 44.6	85 54 53	SBb	2003ij	05 55 41.2	85 54 22	5675	13	5809	18	5471	11	0.018383	0.000037	…	…	209	9
UGC 3375	05 55 25.3	51 54 38	SAc	2001gc	05 55 26.1	51 54 34	5851	7	5941	10	5790	7	0.019290	0.000023	508	9	471	15
UGC 3379	05 58 25.4	68 27 40	SABb	1996by	05 58 24.7	68 27 11	4233	12	4360	16	4099	11	0.013723	0.000037	…	…	346	15
UGC 3432	06 16 13.6	57 03 05	Scd	1996bv	06 16 13.0	57 03 09	5077	12	5188	14	5016	11	0.016672	0.000037	…	…	266	9
UGC 3576	06 53 07.0	50 02 03	SBb	1998ec	06 53 06.1	50 02 22	6012	4	6120	8	6032	6	0.019900	0.000013	369	4	319	14
UGC 3845	07 26 42.7	47 05 38	SBbc	1997do	07 26 42.5	47 05 36	3062	7	3210	12	3140	10	0.010120	0.000023	227	22	182	12
UGC 3885	07 31 07.0	59 28 54	Sbc	2001eg	07 31 05.9	59 28 39	3883	8	4031	12	3877	8	0.012705	0.000023	195	28	143	7
UGC 4195	08 05 06.9	66 46 59	SBb	2000ce	08 05 09.4	66 47 15	4986	12	5135	16	4946	12	0.016305	0.000037	…	…	341	21

Table 3.1: End

1	2	3	4	5	6	7	8	9	10	11	12	13	14	15	16	17	18	19
		Galaxy			SNe Ia		GSR		Virgo infall		3K CMB							
GALAXY		J2000 Epoch			J2000 Epoch		21 cm		velocity		velocity		z		W_{20}		W_{50}	
NAME	RA	DEC	TYPE		RA	DEC	km s^{-1}	σ	km s^{-1}	σ	km s^{-1}	σ	z	σ	km s^{-1}	σ	km s^{-1}	σ
UGC 5129	09 37 58.0	25 29 41	Sa	2001fe	09 37 57.1	25 29 41	3995	7	4170	16	4344	21	0.013539	0.000020	313	6	290	14
UGC 5301	09 53 20.9	42 50 40	Sd	2001er	09 53 20.6	42 50 45	4868	8	5049	15	5086	18	0.016218	0.000027	…	…	202	9
UGC 9391	14 34 37.0	59 20 16	SBdm	2003du	14 34 35.8	59 20 04	2055	7	2307	19	1994	7	0.006384	0.000013	133	16	102	4
UGC 10743	17 11 30.7	07 59 41	Sa	2002er	17 11 29.9	07 59 45	2679	8	2825	14	2564	7	0.008569	0.000023	245	8	236	13
UGC 11198	18 18 59.2	16 14 57	Sab	2000dm	18 18 59.0	16 14 53	4682	21	4775	23	4403	21	0.015034	0.000147	…	…	405	20
UGC 11994	22 20 53.1	33 17 43	Sc	2002dl	22 20 53.9	33 17 34	5088	13	5094	22	4547	25	0.016251	0.000033	…	…	400	14

Table 3.1: Column Description and References

Column 1. Galaxy name

Column 2. Galaxy J2000 Epoch coordinates for right ascension

Column 3. Galaxy J2000 Epoch coordinates for declination

Column 4. Galaxy morphology classification

Column 5. Type Ia (SN Ia) Supernova name

Column 6. SN Ia J2000 Epoch coordinates for right ascension

Column 7. SN Ia J2000 Epoch coordinates for declination

Column 8. 21 cm barycentric velocity corrected to Galactic Standard Rest in km s^{-1}

Column 9. 21 cm barycentric velocity uncertainty in km s^{-1}

Column 10. GSR corrected for the Virgo infall in km s^{-1}

Column 11. Virgo infall velocity uncertainty in km s^{-1}

Column 12. 3K CMB velocity in km s^{-1}

Column 13. 3K CMB velocity uncertainty in km s^{-1}

Column 14. Redshift

Column 15. Redshift uncertainty

Column 16. W_{20} in km s^{-1} (references below)

Column 17. Velocity uncertainty in km s^{-1}

Column 18. W_{50} in km s^{-1} from HyperLeda (references below)

Column 19. Velocity uncertainty in km s^{-1}

Reference for columns 2 through 15. NED

Reference for columns 16 through 17.

- Dixon and Sonneborn (1980)
- Fisher and Tully (1981)
- Sandage and Tammann (1987)
- Sulentic and Tifft (1977)
- Theureau et al. (1998)
- Tully (1988)

Reference for columns 18 and 19. HyperLeda, Paturel et al. (2003)

Table 3.2: Apparent Magnitude B for the SNe Ia, Apparent Magnitude B_T, H^c, and K_s, and $W_R{}^i$ for the Literature Sample

1	2	3	4	5	6	7	8	9	10	11	12	13	14	15	16	17	18	19	20	21	22
GALAXY			SNe Ia				B_T				2MASS	H Isophotal			K_s Isophotal			Corrected Velocity Width			
NAME		B	$\Delta m_{15}(B)$	$B-V_{max}$	ref	$E(B-V)$	B_T	σ	b/a	$B_T{}^{bik}$	b/a	H	σ	$H^{c\,bik}$	K_s	σ	$K_s{}^{bik}$	W_{20}^i	σ	W_{50}^i	σ
IC 1151	1991M	14.37	1.00	0.18	11, 14	0.038	13.49	0.13	0.339	12.69	0.500	10.964	0.04	10.56	10.745	0.08	10.32	257	6	223	2
IC 1731	1983R	14.10	0.50	0.36	27, 32	0.074	…	…	…	…	0.840	11.671	0.06	11.09	11.421	0.11	10.81	272	14	250	3
IC 4182	1937C	8.80	0.87	0.02	11	0.014	…	…	…	…	…	…	…	…	…	…	…	…	…	..	…
IC 4221	2002bs	14.10	1.40	…	24	0.082	…	…	…	…	0.520	10.720	0.03	10.36	10.480	0.06	10.21	269	5	287	6
MGC																					
-01-04-044	1998dm	14.70	1.07	0.20	15, 21	0.044	…	…	…	…	0.200	10.914	0.05	10.29	10.635	0.07	10.29	274	9	236	4
-02-16-002	2003kf	14.30	0.70	…	24	0.316	…	…	…	…	0.220	11.337	0.08	…	10.935	0.11	…	283	14	224	4
-03-34-008	1998dg	14.90	1.10	…	7	0.073	…	…	…	…	…	11.224	0.05	…	10.967	0.09	…	…	…	…	…
00-32-001	1987D	13.70	0.90	0.60	27, 29	0.024	14.90	0.20	0.275	13.42	…	12.146	0.08	…	12.011	0.11	…	647	…	…	…
02-20-009	1987O	15.90	1.10	…	7	0.036	…	…	…	…	0.340	10.579	0.03	…	10.271	0.04	…	…	…	389	6
02-54-010	1990R	15.40	1.00	…	12	0.093	…	…	…	…	…	13.607	0.08	13.18	13.398	0.13	13.04	…	…	…	…
05-29-024	1999gr	18.50	1.10	…	7	0.019	…	…	…	…	…	14.558	0.11	…	14.036	0.12	…	…	…	…	…
06-06-062	1961P	14.30	0.60	…	18	0.048	…	…	…	…	0.680	11.123	0.06	…	10.845	0.09	…	331	18	273	5
06-49-036	1978E	15.32	1.10	0.11	26, 27	0.140	…	…	…	…	…	12.828	0.08	…	12.687	0.13	…	…	…	…	…
07-16-008	1988C	17.00	1.10	…	7	0.053	14.19	0.14	0.724	13.61	0.520	11.305	0.04	10.99	11.033	0.06	10.64	499	11	463	7
08-17-043	2001G	14.20	1.10	0.01	24, 27	0.016	…	…	…	…	…	12.180	0.04	…	11.898	0.05	…	…	…	…	…
09-20-051	1964E	12.90	0.61	…	18	0.027	13.12	0.08	0.692	12.78	…	14.115	0.16	12.20	13.386	0.12	11.71	264	5	214	4
10-12-078	2003cp	16.20	1.10	…	24	0.046	…	…	…	…	…	12.249	0.05	…	11.941	0.08	…	…	…	…	…
10-25-014	1999bv	17.00	1.10	…	7	0.026	…	…	…	…	…	13.659	0.10	…	13.351	0.15	…	…	…	…	…
NGC 105	1997cw	16.00	1.02	0.43	15, 21	0.073	…	…	…	…	…	…	…	…	…	…	…	…	…	…	…
NGC 477	2002jy	15.28	1.01	…	7	0.054	…	…	…	…	0.860	10.987	0.06	10.57	10.678	0.07	10.13	422	23	352	7
NGC 495	1999ej	15.65	1.41	-0.01	15, 21	0.072	…	…	…	…	0.640	10.437	0.04	…	10.116	0.04	…	…	…	…	…
NGC 523	2001en	14.20	0.70	…	19	0.054	…	…	…	…	0.380	10.114	0.02	9.64	9.790	0.02	9.55	485	13	457	8
NGC 673	1996bo	16.15	1.30	0.31	21	0.077	13.20	0.13	0.776	12.60	0.680	10.119	0.03	9.70	9.818	0.05	9.52	523	7	451	5
NGC 976	1999dq	14.88	0.88	0.33	15, 21	0.110	12.82	0.15	0.830	12.14	0.740	9.520	0.02	9.37	9.177	0.02	9.05	574	6	503	…

Table 3.2: Continued

1	2	3	4	5	6	7	8	9	10	11	12	13	14	15	16	17	18	19	20	21	22
GALAXY			SNe Ia				B_T				2MASS	H Isophotal			K_s Isophotal			Corrected Velocity Width			
NAME		B	$\Delta m_{15}(B)$	$B-V_{max}$	ref	$E(B-V)$	B_T	σ	b/a	B_T^{bik}	b/a	H	σ	$H^{c\,bik}$	K_s	σ	K_s^{bik}	W_{20}^i	σ	W_{50}^i	σ
NGC 1003	1937D	12.80	0.13	0.84	34, 36	0.070	12.00	0.18	0.339	11.11	0.330	9.888	0.02	9.30	9.662	0.03	9.26	242	5	202	5
NGC 1084	1963P	14.00	0.91	…	18	0.027	11.31	0.10	0.562	10.71	0.600	8.294	0.02	8.04	8.013	0.02	7.86	419	5	356	5
NGC 1164	1993ab	17.00	1.00	…	7	0.154	…	…	…	…	0.760	10.401	0.03	…	10.064	0.03	…	…	…	441	14
NGC 1309	2002fk	12.45	1.10	…	19	0.040	11.97	0.13	0.933	11.73	0.820	9.467	0.02	9.34	9.216	0.03	9.08	…	…	…	…
NGC 1320	1994aa	15.90	1.10	…	7	0.047	13.32	0.13	0.339	…	0.340	9.781	0.02	…	9.440	0.02	…	…	…	…	…
NGC 1640	1990aj	12.50	1.10	…	33	0.034	12.42	0.13	0.776	12.12	0.700	9.247	0.02	9.07	9.021	0.03	8.87	244	14	…	…
NGC 1961	1998eb	16.70	1.10	…	7	0.124	11.73	0.14	0.646	10.64	0.730	8.263	0.02	7.78	7.951	0.02	7.51	877	…	…	…
NGC 2268	1982B	13.65	0.94	0.22	6, 27	0.064	12.24	0.13	0.617	11.50	0.600	8.967	0.02	8.69	8.670	0.02	8.50	498	5	425	7
NGC 2336	1987L	14.20	1.10	…	7	0.033	11.05	0.13	0.550	10.31	0.605	8.279	0.02	7.70	8.059	0.02	7.61	543	4	490	8
NGC 2441	1995E	16.82	1.19	0.71	21, 23	0.027	13.00	0.20	0.871	12.76	0.700	10.196	0.04	10.13	9.952	0.05	9.93	…	…	…	…
NGC 2487	1975O	15.30	1.40	0.23	18, 33	0.052	13.23	0.13	0.813	12.78	0.440	10.284	0.03	9.83	10.007	0.04	9.66	510	8	408	9
NGC 2595	1999aa	14.91	0.85	0.04	15, 21	0.040	12.93	0.14	0.759	12.46	0.580	10.284	0.04	9.79	9.978	0.04	9.61	554	4	478	7
NGC 2608	2001bg	13.60	1.00	…	19	0.039	13.01	0.13	0.603	12.47	0.560	10.619	0.03	9.47	10.526	0.05	9.27	324	11	235	7
NGC 2748	1985A	14.50	1.00	…	35	0.027	12.40	0.30	0.380	…	0.390	9.158	0.02	…	8.845	0.02	…	…	…	…	…
NGC 2775	1993Z	13.90	1.74	0.71	13	0.043	11.03	0.10	0.776	10.56	0.750	7.468	0.02	7.30	7.113	0.02	6.98	673	4	595	…
NGC 2841	1957A	14.00	1.21	0.80	4, 34	0.016	10.09	0.10	0.437	9.14	0.495	6.390	0.02	5.99	6.158	0.02	5.94	654	4	637	12
NGC 2841	1999by	13.66	1.90	…	21, 27	0.016	10.09	0.10	0.437	9.14	0.495	6.390	0.02	5.99	6.158	0.02	5.94	654	4	637	12
NGC 3021	1995al	13.36	0.89	0.13	21	0.014	…	…	…	…	0.600	9.517	0.01	9.31	9.235	0.02	9.12	354	5	274	7
NGC 3147	1997bq	14.57	1.01	0.30	15, 21	0.024	11.43	0.16	0.891	11.17	0.880	7.835	0.02	7.69	7.498	0.02	7.38	…	…	…	…
NGC 3169	2003cg	14.30	1.10	1.40	24, 27	0.031	11.08	0.10	0.631	10.45	0.660	7.661	0.02	7.39	7.375	0.02	7.21	642	5	685	25
NGC 3190	2002bo	14.04	1.13	0.46	21	0.025	12.12	0.10	0.355	10.93	0.396	7.851	0.02	7.40	7.555	0.02	7.30	626	6	415	20
NGC 3190	2002cv	15.50	1.10	…	10	0.025	12.12	0.10	0.355	10.93	0.396	7.851	0.02	7.40	7.555	0.02	7.30	626	6	415	20
NGC 3227	1983U	13.10	1.90	0.47	9, 27	0.023	11.10	0.20	0.676	10.61	0.570	8.101	0.02	7.80	7.802	0.02	7.58	553	4	662	13
NGC 3251	1999gj	17.50	1.10	…	7	0.028	…	…	…	…	0.260	10.161	0.02	9.59	9.851	0.02	9.57	…	…	431	…
NGC 3294	1992G	14.00	1.10	0.73	14, 27	0.020	12.20	0.30	0.513	11.52	0.440	8.622	0.02	8.42	8.383	0.02	8.30	454	7	420	8

Table 3.2: Continued

1	2	3	4	5	6	7	8	9	10	11	12	13	14	15	16	17	18	19	20	21	22
GALAXY			SNe Ia				B_T				2MASS	H Isophotal			K_s Isophotal			Corrected Velocity Width			
NAME		B	$\Delta m_{15}(B)$	$B-V_{max}$	ref	$E(B-V)$	B_T	σ	b/a	B_T^{bik}	b/a	H	σ	$H^{c\,bik}$	K_s	σ	K_s^{bik}	W_{20}^i	σ	W_{50}^i	σ
NGC 3367	1986A	14.35	1.10	0.20	27, 31	0.029	12.05	0.14	0.871	11.78	0.900	9.202	0.02	9.06	8.932	0.03	8.73	…	…	…	…
NGC 3367	2003aa	16.00	0.87	…	24	0.029	12.05	0.14	0.871	11.78	0.900	9.202	0.02	9.06	8.932	0.03	8.73	…	…	…	…
NGC 3368	1998bu	12.22	1.15	0.36	11	0.025	10.11	0.13	0.692	9.66	0.726	6.648	0.02	6.57	6.403	0.02	6.27	483	4	435	8
NGC 3370	1994ae	13.15	0.87	0.05	21, 22	0.031	…	…	…	…	0.720	9.800	0.03	9.53	9.544	0.03	9.36	333	9	298	5
NGC 3389	1967C	13.00	0.90	0.15	11,18	0.027	…	…	…	…	…	…	…	…	…	…	…	…	…	…	…
NGC 3435	1999bh	15.70	1.10	…	7	0.015	…	…	…	…	0.500	11.191	0.04	10.92	10.895	0.05	10.67	465	11	438	14
NGC 3625	1983W	13.30	1.10	…	30	0.014	…	…	…	…	0.380	11.418	0.06	10.91	11.209	0.07	10.87	255	13	226	6
NGC 3627	1989B	12.34	1.31	0.33	11, 34	0.032	9.65	0.13	0.457	8.86	0.539	6.215	0.02	5.93	5.951	0.02	5.78	412	4	362	7
NGC 3687	1989A	14.10	1.10	0.10	28, 34	0.022	…	…	…	…	…	10.196	0.03	…	9.914	0.03	…	…	…	…	…
NGC 3735	1998cn	14.70	1.10	…	7	0.017	12.50	0.14	0.200	10.91	0.220	8.850	0.01	8.24	8.513	0.02	8.25	…	…	…	…
NGC 3786	2004bd	14.30	0.99	…	7	0.024	13.24	0.18	0.589	12.60	0.520	9.761	0.03	9.47	9.460	0.03	9.31	539	4	378	14
NGC 3811	1969C	14.10	1.00	0.12	18, 31	0.019	12.90	0.40	0.759	12.57	0.680	10.169	0.02	9.91	9.891	0.03	9.66	423	8	…	…
NGC 3913	1963J	13.70	1.10	…	18	0.013	13.17	0.10	0.977	13.10	0.840	11.458	0.04	11.03	11.290	0.07	10.79	…	…	…	…
NGC 3913	1979B	13.85	1.25	0.30	3, 31	0.013	13.17	0.10	0.977	13.10	0.840	11.458	0.04	11.03	11.290	0.07	10.79	…	…	…	…
NGC 3953	2001dp	14.50	0.90	…	24	0.030	10.84	0.10	0.501	10.08	0.517	7.476	0.02	7.12	7.196	0.02	6.95	480	7	438	8
NGC 3982	1998aq	12.22	1.12	-0.05	21	0.014	…	…	…	…	0.840	9.172	0.02	9.03	8.922	0.02	8.83	…	…	…	…
NGC 3987	2001V	14.64	0.99	0.48	21, 27	0.020	13.89	0.13	0.186	12.09	0.200	9.533	0.01	8.90	9.099	0.02	8.81	…	…	…	…
NGC 3992	1956A	12.30	1.10	0.13	5, 11	0.029	10.60	0.13	0.617	9.98	0.638	7.376	0.02	7.02	7.139	0.02	6.86	592	3	548	7
NGC 4045	1985B	13.00	1.88	…	35	0.023	12.79	0.13	0.692	12.35	0.940	9.192	0.02	8.95	8.870	0.03	8.70	440	7	386	6
NGC 4096	1960H	14.50	0.60	…	34	0.018	11.48	0.10	0.269	10.47	0.330	8.275	0.02	7.78	8.009	0.02	7.68	330	4	296	9
NGC 4178	1963I	13.50	1.21	0.37	17, 27	0.028	11.90	0.07	0.355	11.10	0.220	9.829	0.05	9.15	9.575	0.07	9.48	299	6	249	4
NGC 4185	1982C	16.40	1.10	…	7	0.021	…	…	…	…	0.660	10.071	0.03	9.66	9.791	0.04	9.43	556	6	491	10
NGC 4414	1974G	12.48	1.11	0.18	11	0.019	…	…	…	…	0.660	7.297	0.01	7.06	7.005	0.01	6.87	484	16	435	10
NGC 4419	1984A	12.50	1.10	0.24	11, 28	0.033	12.08	0.10	0.339	11.24	0.380	8.083	0.01	…	7.787	0.01	…	…	…	…	…
NGC 4495	1994S	14.79	1.02	-0.03	21	0.021	14.05	0.18	0.550	13.40	0.460	10.622	0.03	10.31	10.242	0.03	10.07	459	6	392	11

Table 3.2: Continued

1	2	3	4	5	6	7	8	9	10	11	12	13	14	15	16	17	18	19	20	21	22
GALAXY			SNe Ia				B_T				2MASS	H Isophotal			K_s Isophotal			Corrected Velocity Width			
NAME		B	$\Delta m_{15}(B)$	$B-V_{max}$	ref	$E(B-V)$	B_T	σ	b/a	B_T^{bik}	b/a	H	σ	$H^{c\,bik}$	K_s	σ	K_s^{bik}	W_{20}^i	σ	W_{50}^i	σ
NGC 4496A	1960F	11.77	1.06	…	11	0.025	11.94	0.13	0.794	11.67	0.520	10.383	0.05	9.72	10.121	0.08	9.53	282	7	234	3
NGC 4501	1999cl	15.11	1.19	1.20	15, 21	0.038	10.36	0.04	0.537	9.54	0.506	6.626	0.02	6.33	6.334	0.02	6.17	616	5	568	9
NGC 4527	1991T	11.69	0.94	0.20	1, 34	0.022	11.38	0.13	0.339	10.40	0.330	7.343	0.02	6.96	7.021	0.02	6.81	401	4	351	7
NGC 4536	1981B	12.04	1.10	0.06	11	0.018	11.16	0.08	0.427	10.43	0.460	8.050	0.02	7.66	7.698	0.02	7.43	363	3	327	6
NGC 4579	1989M	12.70	1.10	0.26	21, 34	0.041	10.48	0.08	0.794	10.06	0.946	6.858	0.02	6.62	6.622	0.02	6.44	585	9	543	…
NGC 4639	1990N	12.75	1.05	0.02	11, 31	0.026	12.24	0.10	0.676	11.77	0.780	9.146	0.02	8.91	8.918	0.03	8.75	470	8	347	…
NGC 4675	1997Y	15.28	1.25	0.02	15	0.017	…	…	…	…	0.320	11.077	0.03	…	10.725	0.04	…	…	…	…	…
NGC 4902	1991X	11.70	1.10	…	12	0.050	11.61	0.15	0.891	11.26	0.820	8.658	0.01	8.50	8.416	0.02	8.28	…	…	…	…
NGC 4948	1994U	13.46	1.10	…	22	0.057	…	…	…	…	0.320	10.991	0.04	10.87	10.751	0.08	10.69	177	6	151	8
NGC 4981	1968I	13.50	1.10	…	5	0.042	…	…	…	…	0.640	8.902	0.02	8.70	8.630	0.03	8.44	386	9	340	6
NGC 5005	1996ai	16.96	0.85	1.72	21	0.014	10.61	0.08	0.479	9.78	0.484	6.790	0.02	6.47	6.501	0.02	6.33	617	10	548	14
NGC 5054	2004ab	14.50	0.82	…	24	0.082	11.67	0.13	0.575	10.85	0.630	8.082	0.02	7.66	7.819	0.02	7.50	403	7	357	6
NGC 5055	1971I	11.70	1.64	0.17	20, 34	0.018	9.31	0.10	0.575	8.74	0.660	5.957	0.02	5.66	5.728	0.02	5.54	471	4	431	8
NGC 5378	1991ak	14.40	1.10	…	7	0.013	…	…	…	…	0.680	10.297	0.03	…	10.049	0.04	…	…	…	…	…
NGC 5426	1991B	12.70	0.80	…	12	0.028	12.68	0.13	0.550	12.01	0.510	9.949	0.02	9.50	9.711	0.03	9.41	477	6	409	9
NGC 5427	1976D	14.50	1.10	…	7	0.028	11.93	0.13	0.851	11.61	0.980	9.046	0.02	8.74	8.797	0.02	8.55	…	…	…	…
NGC 5440	1998D	15.60	1.10	1.07	7, 27	0.015	…	…	…	…	0.440	9.266	0.02	8.79	9.010	0.03	8.75	656	5	610	9
NGC 5468	1999cp	14.20	1.40	…	16	0.024	13.00	0.30	0.912	12.81	0.660	10.889	0.04	10.29	10.624	0.07	10.38	…	…	…	…
NGC 5468	2002cr	14.15	1.00	1.00	24, 27	0.024	13.00	0.30	0.912	12.81	0.660	10.889	0.04	10.29	10.624	0.07	10.38	…	…	…	…
NGC 5668	1954B	12.90	1.00	-0.03	18, 31	0.037	12.20	0.20	0.912	11.98	…	11.952	0.06	11.18	11.775	0.11	11.69	…	…	…	…
NGC 5708	2002jo	16.40	1.10	…	24	0.013	…	…	…	…	0.360	10.998	0.04	…	10.739	0.05	…	…	…	…	…
NGC 5746	1983P	13.00	1.10	…	9	0.040	11.29	0.13	0.178	9.27	0.220	7.223	0.02	6.54	6.927	0.02	6.61	660	4	647	18
NGC 6063	1999ac	14.34	1.00	0.04	15, 21	0.046	…	…	…	…	0.640	10.961	0.05	10.54	10.787	0.09	10.47	324	15	280	8
NGC 6384	1971L	13.60	1.10	0.50	28, 31	0.123	11.14	0.14	0.661	10.22	0.680	7.966	0.02	7.44	7.814	0.02	7.43	491	11	443	7
NGC 6616	2002dk	17.50	1.10	…	24	0.146	…	…	…	…	0.460	9.807	0.02	…	9.493	0.02	…	…	…	…	…

Table 3.2: Continued

1	2	3	4	5	6	7	8	9	10	11	12	13	14	15	16	17	18	19	20	21	22
GALAXY			SNe Ia				B_T				2MASS	H Isophotal			K_s Isophotal			Corrected Velocity Width			
NAME		B	$\Delta m_{15}(B)$	$B-V_{max}$	ref	$E(B-V)$	B_T	σ	b/a	B_T^{bik}	b/a	H	σ	$H^{c\,bik}$	K_s	σ	K_s^{bik}	W_{20}^i	σ	W_{50}^i	σ
NGC 6627	1998V	15.88	1.06	0.01	15, 21	0.196	14.30	0.20	0.912	13.36	0.740	10.263	0.03	10.01	9.910	0.03	9.72	…	…	…	…
NGC 6636	1989P	16.50	1.10	…	7	0.047	…	…	…	…	…	…	…	…	…	…	…	…	…	…	…
NGC 6835	1962J	13.60	0.80	…	18	0.144	13.41	0.13	0.219	12.18	…	…	…	…	…	…	…	179	6	138	7
NGC 6916	2002cd	16.40	0.90	…	7	0.408	14.30	0.30	0.646	12.13	0.560	9.736	0.03	9.35	9.436	0.04	9.09	459	9	408	10
NGC 6951	2000E	14.31	0.94	0.15	21	0.366	11.64	0.15	0.832	9.87	0.640	7.632	0.02	7.36	7.358	0.02	7.06	569	6	502	6
NGC 7253B	2002jg	15.80	1.00	…	7	0.066	…	…	…	…	0.220	…	…	…	…	…	…	…	…	229	10
NGC 7448	1997dt	15.64	1.04	0.53	15, 21	0.057	12.20	0.13	0.457	11.38	0.520	9.403	0.02	…	9.114	0.03	…	335	7	287	6
NGC 7495	1973N	14.73	1.10	0.08	14, 31	0.086	13.73	0.13	0.912	13.24	0.840	11.403	0.06	11.15	10.886	0.09	10.55	…	…	…	…
NGC 7541	1998dh	14.24	1.23	0.21	15, 21	0.068	12.42	0.13	0.355	11.16	0.340	8.757	0.01	8.42	8.351	0.01	8.20	495	4	423	9
NGC 7606	1987N	13.52	1.10	-0.15	25, 27	0.037	11.51	0.14	0.398	10.43	0.473	7.983	0.02	7.38	7.780	0.02	7.50	559	9	…	…
NGC 7678	2002dp	15.10	0.90	…	24	0.049	12.41	0.16	0.708	11.89	0.840	9.661	0.03	9.43	9.334	0.04	9.08	433	6	383	7
NGC 7723	1975N	13.75	1.10	0.20	28, 31	0.029	11.94	0.13	0.676	11.45	0.680	8.720	0.02	8.49	8.398	0.03	8.22	466	34	378	5
NGC 7742	1993R	17.00	1.10	…	7	0.055	…	…	…	…	…	8.987	0.02	…	8.699	0.02	…	…	…	…	…
UGC 646	1998ef	15.21	0.97	0.01	15, 21	0.073	…	…	…	…	0.400	10.835	0.28	…	10.559	0.04	…	…	…	384	12
UGC 1087	1999dk	15.04	1.28	0.05	21	0.054	…	…	…	…	0.920	11.793	0.06	…	11.529	0.07	…	…	…	…	…
UGC 3261	2003F	15.50	1.10	…	7	0.329	14.70	0.30	0.617	…	0.720	11.253	0.07	…	10.988	0.08	…	…	…	292	6
UGC 3329	1999ek	17.97	1.13	0.24	15, 21	0.553	…	…	…	…	0.420	11.307	0.05	…	10.943	0.08	…	…	…	487	12
UGC 3336	2003ij	18.30	1.10	…	24	0.101	…	…	…	…	0.600	11.882	0.06	…	11.577	0.07	…	…	…	271	9
UGC 3375	2001gc	16.20	0.70	…	24	0.209	…	…	…	…	0.520	9.891	0.03	9.44	9.586	0.03	9.29	570	9	535	15
UGC 3379	1996by	16.50	1.37	…	23	0.102	…	…	…	…	0.400	10.223	0.02	…	9.938	0.03	…	…	…	452	15
UGC 3432	1996bv	15.77	0.84	0.16	21	0.105	…	…	…	…	…	12.172	0.05	…	11.860	0.08	…	…	…	269	9
UGC 3576	1998ec	16.44	1.08	0.17	15, 21	0.085	…	…	…	…	0.480	11.055	0.04	10.63	10.765	0.04	10.44	427	4	375	14
UGC 3845	1997do	14.56	0.99	0.07	15, 21	0.063	…	…	…	…	0.640	11.526	0.06	10.93	11.280	0.09	10.69	307	22	253	12
UGC 3885	2001eg	17.80	1.90	…	7	0.049	…	…	…	…	0.600	11.410	0.05	11.10	11.156	0.07	10.84	…	…	…	…
UGC 4195	2000ce	17.31	1.00	0.62	15, 21	0.057	…	…	…	…	0.580	10.850	0.03	…	10.573	0.05	…	…	…	386	21

Table 3.2: End

1	2	3	4	5	6	7	8	9	10	11	12	13	14	15	16	17	18	19	20	21	22
GALAXY			SNe Ia				B_T				2MASS	H Isophotal			K_s Isophotal			Corrected Velocity Width			
NAME		B	$\Delta m_{15}(B)$	$B-V_{max}$	ref	$E(B-V)$	B_T	σ	b/a	B_T^{bik}	b/a	H	σ	$H^{c\,bik}$	K_s	σ	K_s^{bik}	W_{20}^i	σ	W_{50}^i	σ
UGC 5129	2001fe	14.90	1.10	…	24	0.022	14.11	0.18	0.447	13.39	0.600	10.885	0.04	10.46	10.731	0.05	10.46	338	6	320	14
UGC 5301	2001er	17.20	1.10	…	24	0.014	…	…	…	…	…	13.100	0.09	…	12.680	0.11	…	…	…	…	…
UGC 9391	2003du	13.53	1.04	0.08	2, 27	0.010	14.79	0.15	0.589	14.57	…	…	…	…	…	…	…	159	16	129	4
UGC 10743	2002er	14.89	1.33	0.16	8, 21	0.157	…	…	…	…	0.320	10.735	0.03	10.39	10.493	0.04	10.25	254	8	251	13
UGC 11198	2000dm	16.10	1.10	…	19	0.186	…	…	…	…	0.300	10.879	0.02	…	10.611	0.04	…	…	…	…	…
UGC 11994	2002dl	17.70	1.10	…	24	0.078	…	…	…	…	0.220	10.543	0.02	…	10.201	0.03	…	…	…	403	14

Column 1. Galaxy name

Column 2. Type Ia Supernova (SN Ia) name

Column 3. SN Ia B-band peak apparent magnitude

Column 4. SN Ia $\Delta m_{15}(B)$

Column 5. SN Ia $B_{max} - V_{max}$ at peak apparent magnitude

Column 6. Reference for SN Ia data

Column 7. Extinction reddening

Column 8. RC3 B_T apparent magnitude where B_T is the total observed magnitude

Column 9. RC 3 B_T uncertainty

Column 10. B-band galaxy b/a axis ratio

Column 11. RC3 B_T apparent magnitude adjusted for reddening and includes the corrections $B^{bik} = B_T - A_B{}^b - A_B{}^{i\text{-}o\text{-}} - A_B{}^k$

Column 12. 2MASS co-added bands JHK axis ratio

Column 13. Isophotal near-infrared magnitude in H-band

Column 14. Isophotal near-infrared magnitude in H-band uncertainty

Column 15. Isophotal near-infrared magnitude in H-band corrected for b,i,k

Column 16. Isophotal near-infrared magnitude in K_s-band

Column 17. Isophotal near-infrared magnitude in K_s-band uncertainty

Table 3.2: Column Description and References Continued

Column 18. K_s-band isophotal near-infrared apparent magnitude adjusted for reddening and includes the corrections $K_s^{bik} = K_s - A_K^b - A_K^{i\text{-}o} - K_s^k$

Column 19. W_{20} corrected for inclination, broadening, random and rotation motion in km s^{-1} (reference HyperLeda, Paturel et al. 003)

Column 20. W_{20} uncertainty in km s^{-1}

Column 21. W_{50} corrected for inclination, broadening, random and rotation motion in km s^{-1} (reference HyperLeda, Paturel et al. 2003)

Column 22. W_{50} uncertainty in km s^{-1}

References for columns 3 through 6.

1-Altevilla et al. (2004)
2-Anupama et al. (2005)
3-Barbon et al. (1982)
4-Branch and Doggett (1985)
5-Casebeer et al. (2000)
6-Ciatti et al. (1988)
7-CfA (2008)
8-Christensen et al. (2003)
9-de Roberts et al. (1985)
10-Di Paola et al. (2002)
11-Gibson et al. (2000)
12-Gomez et al. (1996)
13-Ho et al. (2001)
14-Hölfich and Khokhlov (1996)
15-Jha (2002)
16-Krisniunas et al. (1999)
17-Kukarkin (1963)
18-Leibundgut et al. (1991)
19-Marion et al. (2003)
20-Phillips (1993)
21-Reindl et al. (2005)
22-Riess et al. (1998)
23-Riess et al. (1999)
24-Rochester (2008)
25-Ruiz-Lapuente et al. (1989)
26-Ruiz-Lapuente et al. (1995)
27-SAI (2008)
28-Schaefer (1995)
29-Schneider et al. (1987)
30-Tammann and Leibundgut (1990)
31-Tammann and Sandage (1995)
32-Tsvetkou (1988)
33-van Dyk et al. (1996)
34-Vaughan et al. (1995)
35-Wegner and McMahan (1987)
36-Zwicky and Karpowicz (1964)

Reference for column 7. NED

Reference for columns 8 and 9. RC3 (de Vaucouleurs et al. 1991 RC3)

Reference for columns 10 and 11. Calculations made using the RC3 B_T axis measurements

Reference for column 12 through 14. 2MASS

Reference for column 15. Calculations made using calibration equations from § 2

Reference for columns 16 and 17. 2MASS

Reference for columns 18 through 22. Calculations made using calibration equations from § 2

Table 3.3: Absolute Magnitude, Apparent Magnitude, and Distance Modulus for the Literature Sample

1	2	3	4	5	6	7	8	9	10	11	12	13	14	15	16	17	18
GALAXY		Phillips Template SN Ia				Tully Template W_{20} B_T				Masters Template W_{50} H^F				Masters Template W_{50} K_s			
NAME		MB	mB	μ	σ	M_B	B_T^{bik}	μ	σ	M_H	$H^{F\,bik}$	μ	σ	M_K	K_s^{bik}	μ	σ
IC 1151	1991M	-19.59	13.29	32.61	0.09	-19.99	12.69	32.68	0.13	-21.21	10.56	31.77	0.05	-21.43	10.32	31.75	0.08
IC 1731	1983R	-19.75	12.60	32.08	0.08	-20.17	…	…	…	-22.44	11.09	33.53	0.09	-22.67	10.81	33.48	0.12
IC 4182	1937C	-19.74	8.32	27.79	0.06	…	…	…	…	…	…	…	…	…	…	…	…
IC 4221	2002bs	-19.30	14.10	…	…	-20.14	…	…	…	-22.42	10.36	32.78	0.03	-22.65	10.21	32.86	0.05
MGC																	
-01-04-044	1998dm	-19.55	13.57	32.85	0.10	-20.19	…	…	…	-21.19	10.29	31.48	0.04	-21.42	10.29	31.71	0.04
-02-16-002	2003kf	-19.74	14.30	…	…	-20.29	…	…	…	-20.95	…	…	…	-21.17	…	…	…
-03-34-008	1998dg	-19.52	14.90	…	…	…	…	…	…	…	…	…	…	…	…	…	…
00-32-001	1987D	-19.65	11.20	30.58	0.10	-22.90	13.42	36.32	0.11	…	…	…	…	…	…	…	…
02-20-009	1987O	-19.52	14.90	…	…	…	…	…	…	…	…	…	…	…	…	…	…
02-54-010	1990R	-19.59	15.40	…	…	…	…	…	…	…	13.18	…	…	…	13.04	…	…
05-29-024	1999gr	-19.52	18.50	…	…	…	…	…	…	…	…	…	…	…	…	…	…
06-06-062	1961P	-19.75	14.30	…	…	-20.79	…	…	…	…	…	…	…	…	…	…	…
06-49-036	1978E	-19.52	14.94	34.19	0.09	…	…	…	…	…	…	…	…	…	…	…	…
07-16-008	1988C	-19.52	17.00	…	…	-22.09	13.61	35.70	0.14	-24.62	10.99	35.61	0.05	-24.87	10.64	35.51	0.05
08-17-043	2001G	-19.52	16.06	…	…	…	…	…	…	…	…	…	…	…	…	…	…
09-20-051	1964E	-19.75	12.90	…	…	-20.08	12.78	32.86	0.08	…	12.20	12.20	0.08	…	11.71	11.71	0.08
10-12-078	2003cp	-19.52	16.20	…	…	…	…	…	…	…	…	…	…	…	…	…	…
10-25-014	1999bv	-19.52	17.00	…	…	…	…	…	…	…	…	…	…	…	…	…	…
NGC 105	1997cw	-19.58	13.88	33.19	0.09	…	…	…	…	…	…	…	…	…	…	…	…
NGC 477	2002jy	-19.58	15.28	…	…	-21.56	…	…	…	-24.09	10.57	34.66	0.09	-24.34	10.13	34.47	0.08
NGC 495	1999ej	-19.21	15.54	34.48	0.15	…	…	…	…	…	…	…	…	…	…	…	…
NGC 523	2001en	-19.74	14.20	33.67	0.05	-22.00	…	…	…	-24.41	9.64	34.05	0.02	-24.67	9.55	34.22	0.02
NGC 673	1996bo	-19.36	14.65	33.74	0.07	-22.23	12.60	34.83	0.13	-24.79	9.70	34.49	0.03	-25.04	9.52	34.56	0.05
NGC 976	1999dq	-19.66	13.18	32.57	0.09	-22.52	12.14	34.66	0.15	-25.45	9.37	34.82	0.03	-25.71	9.05	34.76	0.05

Table 3.3: Continued

1	2	3	4	5	6	7	8	9	10	11	12	13	14	15	16	17	18
GALAXY		Phillips Template SN Ia				Tully Template W_{20} B_T				Masters Template W_{50} H^c				Masters Template W_{50} K_s			
NAME		MB	mB	μ	σ	M_B	B_T^{bik}	μ	σ	M_H	$H^{c\,bik}$	μ	σ	M_K	K_s^{bik}	μ	σ
NGC 1003	1937D	-19.75	9.10	28.58	0.08	-19.80	11.11	30.91	0.18	-20.56	9.30	29.86	0.04	-20.78	9.26	30.04	0.06
NGC 1084	1963P	-19.64	14.00	…	…	-21.53	10.71	32.24	0.10	-23.61	8.04	31.65	0.02	-23.85	7.86	31.71	0.02
NGC 1164	1993ab	-19.59	17.00	…	…	…	…	…	…	…	…	…	…	…	…	…	…
NGC 1309	2002fk	-19.52	13.00	…	…	…	11.73	…	…	…	9.34	…	…	…	9.08	…	…
NGC 1320	1994aa	-19.52	15.90	…	…	…	…	…	…	…	0.00	…	…	…	…	…	…
NGC 1640	1990aj	-19.52	12.50	…	…	-19.83	12.12	…	…	…	9.07	…	…	…	8.87	…	…
NGC 1961	1998eb	-19.52	15.70	…	…	-23.86	10.64	…	…	…	7.78	…	…	…	7.51	…	…
NGC 2268	1982B	-19.63	12.73	32.09	0.09	-22.08	11.50	33.58	0.13	-24.42	8.69	33.11	0.02	-24.67	8.50	33.17	0.02
NGC 2336	1987L	-19.52	14.20	…	…	-22.35	10.31	32.66	0.13	-25.09	7.70	32.79	0.05	-25.34	7.61	32.95	0.05
NGC 2441	1995E	-19.43	13.62	32.78	0.11	…	12.76	…	…	…	10.13	…	…	…	9.93	…	…
NGC 2487	1975O	-19.23	14.18	33.14	0.15	-22.16	12.78	34.94	0.13	-23.95	9.83	33.78	0.03	-24.20	9.66	33.86	0.05
NGC 2595	1999aa	-19.67	14.34	33.74	0.07	-22.41	12.46	34.87	0.14	-24.90	9.79	34.69	0.04	-25.16	9.61	34.77	0.05
NGC 2608	2001bg	-19.59	13.60	…	…	-20.72	12.47	33.19	0.13	-21.54	9.47	31.01	0.02	-21.77	9.27	31.04	0.03
NGC 2748	1985A	-19.59	14.50	…	…	…	…	…	…	…	…	…	…	…	…	…	…
NGC 2775	1993Z	-18.76	10.95	29.44	0.19	-23.03	10.56	33.59	0.10	-26.33	7.30	33.63	0.04	-26.59	6.98	33.57	0.04
NGC 2841	1957A	-19.41	10.42	29.56	0.08	-22.94	9.14	32.08	0.10	-26.16	5.99	32.15	0.02	-26.43	5.94	32.37	0.02
NGC 2841	1999by	-18.46	13.66	…	…	-22.94	9.14	32.08	0.10	-26.16	5.99	32.15	0.02	-26.43	5.94	32.37	0.02
NGC 3021	1995al	-19.64	12.43	31.80	0.08	-21.00	…	…	…	-22.36	9.31	31.67	0.01	-22.59	9.12	31.71	0.02
NGC 3147	1997bq	-19.58	13.66	32.97	0.08	…	11.17	…	…	…	7.69	…	…	…	7.38	…	…
NGC 3169	2003cg	-19.52	8.48	…	…	-22.88	10.45	33.33	0.10	-26.75	7.39	34.14	0.02	-27.02	7.21	34.23	0.02
NGC 3190	2002bo	-19.50	11.84	31.07	0.09	-22.80	10.93	33.73	0.10	-24.03	7.40	31.43	0.02	-24.28	7.30	31.58	0.02
NGC 3190	2002cv	-19.52	15.50	…	…	-22.80	10.93	33.73	0.10	-24.03	7.40	31.43	0.02	-24.28	7.30	31.58	0.02
NGC 3227	1983U	-18.46	11.14	29.33	0.08	-22.41	10.61	33.02	0.20	-26.44	7.80	34.24	0.02	-26.70	7.58	34.28	0.03
NGC 3251	1999gj	-19.52	17.50	…	…	…	…	…	…	…	9.59	….	…	...	9.57	…	…
NGC 3294	1992G	-19.52	10.96	30.21	0.09	-21.78	11.52	33.30	0.30	-24.14	8.42	32.56	0.01	-24.39	8.30	32.69	0.02

Table 3.3: Continued

1	2	3	4	5	6	7	8	9	10	11	12	13	14	15	16	17	18
GALAXY		Phillips Template SN Ia				Tully Template W_{20} B_T				Masters Template W_{50} H^c				Masters Template W_{50} K_s			
NAME		MB	mB	μ	σ	M_B	B_T^{bik}	μ	σ	M_H	$H^{c\,bik}$	μ	σ	M_K	K_s^{bik}	μ	σ
NGC 3367	1986A	-19.52	13.52	…	…	…	11.78	…	…	…	9.06	…	…	…	8.73	…	…
NGC 3367	2003aa	-19.65	16.00	…	…	…	11.78	…	…	…	9.06	…	…	…	8.73	…	…
NGC 3368	1998bu	-19.51	10.39	29.63	0.09	-21.98	9.66	31.64	0.13	-24.82	6.57	31.39	0.02	-25.07	6.27	31.34	0.02
NGC 3370	1994ae	-19.66	12.61	32.00	0.10	-20.81	…	…	…	-22.98	9.53	32.51	0.02	-23.22	9.36	32.58	0.03
NGC 3389	1967C	-19.65	11.99	31.37	0.08	…	…	…	…	…	…	…	…	…	…	…	…
NGC 3435	1999bh	-19.52	15.70	…	…	-21.86	…	…	…	-24.34	10.92	35.26	0.04	-24.59	10.67	35.26	0.05
NGC 3625	1983W	-19.52	13.30	…	…	-19.97	…	…	…	-21.12	10.91	32.03	0.06	-21.34	10.87	32.21	0.06
NGC 3627	1989B	-19.35	10.81	29.89	0.15	-21.48	8.86	30.34	0.13	-23.58	5.93	29.51	0.02	-23.82	5.78	29.60	0.02
NGC 3687	1989A	-19.52	13.39	32.64	0.08	…	…	…	…	…	…	…	…	…	…	…	…
NGC 3735	1998cn	-19.52	14.70	…	…	…	10.91	…	…	…	8.24	…	…	…	8.25	…	…
NGC 3786	2004bd	-19.60	14.30	…	…	-22.33	12.60	34.93	0.18	-23.72	9.47	33.19	0.03	-23.97	9.31	33.28	0.03
NGC 3811	1969C	-19.59	13.27	32.59	0.09	-21.56	12.57	…	…	…	9.91	…	…	…	9.66	…	…
NGC 3913	1963J	-19.52	13.70	…	…	…	13.10	…	…	…	11.03	…	…	…	10.79	…	…
NGC 3913	1979B	-19.40	12.39	31.52	0.07	…	13.10	…	…	…	11.03	…	…	…	10.79	…	…
NGC 3953	2001dp	-19.65	14.50	…	…	-21.96	10.08	32.04	0.10	-24.43	7.12	31.55	0.02	-24.68	6.95	31.63	0.03
NGC 3982	1998aq	-19.51	12.15	31.39	0.09	…	…	…	…	…	9.03	…	…	…	8.83	…	…
NGC 3987	2001V	-19.60	12.64	…	…	…	12.09	…	…	…	8.90	…	…	…	8.81	…	…
NGC 3992	1956A	-19.52	11.46	30.71	0.08	-22.63	9.98	32.61	0.13	-25.67	7.02	32.69	0.03	-25.93	6.86	32.79	0.03
NGC 4045	1985B	-18.53	13.00	…	…	-21.69	12.35	34.04	0.13	-24.92	8.95	33.87	0.02	-25.18	8.70	33.88	0.03
NGC 4096	1960H	-19.75	14.50	…	…	-20.78	10.47	31.25	0.10	-22.39	7.78	30.17	0.02	-22.63	7.68	30.31	0.03
NGC 4178	1963I	-19.41	11.96	31.10	0.09	-20.46	11.10	31.56	0.07	-21.48	9.15	30.63	0.07	-21.71	9.48	31.19	0.03
NGC 4185	1982C	-19.52	16.40	…	…	-22.42	…	…	…	-25.16	9.66	34.82	0.03	-25.41	9.43	34.84	0.04
NGC 4414	1974G	-19.52	11.34	30.59	0.08	-21.98	…	…	…	-24.63	7.06	31.69	0.01	-24.88	6.87	31.75	0.01
NGC 4419	1984A	-19.52	11.11	30.36	0.09	…	11.24	…	…	…	…	…	…	…	…	…	…
NGC 4495	1994S	-19.58	14.58	33.89	0.08	-21.82	13.40	35.22	0.18	-23.77	10.31	34.08	0.03	-24.02	10.07	34.09	0.03

Table 3.3: Continued

1	2	3	4	5	6	7	8	9	10	11	12	13	14	15	16	17	18
GALAXY		Phillips Template SN Ia				Tully Template W_{20} B_T				Masters Template W_{50} H^c				Masters Template W_{50} K_s			
NAME		MB	mB	μ	σ	M_B	B_T^{bik}	μ	σ	M_H	$H^{c\,bik}$	μ	σ	M_K	K_s^{bik}	μ	σ
NGC 4496A	1960F	-19.53	11.77	31.03	0.09	-20.29	11.67	31.96	0.13	-21.47	9.72	31.19	0.05	-21.69	9.53	31.22	0.08
NGC 4501	1999cl	-19.43	9.87	29.03	0.09	-22.75	9.54	32.29	0.04	-25.60	6.33	31.93	0.02	-25.86	6.17	32.03	0.02
NGC 4527	1991T	-19.62	10.48	29.83	0.07	-21.40	10.40	31.80	0.13	-23.17	6.96	30.13	0.02	-23.42	6.81	30.23	0.02
NGC 4536	1981B	-19.52	11.38	30.63	0.06	-21.08	10.43	31.51	0.08	-22.96	7.66	30.62	0.03	-23.20	7.43	30.63	0.03
NGC 4579	1989M	-19.52	11.32	30.57	0.08	-22.58	10.06	32.64	0.08	-26.53	6.62	33.15	0.04	-26.80	6.44	33.24	0.03
NGC 4639	1990N	-19.55	12.34	31.62	0.07	-21.89	11.77	33.66	0.10	-23.86	8.91	32.77	0.03	-24.11	8.75	32.86	0.03
NGC 4675	1997Y	-19.40	14.98	34.11	0.08	…	…	…	…	…	…	…	…	…	…	…	…
NGC 4902	1991X	-19.52	11.70	…	…	…	11.26	…	…	…	8.50	…	…	…	8.28	…	…
NGC 4948	1994U	-19.52	13.46	…	…	-18.81	…	…	…	-19.16	10.87	30.03	0.04	-19.36	10.69	30.05	0.04
NGC 4981	1968I	-19.52	13.50	…	…	-21.28	…	…	…	-23.47	8.70	32.17	0.08	-23.71	8.44	32.15	0.03
NGC 5005	1996ai	-19.67	9.39	28.79	0.06	-22.75	9.78	32.53	0.08	-25.42	6.47	31.89	0.02	-25.68	6.33	32.01	0.02
NGC 5054	2004ab	-19.69	14.50	…	…	-21.41	10.85	32.26	0.13	-23.65	7.66	31.31	0.02	-23.90	7.50	31.40	0.04
NGC 5055	1971I	-18.88	10.96	29.57	0.17	-21.90	8.74	30.64	0.10	-24.60	5.66	30.26	0.02	-24.85	5.54	30.39	0.02
NGC 5378	1991ak	-19.52	14.40	…	…	…	…	…	…	…	…	…	…	…	…	…	…
NGC 5426	1991B	-19.69	12.70	…	…	-21.94	12.01	33.95	0.13	-24.09	9.50	33.59	0.03	-24.34	9.41	33.75	0.04
NGC 5427	1976D	-19.52	14.50	…	…	…	11.61	…	…	…	8.74	…	…	…	8.55	…	…
NGC 5440	1998D	-19.52	11.15	…	…	-22.95	…	…	…	-25.85	8.79	34.64	0.02	-26.12	8.75	34.87	0.03
NGC 5468	1999cp	-19.23	14.20	…	…	…	12.81	…	…	…	10.29	…	…	…	10.38	…	…
NGC 5468	2002cr	-19.59	9.99	…	…	…	12.81	…	…	…	10.29	…	…	…	10.38	…	…
NGC 5668	1954B	-19.59	12.69	32.01	0.09	…	11.98	…	…	…	11.18	…	…	…	11.69	…	…
NGC 5708	2002jo	-19.52	16.40	…	…	…	…	…	…	…	…	…	…	…	…	…	…
NGC 5746	1983P	-19.52	13.00	…	…	-22.97	9.27	32.24	0.13	-25.96	6.54	32.50	0.02	-26.23	6.61	32.84	0.02
NGC 6063	1999ac	-19.59	13.84	33.16	0.07	-20.72	…	…	…	-22.53	10.54	33.07	0.05	-22.76	10.47	33.23	0.08
NGC 6384	1971L	-19.52	11.22	30.47	0.08	-22.03	10.22	32.25	0.14	-24.74	7.44	32.18	0.03	-25.00	7.43	32.43	0.04
NGC 6616	2002dk	-19.52	17.50	…	…	…	…	…	…	…	…	…	…	…	…	…	…

Table 3.3: Continued

1	2	3	4	5	6	7	8	9	10	11	12	13	14	15	16	17	18
GALAXY		Phillips Template SN Ia				Tully Template W_{20} B_T				Masters Template W_{50} H^c				Masters Template W_{50} K_s			
NAME		MB	mB	μ	σ	M_B	B_T^{bik}	μ	σ	M_H	$H^{c\,bik}$	μ	σ	M_K	K_s^{bik}	μ	σ
NGC 6627	1998V	-19.54	15.52	…	…	…	13.36	…	…	…	10.01	…	…	…	9.72	…	…
NGC 6636	1989P	-19.52	16.50	…	…	…	…	…	…	…	…	…	…	…	…	…	…
NGC 6835	1962J	-19.69	13.60	…	…	-18.84	12.18	31.02	0.13	…	…	…	…	…	…	…	…
NGC 6916	2002cd	-19.65	16.40	…	…	-21.82	12.13	33.95	0.30	-24.13	9.35	33.48	0.03	-24.38	9.09	33.47	0.03
NGC 6951	2000E	-19.62	13.31	32.66	0.07	-22.50	9.87	32.37	0.15	-25.30	7.36	32.66	0.02	-25.56	7.06	32.62	0.03
NGC 7253B	2002jg	-19.59	15.80	…	…	…	…	…	…	-21.02	…	…	…	-21.25	…	…	…
NGC 7448	1997dt	-19.56	13.11	32.40	0.08	-20.83	11.38	32.21	0.13	-22.43	…	…	…	-22.66	…	…	…
NGC 7495	1973N	-19.52	14.10	33.35	0.09	…	13.24	…	…	…	11.15	…	…	…	10.55	…	…
NGC 7541	1998dh	-19.41	13.14	32.28	0.08	-22.06	11.16	33.22	0.13	-24.04	8.42	32.46	0.01	-24.29	8.20	32.49	0.01
NGC 7606	1987N	-19.52	14.14	…	…	-22.44	10.43	32.87	0.12	…	7.38	…	…	…	7.50	…	…
NGC 7678	2002dp	-19.65	15.10	…	…	-21.64	11.89	33.53	0.16	-24.46	9.43	33.89	0.04	-24.71	9.08	33.79	0.04
NGC 7723	1975N	-19.52	12.62	31.87	0.08	-21.87	11.45	33.32	0.13	-24.00	8.49	32.49	0.02	-24.25	8.22	32.47	0.03
NGC 7742	1993R	-19.52	17.00	…	…	…	…	…	…	…	…	…	…	…	…	…	…
UGC 646	1998ef	-19.61	14.81	…	…	…	…	…	…	…	…	…	…	…	…	…	…
UGC 1087	1999dk	-19.39	14.63	33.75	0.09	…	…	…	…	…	…	…	…	…	…	…	…
UGC 3261	2003F	-19.52	15.50	…	…	…	…	…	…	-22.82	…	…	…	-23.06	…	…	…
UGC 3329	1999ek	-19.50	14.78	34.01	0.07	…	…	…	…	-24.75	…	…	…	-25.00	…	…	…
UGC 3336	2003ij	-19.52	18.30	…	…	…	…	…	…	-22.24	…	…	…	-22.48	…	…	…
UGC 3375	2001gc	-19.74	16.20	…	…	-22.50	…	…	…	-25.30	9.44	34.74	0.03	-25.56	9.29	34.85	0.03
UGC 3379	1996by	-19.27	16.50	…	…	…	…	…	…	-24.40	…	…	…	-24.65	…	…	…
UGC 3432	1996bv	-19.68	14.69	34.10	0.06	…	…	…	…	…	…	…	…	…	…	…	…
UGC 3576	1998ec	-19.54	15.42	34.69	0.07	-21.59	…	…	…	-23.57	10.63	34.20	0.04	-23.82	10.44	34.26	0.04
UGC 3845	1997do	-19.60	13.93	33.26	0.08	-20.55	…	…	…	-22.04	10.93	32.97	0.06	-22.27	10.69	32.96	0.08
UGC 3885	2001eg	-18.46	17.80	…	…	…	…	…	…	…	11.10	…	…	…	10.84	…	…
UGC 4195	2000ce	-19.59	14.49	33.81	0.08	…	…	…	…	-23.90	…	…	…	-24.14	…	…	…

Table 3.3: End

1	2	3	4	5	6	7	8	9	10	11	12	13	14	15	16	17	18
GALAXY		Phillips Template SN Ia				Tully Template W_{20} B_T				Masters Template W_{50} H^c				Masters Template W_{50} K_s			
NAME		MB	mB	μ	σ	M_B	B_T^{bik}	μ	σ	M_H	$H^{c\,bik}$	μ	σ	M_K	K_s^{bik}	μ	σ
UGC 5129	2001fe	-19.52	14.90	…	…	-20.85	13.39	34.24	0.18	-23.05	10.46	33.51	0.04	-23.29	10.46	33.75	0.05
UGC 5301	2001er	-19.52	17.20	…	…	…	…	…	…	…	…	…	…	…	…	…	…
UGC 9391	2003du	-19.55	13.20	…	…	-18.48	14.57	33.05	0.15	…	…	…	…	…	…	…	…
UGC 10743	2002er	-19.31	13.93	32.97	0.08	-19.95	…	…	…	-21.56	10.39	31.95	0.03	-21.79	10.25	32.04	0.04
UGC 11198	2000dm	-19.52	16.10	…	…	…	…	…	…	…	…	…	…	…	…	…	…
UGC 11994	2002dl	-19.52	17.70	…	…	…	…	…	…	-23.69	…	…	…	-23.94	…	…	…

Column 1. Galaxy name

Column 2. Type Ia Supernova (SN Ia) name

Column 3. SN Ia absolute magnitude

Column 4. SN Ia apparent magnitude

Column 5. SN Ia distance modulus reduced by 0.27 for the Cepheid zero point

Column 6. SN Ia distance modulus uncertainty

Columns 7 through 18. W_R^i absolute magnitude, apparent magnitude, and distance modulus with uncertainty for bands B_T, H^c and K_s

Reference for columns 3 through 6. Calculations made using Phillips et al. (1999) $\Delta m_{15}(B)$ decline rate relation

Reference for columns 7 through 18. Calculations made using the calibration equations from § 2

REFERENCES

Altevilla, G., Fiorentino, G., Marconi, M., Musella, I., Cappellaro, E., Barbon, R., Bennetti, S., Pastorello, A., Riello, M., Turatto, M., & Zampieri, L. 2004, MNRAS, 349, 1344

Anupama, G. C., Sahu, D. K., & Jose, J. 2005, A&A, 429, 667

Barbon, R., Ciatti, F., Rosino, L., Ortolani, S., & Rafanelli, P. 1982, A&A, 116, 43

Branch, D., & Doggett, J. B. 1985, AJ, 90, 2218

Carpenter, J. M. 2001, AJ, 121, 2851

Casebeer, D., Branch, D., Blaylock, M., Millard, J., Baron, E., Richardson, D., & Archeta, C. 2000, PASP, 112, 1433

Ciatti, F., Barbon, R., Cappellaro, E., & Rosino, L. 1988, A&A, 202, 15

CfA 2008, Supernova (Cambridge: Harvard University)

Christensen, L., Becker, T., Jahnke, K., Kelz, A., Roth, M. M., Sánchez, S. F., & Wisotzki, L. 2003, A&A, 401, 479

de Robertis, M. M., & Pinto, P. A. 1985, ApJ, 293, 77

de Vaucouleurs, G., de Vaucouleurs, A., Corwin, H. G., Jr., Buta, R. J., Pautrel, G., & Fouqué, P. 1991, Third Reference Catalogue of Bright Galaxies (New York: Springer) (RC3)

Di Paola, A., Larionov, V., Arkharou, A., Bernardi, F., Caratti o Garatti, A., Doki, M., Di Carlo, E., & Valentini, G. 2002, A&A, 393, 21

Dixon, R. S., & Sonneborn, G. 1980, A Master List of Nonstellar Optical Astronomical Objects (Columbus: Ohio State University Press)

Fisher, J. R., & Tully, R. B. 1981, ApJS, 47, 139

Gibson, B. K., Stetson, P. B., Freedman, W. L., Mould, J. R., Kennicutt, R. C., Jr., Huchra, J. P., Sakai, S., Graham, J. A., Fassett, C. I., Kelson, D. D., Ferrarese, L., Hughes, S. M. G., Illingworth, G. D., Macri, L. M., Madore, B. F., Sebo, K. M., & Silbermann, N. A. 2000, ApJ 529, 723

Gomez, G., Lopez, R., & Sanchez, F. 1996, AJ, 112, 2094

Ho, W. C. G., van Dyk, S. D., Peng, C. Y., Filippenko, A. V., Leonard, D. C., Matheson, T., Treffers, R. R., & Richmond, M. W. 2001, PASP, 113, 1349

Hölfich, P., & Khokhlov, A. 1996, ApJ, 457, 500

Jarrett, T. H., Chester, T., Cutri, R., Schneider, S., Skrutskie, M., & Hucra, J. P. 2000, AJ, 119, 2498

Jha, S. 2002, Exploding Stars, Near and Far, PhD Thesis (Cambridge: Harvard University)

Karachentsev, I. D., Mitronova, S. N., Karachentseva, V. E., Kudrya, Y. N., & Jarrett, T. H. 2002, A&A, 396, 431

Krisciunas, K., Hastings, N. C., Looms, K., McMillan, R., Rest, A., Riess, A. G., & Stubbs, C. 1999, arXiv:9912219 [astro-ph.60]

Kukarkin, B. V. 1963, IBVS, 28, 1

Leibundgut, B., Tammann, G. A., Cadonau, R., & Cerrito, D. 1991, A&AS, 89, 537

Marion, G. H., Hölfich, P., Vacca, W. D., & Wheeler, J. C. 2003, ApJ, 591, 316

Masters, K. L., Springob, C. M., & Hucra, J. P. 2008, Erratum 2014, AJ, 135, 1738

NED – NASA/IPAC Extragalactic Database – http://ned.ipac.caltech.edu/

Paturel, G., Petit, C., Prugniel, Ph., Theureau, G., Rousseau, J., Brouty, M., Dubois, P., & Cambrésy, L. 2003, A&A, 412, 45

Phillips, M. M. 1993, ApJ, 413, 105

Phillips, M. M., Lira, P., Suntzeff, N. B., Schommer, R. A., Hamuy, M., & Maza, J. 1999, AJ, 118, 1766

Reindl, B., Tammann, G. A., Sandage, A., & Saha, A. 2005, ApJ, 624, 532

Riess, A. G., Filippenko, A. V., Li, W., Treffers, R. R., Schmidt, B, P., Qiu, Y., Hu, J., Armstrong, M., Faranda, C., Thouvenot, E., & Buil, C. 1999, AJ, 118, 2675

Riess, A. G., Nugent, P., Filippenko, A. V., Kirshner, R. P., & Perlmutter, S. 1998, ApJ, 504, 935

Riess, A. G., Li, W., Stetson, P. B., Filippenko, A. V., Jha, S., Kirshner, R. P., Challis, P. M., Garnavich, P. M., & Chornock, R. 2005, ApJ, 627, 579

Rochester Astronomy Supernovae 2008, (Rochester: Rochester Academy of Science)

Ruiz-Lapuente, P., Kirschner, R. P., Phillips, M. M., Challis, P. M., Schmidt, B. P., Filippenko, A. V., & Wheeler, J. C. 1995, ApJ, 439, 60

Ruiz-Lapuente, P., Lopez, R., & Dominguez, I. 1989, Ap&SS 157, 65

Said, K., Kraan-Korteweg, R. C., & Jarrett, T. H. 2015, MNRAS, 447, 1618

Sandage, A., & Tammann, G. A. 1987, A Revised Shapley-Ames Catalogue of Bright Galaxies (Washington: Carnegie Institute of Washington)

Schaefer, B. E. 1995, ApJ, 450, 5

Schlegel, D., Finkbeiner, D., & Davis, M. 1998, ApJ, 500, 525

Schneider, D. P., Mould, J. R., Porter, A. C., Schmidt, M., Bothun, G. P., & Gunn, J. E. 1987, PASP, 99, 1167

Sternberg Astronomical Institute (SAI) 2008, Supernova Catalogue (Moscow: Moscow University)

Sulentic, J., & Tifft, W. G. 1977, The Revised New General Catalogue of Nonstellar Astronomic Objects (Tucson: The University Press)

Tammann, G. A., & Leibundgut, B. 1990, A&A, 236, 9

Tammann, G. A., & Sandage, A. 1995, ApJ, 452, 16

Theureau, G., Bottinelli, L., Coudreau-Durand, N., Gouguenheim, L., Hallet, N., Loulergue, M., Paturel, G., & Teerikorpi, P. 1998, A&AS, 130, 333

Tsvetkou, D. Y. 1988, SvA, 32, 72

Tully, R. B. 1988, Nearby Galaxies Catalogue (New York: Cambridge University Press)

Tully, R. B. 1998, MmSAI, 69, 237

2MASS – www.ipac.caltech.edu/2mass/releases/allsky/

van Dyk, S. D., Hamuy, M., & Filippenko, A. V. 1996, AJ, 111, 2017

Vaughan, T. E., Branch, D., Miller, D. L., & Perlmutter, S. 1995, ApJ, 439, 558

Wegner, G., & McMahan, R. K. 1987, AJ, 93, 287

Zwicky, F., & Karpowicz, M. 1964, AJ, 69, 759

CHAPTER 4
PARKES OBSERVATIONS OF HOST GALAXIES WITH WELL-OBSERVED SNe Ia

4.1 The Joint Parkes and SNe Ia Sample (the Parkes Sample)

The preceding chapter was a literature study of the optical, IR and HI properties of host galaxies with well-observed SN Ia. This chapter extends this study to an independent sample of the remaining 46 SN 1a host galaxies without existing HI observations as of the commencement of this study. The SN Ia designations are from 1968I to 2005df. The new 21 cm observations for this sample were taken at the Parkes 64 m radio telescope in April and October 2005. Although data from the HIPASS catalogue (Meyer et al. 2004) is available for all nearby galaxies in the southern hemisphere, HIPASS has insufficient velocity resolution for TF studies and, often, insufficient S/N ratio since the integration time per beam for HIPASS is only ~4 mins.

4.2 The Parkes Multibeam Receiver

This sample of 46 galaxies was observed in 2005 April and October using the ATNF Parkes 64 m Radio Telescope and the 21 cm Multibeam Receiver. The Multibeam Receiver consists of a hexagonal array of 13 circular feed-horns positioned at prime focus of the dish (Staveley-Smith 1996). As projected onto the sky, Beam 1 is the centre beam. Beams 2 through 7 are within a hexagonal inner ring surrounding the centre beam, and beams 8 through 13 comprise a hexagonal outer ring. The current 21 cm observations used only the seven inner beams of the Multibeam Receiver that have higher efficiency than the outer beams. Beam 1 has a FWHP (Full Width Half Peak) beam width of 14.0 arcmin and Beams 2 – 7 have a FWHP beam width of 14.1 arcmin. The FWHP beam radial ellipticity is 0.00 for Beam 1, and Beams 2 through 7 is 0.03. The efficiency of Beam 1 is 1.36 Jy K^{-1}; the efficiency of Beams 2 through 7 is 1.45 Jy K^{-1}. The average system temperature (Jy) at Elev = 55° is 29 Jy for Beam 1 and 30 Jy for Beams 2 through 7. There is no coma lobe for Beam 1; Beams 2 – 7 have a modest coma lobe of -17 dB.

The A and B polarisations for all of the beams correspond to two orthogonal linear polarisations. The spectrometer for the Multibeam Receiver is based on the Canares chip and is a 1024-lag, three-level auto-correlation device. The correlator

board itself contains two of the Canares chips forming a pair of 1024-lag auto-correlations. The correlator chip accepts two data streams at a sample rate of 128 MHz (Staveley-Smith 1996) and can operate at a bandwidth up to 64 MHz. The maximum number of channels per polarisation is 1024 for a bandwidth of 64 MHz and 2048 for both 8 and 4 MHz bandwidth. The channel separation is 62.5 kHz for a bandwidth of 64 MHz, 3.91 kHz for 8 MHz and 1.95 kHz for 4 MHz. The frequency resolution is 75.6 kHz for a bandwidth of 64 MHz, 4.73 kHz for 8 MHz and 2.36 kHz for 4 MHz. The velocity resolution for the bandwidths 64 MHz, 8 MHz and 4 MHz are 16.0, 1.00, and 0.50 km s^{-1} respectively (at 21 cm). Table 4.1 provides more details of the Parkes 21 cm Multibeam receiver and correlator.

The flux density scale is based on observations of Hydra A, that has an assumed value of 40.6 Jy, accounting for 8% beam dilution at 1394.5 MHz.

	Beam 1	Beam 2	Beam 3	Beam 4	Beam 5	Beam 6	Beam 7
Frequency Range GHz	1.23 to 1.53	1.22 to 1.52	1.22 to 1.52	1.22 to 1.52	1.22 to 1.52	1.22 to 1.52	1.22 to 1.52
FWHP beam width arcmin	14.00	14.10	14.10	14.10	14.10	14.10	14.10
FWHP beam radial ellipticity	0.00	0.03	0.03	0.03	0.03	0.03	0.03
Beam efficiency in Jy K^{-1}	1.36	1.45	1.45	1.45	1.45	1.45	1.45
Average Temp @ Elev 55°	29 Jy	30 Jy	30 Jy	30 Jy	30 Jy	30 Jy	30 Jy
Average Cal Temp	1.60 Jy	1.80 Jy	1.80 Jy	1.80 Jy	1.80 Jy	1.80 Jy	1.80 Jy
Coma Lobe	0.00	-17 dB	-17 dB	-17 dB	-17 dB	-17 dB	-17 dB

Bandwidth	4 MHz	8 MHz	64 MHz
Beams	7	7	13
Polarisations / Beam	2 or 4	2 or 4	2
Max No. Channels	2048	2048	1024
Channel Separation (kHz)	1.95	3.91	62.5
Frequency Resolution (kHz)	2.36	4.73	75.6
Velocity Resolution (km s^{-1})	0.50	1.00	16.00
Velocity Resolution with Hanning Smoothing (km s^{-1})	0.82	1.65	26.40

Table 4.1: Parkes 21cm Multibeam receiver and correlator parameters.

The Parkes Radio Telescope, like most other single dish telescopes, is susceptible to baseline spectral ripple. Continuum sources that are in any of the beams, or even in the telescope side lobes, will generate standing waves that result in a sinusoidal ripple across the spectral bandpass. Padman (1977) and MacA. Thomas et al. (1998) studied the baseline ripple at Parkes and determined that the baseline ripple is a frequency-dependent scattering and reflection that comes from several possible sources. The two types of baseline ripple are on-axis ripple that is produced by sources in the beam, or off-axis ripple. The scattering may occur from the physical structure of the dish such as the feed supports, the focus cabin and the dish surface. The off-axis source is more problematic, and is often caused by strong sources such as the Sun (Barnes et al. 1998; Reynolds 2006).

Radio-frequency interference (RFI) is also an issue with the potential to contaminate the data. The data reduction algorithms therefore include statistical robustness against RFI.

4.2.1 Observations and Reduction

The nominal frequency for the 21 cm observations was offset from the rest frequency of 1420.4058 MHz according to the already-known redshift of each galaxy. An observing bandwidth of 8 MHz was used. The polarisation configuration was set to two per beam. Observations were taken in so-called MX mode where each galaxy was observed with each of the inner seven beams in turn. The observation schedule files for each galaxy listed the recession velocity. The Telescope Control System (TCS) used this to correct the observing frequency for Doppler shift to the topocentric (telescope) frame. Each galaxy was observed for 24 integration cycles of 5 seconds each per beam, equating to 120 seconds per beam. For seven beams, a total of 14 minutes of on-sky integration was therefore accumulated. Each galaxy was initially observed twice, resulting in a minimum of 28 minutes integration time. Additional observations were taken in cases where the S/N remained insufficient.

The multibeam correlator automatically saves data in RPFITS format. The ATNF LiveData package was subsequently used for bandpass calibration and fine Doppler shifting to the solar system barycentre. The on-source scan for a particular beam was bandpass-calibrated using the off-source scans for the same beam both before and after the on-source scan. Data was then saved in Single Dish Flexible Image Transport System (SDFITS) format. The ATNF Multibeam Gridder ‘GRIDZILLA’

was then used to combine the individual spectra for each galaxy. Two gridding algorithms - mean and 'median' - were used. The best S/N ratio spectrum was chosen. Generally, this was the mean spectrum unless RFI or bad data was present. No smoothing was applied during data reduction. The Parkes Multibeam Gridder system (GRIDZILLA) saved the data in image FITS format.

The Karma Visualisation tool (KVIS) program provided the capability to view and print the reduced data. The MIRIAD data reduction package (task MBSPECT) is also able to plot the data. In addition, it can apply Hanning smoothing, perform robust baseline fitting, and measure various profile parameters.

The observations were calibrated four times during the two observation periods of 2005, April and October to ensure a correct flux scale (although this does not affect velocity widths). The calibrator used is a galaxy identified as PKS B1934-638. Owing to its compact nature and high flux density, this is the standard calibrator for ATNF Compact Array and Parkes observations. Each calibration consisted of a 14-minute observation using all beams. At a frequency of 1420 MHz, the average flux density across all seven beams was recorded to be 14.74 ± 0.71 Jy, 14.85 ± 0.58 Jy, 15.07 ± 1.14 Jy, and 14.65 ± 0.81 Jy for the four calibrations, respectively (where the error indicates the *rms* for the different beams and polarisations). All calibrations agreed with the nominal 1934-638 flux density of 14.9 Jy.

The bandpass removal normally yields spectra that are flat, excluding receiver noise and line emission. Non-flat baselines may be caused by ringing associated with strong Galactic HI emission, and standing wave patterns that can cause residual ripple even after bandpass removal. During final data reduction, a polynomial was therefore subtracted from the spectra. A Hanning 3-point smoothing kernel was also applied to reduce the local noise level and to suppress any ringing. The resultant velocity resolution was therefore 1.65 km s^{-1}.

4.3 Parameterisation

The mean data combination algorithm produced the best S/N for 43 of the 46 galaxies. The 'median' algorithm produced the best S/N for IC 4758, NGC 977, and UGC 52. The lowest acceptable order of polynomial fit (usually three) was used in each case. Twenty-four of the 46 galaxies had well-defined lines with sufficient S/N ratio to give acceptable results in a first pass of automated data reduction and parameterisation. The data for the remaining 22 galaxies, in Table 4.2, had lower S/N

ratio, or noise spikes, and required manual measurement of W_{20}, W_{50}, or V_{50}. The baseline order fit was set to zero for these objects.

ESO 478-G6	MCG -01-30-011	NGC 3450	UGC 52
IC 603	MCG -05-16-021	NGC 4679	UGC 5100
IC 4221	MCG -05-25-032	NGC 6708	UGC 10743
IC 4758	MCG 00-32-001	NGC 6754	UGC 11816
IC 4769	NGC 706	NGC 6901	
MCG -01-02-001	NGC 977	NGC 7782	

Table 4.2: Manually measured galaxies for the Parkes sample.

Several profiles required masking of the baseline to remove the effect of unwanted noise (e.g., RFI) on the fit. The objective was to eliminate as much noise as possible without affecting the measurement of the line width. Figure 4.1 is an example of the final data reduction of NGC 1448 and the use of masking in order to fit a baseline and measure the profile width. A polynomial order of three was fitted. The width-maximised and width-minimised points were averaged for the small number of cases where the points diverged due to noise. For profiles with low S/N ratio or where significant noise spikes were present, a manual width measurement procedure was used. Figure 4.1 is the spectral profile for NGC 1448, this galaxy has the highest peak S/N $= 92.88$ and integrated flux density 143.6 Jy km s^{-1} of the 46 galaxies observed. Figure 4.2 shows the 21 cm line width velocity integration profiles for all 46 galaxies.

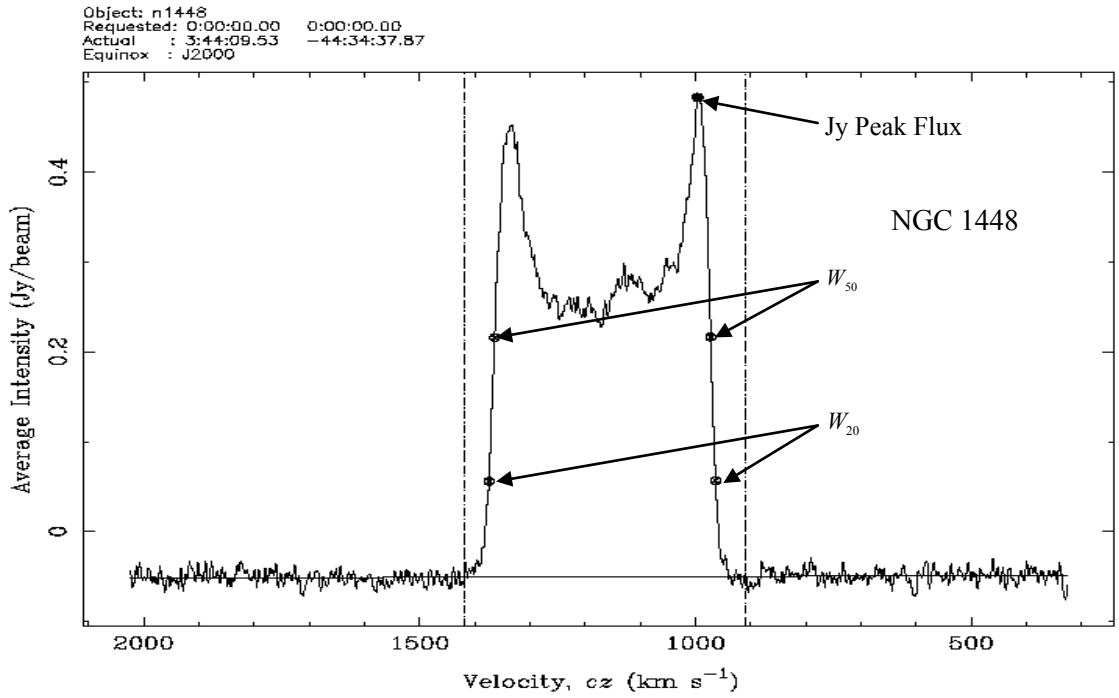

Figure 4.1: Example NGC 1448

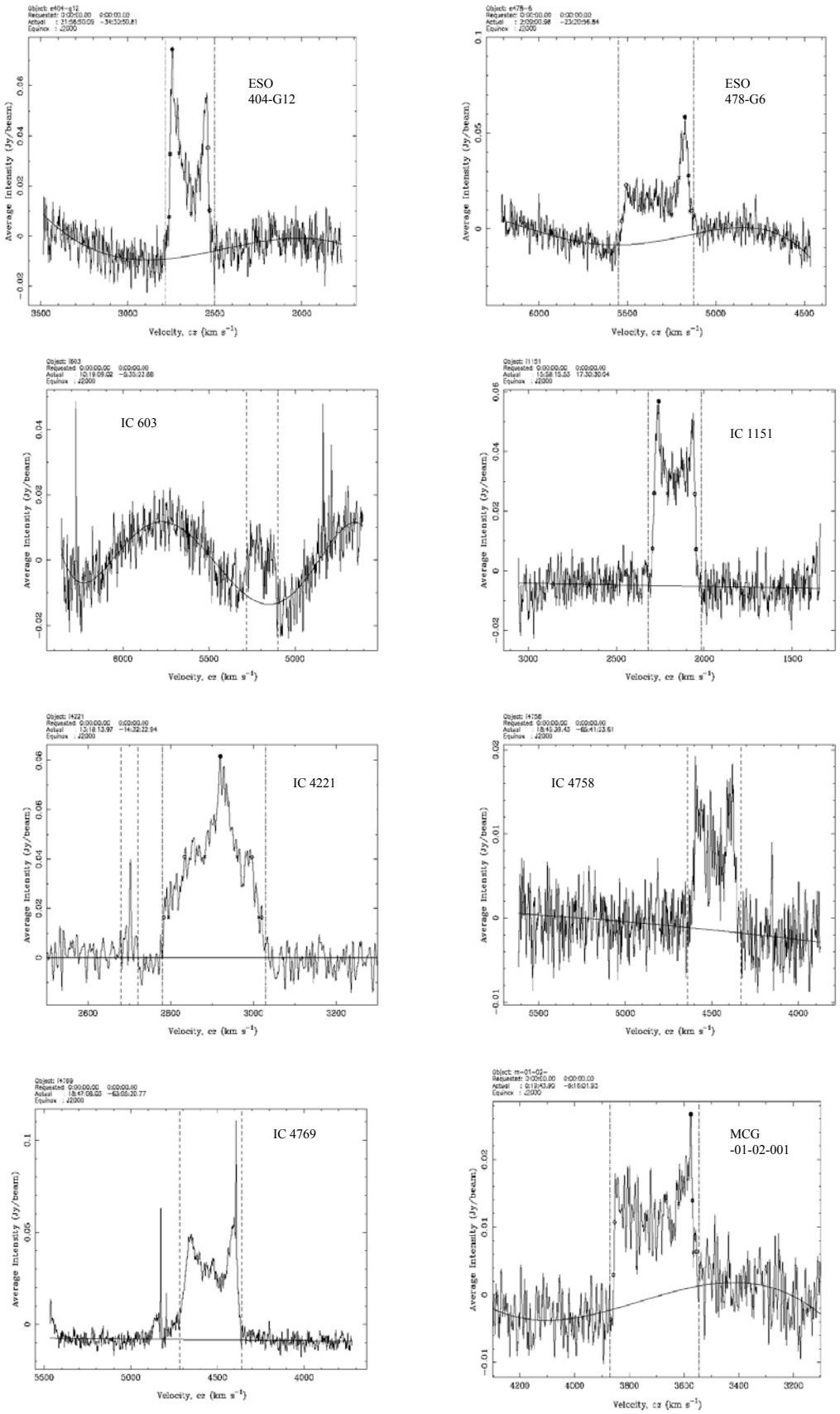

Figure 4.2: New 21 cm HI integrations

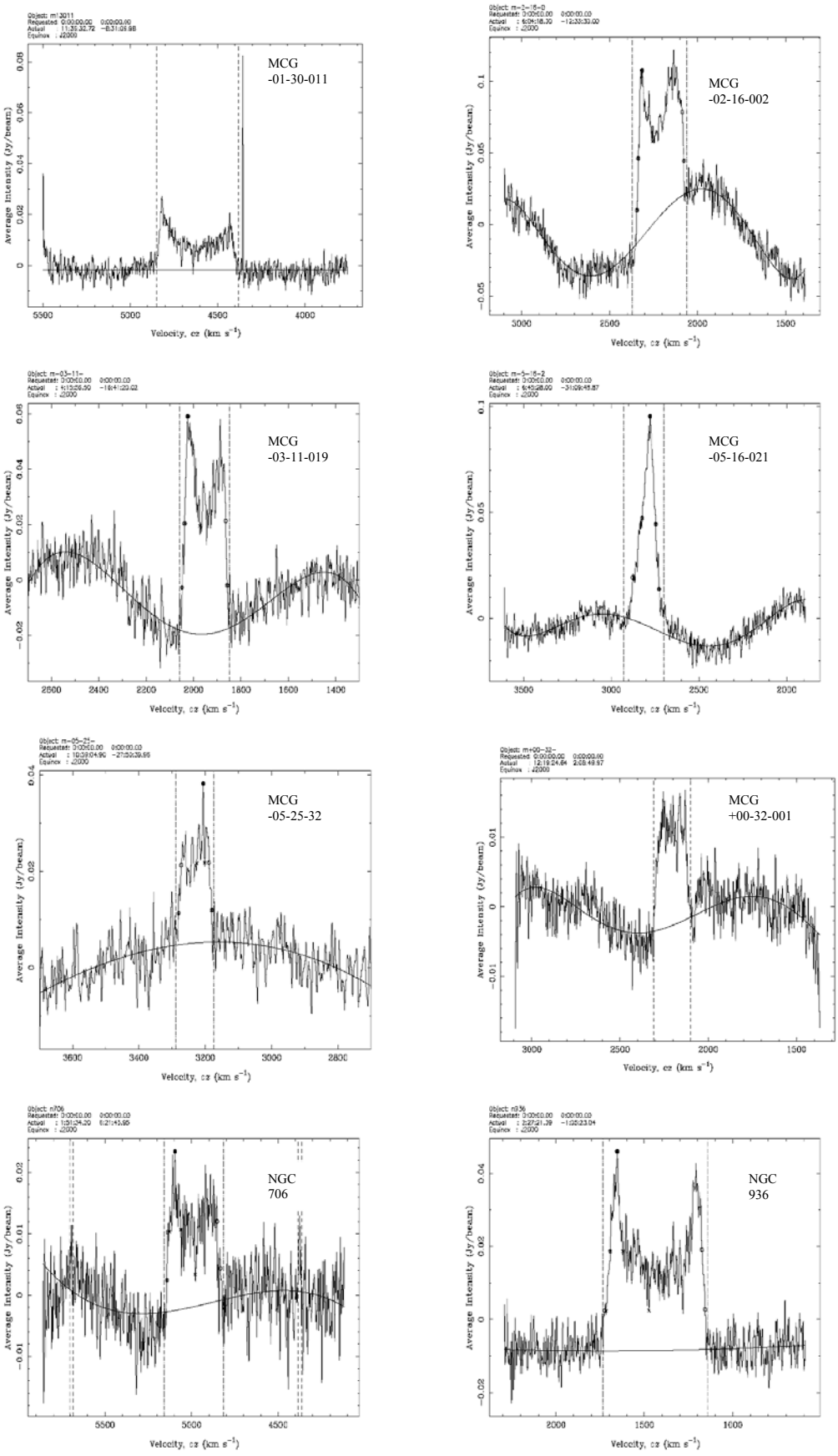

Figure 4.2: Continued

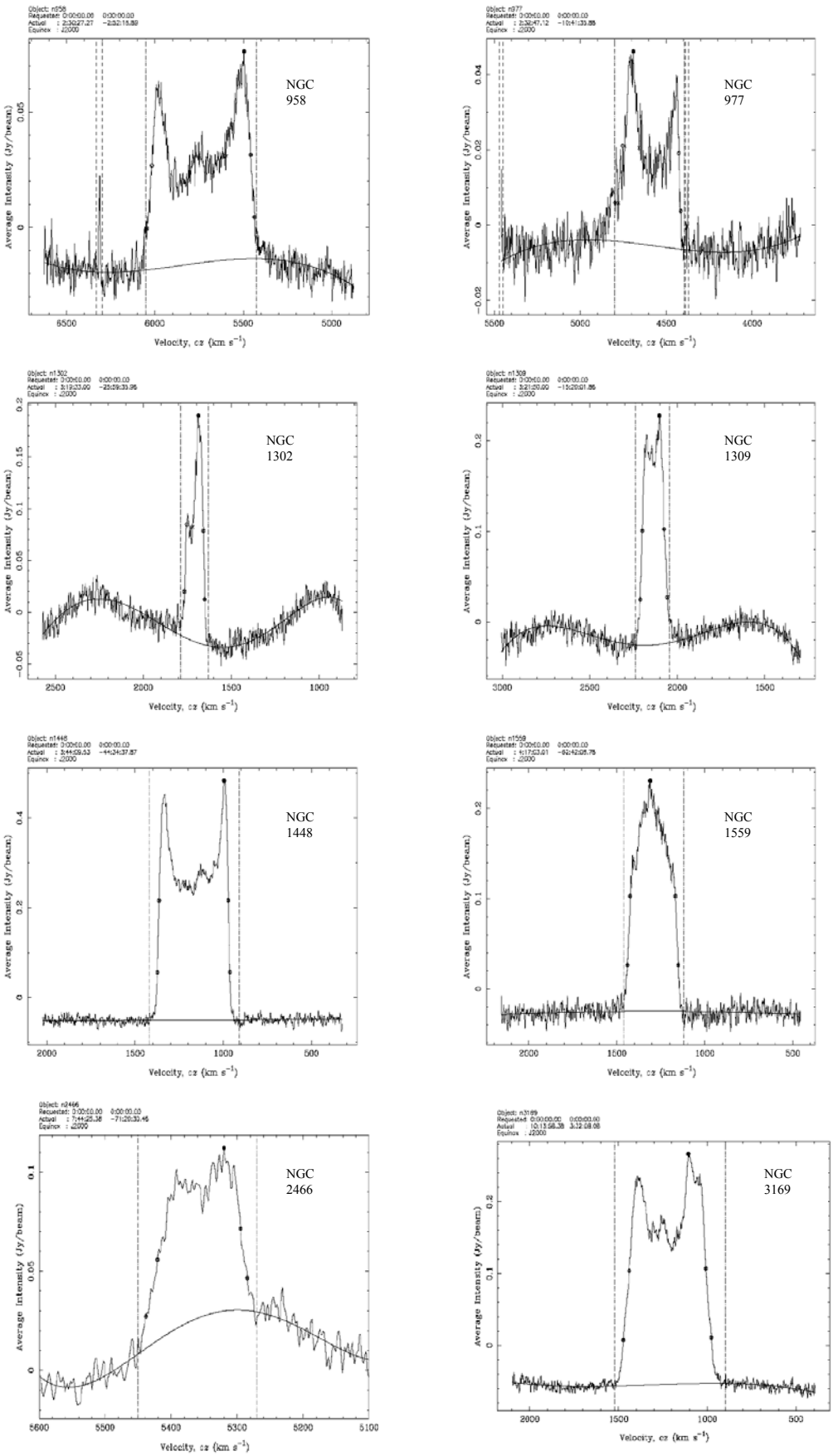

Figure 4.2: Continued

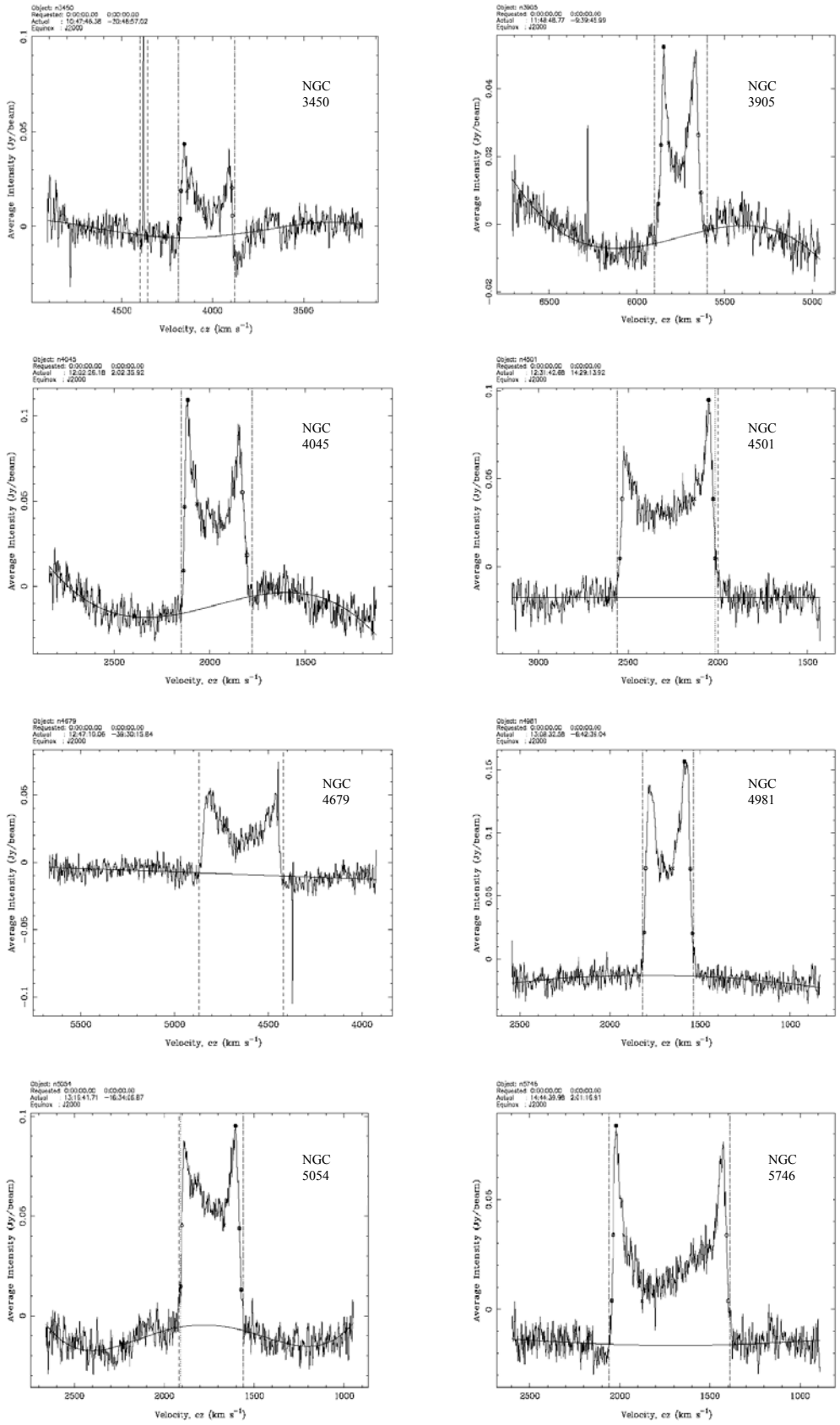

Figure 4.2: Continued

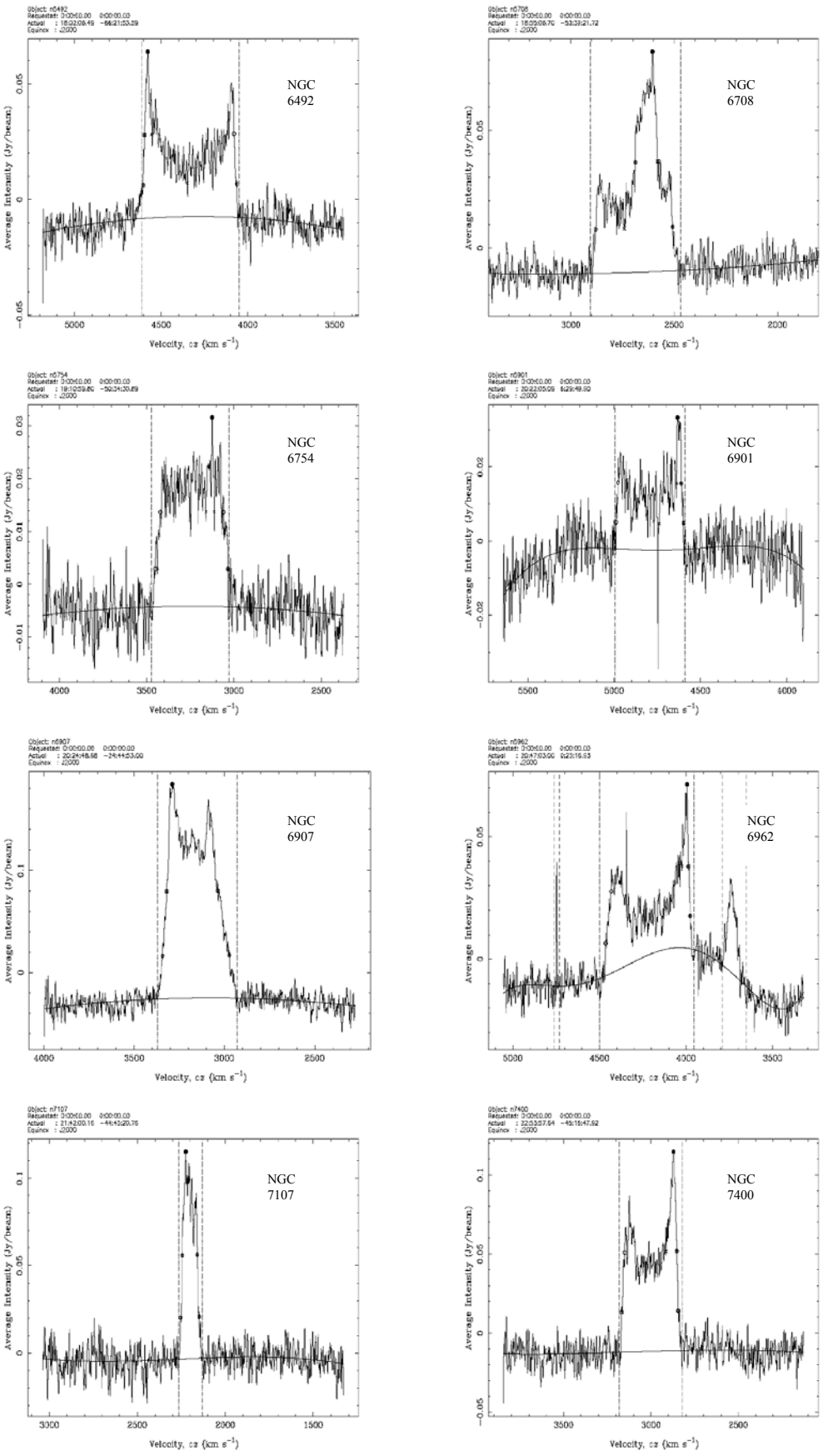

Figure 4.2: Continued

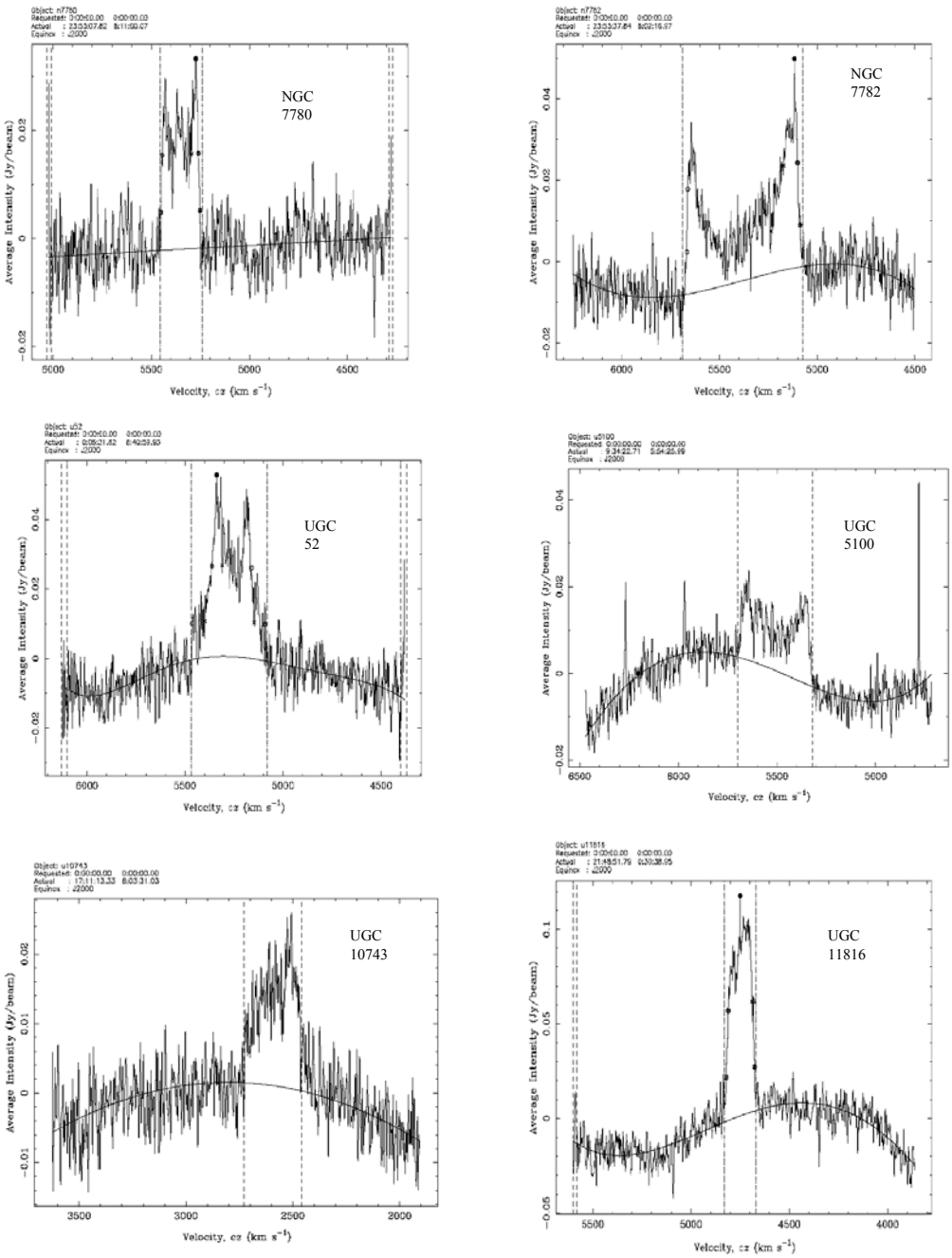

Figure 4.2: End

4.4 Tabulation of the Parkes Data

The 21 cm profiles were firstly categorised to indicate the quality of the final observation. The categories are:

Category 1 = normal double-horned profile with an S/N ratio ≥ 5, steep sides and good automated data parameterisation.

Category 2 = normal double-horned profile with a S/N ≥ 5, steep sides but a profile that includes a narrow but significant noise spike on one side of the profile.

Category 3 = double-horned profile is poorly defined or with an S/N ratio < 5 and / or has confusing noise.

Category 4 = profile shape has a central peak rather than the normal double-horned profile.

The observed mean values of flux are listed in Table 4.3 as a function of category. Category 1 and 4 contain the highest flux and S/N ratios; category 3 contains the lowest.

Category	No. of Galaxies	Peak S/N	mean S/N	mean Jy km s^{-1}
1	23	29.53	15.57	28.98
2	6	23.00	9.53	12.35
3	14	10.77	5.11	5.41
4	3	32.45	16.56	24.15

Table 4.3: Quality categories assigned to the Parkes Sample.

The mean S/N for all manually measured profiles is 8.12; the mean flux is 10.37 Jy km s^{-1}. Nine of the 22 galaxies that were manually measured resulted in a S/N < 5. The findings agreed with the studies by Roth et al. (1994) and Donley et al. (2005), and showed that integrations with an S/N < 5 require a manual measurement to determine the line widths. Owing to their low S/N ratio, these measurements have higher errors.

The mean S/N ratio for the 'automatically' measured galaxies is 16.3 with a mean flux of 31.0 Jy km s^{-1}. The S/N range is 6.1 to 49.0 and the flux range extends from 4.2 to 143.6 Jy km s^{-1}. The galaxy with the greatest S/N in the sample was NGC 1448 with a peak S/N of 92.9 and a mean S/N of 49.0.

Existing 21 cm and recession velocity data that are available in the literature are listed in Table 4.4. Data are from are the NASA / IPAC Extragalactic Database (NED). This table also lists morphology classification - there are nine galaxies with a morphology Sa to Sc; eleven defined as SAc to SAcd, ten ranging from SABa to SABbc and sixteen galaxies that are SB to SBdm (RC3; de Vaucouleurs 1991).

Table 4.5 is a compilation of the photometric data that is available in the literature for the B_T, H^c and K_s apparent magnitudes of the galaxies. The table also lists the SNe Ia B magnitude and the $\Delta m_{15}(B)$ values. The SNe Ia in the current sample range from 1968I to 2005df with the latter date being fixed by the date of the commencement of the observations. The same corrections and extinction coefficients are used as for the previous (literature-only) sample in Chapter 3. To maintain the quality and homogeneity of the photometric data for SN Ia and their host galaxies, this was again gathered from as few sources as possible. Details are summarised at the end

Table 4.6 contains the new W_{20}, W_{50}, and V_{50} measurements for the 46 newly-observed galaxies. The S/N ratio ('peak' and mean) and the flux in Jy km s^{-1} are also included in this Table. Corrections for inclination and reference frame are given in Table 4.7. Velocities are given in frames relative to the Galactic Standard of Rest, corrected for Virgo infall, and in the frame in which the 3K CMB has no dipole anisotropy (equation (2.14)).

The B_T -band axial ratio calculation data are from the RC3 axis measurements. The H^c and K_s -band axial ratio data, from the 2MASS H and K_s isophotal elliptical aperture photometry axis measurements, optical, and NIR images were manually measured and calculated to verify the catalogue data; no discrepancies were noted. All of the calculations to correct B_T and K_s apparent magnitudes were made using the corrections in § 2. The H apparent magnitudes were corrected for Galactic extinction and k-correction using the equation (2.5).

The HI line width velocities were adjusted for cosmological broadening using $W_R^c = W_R / 1+z$ followed by a correction for inclination with equation 2.6 for W_{20} and correction for internal extinction and random motion (equations 2.7 and 2.8). Equations 2.9, 2.10, 2.11, and 2.12 were correspondingly used to correct W_{50}. The absolute magnitudes M_B, M_H, and M_K, were determined with the template equations (2.13) and the distance moduli were calculated using: $m - M = 5\log d - 5$.

Table 4.8 contains the new apparent and absolute magnitudes in the three colour bands B_T, H^c, and K_s for the galaxies with a corresponding W_{20} and W_{50}. The corrections for the SNe Ia are the same as in § 3. Extinction equations are in § 2.2. The *k*-corrections are made using the § 2 (Table 2.1). The unreddened SNe Ia and absolute magnitudes were determined using the Phillips et al. (1999) correlation of the peak luminosity and initial decline rate. The SNe Ia distance determinations were obtained using the Riess et al. (2005) (0.27 mag) adjustment to the Cepheid zero point. The μ deltas between the different templates and passbands are owing to the inaccuracy of the data in the passband. Observational errors are also listed for the distance moduli.

4.5 Results

Values for W_{20} and W_{50} were obtained for the majority of the galaxies. Figure 4.3 shows a comparison of the measured W_{50} and W_{20} parameters. As expected, there is a much lower scatter than for the literature sample of the previous chapter. The difference for the W_{50} and W_{20} parameters is 27 km s^{-1} with an *rms* of 32 km s^{-1}. Once corrected for inclination etc., the mean difference reduced to only 3 km s^{-1} with an *rms* of 16 km s^{-1} (Figure 4.4), consistent with measurement error.

Figures 4.5 through 4.7 compare the distance moduli calculated from the TF relation using the Parkes W_{20} and W_{50} observations, with inclination, random motion and cosmological corrections applied, for the three bands B_T, H^c, and K_s. The inclination criterion is the same as for Chapter 3 ($35° < i < 85°$). This removes five galaxies from subsequent discussion of TF distance moduli. The *rms* scatter of the B_T-band TF moduli against the IR moduli is moderate: 0.78 mag against H^c-band, and 0.83 mag for K_s-band. However, the scatter between the H^c and K_s-band distance moduli calculated using the TF relation, is very impressively small: 0.14 mag.

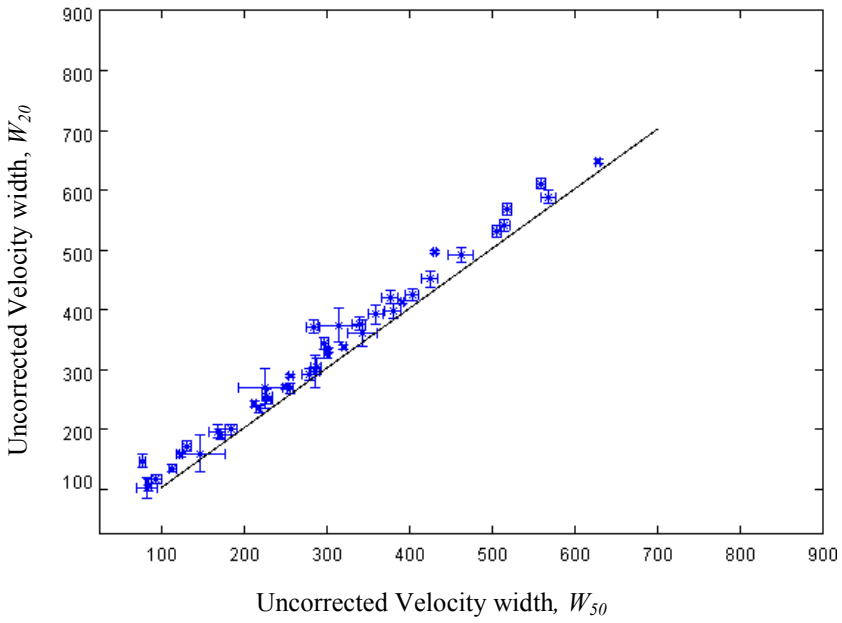

Figure 4.3: Comparison of W_{50} and W_{20} for 43 galaxies in the Parkes sample. The mean difference is 27 km s^{-1}, with an *rms* scatter of 32 km s^{-1}. The galaxies with large error bars are owing to low S/N ratio; several galaxies have inclination values that are beyond the parameter $35° < i < 80°$ and are later excluded.

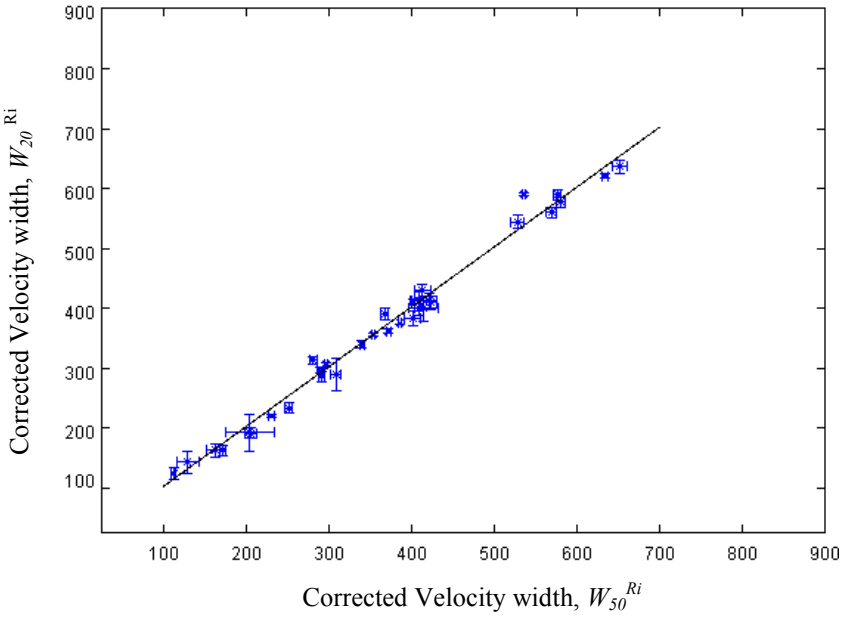

Figure 4.4: Comparison of velocity widths of W_{50}^{Ri} plotted against W_{20}^{Ri} using the RC3 data for the inclination correction for 36 galaxies in the Parkes sample. The mean difference is 3 km s^{-1}, with an *rms* scatter of 16 km s^{-1}. The galaxies with large error bars have the lowest S/N ratio; several galaxies have inclination values that are beyond the parameter $35° < i < 80°$ and are later excluded.

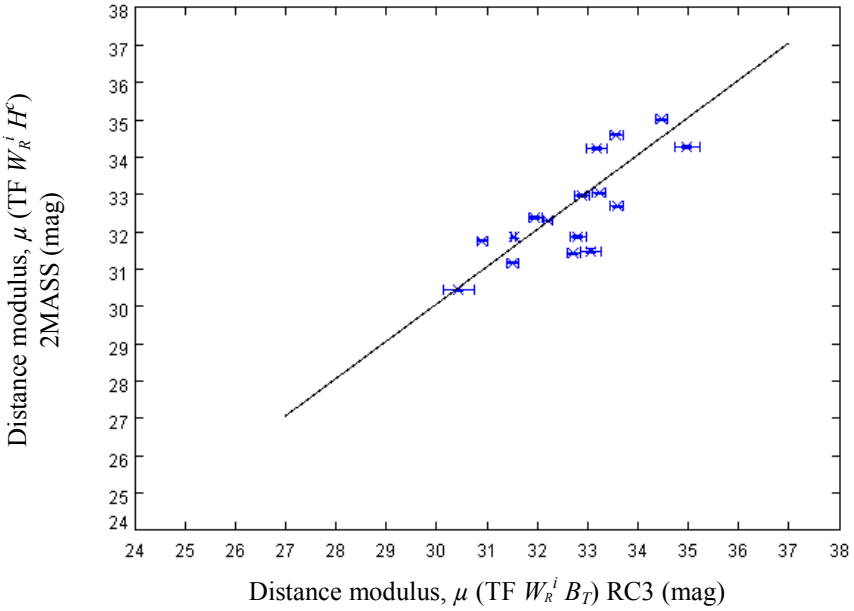

Figure 4.5: Distribution of 16 galaxies, based on the TF distance modulus derived from W_R^i for the RC3 B_T -band based results versus distance modulus derived from W_R^i for the 2MASS H^c -band based data. The reference line is through the origin with a slope = 1.000. The mean difference is 0.14 mag, with an *rms* scatter of 0.78 mag and the MAD is 0.31 mag.

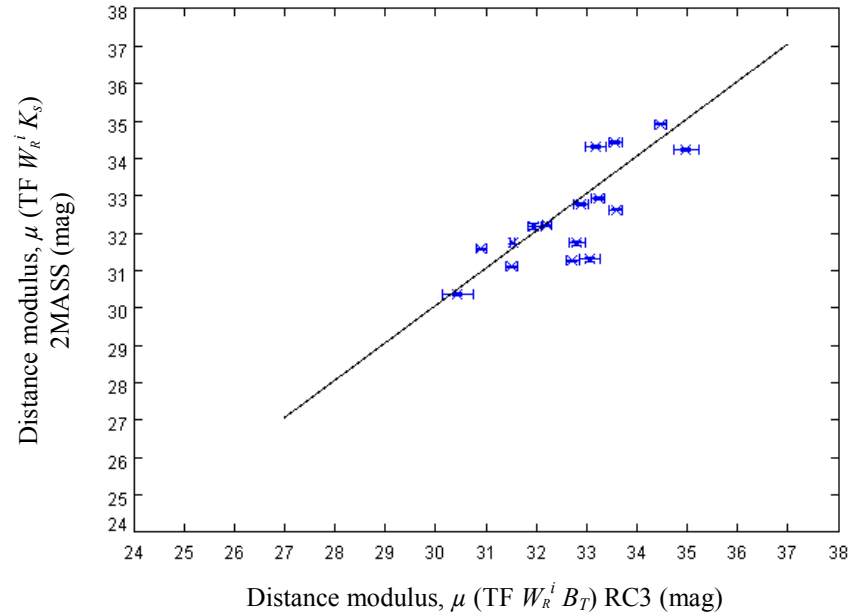

Figure 4.6: Distribution of 16 galaxies, based on the TF distance modulus derived from W_R^i for the RC3 B_T -band based results versus distance modulus derived from W_R^i for 2MASS K_s -band based data. The reference line is through the origin with a slope = 1.000. The mean difference is 0.25 mag, with an *rms* scatter of 0.83 mag and the MAD is 0.39 mag.

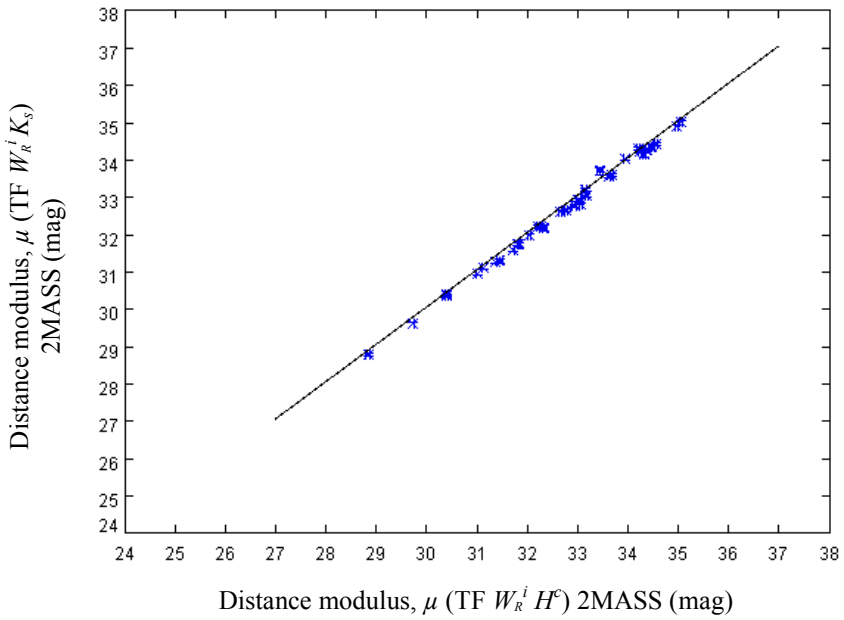

Figure 4.7: Distribution of 35 galaxies, based on the TF distance modulus derived from W_R^i for the 2MASS H^c -band based results versus distance modulus derived from W_R^i for the 2MASS K_s -band based data. The reference line is through the origin with a slope = 1.000. The mean difference is 0.10 mag, with an *rms* scatter of 0.14 mag and the MAD is 0.02 mag.

Unfortunately, the majority of the SNe Ia (36) in the literature do not include $B-V_{\max}$ at peak apparent magnitude, required to correct the observed maximum-light magnitude for reddening. In the absence of this data, a mean value $B_{\max}-V_{\max}=0.45$ was used. Although this diminishes the effectiveness of the 'standard' candle approach, the largest errors, due to extreme values of reddening, are avoided by our exclusion of edge-on host galaxies. Additionally, values of $\Delta m_{15}(B)$ were not available for 22 SNe Ia. These were assigned the mean decline rate of 1.10 mag over 15 days. The majority of the SNe Ia data for the Parkes sample are therefore limited by incomplete light curve data. Only five have complete data.

Figures 4.8 and 4.9 compare the corrected velocity width and the absolute H^c -band and K_s -band magnitude computed from the redshift, as opposed to the template relation. This diagram (which is the usual way that the Tully-Fisher relation is plotted) has an *rms* of 1.20 and 1.20 mag respectively, around the template regression line. Figures 4.10, 4.11, 4.12 and 4.13 show the Hubble diagram for the galaxies using the redshift – i.e., measured distance modulus as a function of redshift (log *cz*) for the IR Tully-Fisher relation applied to the host galaxies, and their corresponding SNe Ia, respectively. The *rms* scatter of B_T is 0.83 mag, the IR H^c and K_s TF moduli is 1.16 mag and 1.18 mag respectively, compared with 1.31 mag for the SNe Ia. The high

quality of the Parkes data and the IR data ensure that the TF distance accuracy is high. Unfortunately the SNe Ia data appears to give poorer distance accuracy. This is reflected in Figures 4.14, 4.15 and 4.16, that compares the SNe Ia distance moduli with the TF moduli for the B_T, H^c and K_s bands, respectively including the MAD results. The scatter is 1.61 mag for B_T -band, 1.84 mag and 1.81 mag for the IR H^c and K_s bands resulting in a mean rms scatter of 1.75 mag. The high scatter appears to be the result of increased observational scatter arising from the heterogeneous nature of the SNe Ia observations – e.g. multiple telescopes and detectors and limited time span for the light curve observations.

4.6 Summary

This chapter provides new distance moduli for a sample of SN Ia and their host galaxies. The distance moduli for the host galaxies were obtained with new 21 cm observations, producing less dispersion. Nevertheless, the dispersion remains owing to the photometric B_T -band data that was obtained from the literature. The data presented in Chapter 5 provides new 21 cm and IR observational data, and comparative detail is provided in chapter 6.

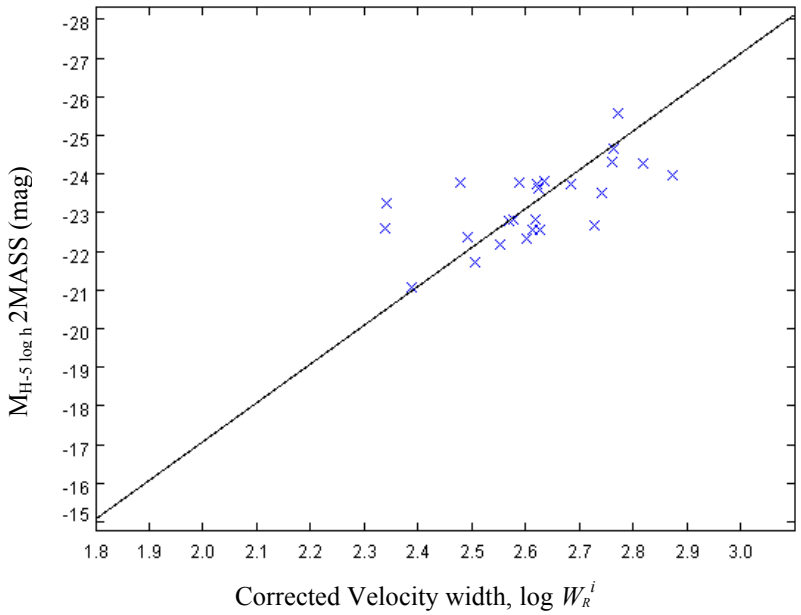

Figure 4.8: 21cm line width velocity corrected for broadening, inclination, random and rotation motion versus 2MASS H^c -band based absolute magnitude, calculated from redshift for 25 galaxies in the Parkes sample. The difference from the template relation is 0.09 mag, with an *rms* scatter of 1.20 mag.

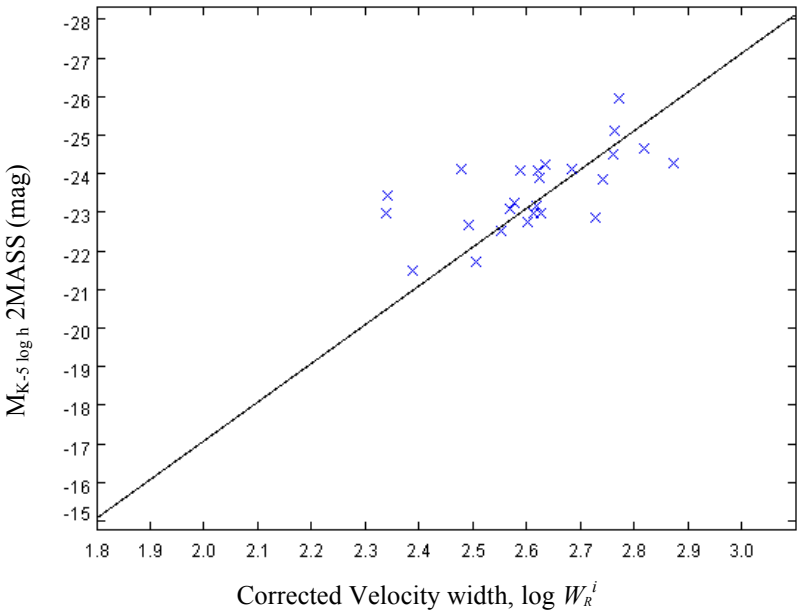

Figure 4.9: 21cm line width velocity corrected for broadening, inclination, random and rotation motion versus 2MASS K_s -band based absolute magnitude, calculated from redshift for 25 galaxies in the Parkes sample. The difference from the template relation is 0.12 mag, with an *rms* scatter of 1.20 mag.

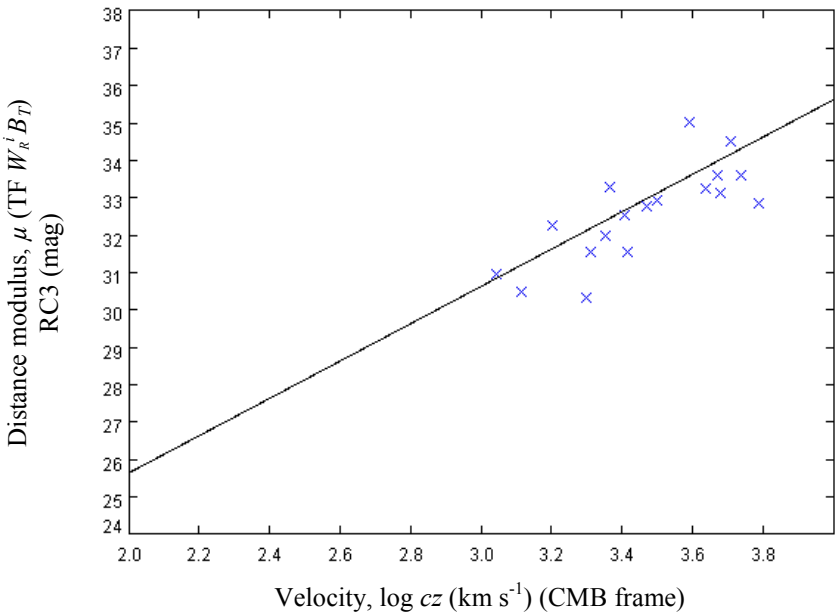

Figure 4.10: A comparison of the log *cz* (CMB frame) versus TF RC3 B_T -band based distance modulus for 18 galaxies. The offset is -0.24 mag, with an *rms* scatter of 0.83 mag.

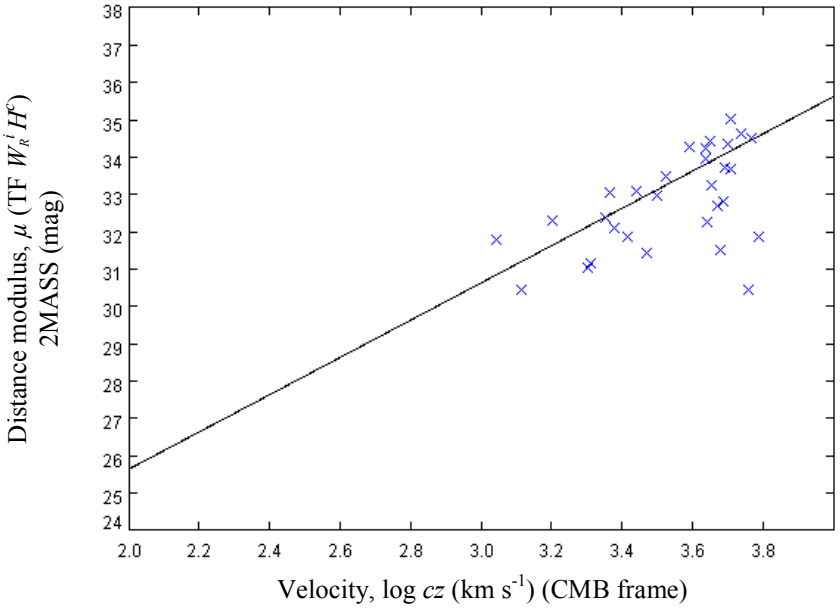

Figure 4.11: A comparison of the log *cz* (CMB frame) versus TF 2MASS H^c -band based distance modulus for 29 galaxies. The offset is -0.34 mag, with an *rms* scatter of 1.16 mag.

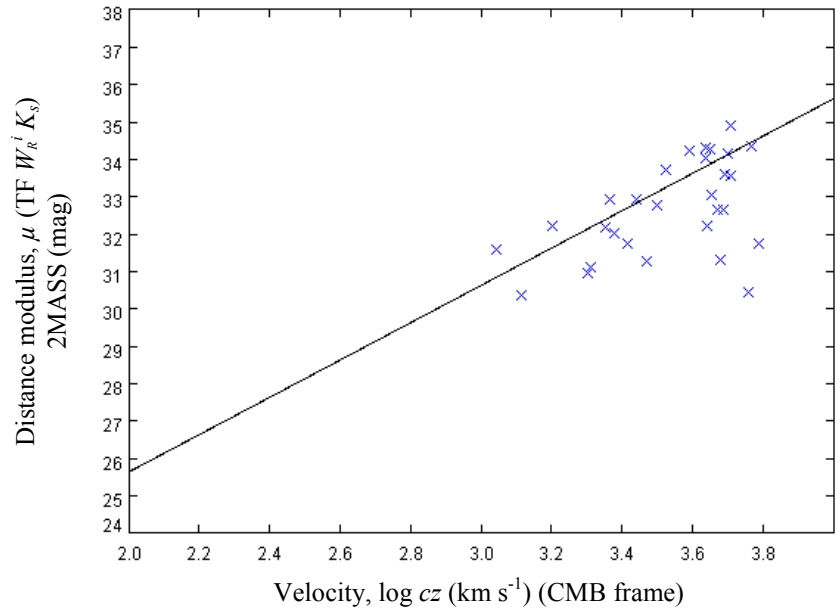

Figure 4.12: A comparison of the log *cz* (CMB frame) versus TF 2MASS K_s -band based distance modulus for 29 galaxies. The offset is -0.22 mag, with an *rms* scatter of 1.18 mag.

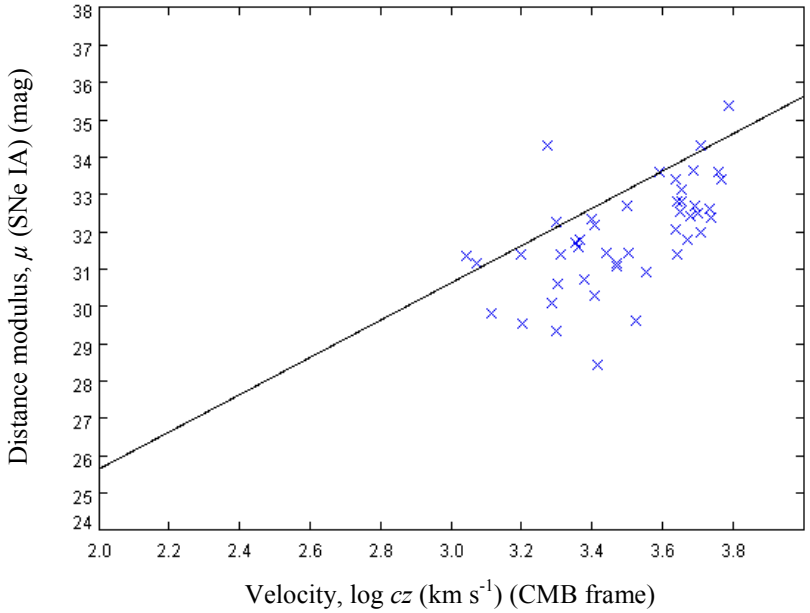

Figure 4.13: A comparison of the log *cz* (CMB frame) versus SNe Ia distance modulus for 46 galaxies. The offset is -0.62 mag, with an *rms* scatter of 1.31 mag.

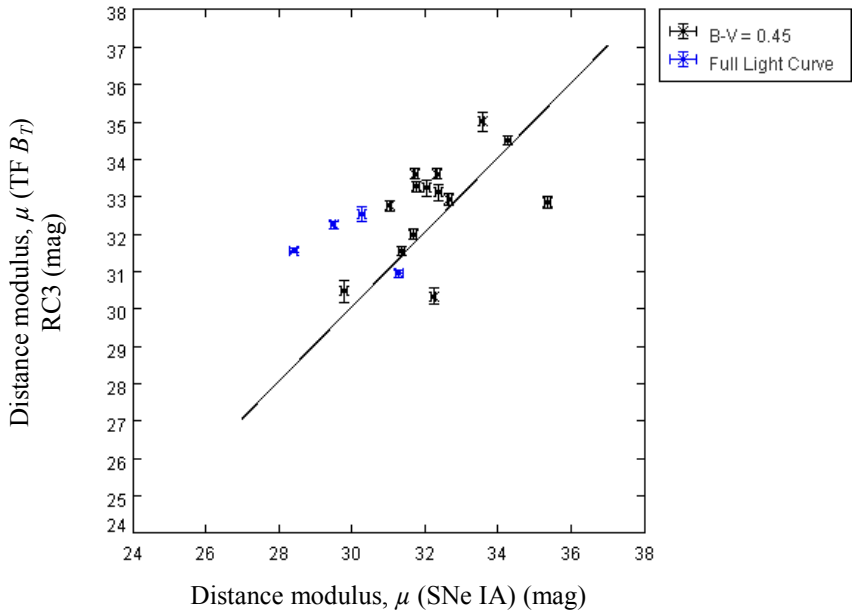

Figure 4.14: Comparison of 18 SN Ia distance moduli and RC3 B_T -band based TF results. There are 14 SNe Ia without measured B–V_{max}, so $B - V_{max} = 0.45$ was assumed; 4 SNe Ia have complete SNe Ia light curves. The reference line is through the origin with a slope = 1.000. The mean difference is 0.79 mag, with an *rms* scatter of 1.61 mag and the MAD is 0.85 mag.

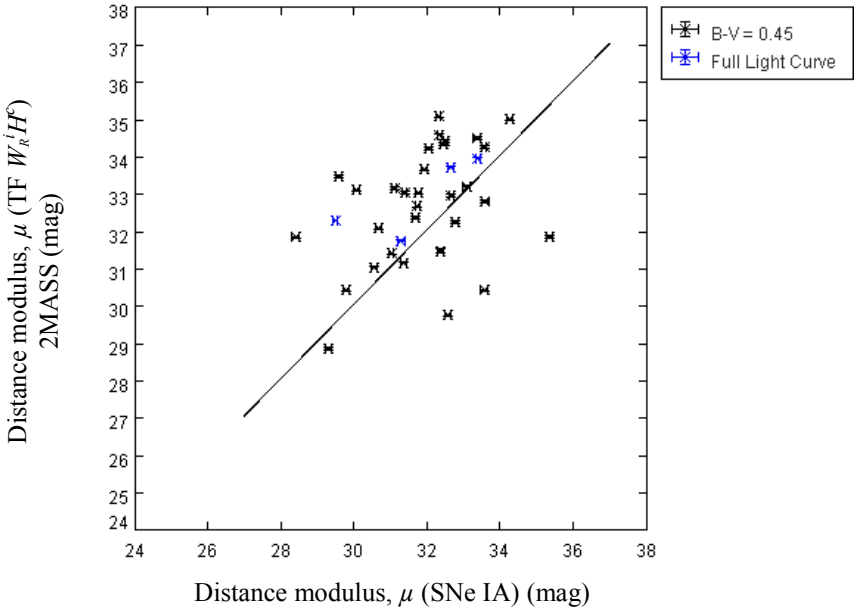

Figure 4.15: Comparison of 20 SN Ia distance moduli and the 2MASS H^c –band based TF distance moduli. 31 SNe Ia are without measured B–V_{max}, so $B-V_{max}=0.45$ was assumed; 4 SNe Ia have complete SNe Ia light curves. The reference line is through the origin with a slope = 1.000. The mean difference is -0.78 mag, with an *rms* scatter of 1.84 mag and the MAD is 0.68 mag.

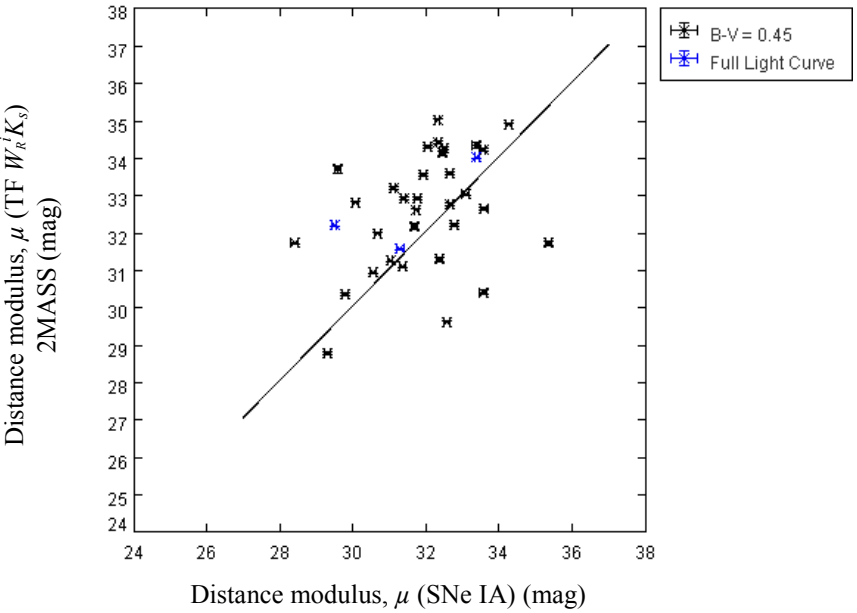

Figure 4.16: Comparison of 20 SN Ia distance moduli and the 2MASS K_s -band based TF distance moduli. 32 SNe Ia are without measured B–V_{max}, so $B-V_{max}=0.45$ was assumed; 3 SNe Ia have complete SNe Ia light curves. The reference line is through the origin with a slope = 1.000. The mean difference is -0.68 mag, with an *rms* scatter of 1.81 mag and the MAD is 0.69 mag.

Table 4.4: The Parkes Sample

1	2	3	4	5	6	7	8	9	10	11	12	13	14	15	16
	Galaxy				SNe Ia										
GALAXY	J2000 Epoch				J2000 Epoch		21 cm			z		W_{20}		W_{50}	
NAME	RA	DEC	TYPE	SN Ia	RA	DEC	km s^{-1}	σ	$E(B-V)$	z	σ	km s^{-1}	σ	km s^{-1}	σ
ESO															
404-G12	21 57 07.2	-34 34 56	SABc	2004eq	21 57 09.4	-34 34 51	2643	7	0.022	0.008843	0.000010	…	..	218	…
478-G6	02 09 18.1	-23 24 54	Sbc	2003em	02 09 20.2	-23 24 53	5176	9	0.017	0.017265	0.000030	…	…	359	…
IC 603	10 19 25.0	-05 39 22	SBa	2002jm	10 19 25.2	-05 39 15	5400	61	0.051	0.018012	0.000203	…	…	148	…
IC 1151	15 58 32.3	17 26 30	SBc	1991M	15 58 34.8	17 27 29	2169	6	0.038	0.007235	0.000004	249	6	230	6
IC 4221	13 18 30.3	-14 36 32	SAc	2002bs	13 18 30.3	-14 36 32	2895	5	0.082	0.009637	0.000010	…	…	…	…
IC 4758	18 46 18.3	-65 45 24	Sc	2001cn	18 46 17.8	-65 45 42	4647	25	0.059	0.015114	0.000150	…	…	228	…
IC 4769	18 47 44.0	-63 09 25	SBbc	2004ac	18 47 43.7	-63 08 55	4534	10	0.108	0.015124	0.000033	…	…	298	…
MCG															
-01-02-001	00 20 00.0	-06 20 02	Sbab	1999cw	00 20 01.4	-06 20 04	3709	4	0.036	0.012372	0.000013	…	…	286	…
-01-30-011	11 36 48.8	-08 35 11	SAb	2001L	11 36 48.8	-08 35 07	4567	37	0.035	0.015234	0.000003	…	…	425	…
-02-16-002	06 04 34.9	-12 37 29	Sb	2003kf	06 04 35.4	-12 37 43	2220	6	0.316	0.007388	0.000017	…	…	256	…
-03-11-019	04 16 12.5	-16 45 02	SBdm	2004ea	04 16 13.2	-16 45 20	1955	7	0.036	0.006514	0.000007	…	…	173	…
-05-16-021	06 45 46.7	-31 13 49	Sc	2004S	06 45 43.5	-31 13 52	2787	6	0.101	0.009360	0.000013	…	…	78	…
-05-25-032	10 39 25.0	-27 54 45	SBbc	2004gi	10 39 23.3	-27 54 40	3244	10	0.060	0.010821	0.000003	..	…	83	…
00-32-001	12 19 40.3	02 04 50	SBbc	1987D	12 19 41.0	02 04 26	2217	40	0.024	0.007395	0.000133	…	…	168	…
NGC 706	01 51 50.5	06 17 49	Sbc	2001ed	01 51 51.1	06 17 27	4984	7	0.058	0.016611	0.000017	313	10	288	8
NGC 936	02 27 37.4	-01 09 23	SB	2003gs	02 27 38.3	-01 09 35	1204	13	0.035	0.004770	0.000014	500	6	519	…
NGC 958	02 30 42.8	-02 56 20	SBc	2005A	02 30 43.2	-02 56 20	5739	7	0.030	0.019143	0.000022	591	34	560	25
NGC 977	02 33 03.4	-10 45 36	SABa	1976J	02 33 02.8	10 45 51	4579	11	0.027	0.015274	0.000037	…	…	316	…
NGC 1302	03 19 51.2	-26 03 38	SABa	2003if	03 19 52.6	-26 03 51	1703	5	0.021	0.005704	0.000010	103	6	94	5
NGC 1309	03 22 06.5	-15 24 00	SAbc	2002fk	03 22 05.7	-15 24 03	2136	5	0.040	0.007125	0.000013	142	4	124	5
NGC 1448	03 44 31.9	-44 38 41	SAcd	2001el	03 44 30.6	-44 38 23	1167	5	0.014	0.003896	0.000007	405	5	392	6
NGC 1559	04 17 35.8	-62 47 01	SBcd	2005df	04 17 37.8	-62 46 10	1301	5	0.030	0.004350	0.000013	296	5	257	7
NGC 2466	07 45 16.0	-71 24 38	SAc	2003gh	07 45 17.9	-71 24 37	5364	9	0.165	0.017722	0.000020	172	12	131	…
NGC 3169	10 14 15.0	03 27 58	SAa	2003cg	10 14 16.0	03 28 02	1221	5	0.031	0.004130	0.000013	508	5	431	25
NGC 3450	10 48 03.6	-20 50 57	SBb	2005as	10 48 03.5	-20 50 57	4027	4	0.055	0.013433	0.000013	…	…	279	…
NGC 3905	11 49 04.9	-09 43 47	SBc	2001E	11 49 05.0	09 44 11	5774	7	0.039	0.019260	0.000023	266	9	213	…

Table 4.4: End

1	2	3	4	5	6	7	8	9	10	11	12	13	14	15	16
	Galaxy				SN Ia										
GALAXY	J2000 Epoch				J2000 Epoch		21 cm			z		W_{20}		W_{50}	
NAME	RA	DEC	TYPE	SN Ia	RA	DEC	km s^{-1}	σ	$E(B-V)$	z	σ	km s^{-1}	σ	km s^{-1}	σ
NGC 4045	12 02 42.2	01 58 36	SABa	1985B	12 02 44.0	01 58 45	1981	6	0.023	0.006591	0.000010	324	7	302	7
NGC 4501	12 31 59.1	14 25 13	SAb	1999cl	12 31 56.0	14 25 35	2281	7	0.038	0.007609	0.000010	532	5	506	4
NGC 4679	12 47 30.2	-39 34 15	SAbc	2001cz	12 47 30.2	-39 34 48	4648	10	0.091	0.015489	0.000026	419	12	404	9
NGC 4981	13 08 48.7	-06 46 39	SABbc	1968I	13 08 49.3	-06 46 40	1678	5	0.042	0.005604	0.000013	265	9	250	11
NGC 5054	13 16 58.5	-16 38 05	SAbc	2004ab	13 16 58.2	-16 37 53	1746	10	0.082	0.005807	0.000020	340	7	321	8
NGC 5746	14 44 55.9	01 57 18	SABb	1983P	14 44 56.0	01 57 12	1720	4	0.040	0.005751	0.000033	652	4	629	5
NGC 6492	18 02 48.3	-66 25 50	SABb	2004fv	18 02 46.4	-66 25 55	4282	40	0.062	0.014482	0.000026	…	…	516	6
NGC 6708	18 55 35.6	-53 43 24	Sb	2004do	18 55 33.7	-53 43 23	2579	13	0.070	0.008603	0.000043	…	…	369	7
NGC 6754	19 11 25.7	-50 38 31	SABbc	2000do	19 11 26.2	-50 38 25	3254	10	0.070	0.010864	0.000033	407	12	377	9
NGC 6901	20 22 21.5	06 25 47	SBab	2004da	20 22 21.2	06 25 50	4761	25	0.123	0.015881	0.000083	…	…	381	6
NGC 6907	20 25 06.6	-24 48 34	SBbc	2004bv	20 25 06.3	-24 48 54	3182	5	0.064	0.010614	0.000013	384	8	284	11
NGC 6962	20 47 19.1	00 19 15	SABab	2003dt	20 47 17.5	00 18 43	4221	6	0.098	0.014046	0.000020	503	9	463	8
NGC 7107	21 42 26.5	-44 47 25	SBcd	2005dc	21 42 22.6	-44 47 21	2205	6	0.025	0.007354	0.000019	100	16	85	12
NGC 7400	22 54 20.8	-45 20 49	SABb	2002ge	22 54 21.5	-45 20 27	3002	6	0.013	0.010012	0.000020	…	…	300	5
NGC 7780	23 53 32.2	08 07 05	Sab	2001da	23 53 32.8	08 07 03	5155	60	0.055	0.017195	0.000193	…	…	185	4
NGC 7782	23 53 53.9	07 58 14	SAb	2003gl	23 53 54.0	07 57 24	5379	7	0.050	0.017942	0.000023	570	18	568	8
UGC 52	00 06 49.5	08 37 43	SAc	2002hw	00 06 49.0	08 37 49	5255	9	0.111	0.017535	0.000007	…	…	225	4
UGC 5100	09 34 38.6	05 50 29	SBb	2002au	09 34 37.6	05 50 16	5514	10	0.038	0.018393	0.000033	…	…	344	7
UGC 10743	17 11 30.7	07 59 41	Sa	2002er	17 11 29.9	07 59 45	2569	7	0.157	0.008569	0.000023	245	…	…	…
UGC 11816	21 49 07.3	00 26 50	SBc	2004ey	21 49 07.8	00 26 39	4750	7	0.130	0.015786	0.000022	137	6	114	7

Table 4.4: Column Description and References

Column 1. Galaxy name

Column 2. Galaxy J2000 Epoch coordinates for right ascension

Column 3. Galaxy J2000 Epoch coordinates for declination

Column 4. Galaxy morphology classification

Column 5. Type Ia Supernova (SN Ia) name

Column 6. SN Ia J2000 Epoch coordinates for right ascension

Column 7. SN Ia J2000 Epoch coordinates for declination

Column 8. 21 cm barycentric velocity in km s^{-1}

Column 9. Velocity uncertainty in km s^{-1}

Column 10. Reddening extinction $E(B-V)$

Column 11. Redshift

Column 12. Redshift uncertainty

Column 13. W_{20} in km s^{-1}

Column 14. Velocity uncertainty in km s^{-1}

Column 15. W_{50} in km s^{-1}

Column 16. Velocity uncertainty in km s^{-1}

Reference for columns 2 and 3. NED J2000 Epoch

Reference for column 4. NED

Reference for columns 6 and 7. NED J2000 Epoch

Reference for columns 8 through 12. NED

Reference for columns 13 and 14. RC3 (de Vaucouleurs et al. 1991 RC3)

Reference for columns 15 and 16. HyperLeda, Paturel et al. (2003)

Table 4.5: *B*-band photometry data for the SNe Ia, and Galaxy Apparent Magnitudes, B_T, H^c, and K_s, for the Parkes 46 galaxy sample

1	2	3	4	5	6	7	8	9	10	11	12	13	14	15	16	17	18
GALAXY			SNe Ia					B_T *Total*				H^c Total			K_s Total		2MASS
NAME		B	$\Delta m_{15}(B)$	$B-V_{max}$	ref	$E(B-V)$	B_T	σ	b/a	B^{bik}	H	σ	$H^{c\,bik}$	K_s	σ	$K_s{}^{bik}$	b/a
ESO																	
404-G12	2004eq	13.40	0.70	…	10	0.022	…	…	…	…	9.763	0.021	9.74	9.457	0.031	9.43	0.900
478-G6	2003em	14.70	0.80	…	10	0.017	…	..	…	…	9.888	0.021	9.85	9.582	0.026	9.50	0.620
IC 603	2002jm	16.50	…	…	10	0.051	…	…	…	…	10.656	0.034	10.61	10.431	0.055	10.39	0.620
IC 1151	1991M	14.60	…	…	4	0.038	13.49	0.13	0.351	12.78	10.769	0.043	10.75	10.412	0.084	10.32	0.500
IC 4221	2002bs	14.10	0.40	…	10	0.082	…	…	…	…	10.471	0.033	10.45	10.271	0.060	10.20	0.520
IC 4758	2001cn	14.80	0.90	0.25	7, 12	0.059	…	…	…	…	10.821	…	10.77	10.419	…	…	…
IC 4769	2004ac	15.80	0.43	…	10	0.108	…	…	…	…	10.540	0.028	10.49	10.152	0.033	10.06	0.480
MCG																	
-01-02-001	1999cw	14.30	0.94	0.89	1, 12	0.036	…	…	…	…	10.975	0.050	10.95	11.016	0.087	10.94	0.460
-01-30-011	2001L	15.40	…	…	10	0.035	…	…	…	…	10.246	0.023	10.21	9.916	0.036	9.74	0.260
-02-16-002	2003kf	14.30	0.80	…	10	0.316	…	…	…	…	…	…	…	…	…	…	0.220
-03-11-019	2004ea	17.20	…	…	10	0.036	…	…	…	…	13.023	0.102	13.00	13.346	0.128	13.28	…
-05-16-021	2004S	13.60	1.30	0.27	8, 12	0.101	…	…	…	…	11.251	…	11.19	10.966	…	…	…
-05-25-032	2004gi	13.80	…	…	10	0.060	…	…	…	…	12.085	0.062	12.05	11.929	0.102	11.90	…
00-32-001	1987D	13.70	…	0.60	3, 12	0.024	14.90	0.20	0.275	14.35	…	…	-0.02	…	…	…	…
NGC 706	2001ed	14.50	0.80	…	10	0.058	13.20	0.13	0.741	12.68	9.823	0.026	9.79	9.518	0.031	9.50	0.680
NGC 936	2003gs	14.05	…	…	10	0.035	11.12	0.10	0.871	10.77	7.140	0.016	7.13	6.913	0.017	6.87	0.825
NGC 958	2005A	15.10	0.80	…	10	0.030	12.89	0.13	0.347	11.66	9.105	0.013	9.07	8.800	0.020	8.64	0.420
NGC 977	1976J	14.80	0.90	-0.10	9, 13	0.027	…	…	…	…	10.580	0.023	10.55	10.397	0.038	10.36	0.720
NGC 1302	2003if	14.30	…	…	10	0.021	11.60	0.13	0.955	11.46	8.029	0.020	8.02	7.827	0.030	7.81	0.820
NGC 1309	2002fk	12.45	1.00	…	13	0.040	11.97	0.13	0.933	11.73	9.379	0.020	9.36	9.102	0.030	9.08	0.820
NGC 1448	2001el	12.70	…	0.08	5, 11	0.014	11.40	0.13	0.224	10.18	7.944	0.016	7.93	7.660	0.017	7.49	0.264
NGC 1559	2005df	12.50	0.70	…	10	0.030	11.00	0.30	0.575	10.50	8.279	0.017	8.26	8.018	0.026	7.96	0.520
NGC 2466	2003gh	15.50	…	…	10	0.165	13.54	0.13	0.891	12.72	9.946	0.040	9.89	9.604	0.053	9.53	0.880

Table 4.5: End

1	2	3	4	5	6	7	8	9	10	11	12	13	14	15	16	17	18
GALAXY			SNe Ia					B_T *Total*			H^c Total				K_s Total		2MASS
NAME		B	$\Delta m_{15}(B)$	$B-V_{max}$	ref	$E(B-V)$	B_T	σ	b/a	B^{bik}	H^c	σ	$H^{c\ bik}$	K_s	σ	$K_s{}^{bik}$	b/a
NGC 3169	2003cg	14.30	…	0.90	12, 13	0.031	11.08	0.10	0.633	10.47	7.564	0.016	7.21	7.283	0.017	7.21	0.660
NGC 3450	2005as	13.90	0.89	…	10	0.055	…	…	…	…	8.784	0.033	8.46	8.501	0.045	8.46	0.920
NGC 3905	2001E	16.60	…	…	3	0.039	13.38	0.16	0.724	12.97	10.251	0.039	9.84	9.884	0.070	9.84	0.740
NGC 4045	1985B	13.00	…	…	3	0.023	12.79	0.13	0.692	12.37	9.070	0.019	8.70	8.751	0.027	8.70	0.940
NGC 4501	1999cl	14.11	1.19	1.20	11	0.038	10.36	0.04	0.537	9.56	6.560	0.016	6.17	6.267	0.016	6.17	0.560
NGC 4679	2001cz	14.50	1.05	0.20	5, 12	0.091	…	…	…	…	9.722	0.020	9.28	9.419	0.032	9.28	0.420
NGC 4981	1968I	13.50	…	…	2	0.042	…	…	...	…	8.793	0.019	8.44	8.487	0.033	8.44	0.640
NGC 5054	2004ab	14.30	…	…	10	0.082	11.67	0.13	0.575	10.89	7.823	0.017	7.50	7.589	0.020	7.50	0.630
NGC 5746	1983P	13.00	…	…	3	0.040	11.29	0.13	0.178	9.32	7.169	0.015	6.61	6.878	0.016	6.61	0.220
NGC 6492	2004fv	14.80	0.78	…	10	0.062	12.30	0.20	0.490	11.30	8.960	0.024	8.73	8.847	0.031	8.73	0.540
NGC 6708	2004do	15.10	1.00	…	10	0.070	…	…	…	…	10.318	0.034	9.98	10.044	0.040	9.98	0.920
NGC 6754	2000do	15.60	…	…	3	0.070	12.89	0.15	0.490	11.96	9.252	0.034	8.75	8.856	0.040	8.75	0.420
NGC 6901	2004da	15.20	0.70	…	10	0.123	…	…	…	…	10.815	0.037	10.34	10.480	0.049	10.34	0.320
NGC 6907	2004bv	13.90	1.00	…	10	0.064	11.90	0.14	0.813	11.39	8.667	0.017	8.25	8.301	0.022	8.25	0.620
NGC 6962	2003dt	16.50	…	…	10	0.098	13.00	0.25	0.794	12.27	9.063	0.028	8.71	8.786	0.031	8.71	0.760
NGC 7107	2005dc	15.10	1.00	…	10	0.025	13.30	0.20	0.741	13.12	…	…	…	…	…	…	…
NGC 7400	2002ge	14.10	0.70	…	10	0.013	…	…	…	…	10.375	0.034	9.99	10.134	0.049	9.99	0.400
NGC 7780	2001da	15.40	…	…	10	0.055	14.80	0.20	0.537	14.25	10.885	0.046	10.45	10.506	0.058	10.45	0.520
NGC 7782	2003gl	17.20	…	…	10	0.050	13.08	0.13	0.537	12.17	9.323	0.023	8.93	9.039	0.030	8.93	0.520
UGC 52	2002hw	16.40	0.90	…	10	0.111	…	…	…	…	10.772	0.055	10.35	10.405	0.069	10.35	0.800
UGC 5100	2002au	16.30	…	…	10	0.038	…	…	…	…	11.341	0.057	10.88	10.956	0.083	10.88	0.320
UGC 10743	2002er	13.90	1.33	0.12	9, 12	0.157	…	…	…	…	10.611	0.029	10.24	10.375	0.043	10.24	0.320
UGC 11816	2004ey	14.60	…	…	10	0.130	…	…	…	…	11.537	0.068	11.40	11.451	0.106	11.40	…

Table 4.5: Column Description and References

Column 1. Galaxy name

Column 2. Type Ia Supernova (SN Ia) name

Column 3. SN Ia *B*-band peak apparent magnitude

Column 4. SN Ia $\Delta m_{15}(B)$

Column 5. SN Ia $B_{max} - V_{max}$ at peak apparent magnitude

Column 6. Reference for SN Ia data

Column 7. Extinction reddening

Column 8. RC3 B_T apparent magnitude where B_T is the total observed magnitude

Column 9. RC 3 B_T uncertainty

Column 10. *B*-band galaxy *b/a* axis ratio

Column 11. RC3 B_T apparent magnitude adjusted for reddening and includes the corrections $B^{b,i,k} = B_T - A_B{}^b - A_B{}^{i\text{-}o\text{-}} - A_B{}^k$

Column 12. H^c -band-total near-infrared magnitude

Column 13. H^c-band-total near-infrared magnitude uncertainty

Column 14. *H*-band-total near-infrared magnitude corrected for galactic extinction and redshift *z, (bik)*

Column 15. K_s-band-total near-infrared magnitude

Column 16. K_s-band-total near-infrared magnitude uncertainty

Column 17. K_s-band-total near-infrared apparent magnitude adjusted for reddening and includes the corrections $K_s{}^{b,i,k} = K_s - A_K{}^b - A_K{}^{i\text{-}o\text{-}}$

Column 18. 2MASS co-added bands *JHK* axis ratio

Reference for columns 3 through 5.

1-Bufano et al. (2005)
2-Casebeer et al. (2000)
3-CfA (2008)
4-Hölfich and Khokhlov (1996)
5-Jha (2002)
6-Krisciunas et al. (2003)
7-Krisciunas et al. (2004)
8-Misra et al. (2005)
9-Patat et al. (1997)
10-Pelle (2008)
11-Reindl et al. (2005)
12-SAI (2008)
13-Tammann and Sandage (1995)
14-Wang et al. (2005)

Reference for column 7. NED

Reference for columns 8 through 10. RC3 (de Vaucouleurs et al. 1991 RC3)

Reference for columns 11 through 17. Calculations made using calibration equations from § 2

Reference for column 18. 2MASS

Table 4.6: New Uncorrected Observation Data for the Parkes Sample from Table 4.1

1	2	3	4	5	6	7	8	9	10	11	12	13
GALAXY	W_{20}		W_{50}		21 cm				Peak	mean		
NAME	km s^{-1}	σ	km s^{-1}	σ	km s^{-1}	σ	z	σ	S/N	S/N	Jy km s^{-1}	Cat
ESO												
404-G12	233	6	218	3	2649	3	0.008843	0.000013	18.06	7.42	9.844	1
478-G6	391	16	359	9	5328	4	0.017786	0.000027	16.24	6.30	10.250	2
IC 603	158	31	148	29	5188	5	0.018344	0.000028	5.73	3.08	2.667	3
IC 1151	248	3	230	4	2169	6	0.007288	0.000011	16.37	8.73	9.900	1
IC 4221	237	27	…	…	2902	7	0.009751	0.000015	20.17	9.76	9.905	4
IC 4758	253	12	228	6	4488	7	0.015745	0.000024	9.03	4.48	2.700	3
IC 4769	342	10	298	5	4532	3	0.015243	0.000023	44.74	14.89	14.246	2
MCG												
-01-02-001	296	27	286	6	3711	4	0.012373	0.000019	9.56	4.47	3.915	3
-01-30-011	449	14	425	10	4626	4	0.015470	0.000023	12.82	5.04	5.264	3
-02-16-002	267	9	256	4	2211	3	0.007389	0.000011	18.58	10.27	19.998	1
-03-11-019	190	8	173	4	1951	3	0.006515	0.000010	17.65	10.76	9.944	1
-05-16-021	145	11	78	4	2786	4	0.009110	0.000014	32.41	12.27	8.683	4
-05-25-032	100	18	83	13	3231	2	0.010821	0.000016	11.11	5.35	1.826	3
00-32-001	194	11	168	10	2208	4	0.007451	0.000011	9.70	6.03	2.518	3
NGC 706	303	13	288	6	4995	4	0.016612	0.000025	7.55	3.59	4.247	3
NGC 936	565	10	519	5	1434	3	0.004771	0.000007	16.88	7.97	15.374	1
NGC 958	609	9	560	5	5737	4	0.019141	0.000029	26.17	14.22	30.595	1
NGC 977	372	29	316	25	4585	21	0.015275	0.000023	17.01	8.59	10.464	3
NGC 1302	115	8	94	6	1706	3	0.005705	0.000009	32.84	15.25	16.310	1
NGC 1309	156	3	124	2	2137	2	0.007126	0.000011	42.93	25.82	29.791	1
NGC 1448	411	2	392	2	1168	1	0.003897	0.000006	92.88	49.05	143.639	1

Table 4.6: Continued

1	2	3	4	5	6	7	8	9	10	11	12	13
GALAXY	W_{20}		W_{50}				21 cm		Peak	mean		
NAME	km s^{-1}	σ	km s^{-1}	σ	km s^{-1}	σ	z	σ	S/N	S/N	Jy km s^{-1}	Cat
NGC 1559	288	3	257	2	1296	2	0.004350	0.000007	44.77	27.65	53.869	4
NGC 2466	170	9	131	6	5355	5	0.017723	0.000027	25.36	15.52	13.607	1
NGC 3169	495	3	431	2	1224	2	0.004225	0.000006	82.80	46.88	112.380	1
NGC 3450	290	11	279	8	4036	5	0.013433	0.000020	11.15	4.55	6.231	2
NGC 3905	241	5	213	3	5757	3	0.019490	0.000029	20.60	8.97	7.543	1
NGC 4045	330	4	302	3	1981	3	0.006652	0.000010	24.76	11.48	21.280	1
NGC 4501	529	9	506	6	2281	3	0.007668	0.000012	25.46	12.90	31.136	1
NGC 4679	423	11	404	8	4646	3	0.015983	0.000024	20.19	8.43	15.206	2
NGC 4981	269	3	250	2	1678	2	0.005640	0.000008	38.66	23.91	29.886	1
NGC 5054	336	4	321	3	1742	2	0.006011	0.000009	22.07	14.17	22.877	1
NGC 5746	646	4	629	3	1722	2	0.005785	0.000009	24.84	10.20	27.350	1
NGC 6492	539	9	516	6	4338	4	0.014454	0.000022	17.81	7.27	16.493	1
NGC 6708	375	11	340	8	2686	6	0.008603	0.000013	25.69	10.39	16.455	2
NGC 6754	419	11	377	10	3240	8	0.010865	0.000016	12.73	7.27	8.994	3
NGC 6901	396	12	381	10	4795	9	0.015992	0.000024	8.40	3.63	6.257	3
NGC 6907	370	11	284	8	3177	8	0.010545	0.000016	36.91	20.76	51.979	1
NGC 6962	490	13	463	15	4214	5	0.014395	0.000022	20.41	6.77	12.130	1
NGC 7107	106	10	85	3	2202	3	0.007352	0.000011	23.54	12.92	8.720	1
NGC 7400	325	8	300	3	3001	3	0.010011	0.000015	22.71	10.82	21.575	1
NGC 7780	198	9	185	7	5352	4	0.017196	0.000026	10.92	6.09	4.218	1
NGC 7782	586	11	568	9	5381	4	0.017943	0.000027	14.70	4.80	10.345	3

Table 4.6: End

1	2	3	4	5	6	7	8	9	10	11	12	13
GALAXY	W_{20}		W_{50}		21 cm				Peak	mean		
NAME	km s^{-1}	σ	km s^{-1}	σ	km s^{-1}	σ	z	σ	S/N	S/N	Jy km s^{-1}	Cat
UGC 52	267	34	225	32	5302	8	0.017536	0.000026	13.35	5.84	8.921	3
UGC 5100	359	21	344	18	5507	4	0.018738	0.000028	9.71	4.70	4.221	3
UGC 10743	262	37	…	…	2596	4	0.009146	0.000014	9.43	4.71	3.416	3
UGC 11816	133	6	114	5	4738	4	0.015845	0.000024	19.98	12.60	11.724	2

Column 1. Galaxy name
Column 2. W_{20} in km s^{-1}
Column 3. Velocity uncertainty in km s^{-1}
Column 4. W_{50} in km s^{-1}
Column 5. Velocity uncertainty in km s^{-1}
Column 6. 21 cm barycentric velocity in km s^{-1}
Column 7. Velocity uncertainty in km s^{-1}
Column 8. Redshift z
Column 9. Redshift z uncertainty
Column 10. Peak signal to noise ratio S/N
Column 11. Mean S/N ratio
Column 12. Observed flux for the 21 cm measurements in Jy km s^{-1}
Column 13. Category 1 = normal double-horned profile, S/N ≥ 5, steep sides and the integration sufficient to accept the automated data reduction
Category 2 = normal double-horned profile with a noise spike, S/N ≥ 5
Category 3 = double-horned profile that is poorly defined and has a S/N < 5 and / or confusing noise
Category 4 = central peak rather than a double-horned profile

Reference for columns 2 through 13. New observations obtained with the Parkes 64 m Radio Telescope

Table 4.7: Inclination and z Corrected to W_R^i Observation Data for Parkes Sample from Table 4.6

1	2	3	4	5	6	7	8	9	10	11	12	13	14	15	16
	New Observations						GSR		Virgo infall		3K CMB			Corrected	
GALAXY	W_{20}		W_{50}		21 cm		21 cm		velocity		velocity			W_{20}^i	W_{50}^i
NAME	km s^{-1}	σ	km s^{-1}	σ	km s^{-1}	σ	km s^{-1}	σ	km s^{-1}	σ	km s^{-1}	σ	i	km s^{-1}	km s^{-1}
ESO															
404-G12	233	6	218	3	2649	3	2677	3	2598	8	2390	19	38	337	357
478-G6	391	16	359	9	5328	4	5292	9	5167	14	5108	18	59	410	418
IC 603	158	31	148	29	5188	5	5238	6	5369	64	5761	66	43	191	220
IC 1151	248	3	230	4	2169	6	2261	4	2479	17	2266	7	74	219	244
IC 4221	237	27	…	…	2902	7	2784	7	2980	22	3204	22	53	256	…
IC 4758	253	12	228	6	4488	7	4428	45	4377	46	4512	45	…	…	…
IC 4769	342	10	298	5	4532	3	4440	11	4391	13	4507	10	52	389	379
MCG															
-01-02-001	296	27	286	6	3711	4	3787	5	3688	14	3364	24	64	287	321
-01-30-011	449	14	425	10	4626	4	4492	11	4650	23	5004	28	81	410	430
-02-16-002	267	9	256	4	2211	3	2066	8	2085	12	2306	8	79	232	…
-03-11-019	190	8	173	4	1951	3	1852	5	1811	7	1881	5	74	161	185
-05-16-021	145	11	78	4	2786	4	2604	9	2607	16	2955	11	…	…	…
-05-25-032	101	18	83	13	3231	2	3040	13	3160	25	3587	26	35	141	150
00-32-001	194	11	168	10	2208	4	2125	40	2424	48	2567	47	79	161	176
NGC 706	303	13	288	6	4995	4	5041	6	4958	14	4694	21	43	399	422
NGC 936	565	10	519	5	1434	3	1446	4	1401	9	1193	17	30	…	…
NGC 958	609	9	560	5	5737	4	5745	4	5648	12	5502	18	73	587	581
NGC 977	372	29	316	25	4585	21	4562	11	4459	15	4362	19	36	585	536
NGC 1302	115	8	94	6	1706	3	1620	5	1553	8	1571	10	18	…	…
NGC 1309	156	3	124	2	2137	2	2074	2	2007	8	1984	11	22	…	…
NGC 1448	411	2	392	2	1168	1	1024	6	978	10	1102	5	84	373	399

Table 4.7: Continued

1	2	3	4	5	6	7	8	9	10	11	12	13	14	15	16
	New Observations						GSR		Virgo infall		3K CMB			Corrected	
GALAXY	W_{20}		W_{50}		21 cm		21 cm		velocity		velocity			W_{20}^{i}	W_{50}^{i}
NAME	km s^{-1}	σ	km s^{-1}	σ	km s^{-1}	σ	km s^{-1}	σ	km s^{-1}	σ	km s^{-1}	σ	i	km s^{-1}	km s^{-1}
NGC 1559	288	3	257	2	1296	2	1126	8	1090	14	1305	4	57	304	311
NGC 2466	170	9	131	6	5355	5	5102	10	5048	18	5428	10	28	…	…
NGC 3169	495	3	431	2	1224	2	1102	7	1340	24	1591	25	52	588	551
NGC 3450	290	11	279	8	4036	5	3837	9	3963	22	4385	25	28	…	…
NGC 3905	241	5	213	3	5757	3	5633	9	5779	21	6140	27	45	296	302
NGC 4045	330	4	302	3	1981	3	1875	5	2212	30	2333	25	47	410	417
NGC 4501	529	9	506	6	2281	3	2235	4	957	86	2605	23	59	575	592
NGC 4679	423	11	404	8	4646	3	4470	10	4553	21	4932	22	69	408	432
NGC 4981	269	3	250	2	1678	2	1590	5	1940	31	2005	23	43	354	371
NGC 5054	336	4	321	3	1742	2	1629	7	1904	28	2056	23	57	360	387
NGC 5746	646	4	629	3	1722	2	1723	10	2000	25	1943	18	78	619	…
NGC 6492	539	9	516	6	4338	4	4229	9	4190	13	4351	8	63	558	577
NGC 6708	399	11	369	8	2693	6	2520	13	2502	14	2520	14	43	542	543
NGC 6754	419	11	377	10	3240	8	3213	10	3181	11	3176	11	63	427	425
NGC 6901	396	12	381	10	4795	9	4934	26	4935	29	4486	31	68	382	411
NGC 6907	370	11	284	8	3177	8	3250	5	3213	7	2951	17	36	585	484
NGC 6962	490	13	463	15	4214	5	4368	9	4348	15	3913	22	38	746	747
NGC 7107	106	10	85	3	2202	3	2192	6	2122	8	1995	16	43	123	130
NGC 7400	325	8	300	3	3001	3	2974	6	2872	10	2776	17	89	…	…
NGC 7780	198	9	185	7	5352	4	5289	58	5124	60	4790	63	59	190	219
NGC 7782	586	11	568	9	5381	4	5513	9	5433	18	5014	26	59	634	658

Table 4.7: End

1	2	3	4	5	6	7	8	9	10	11	12	13	14	15	16
	New Observations						GSR		Virgo infall		3K CMB			Corrected	
GALAXY	W_{20}		W_{50}		21 cm		21 cm		velocity		velocity			W_{20}^{i}	W_{50}^{i}
NAME	km s^{-1}	σ	km s^{-1}	σ	km s^{-1}	σ	km s^{-1}	σ	km s^{-1}	σ	km s^{-1}	σ	i	km s^{-1}	km s^{-1}
UGC 52	267	34	225	32	5302	8	5386	6	5306	17	4896	25	22	…	…
UGC 5100	359	21	344	18	5507	4	5379	11	5510	20	5843	25	54	436	424
UGC 10743	262	37	…	…	2596	4	2679	8	2825	14	2564	7	73	…	…
UGC 11816	133	6	114	5	4738	4	4886	9	4833	17	4388	25	22	…	…

Column 1. Galaxy name
Column 2. W_{20} in km s^{-1}
Column 3. Velocity uncertainty in km s^{-1}
Column 4. W_{50} in km s^{-1}
Column 5. Velocity uncertainty in km s^{-1}
Column 6. 21 cm barycentric velocity in km s^{-1}
Column 7. 21 cm barycentric velocity uncertainty in km s^{-1}
Column 8. 21 cm barycentric velocity corrected to Galactic Standard of Rest in km s^{-1}
Column 9. 21 cm barycentric velocity corrected to Galactic Standard of Rest uncertainty in km s^{-1}
Column 10. Virgo infall velocity in km s^{-1}
Column 11. Virgo infall velocity uncertainty in km s^{-1}
Column 12. 3K CMB velocity in km s^{-1}
Column 13. 3K CMB velocity uncertainty in km s^{-1}
Column 14. Inclination
Column 15 and 16. Neutral hydrogen line width velocity at 20% and 50% corrected for cosmological redshift, inclination, broadening, random and rotation motion, in km s^{-1}

Reference for columns 2 through 7. New observations obtained with the Parkes 64 m Radio Telescope
Reference for columns 8 through 14. NED

Table 4.8: Absolute Magnitude, Apparent Magnitude, and Distance Modulus for the Parkes Sample

1	2	3	4	5	6	7	8	9	10	11	12	13	14	15	16	17	18
GALAXY		Phillips Template SN Ia				Tully Template W_{20} B_T				Masters Template W_{50} H^c				Masters Template W_{50} K_s			
NAME	NAME	MB	mB	μ	σ	M_B	B_T^{bik}	μ	σ	M_H	H^{cbik}	μ	σ	M_K	K_s^{bik}	μ	σ
ESO																	
404-G12	2004eq	-19.74	11.21	30.68	0.08	-21.18	…	…	…	-23.14	9.74	32.88	0.02	-23.38	9.43	32.81	0.03
478-G6	2003em	-19.69	12.51	31.93	0.08	-21.75	…	…	…	-23.88	9.85	33.73	0.02	-24.13	9.50	33.63	0.03
IC 603	2002jm	-19.52	14.31	33.56	0.09	-19.60	…	…	…	-20.84	10.61	31.45	0.03	-21.06	10.39	31.45	0.06
IC 1151	1991M	-19.52	12.43	31.68	0.08	-19.98	12.78	32.76	0.13	-21.34	10.75	32.09	0.04	-21.57	10.32	31.89	0.08
IC 4221	2002bs	-19.74	11.91	31.38	0.08	-20.41	…	…	…	…	10.45	…	…	…	10.20	…	…
IC 4758	2001cn	-19.65	13.38	32.76	0.05	…	…	…	…	…	10.77	…	…	…	…	…	…
IC 4769	2004ac	-19.74	13.61	33.08	0.09	-21.60	…	…	…	-23.42	10.49	33.91	0.03	-23.66	10.06	33.72	0.03
MCG																	
-01-02-001	1999cw	-19.62	10.22	29.57	0.08	-20.73	…	…	…	-22.63	10.95	33.58	0.05	-22.87	10.94	33.81	0.09
-01-30-011	2001L	-19.52	13.21	32.46	0.08	-21.74	…	…	…	-24.02	10.21	…	…	-24.26	9.74	…	…
-02-16-002	2003kf	-19.69	12.11	31.53	0.08	-20.14	…	…	…	…	…	…	…	…	…	…	…
-03-11-019	2004ea	-19.52	15.01	34.26	0.09	-19.14	…	…	…	-20.03	13.00	33.03	0.10	-20.24	13.28	33.52	0.13
-05-16-021	2004S	-19.10	12.27	31.10	0.02	…	…	…	…	…	11.19	…	…	…	…	…	…
-05-25-032	2004gi	-19.52	11.61	30.86	0.08	-18.76	…	…	…	-18.99	12.05	31.04	0.06	-19.20	11.90	31.10	0.10
00-32-001	1987D	-19.52	10.89	30.27	0.08	-19.14	14.35	33.49	0.20	-19.79	…	…	…	-20.00	…	…	…
NGC 706	2001ed	-19.69	12.31	31.73	0.06	-21.67	12.68	34.35	0.13	-23.93	9.79	33.72	0.03	-24.17	9.50	33.67	0.03
NGC 936	2003gs	-19.52	11.86	31.11	0.06	…	10.77	…	…	…	7.13	…	…	…	6.87	…	…
NGC 958	2005A	-19.69	12.91	32.33	0.06	-22.80	11.66	34.46	0.13	-25.43	9.07	…	…	-25.69	8.64	…	…
NGC 977	1976J	-19.65	14.00	33.38	0.06	-22.79	…	…	…	-25.05	10.55	35.60	0.02	-25.30	10.36	35.66	0.04
NGC 1302	2003if	-19.52	12.11	31.36	0.08	…	11.46	…	…	…	8.02	…	…	…	7.81	…	…
NGC 1309	2002fk	-19.30	10.26	29.29	0.08	…	11.73	…	…	…	9.36	…	…	…	9.08	…	…
NGC 1448	2001el	-19.50	12.07	31.30	0.09	-21.48	10.18	31.66	0.10	-23.66	7.56	31.22	0.02	-23.91	7.49	31.40	0.02
NGC 1559	2005df	-19.74	10.31	29.78	0.08	-20.89	10.50	31.39	0.30	-22.50	8.26	…	…	-22.73	7.96	…	…
NGC 2466	2003gh	-19.52	13.31	32.56	0.08	…	12.72	…	…	…	9.89	…	…	…	9.53	…	…

Table 4.8: End

1	2	3	4	5	6	7	8	9	10	11	12	13	14	15	16	17	18
GALAXY		Phillips Template SN Ia				Tully Template W_{20} B_T				Masters Template W_{50} H^c				Masters Template W_{50} K_s			
NAME	NAME	*MB*	*mB*	μ	σ	M_B	B_T^{bik}	μ	σ	M_H	H^{cbik}	μ	σ	M_K	K_s^{bik}	μ	σ
NGC 3169	2003cg	-19.52	10.24	29.49	0.07	-22.80	10.47	33.27	0.10	-25.18	7.55	32.73	0.02	-25.44	7.21	32.65	0.02
NGC 3450	2005as	-19.66	13.40	32.79	0.08	…	…	…	…	…	8.75	…	…	…	8.46	…	…
NGC 3905	2001E	-19.52	16.10	35.35	0.09	-20.82	12.97	33.79	0.16	-22.35	10.21	32.56	0.04	-22.59	9.84	32.43	0.07
NGC 4045	1985B	-19.52	12.50	31.75	0.08	-21.75	12.37	34.12	0.13	-23.87	9.06	32.93	0.02	-24.12	8.70	32.82	0.03
NGC 4501	1999cl	-19.43	9.24	28.40	0.09	-22.73	9.56	32.29	0.04	-25.52	6.55	32.07	0.02	-25.78	6.17	31.95	0.02
NGC 4679	2001cz	-19.58	13.34	32.65	0.09	-21.73	…	…	…	-24.04	9.67	33.71	0.02	-24.29	9.28	33.57	0.03
NGC 4981	1968I	-19.52	11.31	30.56	0.08	-21.32	…	…	…	-23.32	8.78	32.10	0.02	-23.56	8.44	32.00	0.03
NGC 5054	2004ab	-19.52	12.11	31.36	0.08	-21.37	10.89	32.26	0.13	-23.52	7.81	31.33	0.02	-23.76	7.50	31.26	0.02
NGC 5746	1983P	-19.52	10.81	30.06	0.08	…	9.32	…	…	…	7.15	…	…	…	6.61	…	…
NGC 6492	2004fv	-19.70	12.61	32.04	0.08	-22.65	11.30	33.95	0.20	-25.40	8.90	34.30	0.02	-25.66	8.73	34.39	0.03
NGC 6708	2004do	-19.67	12.91	32.31	0.06	-22.56	…	…	…	-25.11	10.28	…	…	-25.37	9.98	…	…
NGC 6754	2000do	-19.52	13.41	32.66	0.06	-21.86	11.96	33.82	0.15	-23.96	9.21	…	…	-24.21	8.75	…	…
NGC 6901	2004da	-19.75	13.01	32.49	0.06	-21.54	0.00	…	…	-23.80	10.75	34.55	0.04	-24.05	10.34	34.39	0.05
NGC 6907	2004bv	-19.59	11.71	31.03	0.06	-22.78	11.39	34.17	0.14	-24.57	8.63	33.20	0.02	-24.83	8.25	33.08	0.02
NGC 6962	2003dt	-19.52	14.31	33.56	0.07	-23.51	12.27	35.78	0.25	-26.60	9.02	35.62	0.03	-26.87	8.71	35.58	0.03
NGC 7107	2005dc	-19.59	12.91	32.23	0.06	-18.38	13.12	31.50	0.20	…	…	…	…	-18.52	…	…	…
NGC 7400	2002ge	-19.74	11.91	31.38	0.06	…	…	…	…	…	10.35	…	…	…	9.99	…	…
NGC 7780	2001da	-19.42	13.21	32.36	0.07	-19.60	14.25	33.85	0.20	-20.82	10.85	31.67	0.05	-21.04	10.45	31.49	0.06
NGC 7782	2003gl	-19.52	15.01	34.26	0.09	-23.02	12.17	35.19	0.13	-26.00	9.28	35.28	0.02	-26.27	8.93	35.20	0.03
UGC 52	2002hw	-19.65	14.21	33.59	0.09	…	…	…	…	…	10.73	…	…	…	10.35	…	…
UGC 5100	2002au	-19.52	14.11	33.36	0.09	-21.66	…	…	…	-23.95	11.30	35.25	0.06	-24.20	10.88	35.08	0.08
UGC 10743	2002er	-19.32	13.09	32.14	0.08	…	…	…	…	…	10.57	…	…	…	10.24	…	…
UGC 11816	2004ey	-19.23	12.41	31.37	0.08	…	…	…	…	…	11.50	…	…	…	11.40	…	…

Table 4.8- Column Definitions and References

Column 1. Galaxy name

Column 2. Type Ia Supernova (SN Ia) name

Column 3. SN Ia absolute magnitude

Column 4. SN Ia apparent magnitude

Column 5. SN Ia distance modulus reduced by 0.27 for the Cepheid zero point

Column 6. SN Ia distance modulus uncertainty

Columns 7 through 18. $W_R{}^i$ absolute magnitude, apparent magnitude, and distance modulus with uncertainty for bands B_T, H^c and K_s

Reference for columns 3 through 6. Calculations made using Phillips et al. (1999) $\Delta m_{15}(B)$ decline rate relation

Reference for columns 7 through 18. Calculations made using the calibration equations from § 2

REFERENCES

Barnes, D. G., Staveley-Smith, L., & Ye, T., Oosterloo, T. 1998, in ASP Conf. Ser. 145, Robust, Realtime Bandpass Removal for the HI Parkes All Sky Survey Project using AIPS++, ed. R. Albrecht, R. N. Hook, & H. A. Bushouse (San Francisco: ASP)

Bufano, F., Turatto, M., Benetti, S., Harutyunyan, A., Elias de LaRosa, N., & Cappellaro, E. 2005, ASPC, 342, 255

Casebeer, D., Branch, D., Blaylock, M., Millard, J., Baron, E., Richardson, D., & Archeta, C. 2000, PASP, 112, 1433

CfA 2008, Supernova (Cambridge: Harvard University)

de Vaucouleurs, G., de Vaucouleurs, A., Corwin, H. G., Jr., Buta, R. J., Pautrel, G., & Fouqué, P. 1991, Third Reference Catalogue of Bright Galaxies (New York: Springer) (RC3)

Donley, J. L., Staveley-Smith, L., Kraan-Kerteweg, R. C., Islas-Islas, J. M., Schröder, A., Henning, P. A., Koribalski, B., Mader, S., & Stewart, I. 2005, AJ, 129, 220

Hölfich, P., & Khokhlou, A. 1996, ApJ, 457, 500

Jha, S. 2002, Exploding Stars, Near and Far, PhD Thesis (Cambridge: Harvard University)

Krisciunas, R., Suntzeff, N. B., Cardin, P., Arenas, J., Espinoza, J., Gonzalez, D., Gonzalez, S., Hölfich, P., Landelt, A. U., Phillips, M. M., & Pizarro, S. 2003, AJ, 125, 166

Krisciunas, K., Suntzeff, N. B., Phillips, M. M., Candia, P., Prieto, J. J., Antezana, R., Chassagne, R., Chen, H. W., Dicknson, M., Eisenhardt, P. R., Espinoza, J., Garnavich, P. M., Gonzales, D., Harrison, T. E., Hamuy, M., Ivanov, V. D., Krzeminski, W., Kulesa, C., McCarthy, P., Moro-Martin, A., Muena, C., Noriega-Crespo, A., Persson. S. E., Pinto, P. A., Roth, M., Rubenstein, E. P., Standford, S. A., Stringfellow, G. S., Zapata, A., Porter, A., & Wischnjewsky, M. 2004, AJ, 128, 3034

MacA. Thomas, B., Graves, G. R., Staveley-Smith, L., Kesteven, M. J., & Price, R. M. 1998, CSIRO ATNF, Technical Report 39.3/084

Meyer, M. J., Zwaan, M. A., Webster, R. L., Staveley-Smith, L., Ryan-Weber, E., Drinkwater, M. J., Barnes, D. G., Howlett, M., Kilborn, V. A., Stevens, J., Waugh, M., Pierce, M. J., Bhatal, R., de Blok, W. J. G., Disney, M. J., Ekers, R. D., Freeman, K. C., Garcia, D. A., Gibson, B. K., Harnett, J., Henning, P. A., Jerjen, H., Kesteven, M. J., Knezek, P. M., Koribalski, B. S., Mader, S., Marquarding, M., Minchin, R. F., O'Brien, J., Oosterloo, T., Price, R. M., Putman, M. E., Ryder, S. D., Sadler, E. M., Stewart, I. M., Stootman, F., & Wright, A. E. 2004, MNRAS, 350, 1195

Misra, K., Kamble, A. P., Bhattacharya, D., & Sagar, R. 2005, MNRAS, 360, 662

NED – NASA/IPAC Extragalactic Database – http://ned.ipac.caltech.edu/

Padman, R. 1977, PASAu, 3, 111

Patat, F., Bardon, R., Cappellaro, E., & Turatto, M. 1997, A&A, 317, 423

Paturel, G., Petit, C., Prugniel, Ph., Theureau, G., Rousseau, J., Brouty, M., Dubois, P., & Cambrésy, L. 2003, A&A, 412, 45

Pelle, J. C. 2008, Supernovae, URL

Phillips, M. M., Lira, P., Suntzeff, N. B., Schommer, R. A., Hamuy, M., & Maza, J. 1999, AJ, 118, 1766

Reindl, B., Tammann, G. A., Sandage, A., & Saha, A. 2005, ApJ, 624, 532

Reynolds, J. 2006, private communication (Parkes: CSIRO ATNF)

Riess, A. G., Li, W., Stetson, P. B., Filippenko, A. V., Jha, S., Kirshner, R. P., Challis, P. M., Garnavich, P. M., & Chornock, R. 2005, ApJ, 627, 579

Roth, J., Mould, J., & Staveley-Smith, L. 1994 AJ, 108, 851

Staveley-Smith, L., Wilson, W. E., Bird, T. S., Disney, M. J., Ekers, R. D., Freeman, K. C., Haynes, R. F., Sinclair, M. W., Vaile, R. A., Webster, R. L., & Wright, A. E. 1996, PASA, 13, 243

Sternberg Astronomical Institute (SAI) 2008, Supernova Catalogue (Moscow: Moscow University)

Tammann, G. A., & Sandage, A. 1995, ApJ, 452, 16

2MASS – www.ipac.caltech.edu/2mass/releases/allsky/

Wang, X. F., Zhou, X., Zhang, T. M., & Li, Z. W. 2005, ASPC, 342, 272

CHAPTER 5
PARKES / NTT SAMPLE
NEW NIR AND 21 CM LINE WIDTH VELOCITY MEASUREMENTS

5.1 The Parkes / NTT Sample

This chapter contains new infrared and radio observations for 88 SNe Ia host galaxies. New NIR observations were made for the galaxies for bands H and K_s at the ESO (European Southern Observatory) La Silla observatory (Grosbøl 2008 priv. comm.). The observations were accomplished in June 1999, May 2000, and November 2000. The observations and data reduction yielded good photometric measurements and more precise inclination values than before. The observations were made with the 3.5 m New Technology Telescope (NTT) using Son of Isaac (SOFI). SOFI is the infrared spectrograph and imaging camera on the NTT. The largest field of view is 4.92 arcmin, and it covers the 0.9-2.5 micron wavelength range with spectral resolution between 0.4 and 4.0 nm. SOFI was equipped with a 1024 x 1024 Hawaii HgCdTe detector. The detector filters included the NIR wavelength J with a central wavelength $1.247\mu m$, H with a central wavelength $1.653\mu m$, and K_s with a central wavelength $2.162\mu m$, (Pierce-Price 2008).

Observations with a varying sky at NIR wavelengths and bad pixels required multiple exposures of each galaxy. The NIR exposures were made using a jitter pattern with 10" offsets frequently interleaved with sky fields around 10' from the galaxy. Bright or extended sources were avoided with the total exposure times of 4^m and 10^m for H and K filters respectively. Standard stars were observed several times during the observing period to establish colour transformations and extinction coefficients. The reduction of standard stars in the transformation to the standard system resulted in errors of 0.02 mag for all colour bands. Grosbøl et al. (2004) determined that the K-band maps better represent the mass distribution in the galaxies and are less affected by the irregular distribution of young objects versus images taken at shorter wavelengths. They applied numerous methods to estimate the inclination of disk galaxies using the surface brightness distribution by presuming the galaxy disks are flat and thin. The methods ranged from a computation of the aspect ratio of the disks at a specified surface brightness level, to fitting of 2D models and Fourier analyses.

New 21 cm line width velocity measurements were made using the CSIRO ATNF 64 m Parkes Radio Telescope for a 51-galaxy sub-sample of the Parkes / NTT group. The observed integration flux ranged from 2.3 to 470.8 Jy km s^{-1} with a mean of 46.20 Jy km s^{-1}. Four galaxies were manually measured due to low S/N ratio. The automated data reductions for the remaining 47 galaxies were accepted.

5.2 Light Curve of SN Ia 2012fr

Type Ia Supernovae events are fairly rare; nevertheless they continue to contribute to the calibration of distances in the local Universe. While finalizing this thesis, a Type Ia Supernovae 2012fr event occurred in host galaxy NGC 1365, a galaxy in this Chapter 5 data set. Observations began 12 days prior to the peak magnitude occurring on 2012 November 11.0 and had continued thereafter beyond 49 days post peak; the light curve is shown in Figure 5.1. Although outside of the time period considered for other SNe Ia in this thesis, it is included in this thesis as it occurred in a very nearby galaxy in the Fornax cluster for which good Cepheid data is available.

Madore et al. (1999) calculated a Cepheid distance modulus for NGC 1365 of $m - M = 31.35 \pm 0.07$ (random) mag. The NED (NASA / IPAC Extragalactic Database) galactic extinction for NGC 1365 is $A_B = 0.024$. Observations with the TAROT telescope located at the ESO observatory in La Silla, Chile yielded a *B*-band apparent magnitude at maximum peak of $B = 11.99$ mag for SN Ia 2012fr. The other bands observed include $V = 11.96$ mag, and $R = 12.00$ mag, resulting in $B - V = 0.03$ mag (Klotz & Childress, 2012). The decline rate for 2012fr was $\Delta m_{15}(B) = 0.77$ establishing an absolute magnitude of -19.38 mag. The distance modulus for SN Ia 2012fr is therefore $m - M = 31.37$ mag. The Tully-Fisher distance modulus results in this paper are: B_T-band, $\mu = 31.49 \pm 0.15$, SOFI - H^c-band, $\mu = 31.91 \pm 0.03$, and SOFI - K_s-band, $\mu = 31.87 \pm 0.04$; whereas 2MASS - H^c-band, $\mu = 31.89 \pm 0.03$, and 2MASS - K_s-band, $\mu = 31.83 \pm 0.04$.

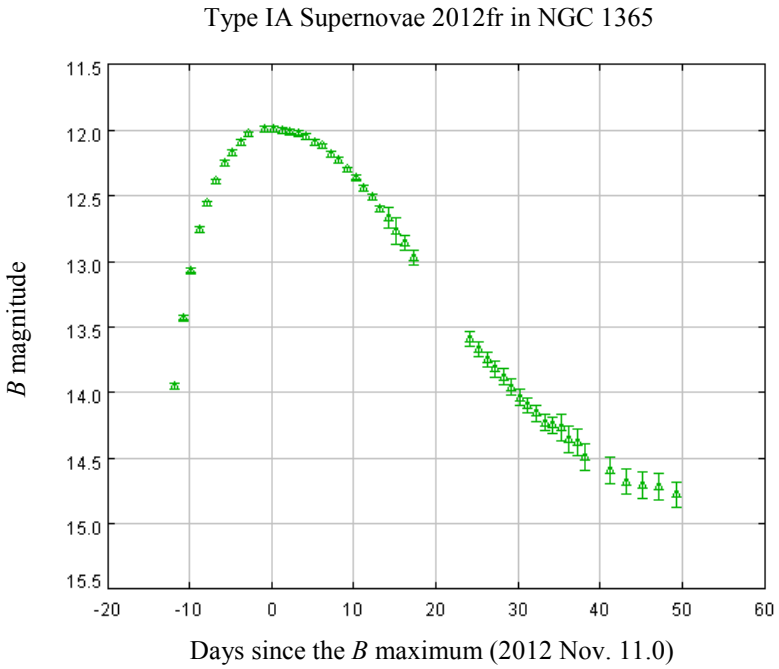

Figure 5.1: Type Ia Supernova 2012fr light curve in host galaxy NGC 1365. Peak magnitude 11.99 mag where $\Delta m_{15}(B) = 0.77$ and $B - V = 0.03$ mag (Klotz & Childress, 2012 priv. comm.).

5.3 The Tully-Fisher Relation Measurements

The ESO VII / 115 catalogue provided the B_T, surface photometry for the ESO-Uppsala Galaxies. The same algorithms for the TF relation and SNe Ia distances as used for the Literature and the Parkes sample were applied for this sample. The calculations to correct the B_T, H^c, and K_s band apparent magnitude extinction and redshift values were made using the coefficient corrections stated in § 2.

The 21 cm HI line width velocities, were adjusted for broadening using $W_R^c = W_R / 1+z$, they were then corrected for inclination and internal extinction inclination-dependence using the equations (2.6) and (2.7). The line width velocities were corrected for random and rotation motion using equation (2.8).

The absolute magnitudes M_B, M_H, and M_K were calculated using the equations (2.13). The recession velocities were corrected to the GSR, corrected for the Virgo infall and corrected to the 3K CMB using the equation (2.14).

The same criteria, as in Chapters 3 and 4, were applied to calculate the TF distance modulus for the W_{20} and W_{50} HI line width velocities in bands B_T, H^c, and

K_s to determine the best calibration for the TF relation in comparison to the SN Ia distance modulus.

The data for the Parkes / NTT sample and the new H^c and K_s band observation results are in Table 5.1. The apparent magnitude in bands B_T, H^c, and K_s along with the SNe Ia data for the Parkes / NTT sub-sample of 51 galaxies are in Table 5.2. Table 5.3 provides the new 21 cm measurements and includes the 21 cm barycentre velocities corrected to the Galactic Standard of Rest, the velocities corrected for Virgo infall, and the velocities corrected to the 3K CMB using equation (2.14). The distance modulus results for the Parkes / NTT 51-galaxy sub-sample are in Table 5.4 for IR apparent magnitudes from SOFI and Table 5.5 for IR apparent magnitudes from 2MASS. The resulting plots of the Parkes / NTT sample indicate less dispersion in the data points when compared to the data in Chapters 3 and 4.

The uncorrected W_{50} versus the uncorrected W_{20}, results in a mean difference of 26 km s^{-1} and an *rms* of 31 km s^{-1} (Figure 5.2). Whereas corrected W_{50} versus corrected W_{20} results in a negligible mean difference -3 km s^{-1}, and an *rms* of 27 km s^{-1} (Figure 5.3).

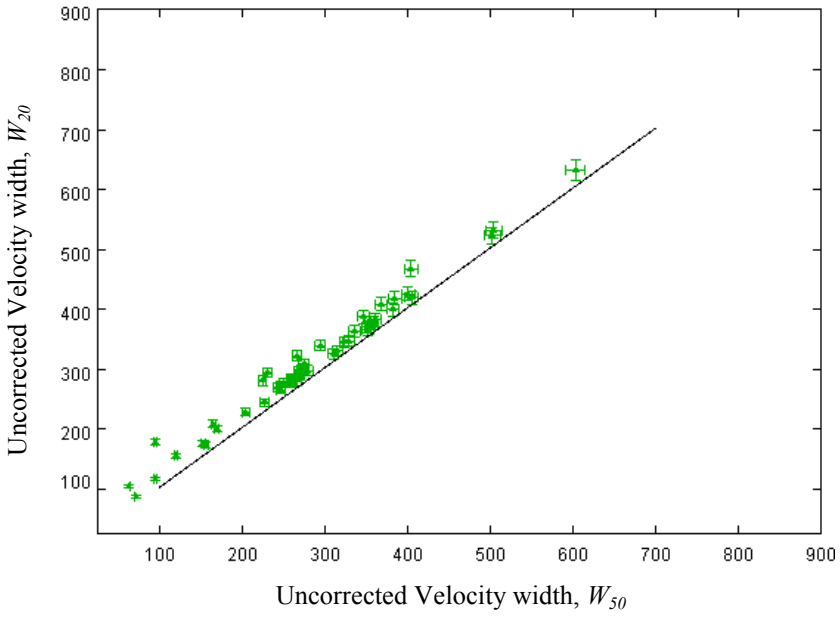

Figure 5.2: Distribution of 50 galaxies of the Parkes / NTT sample W_{50} uncorrected versus W_{20} uncorrected resulted in a mean difference of 26 km s^{-1}, with an *rms* scatter of 31 km s^{-1}. The outliers or large error bars are owing to inclination values that are beyond the parameters $35° < i < 80°$.

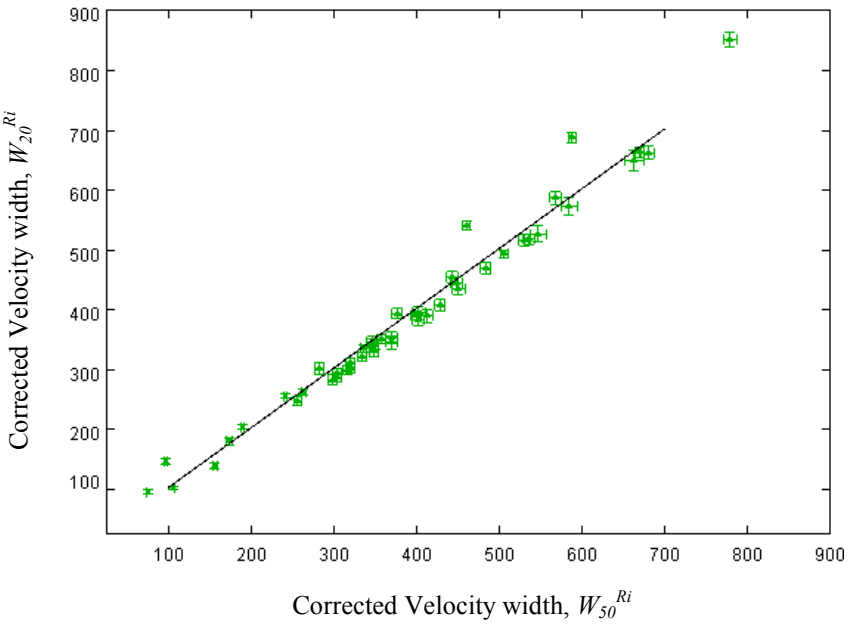

Figure 5.3: Distribution of 38 galaxies of the Parkes / NTT sample corrected W_{50}^{Ri} plotted against W_{20}^{Ri} using the RC3 inclination data resulted in a mean difference of -3 km s^{-1}, with an *rms* scatter of 27 km s^{-1}. The outliers or large error bars are owing to inclination values that are beyond the parameters $35° < i < 80°$.

Figure 5.4 compares the SOFI H^c-band and 2MASS H^c-band data where the *rms* difference is 0.26 mag. Figure 5.5 compares the SOFI K_s -band to 2MASS K_s -band, giving an *rms* of 0.23 mag. The differences may be due to a combination of calibration and flat-field errors, sensitivity to low-surface-brightness features, and differences in methodology used in SOFI and 2MASS photometric measurements. Figures 5.6 through 5.8 and 5.9 through 5.11 are the distance modulus plots for the TF relation contained in Tables 5.4 (SOFI) and 5.5 (2MASS) respectively, and contain only galaxies with an inclination $35° < i < 85°$. The NIR measurements have less dispersion as shown in Figures 5.8 and 5.11. Figure 5.12 is a comparison of the TF and redshift distance moduli for the H^c-band and Figure 5.13 for the K_s-band. Figures 5.14 through 5.17 show the Hubble diagram for the galaxies and supernovae respectively showing an rms scatter ranging from 1.05 to 1.55 mag.

5.4 Calculations for the SNe Ia

The SNe Ia in the Parkes / NTT 51-galaxy sub-sample range of 53 years and are identified as 1959C through 2012fr. The exclusion criterion for the SNe Ia population is the same as in Chapters 3 and 4. The SNe Ia that are not part of the final compilation

of the sample set are due to the SNe Ia peak magnitude, $B_{max} - V_{max}$ or the $\Delta m_{15}(B)$ data not being well defined.

The corrections for the SNe Ia are the same as in chapters 3 and 4 using the extinction and reddening equations in Chapter 2.2, and Table 2.1 from chapter 2. The unreddened SNe Ia and absolute magnitudes were determined using the Phillips et al. (1999) correlation of the peak luminosity and initial decline rate. The SNe Ia distance determinations were further modified using the Riess et al. (2005) 0.27 mag adjustment to the Cepheid zero point. The SNe Ia distance modulus versus the Tully-Fisher B_T distance modulus is shown in Figure 5.18. Figures 5.19 through 5.22 show the SNe Ia distance modulus versus the TF H^c and K_s distance moduli derived using SOFI and 2MASS IR data.

The SOFI-based data in Figures 5.19 and 5.20 are less consistent with the SNe Ia then the 2MASS-based in Figures 5.21 and 5.22. They are due to unknown differences in calibration, resolution, saturation effects, or oversubtraction due to the limited NTT field of view versus 2MASS. There is minimal difference in the *K*-band versus K_s -band of $\Delta = 0.03$ mag (Bonatto et al. 2009).

5.5 Summary

This chapter provides new distance moduli for a sample of SN Ia and their host galaxies. The distance moduli for the host galaxies were obtained with new 21 cm and new IR observations. There is less dispersion about the distance relations owing to the new observations. Comparative detail of the three sample sets and the implications for cosmology are discussed in Chapter 6.

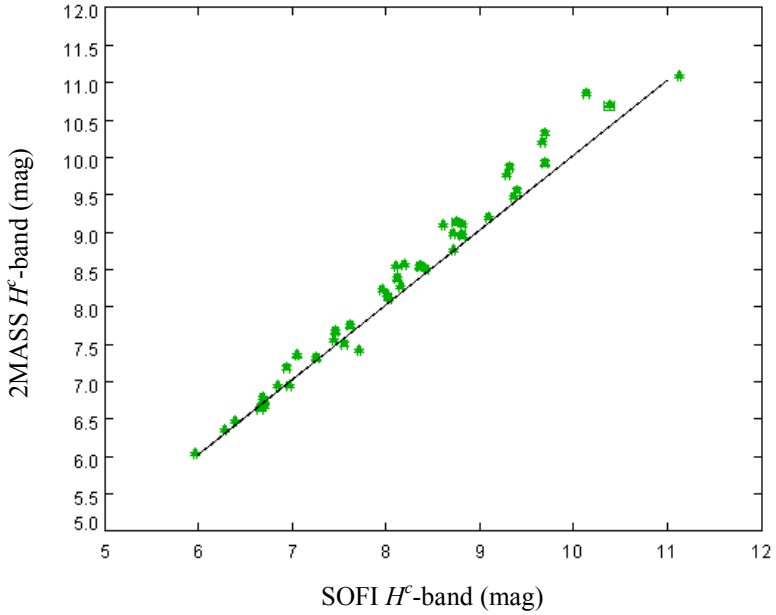

Figure 5.4: Parkes / NTT apparent magnitude for 45 galaxies in SOFI H^c -band based results versus 2MASS H^c -band based data. The mean is 0.17 mag with an *rms* of 0.26 mag.

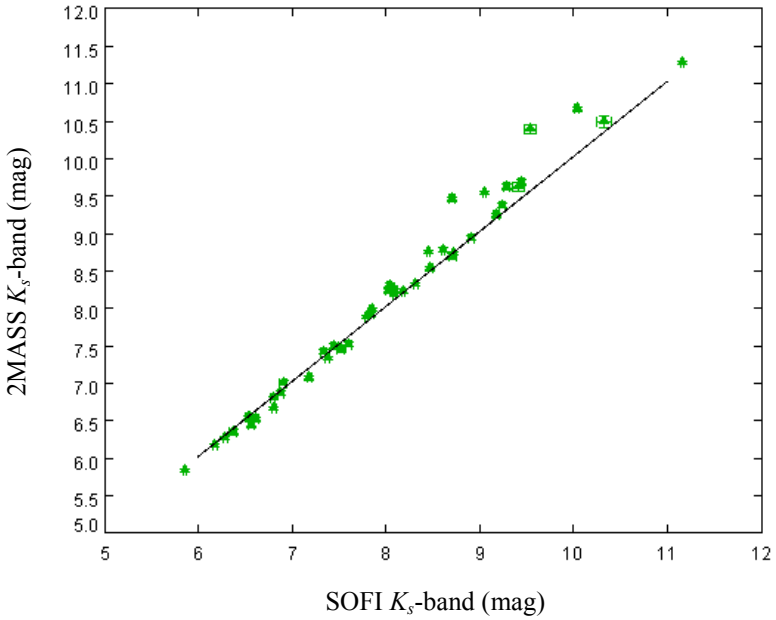

Figure 5.5: Parkes / NTT apparent magnitude for 45 galaxies in SOFI K_s -band based results versus 2MASS K_s -band based data. The mean is 0.10 mag with an *rms* of 0.23 mag.

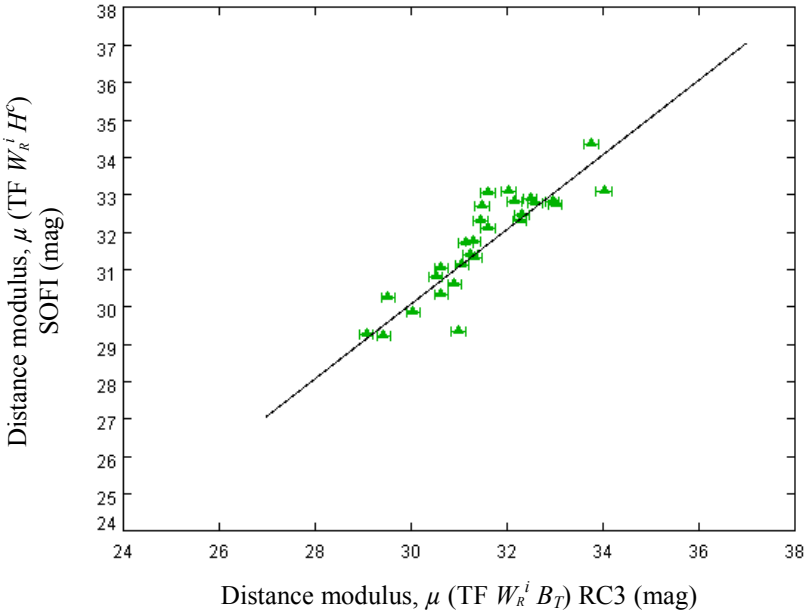

Figure 5.6: SOFI IR - Distribution of 28 galaxies, based on the TF distance modulus derived from W_R^i for the RC3 B_T -band based results versus distance modulus derived from W_R^i for SOFI H^c -band based results. The reference line is through the origin with a slope = 1.000. The mean difference is 0.16 mag, with an *rms* scatter of 0.64 mag and the MAD is 0.18 mag.

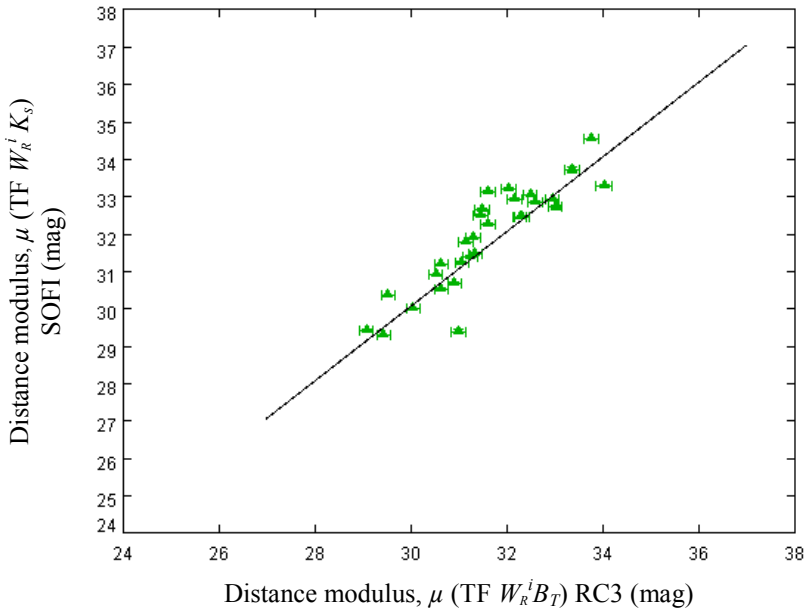

Figure 5.7: SOFI IR - Distribution of 29 galaxies, based on the TF distance modulus derived from W_R^i for the RC3 B_T -band based results versus distance modulus derived from W_R^i for SOFI H^c -band based results. The reference line is through the origin with a slope = 1.000. The mean difference is 0.27 mag, with an *rms* scatter of 0.67 mag and the MAD is 0.18 mag.

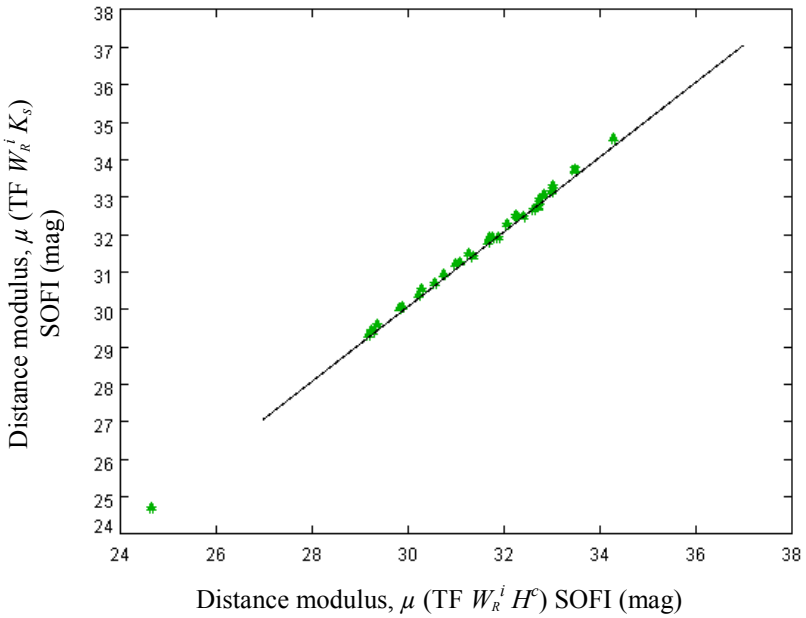

Figure 5.8: SOFI IR - Distribution of 34 galaxies, based on the TF distance modulus derived from W_R^i for SOFI H^c -band based results versus distance modulus derived from W_R^i for SOFI K_s -band based data. The reference line is through the origin with a slope = 1.000. The mean difference is 0.11 mag, with an *rms* scatter of 0.13 mag and the MAD is 0.01 mag.

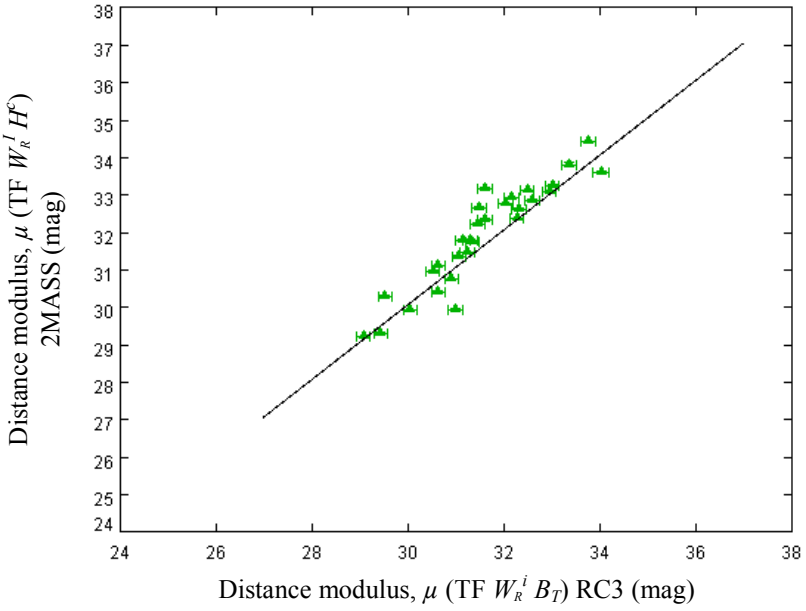

Figure 5.9: 2MASS IR - Distribution of 29 galaxies, based on the TF distance modulus derived from W_R^i for the RC3 B_T -band based results versus distance modulus derived from W_R^i for the 2MASS H^c -band based data. The reference line is through the origin with a slope = 1.000. The mean difference is 0.31 mag, with an *rms* scatter of 0.58 mag and the MAD is 0.13 mag.

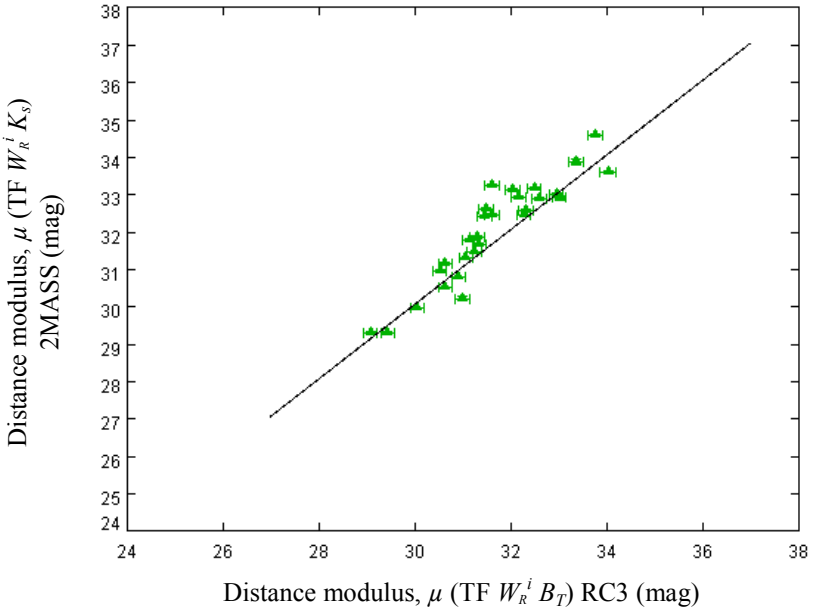

Figure 5.10: 2MASS IR - Distribution of 28 galaxies, based on the TF distance modulus derived from W_R^i for B_T -band based results versus distance modulus derived from W_R^i for 2MASS K_s -band based data. The reference line is through the origin with a slope = 1.000. The mean difference is 0.34 mag, with an *rms* scatter of 0.61 mag and the MAD is 0.20 mag.

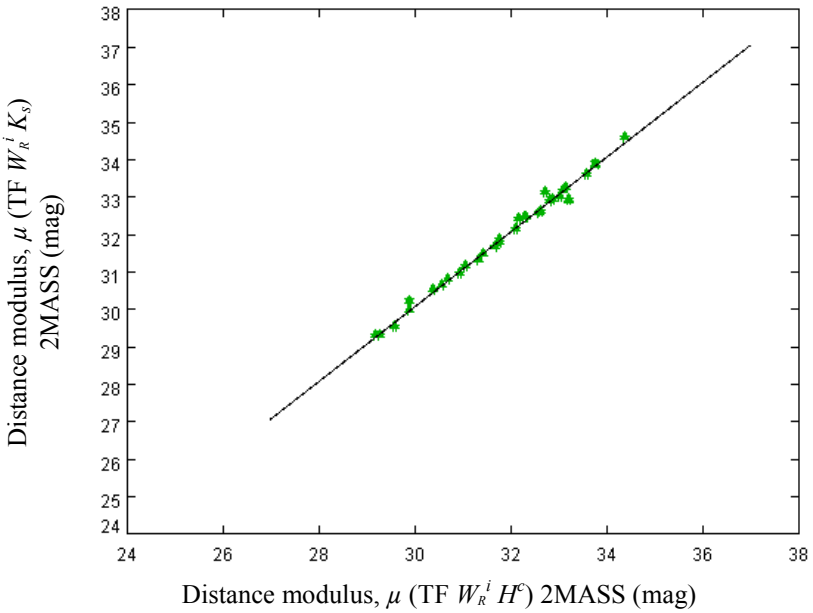

Figure 5.11: 2MASS IR - Distribution of 32 galaxies, based on the TF distance modulus derived from W_R^i for 2MASS H^c -band based results versus distance modulus derived from W_R^i for 2MASS K_s -band based data. The reference line is through the origin with a slope = 1.000. The mean difference is -0.03 mag, with an *rms* scatter of 0.12 mag and the MAD is 0.02 mag.

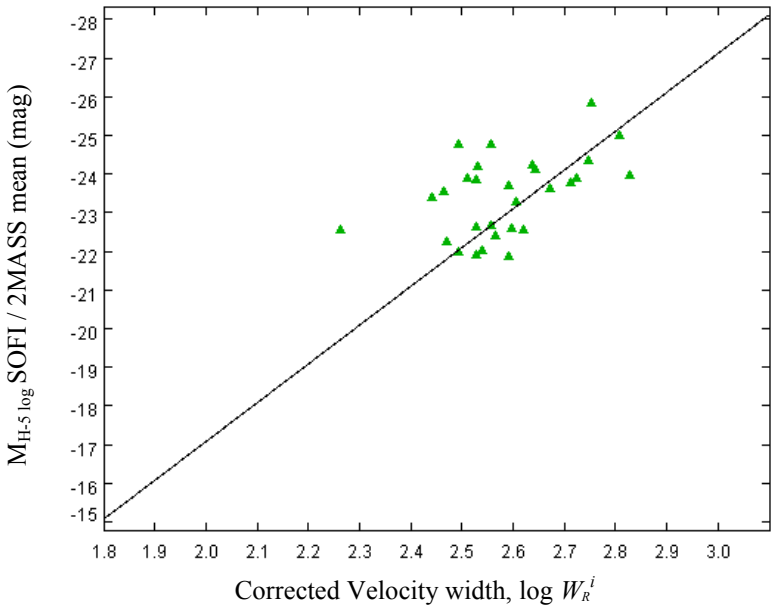

Figure 5.12: Parkes / NTT sample for 29 of the TF log 21 cm line width velocity corrected for broadening, inclination, random and rotation motion versus redshift cz distance modulus for the absolute magnitude of the mean SOFI and 2MASS H^c -band based data. The offset is 0.17 mag with an *rms* scatter of 1.17 mag.

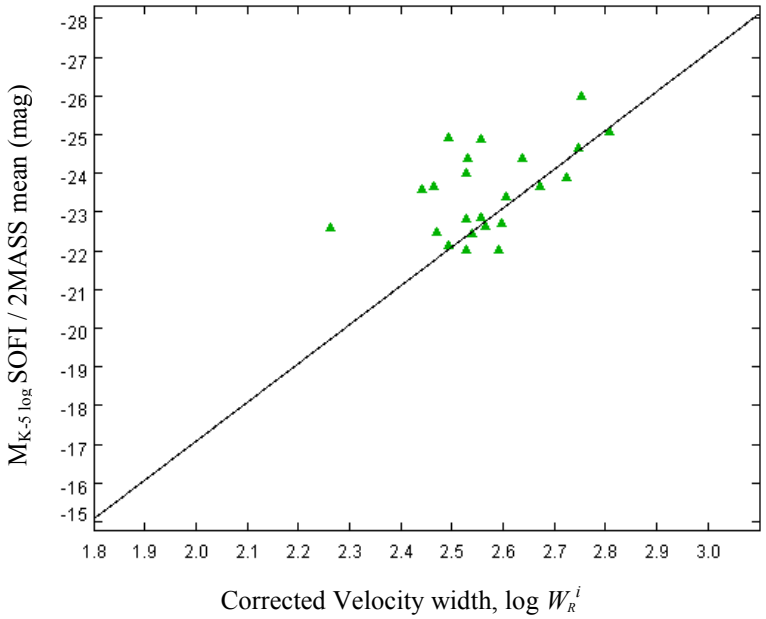

Figure 5.13: Parkes / NTT sample for 23 of the TF log 21 cm line width velocity corrected for broadening, inclination, random and rotation motion versus redshift *cz* distance modulus for the absolute magnitude of the mean SOFI and 2MASS K_s -band based data. The offset is 0.20 mag with an *rms* scatter of 1.17 mag.

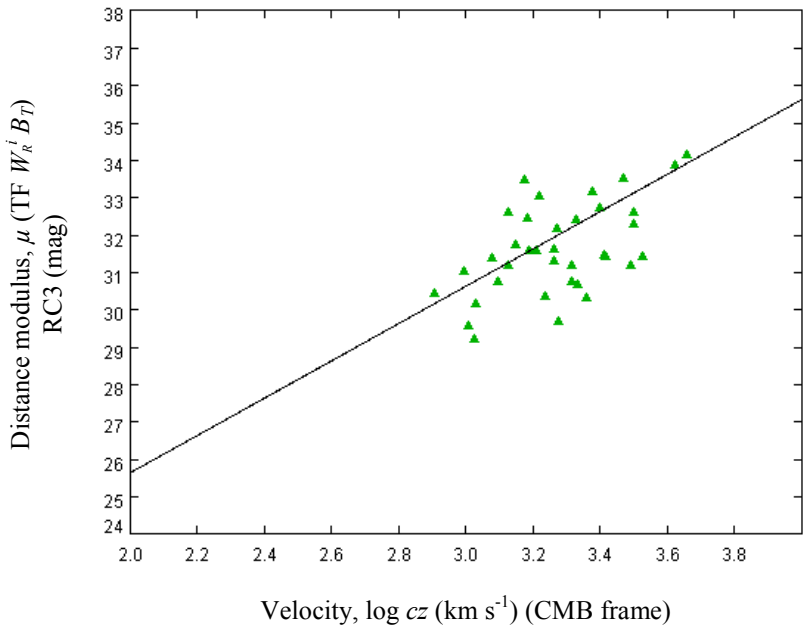

Figure 5.14: Distribution of 36 galaxies for a comparison of the 3K CMB log *cz* versus TF RC3 B_T -band based distance modulus. The offset is -0.19 mag, with an *rms* scatter of 1.05 mag.

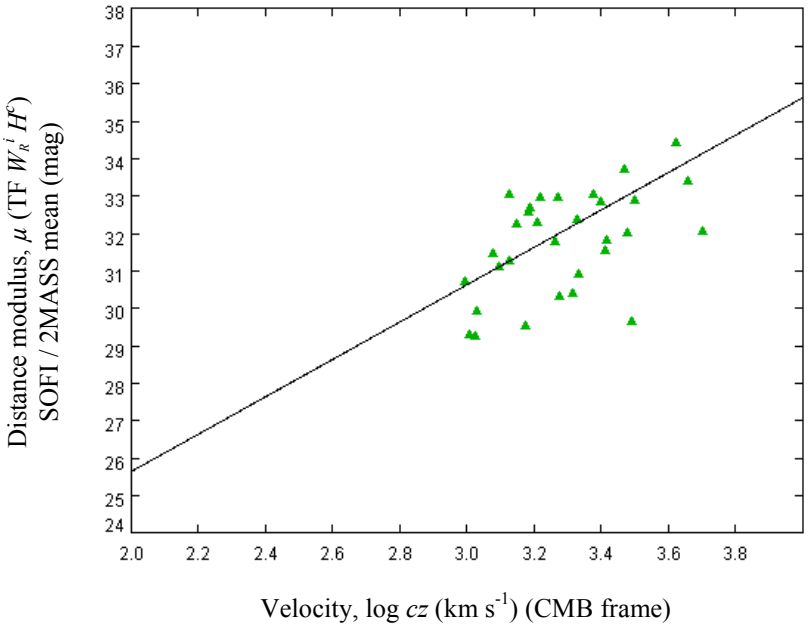

Figure 5.15: SOFI / 2MASS IR - Distribution of 31 galaxies for a comparison of the 3K CMB log *cz* versus TF H^c -band based distance modulus from a mean of SOFI and 2MASS. The offset is -0.25 mag, with an *rms* scatter of 1.21 mag.

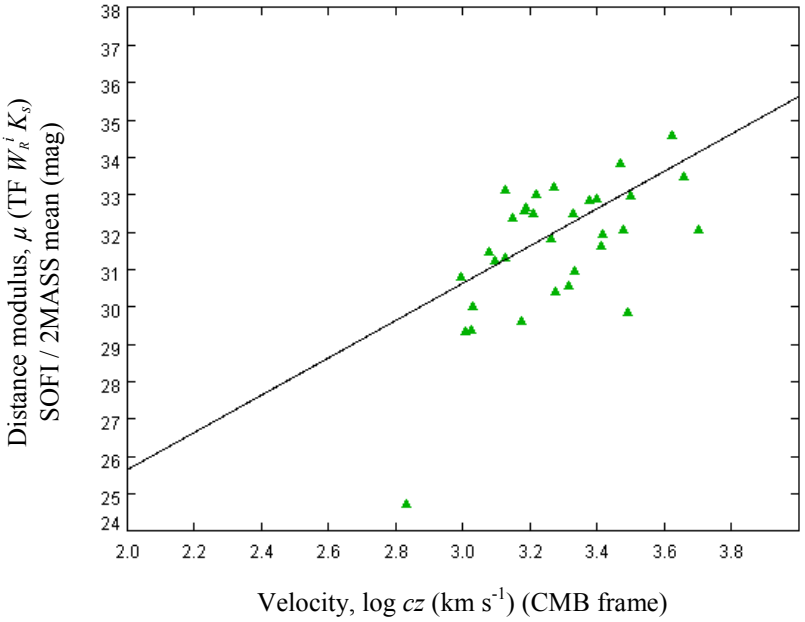

Figure 5.16: SOFI / 2MASS IR - Distribution of 32 galaxies for a comparison of the 3K CMB log *cz* versus TF K_s -band based distance modulus from a mean of SOFI and 2MASS. The offset is -0.32 mag, with an *rms* scatter of 1.23 mag.

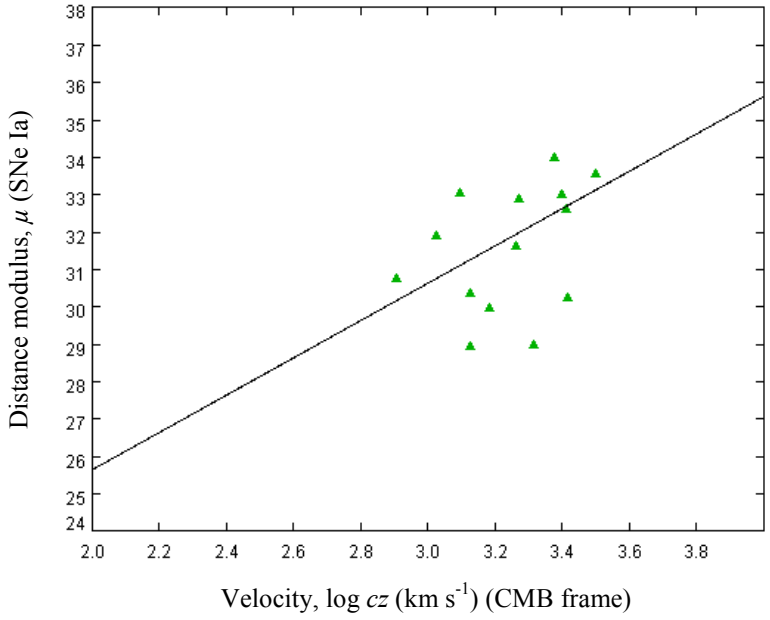

Figure 5.17: Distribution of 14 galaxies for a comparison of the 3K CMB log *cz* versus SNe Ia distance modulus. The offset is -0.26 mag, with an *rms* scatter of 1.55 mag.

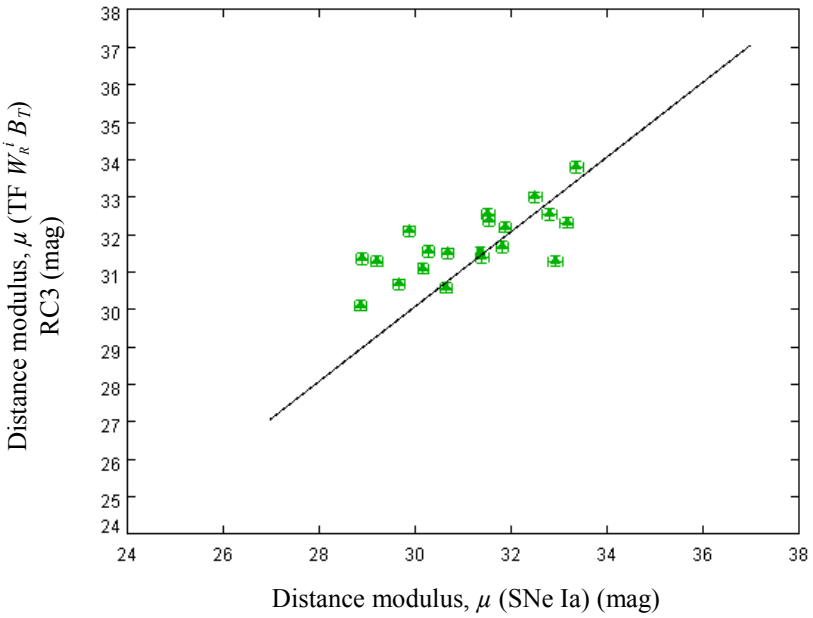

Figure 5.18: Distribution of 20 galaxies, based on the SN Ia distance modulus versus the TF W_R^i RC3 B_T -band based distance modulus. The reference line is through the origin with a slope = 1.000. The mean difference is 0.56 mag, with an *rms* scatter of 1.13 mag and the MAD is 0.54 mag.

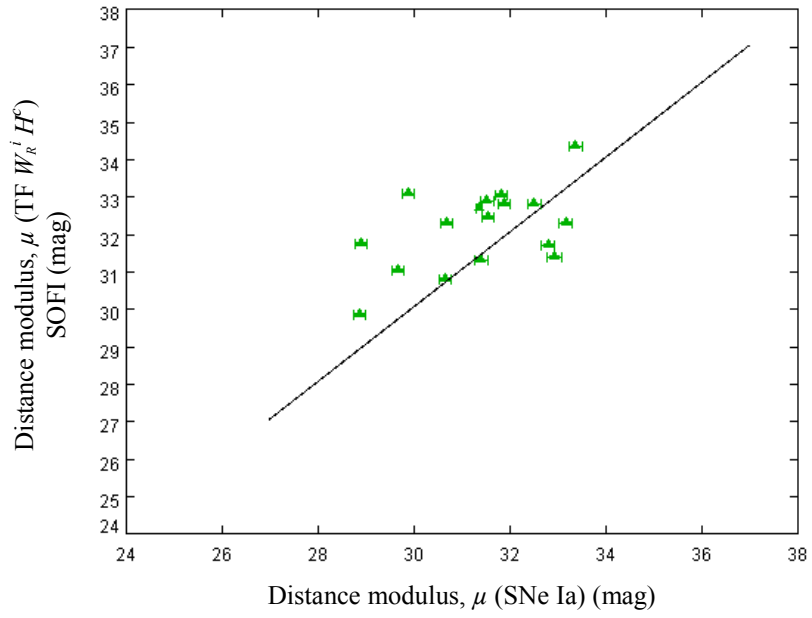

Figure 5.19: SOFI IR - Distribution of 17 galaxies, based on SN Ia distance modulus versus the TF W_R^i SOFI H^c -band based distance modulus. The reference line is through the origin with a slope = 1.000. The mean difference is 0.76 mag, with an *rms* scatter of 1.43 mag and the MAD is 0.25 mag.

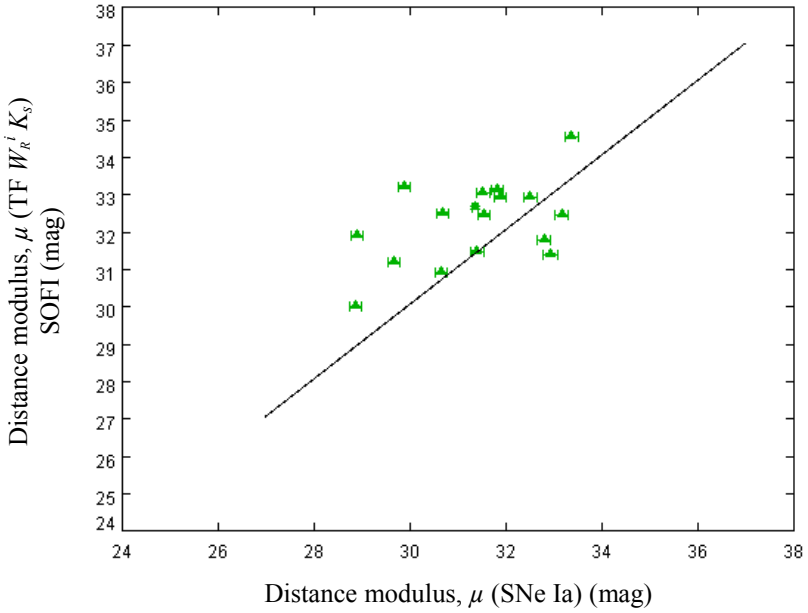

Figure 5.20: SOFI IR - Distribution of 17 galaxies, based on SN Ia distance modulus versus the TF W_R^i SOFI K_s -band based distance modulus. The reference line is through the origin with a slope = 1.000. The mean difference is 0.87 mag, with an *rms* scatter of 1.51 mag and the MAD is .33 mag.

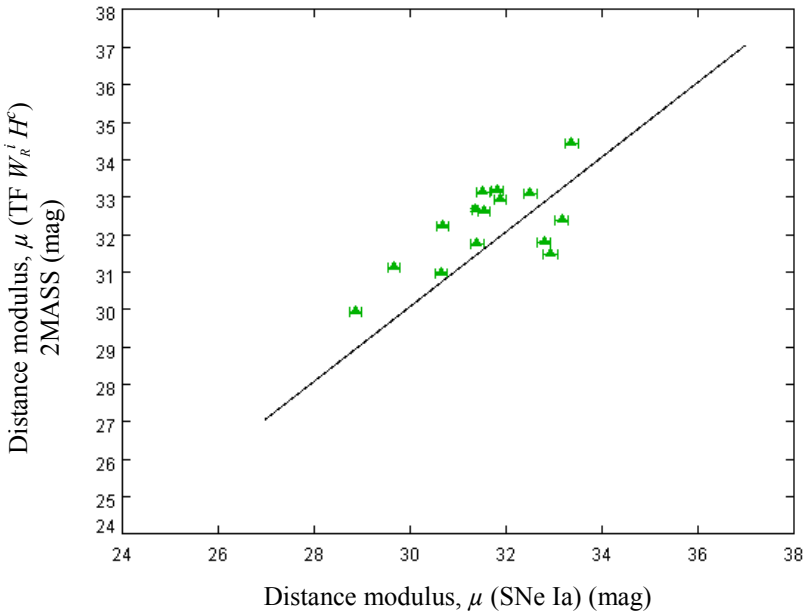

Figure 5.21: 2MASS IR - Distribution of 15 galaxies, based on SN Ia distance modulus versus TF W_R^i 2MASS H^c -band based distance modulus. The reference line is through the origin with a slope = 1.000. The mean difference is 0.58 mag, with an *rms* scatter of 1.11 mag and the MAD is 0.25 mag.

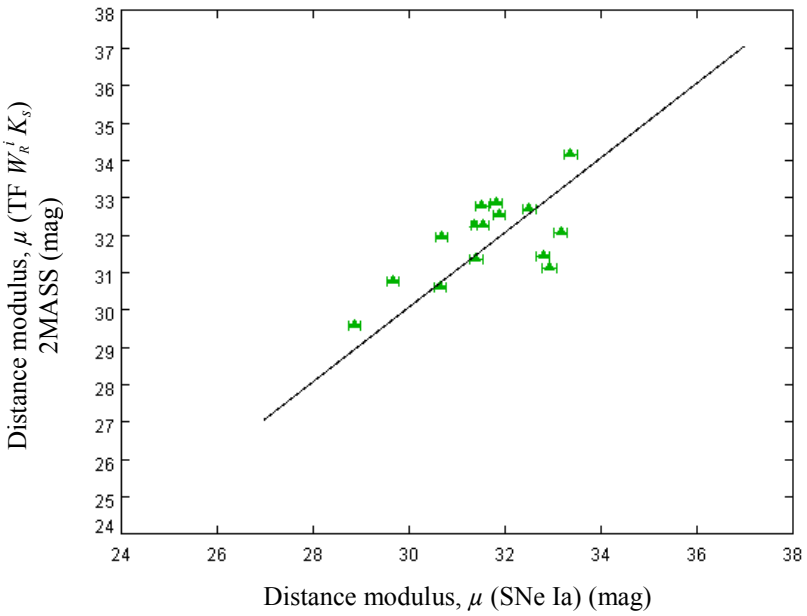

Figure 5.22: 2MASS IR - Distribution of 15 galaxies, based on SN Ia distance modulus versus TF W_R^i 2MASS K_s -band based distance modulus. The reference line is through the origin with a slope = 1.000. The mean difference is 0.24 mag, with an *rms* scatter of 0.98 mag and the MAD is 0.30 mag.

Table 5.1: Apparent Magnitude B_T, H^c and K_s for the Parkes / NTT Sample

1	2	3	4	5	6	7	8	9	10	11	12	13	14
			Galaxy				ESO			SOFI			
GALAXY	J2000 Epoch						VII / 115		H^c Total		K_s Total		2MASS
NAME	RA	DEC	TYPE	$E(B-V)$	z	σ	B_T	i	H^c	Md_h	K_s	Md_k	b/a
ESO													
269-G57	13 10 04.4	-46 26 14	SABb	0.101	0.010360	0.000017	12.49	21.5	8.64	0.0000	8.50	0.0010	0.980
300-G09	03 05 15.8	-39 33 41	SABb	0.022	0.020000	0.002000	15.67	…	…	…	…	…	…
576-G40	13 20 43.7	-22 03 04	SBd	0.113	0.006938	0.000029	14.66	80.5	11.31	0.0019	11.31	0.0011	…
IC 344	03 41 29.5	-04 39 57	SB	0.053	0.018146	0.000020	…	67.8	12.30	-0.0057	11.66	0.0011	…
IC 1151	15 58 32.3	17 26 30	SBc	0.038	0.007235	0.000020	13.49*	63.6	10.49	-0.0002	10.33	0.0005	0.500
IC 2163	06 16 27.6	-21 22 32	SBc	0.087	0.008966	0.000057	12.55	39.8	8.98	0.0151	7.89	0.0007	0.480
IC 4824	19 13 17.8	-62 05 21	…	0.054	0.003179	0.000030	13.90	55.0	11.73	0.0080	11.15	0.0083	…
IC 5179	22 16 09.1	-36 50 37	SAbc	0.020	0.011415	0.000033	12.29	62.9	8.94	0.0000	8.58	0.0004	0.480
IC 5270	22 57 55.0	-35 51 26	SBc	0.014	0.005457	0.000033	13.00	74.5	9.72	-0.0005	9.39	0.0001	0.300
MCG													
0-32-01	12 19 40.3	02 04 50	SBbc	0.024	0.007395	0.000133	14.90*	77.5	11.95	-0.0046	11.68	0.0019	…
01-34-05	13 11 23.2	03 24 41	SBc	0.026	0.010147	0.000027	13.98*	73.0	12.65	0.0076	12.39	0.0161	…
-01-04-44	01 26 14.4	-06 05 39	SBc	0.044	0.006541	0.000023	…	79.5	10.66	0.0001	10.26	0.0013	0.200
NGC 289	00 52 41.7	-31 12 20	SABbc	0.019	0.005440	0.000017	11.36	55.6	8.22	0.0001	7.95	0.0003	0.690
NGC 613	01 34 17.8	-29 25 09	SBbc	0.019	0.004920	0.000017	10.77	73.9	7.32	0.0000	7.05	0.0000	0.616
NGC 976	02 34 00.0	20 58 36	SAc	0.110	0.014327	0.000017	13.26*	39.9	9.38	0.0007	9.04	0.0015	0.740
NGC 977	02 33 03.4	-10 45 36	SABa	0.027	0.015274	0.000037	…	47.7	10.49	-0.0007	10.15	0.0002	0.720
NGC 986	02 33 34.2	-39 02 46	SBb	0.019	0.006688	0.000023	11.74	65.4	…	…	7.92	-0.0002	0.570
NGC 1084	02 45 59.9	-07 34 42	SAc	0.027	0.004693	0.000013	11.31*	51.5	8.15	0.0001	7.86	0.0004	0.600
NGC 1187	03 02 37.6	-22 52 03	SBc	0.022	0.004657	0.000017	11.41	58.6	8.31	0.0003	8.04	0.0008	0.610
NGC 1300	03 19 40.7	-19 24 42	SBbc	0.030	0.005230	0.000020	11.16	42.2	8.11	-0.0002	7.84	0.0001	0.460
NGC 1320	03 24 48.7	-03 02 32	Sa	0.047	0.008883	0.000053	13.32*	71.5	9.64	0.0009	9.32	0.0021	0.340
NGC 1326	03 25 08.5	-36 21 50	SBm	0.017	0.006124	0.000037	13.80	42.4	11.42	0.0124	11.39	0.0143	0.740

Table 5.1: Continued

1	2	3	4	5	6	7	8	9	10	11	12	13	14
			Galaxy				ESO			SOFI			
GALAXY	J2000 Epoch						VII / 115		H^c Total		K_s Total		2MASS
NAME	RA	DEC	TYPE	$E(B-V)$	z	σ	B_T	i	H^c	Md_h	K_s	Md_k	b/a
NGC 1350	03 31 08.1	33 37 43	SBab	0.012	0.006304	0.000030	11.20	61.2	7.54	0.0000	7.28	0.0000	0.572
NGC 1365	03 33 36.4	-36 08 25	SBb	0.020	0.005457	0.000003	10.08	40.4	6.76	-0.0002	6.42	0.0000	0.825
NGC 1398	03 38 51.9	-26 20 10	SBab	0.013	0.004693	0.000020	10.37	42.1	6.95	0.0000	6.71	0.0000	0.990
NGC 1425	03 42 11.5	-29 53 36	SAb	0.013	0.005037	0.000010	11.61	61.2	8.32	0.0006	8.12	-0.0001	0.540
NGC 1566	04 20 00.4	-54 56 16	SAB	0.021	0.005017	0.000007	13.53	37.5	7.00	0.0002	6.91	0.0001	0.737
NGC 1808	05 07 42.3	-37 30 47	SABb	0.030	0.003319	0.000013	10.80	70.7	6.90	0.0000	6.65	0.0002	0.484
NGC 2090	05 47 01.9	-34 15 02	SAb	0.040	0.003072	0.000007	11.70	62.0	8.17	0.0009	7.94	0.0010	0.430
NGC 2207	06 16 21.6	-21 22 18	SABbc	0.087	0.009160	0.000023	11.48	44.0	8.89	0.0172	7.76	0.0002	0.640
NGC 2227	06 25 58.0	-22 00 17	SBc	0.083	0.007532	0.000010	13.40	46.6	9.76	0.0016	9.48	0.0034	0.660
NGC 2487	07 58 20.4	25 08 57	SBc	0.052	0.016148	0.000010	13.23*	30.9	9.74	0.0000	9.48	0.0013	0.440
NGC 2595	08 27 42.0	21 28 45	SABc	0.040	0.014443	0.000013	12.93*	37.9	9.39	0.0027	9.33	0.0017	0.580
NGC 2713	08 57 20.5	02 55 17	SBab	0.042	0.013082	0.000020	12.72*	65.4	8.47	0.0003	8.24	0.0002	0.480
NGC 2775	09 10 20.1	07 02 17	SAab	0.043	0.004516	0.000007	11.03*	36.6	7.13	0.0000	6.96	0.0000	0.750
NGC 2935	09 36 44.8	-21 07 41	SABb	0.064	0.007575	0.000010	11.84	52.4	8.22	-0.0002	8.10	0.0012	0.640
NGC 3227	10 23 30.6	19 51 54	SAB	0.023	0.003859	0.000010	11.10*	66.5	7.84	0.0005	7.52	0.0048	0.570
NGC 3351	10 43 57.7	11 42 14	SBb	0.028	0.002595	0.000013	10.53*	23.5	7.00	0.0000	6.83	0.0000	0.968
NGC 3367	10 46 34.9	13 45 03	SBc	0.029	0.010142	0.000024	12.05*	30.1	8.86	0.0007	8.75	0.0026	0.900
NGC 3368	10 46 45.7	11 49 12	SABab	0.025	0.002992	0.000013	10.11*	48.7	6.51	0.0000	6.35	0.0001	0.726
NGC 3370	10 47 04.0	17 16 25	SAc	0.031	0.004266	0.000013	12.28*	58.0	9.54	-0.0003	9.32	0.0006	0.720
NGC 3389	10 48 27.9	12 31 59	SAc	0.027	0.004340	0.000020	12.36*	63.4	9.58	-0.0001	9.40	0.0000	0.400
NGC 3621	11 18 16.5	-32 48 51	SAd	0.080	0.002435	0.000007	10.18	60.9	6.85	0.0004	6.71	0.0004	0.528
NGC 3627	11 20 14.9	12 59 30	SABb	0.032	0.002425	0.000010	9.65*	51.7	6.10	0.0007	5.93	0.0007	0.539
NGC 3810	11 40 58.7	11 28 16	SAc	0.044	0.003309	0.000002	11.35*	44.8	8.04	0.0000	7.90	0.0001	0.720
NGC 4045	12 02 42.2	01 58 36	SABc	0.023	0.006608	0.000027	12.79*	22.6	8.76	0.0004	8.58	0.0003	0.420

Table 5.1: Continued

1	2	3	4	5	6	7	8	9	10	11	12	13	14
			Galaxy				ESO	SOFI					
GALAXY	J2000 Epoch						VII / 115		H^c Total		K_s Total		2MASS
NAME	RA	DEC	TYPE	$E(B-V)$	z	σ	B_T	i	H^c	Md_h	K_s	Md_k	b/a
NGC 4178	12 12 46.4	10 51 57	SBdm	0.028	0.001248	0.000002	11.90*	76.5	9.01	0.0001	8.84	0.0005	0.220
NGC 4321	12 22 54.8	15 49 19	SABbc	0.026	0.005240	0.000003	10.05*	50.7	6.80	0.0001	6.60	0.0001	0.770
NGC 4462	12 29 21.2	-23 09 59	SBac	0.100	0.005977	0.000013	12.81	68.2	8.69	-0.0001	8.47	0.0003	0.380
NGC 4496	12 31 39.2	03 56 22	SBm	0.025	0.005771	0.000010	11.94*	35.5	9.33	0.0020	9.08	0.0042	0.520
NGC 4501	12 31 59.2	14 25 13	SAb	0.038	0.007609	0.000010	10.36*	59.7	6.51	0.0000	6.29	0.0000	0.506
NGC 4527	12 34 08.4	02 39 13	SABbc	0.022	0.005791	0.000003	11.38*	74.4	7.17	0.0000	6.95	0.0000	0.330
NGC 4535	12 34 20.3	08 11 52	SABc	0.019	0.006551	0.000002	10.59*	53.4	7.56	0.0000	7.44	0.0000	0.880
NGC 4536	12 34 27.1	02 11 17	SABbc	0.018	0.006031	0.000003	11.16*	68.2	7.70	0.0000	7.45	0.0003	0.460
NGC 4548	12 35 26.4	14 29 47	SBb	0.038	0.001621	0.000013	10.96*	48.5	7.34	0.0000	7.24	0.0000	0.924
NGC 4579	12 37 43.5	11 49 05	SABc	0.041	0.005060	0.000002	10.48*	42.6	6.76	0.0000	6.62	0.0000	0.946
NGC 4639	12 42 52.4	13 15 27	SABbc	0.026	0.003395	0.000018	12.24*	43.7	8.80	0.0000	8.66	0.0007	0.780
NGC 4680	12 46 54.7	-11 38 13	…	0.044	0.008312	0.000030	…	28.7	9.93	-0.0008	9.67	0.0006	0.740
NGC 4902	13 00 59.7	-14 30 49	SBb	0.050	0.008916	0.000017	11.61*	22.5	8.22	0.0006	8.07	0.0009	0.820
NGC 4948	13 04 55.9	-07 56 52	SBdm	0.057	0.003746	0.000021	…	81.0	10.30	0.0009	10.15	0.0023	0.320
NGC 4981	13 08 8.7	-06 46 39	SABbc	0.042	0.005624	0.000020	12.10*	54.6	8.66	0.0002	8.52	0.0011	0.640
NGC 5085	13 20 17.7	-24 26 25	SAc	0.102	0.006525	0.000002	11.99	43.8	8.22	0.0000	8.04	0.0003	…
NGC 5134	13 25 19.0	-21 07 59	SABa	0.090	0.005861	0.000030	12.11	64.2	…	…	8.16	0.0012	0.560
NGC 5247	13 38 03.4	-17 52 55	Sabc	0.089	0.004526	0.000017	10.77	33.8	7.77	0.0000	7.69	-0.0001	…
NGC 5253	13 39 55.9	-31 38 24	Sb	0.056	0.001358	0.000010	11.17	58.6	8.34	0.0000	8.22	0.0004	0.520
NGC 5364	13 56 12.0	05 00 52	Sabc	0.027	0.000414	0.000013	11.17*	49.4	8.20	0.0000	8.07	0.0001	0.670
NGC 5426	14 03 24.8	-06 04 09	SAc	0.028	0.008743	0.000023	12.68*	61.0	9.48	0.0019	9.34	0.0033	0.510
NGC 5427	14 03 26.0	-06 01 51	SAc	0.028	0.008733	0.000010	11.93*	32.7	8.76	0.0008	8.64	0.0045	0.980
NGC 5468	14 06 34.9	-05 27 11	SABcd	0.024	0.009480	0.000013	13.00*	39.7	9.72	0.0003	9.57	0.0010	0.660
NGC 5494	14 12 24.1	-30 38 39	SAc	0.077	0.008686	0.000007	12.64	33.3	…	…	8.94	0.0018	0.940

Table 5.1: End

1	2	3	4	5	6	7	8	9	10	11	12	13	14
			Galaxy				ESO	SOFI					
GALAXY	J2000 Epoch						VII / 115		H^c Total		K_s Total		2MASS
NAME	RA	DEC	TYPE	$E(B-V)$	z	σ	B_T	i	H^c	Md_h	K_s	Md_k	b/a
NGC 5668	14 33 24.3	04 27 02	SAd	0.037	0.005260	0.000003	12.20*	23.1	9.49	0.0021	9.43	0.0039	…
NGC 5746	14 44 55.9	01 57 18	SABb	0.040	0.005737	0.000013	11.29*	86.0	7.03	0.0004	6.86	0.0000	0.220
NGC 5861	15 09 16.1	-11 19 18	SABc	0.108	0.006298	0.000017	12.30*	53.2	8.71	0.0000	8.53	0.0006	0.490
NGC 6063	16 07 13.0	07 58 44	Scd	0.046	0.009500	0.000017	13.76*	51.0	10.49	0.0011	10.39	0.0003	0.640
NGC 6384	17 32 24.3	07 03 37	SABbc	0.123	0.005554	0.000004	11.14*	48.5	7.68	0.0001	7.62	0.0000	0.680
NGC 6753	19 11 23.6	-57 02 58	SAb	0.069	0.010570	0.000027	11.84	31.3	7.68	0.0000	7.50	0.0008	0.920
NGC 6754	19 11 25.7	-50 38 31	SABbc	0.070	0.010864	0.000033	12.86	72.9	9.14	0.0001	8.88	0.0020	0.420
NGC 6835	19 54 32.9	-12 34 03	SBa	0.144	0.005374	0.000030	13.41*	79.0	9.19	0.0000	8.94	0.0001	…
NGC 7083	21 35 45.4	-63 54 15	SABc	0.040	0.010371	0.000030	11.93	57.9	8.64	0.0001	8.31	0.0003	0.560
NGC 7329	22 40 23.4	-66 28 44	SBb	0.027	0.010848	0.000019	12.51	55.0	8.91	0.0006	8.65	0.0010	0.620
NGC 7412	22 55 45.2	-42 38 17	SABc	0.012	0.005727	0.000017	11.82	37.1	8.90	0.0003	8.64	0.0026	0.840
NGC 7448	23 00 03.6	15 58 49	SAbc	0.057	0.007318	0.000003	12.20*	62.2	9.25	0.0010	9.00	0.0005	0.520
NGC 7479	23 04 56.6	12 19 22	SBc	0.112	0.007932	0.000010	11.60*	73.3	8.16	0.0000	7.85	0.0001	0.400
NGC 7541	23 14 43.9	04 32 04	SBbc	0.068	0.008943	0.000010	12.42*	73.2	8.60	-0.0002	8.24	0.0001	0.340
NGC 7606	23 19 04.8	-08 29 06	SAb	0.037	0.007442	0.000017	11.51*	66.7	8.01	0.0000	7.74	0.0001	0.473
NGC 7723	23 38 57.1	-12 57 40	SBb	0.029	0.006254	0.000027	11.94*	47.4	8.46	0.0001	8.15	0.0002	0.680
UGC 2936	04 02 48.2	01 57 57	SBd	0.452	0.012719	0.000023	15.00*	75.0	9.24	0.0005	8.83	0.0006	0.300
UGC 11198	18 18 59.2	16 14 58	Sab	0.186	0.015034	0.000147	15.10*	76.0	10.82	-0.0009	10.27	0.0055	…

Table 5.1: Column Description and References

Column 1. Galaxy name

Column 2. Galaxy J2000 Epoch coordinates for right ascension

Column 3. Galaxy J2000 Epoch coordinates for declination

Column 4. Galaxy morphology classification

Column 5. Extinction reddening

Column 6. Redshift *z*

Column 7. Redshift z uncertainty

Column 8. Apparent magnitude for B_T -band from the ESO VII catalogue

Column 9. Inclination

Column 10. Apparent magnitude for H^c - band

Column 11. K-correction for the H^c-band

Column 12. Apparent magnitude for the K_s-band

Column 13. K-correction for the K_s-band

Column 14. 2MASS co-added bands *JHK* axis ratio

Reference for columns 2 through 7. NED

Reference for column 8. ESO VII / 115 catalogue. Apparent magnitudes in column 8 with an (*) are from RC3 (de Vaucouleurs et al. 1991 RC3)

Reference for columns 9 through 13. New observations obtained with SOFI

Reference for column 14. 2MASS

Table 5.2: Apparent Magnitude B_T, H^c and K_s for the Parkes / NTT Sub-Sample

1	2	3	4	5	6	7	8	9	10	11	12	13	14	15	16	17	18	19	20
GALAXY			SNe Ia			ESO VII / 115				New Obs		2MASS H^c		SOFI H^c Total		2MASS K_s		SOFI K_s Total	
NAME		B	$\Delta m_{15}(B)$	$B-V_{max}$	ref	B_T	a/b	i	B_T^{bik}	i	a/b	H^c	$H^{c\,bik}$	H^c	$H^{c\,bik}$	K_s	K_s^{bik}	K_s	K_s^{bik}
ESO																			
269-G57	…	…	…	…	…	12.49	1.40	44	11.94	21.5	1.08	9.10	9.07	8.64	8.61	8.78	8.73	8.50	8.45
300-G09	1992bc	15.12	0.92	0.04	5, 6	15.67	3.00	71		…	…	…	…	…	…	…	…	…	…
576-G40	…	…	…	…	…	14.66	5.17	79	13.37	80.5	6.06	11.24	11.06	11.31	11.13	11.42	11.26	11.31	11.16
IC 5179	1999ee	14.93	0.96	0.26	5, 6	12.29	1.87	58	11.48	62.9	2.19	8.95	8.73	8.94	8.72	8.62	8.51	8.58	8.47
MCG																			
+01-34-05	1959C	14.10	0.74	0.91	5, 6	13.98*	8.33	83	13.26	73.0	3.42	13.65	13.52	…	12.52	13.23	13.14	…	12.30
-01-04-44	1998dm	15.40	0.38	0.16	5, 6	…	…	…	…	…	…	10.654	…	…	…	1.442	…	…	…
NGC 1084	1963P	14.20	1.01	0.06	1, 6	11.31*	1.79	56	10.79	51.5	1.61	8.21	8.09	8.15	8.03	7.93	7.86	7.86	7.79
NGC 1320	1994aa	17.00	…	…	2	13.32*	2.94	70	12.19	71.5	3.15	9.72	9.44	9.64	9.36	9.36	9.22	9.32	9.18
NGC 1326	…	…	…	…	…	13.80	1.04	16	13.66	42.4	1.36	13.85	13.85	…	…	13.56	13.54	…	…
NGC 1365	2012fr	11.99	0.77	0.04	8	10.08	1.40	44	9.70	40.4	1.31	6.74	6.65	6.76	6.67	6.37	6.33	6.42	6.37
NGC 1425	…	…	…	…	…	11.61	2.25	64	10.94	61.2	2.07	8.55	8.36	8.32	8.13	8.31	8.22	8.12	8.03
NGC 1566	…	…	…	…	…	13.53	1.44	46	13.25	37.5	1.26	7.21	7.16	7.00	6.95	6.89	6.85	6.91	6.88
NGC 1808	1993af	16.63	…	…	3	10.80	1.43	46	9.87	70.7	3.02	6.98	6.77	6.90	6.68	6.66	6.53	6.65	6.53
NGC 2090	…	…	…	…	…	11.70	1.80	56	10.98	62.0	2.13	8.30	8.14	8.17	8.01	8.05	7.96	7.94	7.85
NGC 2227	1986O	14.00	…	…	2	13.40	1.82	57	12.73	46.6	1.46	10.26	10.17	9.76	9.67	9.68	9.60	9.48	9.41
NGC 2487	…	…	…	…	…	13.23*	1.23	36	12.83	30.9	1.17	9.95	9.90	9.74	9.69	9.70	9.66	9.48	9.44
NGC 2595	…	…	…	…	…	12.93*	1.32	41	12.50	37.9	1.27	9.92	9.85	9.39	9.32	9.66	9.61	9.33	9.28
NGC 2713	1968E	14.72	0.72	0.06	4, 6	12.72*	2.38	65	11.55	65.4	2.40	8.56	8.24	8.47	8.16	8.31	8.16	8.24	8.09
NGC 2775	1993Z	13.87	0.74	0.06	2, 6	11.03*	1.28	39	10.59	36.6	1.25	7.41	7.33	7.13	7.05	7.04	6.99	6.96	6.91
NGC 2935	1996Z	14.61	1.22	0.51	5, 6	11.84	1.40	44	11.16	52.4	1.64	8.64	8.52	8.22	8.10	8.31	8.23	8.10	8.02
NGC 3351	…	…	…	…	…	10.53*	1.47	47	10.31	23.5	1.09	6.95	6.92	7.00	6.97	6.67	6.64	6.83	6.81

Table 5.2: Continued

1	2	3	4	5	6	7	8	9	10	11	12	13	14	15	16	17	18	19	20
GALAXY			SNe Ia			ESO VII / 115				New Obs		2MASS H^c		SOFI H^c Total		2MASS K_s		SOFI K_s Total	
NAME		B	$\Delta m_{15}(B)$	$B-V_{max}$	ref	B_T	a/b	i	B_T^{bik}	i	a/b	H^c	$H^{c\,bik}$	H^c	$H^{c\,bik}$	K_s	K_s^{bik}	K_s	K_s^{bik}
NGC 3367	1986A	14.45	0.56	0.07	6, 7	12.05*	1.15	30	11.76	30.1	1.16	9.12	9.08	8.86	8.82	8.76	8.72	8.75	8.72
NGC 3368	1998bu	12.22	1.10	0.36	5, 6	10.11*	1.45	46	9.62	48.7	1.52	6.57	6.45	6.51	6.39	6.32	6.26	6.35	6.29
NGC 3370	1994ae	13.15	1.29	0.05	5, 6	12.28*	1.79	56	11.68	58.0	1.89	9.67	9.53	9.54	9.40	9.43	9.35	9.32	9.24
NGC 3621	…	…	…	…	…	10.18	2.00	60	9.34	60.9	2.06	6.80	6.65	6.85	6.70	6.60	6.50	6.71	6.61
NGC 3627	1989B	11.93	1.48	0.43	5, 6	9.65*	2.17	63	9.07	51.7	1.61	6.15	6.01	6.10	5.97	5.88	5.81	5.93	5.86
NGC 3810	…	…	…	…	…	11.35*	1.41	45	10.88	44.8	1.42	8.29	8.21	8.04	7.96	7.95	7.90	7.90	7.85
NGC 4178	1963I	13.10	1.26	0.06	2, 6	11.90*	2.86	70	10.87	76.5	4.29	9.37	9.11	9.01	8.75	9.58	9.44	8.84	8.70
NGC 4321	…	…	…	…	…	10.05*	1.18	32	9.59	50.7	1.58	6.82	6.72	6.80	6.70	6.59	6.53	6.60	6.54
NGC 4462	1998bn	14.31	1.37	0.00	2, 6	12.81	2.59	67	11.53	68.2	2.70	8.74	8.48	8.69	8.43	8.46	8.31	8.47	8.32
NGC 4496	1960F	11.46	0.84	0.06	3, 6	11.94*	1.27	38	11.69	35.5	1.23	9.78	9.74	9.33	9.29	9.56	9.53	9.08	9.05
NGC 4501	1999cl	15.11	1.30	1.22	5, 6	10.36*	1.85	57	9.48	59.7	1.98	6.56	6.33	6.51	6.28	6.27	6.15	6.29	6.18
NGC 4527	…	…	…	…	…	11.38*	2.94	70	10.23	74.4	3.72	7.26	6.93	7.17	6.85	6.93	6.78	6.95	6.80
NGC 4535	…	…	…	…	…	10.59*	1.41	45	10.11	53.4	1.68	7.65	7.53	7.56	7.44	7.38	7.32	7.44	7.38
NGC 4536	1981B	11.93	1.01	0.06	5, 6	11.16*	2.33	65	10.31	68.2	2.70	7.88	7.65	7.70	7.47	7.52	7.40	7.45	7.34
NGC 4548	…	…	…	…	…	10.96*	1.27	38	10.51	48.5	1.51	7.37	7.29	7.34	7.25	7.12	7.06	7.24	7.19
NGC 4579	1989M	12.67	1.37	0.30	1, 6	10.48*	1.27	38	10.00	42.6	1.36	6.71	6.61	6.76	6.66	6.49	6.43	6.62	6.56
NGC 4639	1990N	12.75	1.14	0.05	5, 6	12.24*	1.47	47	11.85	43.7	1.38	9.03	8.95	8.80	8.72	8.81	8.76	8.66	8.61
NGC 4902	1991X	13.70	…	…	2	11.61*	1.12	27	11.28	22.5	1.08	8.56	8.53	8.22	8.19	8.32	8.29	8.07	8.04
NGC 4948	1994U	14.00	…	…	2	…	…	…		81.0	6.41	10.99	10.83	10.30	10.14	10.75	10.64	10.15	10.04
NGC 5253	1972E	8.86	1.42	0.18	5, 6	11.17	2.32	64	10.81	58.6	1.92	8.48	8.52	8.34	8.37	8.25	8.21	8.22	8.18
NGC 5468	1999cp	14.60	…	…	2	13.00*	1.10	25	12.74	39.7	1.30	10.34	10.30	9.72	9.69	10.40	10.37	9.57	9.54
NGC 5668	…	…	…	…	…	12.20*	1.10	25	11.98	23.1	1.09	11.21	11.19	…	…	11.71	11.69	…	…
NGC 6063	…	…	…	…	…	13.76*	2.00	60	13.18	51.0	1.59	10.77	10.66	10.49	10.38	10.55	10.48	10.39	10.32
NGC 6384	1971L	13.05	1.04	0.32	1, 6	11.14*	1.52	49	10.21	48.5	1.51	7.60	7.48	7.68	7.56	7.53	7.43	7.62	7.52
NGC 6753	2000cj	14.56	0.72	0.00	2, 6	11.84	1.12	27	11.32	31.3	1.17	7.80	7.73	7.68	7.62	7.52	7.47	7.50	7.45

Table 5.2: End

1	2	3	4	5	6	7	8	9	10	11	12	13	14	15	16	17	18	19	20
GALAXY			SNe Ia			ESO VII / 115				New Obs		2MASS H^c		SOFI H^c Total		2MASS K_s		SOFI K_s Total	
NAME		B	$\Delta m_{15}(B)$	$B-V_{max}$	ref	B_T	a/b	i	$B_T{}^{bik}$	i	a/b	H^c	$H^{c\ bik}$	H^c	$H^{c\ bik}$	K_s	$K_s{}^{bik}$	K_s	$K_s{}^{bik}$
NGC 6754	1998dq	13.39	0.72	0.10	2, 6	12.86	1.91	58	11.50	72.9	3.40	9.25	8.93	9.14	8.82	8.86	8.68	8.88	8.71
NGC 6835	1962J	12.89	0.76	0.06	2, 6	13.41*	4.55	77	12.13	79.0	5.24	…	0.01	…	…	…	…	…	…
NGC 7448	1997dt	15.64	1.04	0.43	5, 6	12.20*	2.17	63	11.40	62.2	2.15	9.33	9.17	9.25	9.09	9.01	8.92	9.00	8.90
NGC 7606	1987N	12.85	0.72	0.45	3, 6	11.51*	2.50	66	10.42	66.7	2.53	7.69	7.40	8.01	7.71	7.64	7.50	7.74	7.60
NGC 7723	1975N	13.72	1.46	0.31	1, 6	11.94*	1.47	47	11.46	47.4	1.48	8.61	8.51	8.46	8.35	8.28	8.22	8.15	8.09

Column 1. Galaxy name

Column 2. Type Ia Supernova (SN Ia) name

Column 3. SN Ia B-band peak apparent magnitude

Column 4. SN Ia $\Delta m_{15}(B)$

Column 5. SN Ia $B-V_{max}$ at peak apparent magnitude

Column 6. Reference for SN Ia data

Column 7. ESO VII / 115 B_T apparent magnitude where B_T is the total observed magnitude - **Note**: Apparent magnitudes in column 7 with an (*) are from RC3

Column 8. Axis ratio a/b from the B_T apparent magnitude

Column 9. Inclination calculated using the axis measurements from B_T

Column 10. B_T apparent magnitude adjusted for reddening and includes the corrections $B^{b,i,k} = B_T - A_B{}^b - A_B{}^{i\text{-}o\text{-}} - A_B{}^k$

Column 11. New observation inclination

Column 12. Axis ratio a/b from the new observation measurements

Column 13. 2MASS H^c-band total near-infrared apparent magnitude

Column 14. 2MASS H^c-band total apparent magnitude corrected for galactic extinction and redshift z, *(bik)*

Column 15. SOFI H^c-band total near-infrared apparent magnitude

Column 16. SOFI H^c-band total apparent magnitude corrected for galactic extinction and redshift z, *(bik)*

Column 17. 2MASS K_s-band total apparent magnitude

Column 18. 2MASS K_s-band total near-infrared apparent magnitude adjusted for reddening and includes the corrections $K_s{}^{b,i,k} = K_s - A_K{}^b - A_K{}^{i\text{-}o\text{-}} - K_s{}^k$

Column 19. SOFI K_s-band total apparent magnitude

Column 20. SOFI K_s-band total near-infrared apparent magnitude adjusted for reddening and includes the corrections $K_s{}^{b,i,k} = K_s - A_K{}^b - A_K{}^{i\text{-}o\text{-}} - K_s{}^k$

Table 5.2: References

References for columns 3 through 6.

1-Branch and Miller (1993)

2-CfA (2008)

3-Lanoix (1998)

4-Petrosian (2005)

5-Reindl et al. (2005)

6-SAI (2008)

7-Tammann and Leibundgut (1990)

8-Klotz and Childress (2012).

Reference for columns 7 through 10. ESO

Reference for columns 11 and 12. New observations.

Reference for columns 13 and 14. 2MASS

Reference for columns 15 and 16. SOFI

Reference for columns 17 and 18. 2MASS

Reference for columns 19 and 20. SOFI

Table 5.3: The Parkes / NTT Sub-Sample Measurements

1	2	3	4	5	6	7	8	9	10	11	12	13	14	15	16	17	18	19	20
		SN Ia				Obs	GSR		Virgo infall		3K CMB		Parkes New Observations				Corrected		
GALAXY		J2000		Galaxy		21 cm	velocity		velocity		velocity		W_{20}		W_{50}		W_{50}^{i}		Jy
NAME		RA	DEC	z	σ	km s^{-1}	km s^{-1}	σ	km s^{-1}	σ	km s^{-1}	σ	km s^{-1}	σ	km s^{-1}	σ	km s^{-1}	σ	km s^{-1}
ESO																			
269-G57	…	…	….	0.010360	0.000018	3104	2933	9	3021	20	3359	18	345	9	324	6	…	…	36.5
300-G09	1992bc	03 05 16.0	-39 33 35	0.020000	0.002000	6078	5881	7	5751	60	5895	60	324	9	311	6	..	…	3.2
576-G40	…	…	…	0.006938	0.000017	2086	1957	7	2176	25	2386	22	198	5	170	3	…	…	17.6
IC 5179	1999ee	22 16 10.0	-36 50 40	0.011415	0.000033	3414	3436	10	3340	13	3163	21	424	11	401	8	444	7	9.8
MCG																			
+01-34-05	1959C	13 11 23.8	03 24 38	0.010147	0.000270	3042	2984	3	3215	23	3358	24	207	6	166	3	175	3	9.8
-01-04-44	1998dm	01 26 14.0	-06 06 14	0.006535	0.000022	1959	2000	2	1923	13	1659	22	264	7	247	5	…	…	17.9
NGC 1084	1963P	02 46 02.1	-07 23 450	0.004693	0.000013	1409	1391	4	1342	7	1196	15	338	9	295	6	374	6	64.2
NGC 1320	1994aa	03 24 49.4	-03 02 33	0.008883	0.000053	2794	2634	16	2577	17	2500	20	364	10	352	7	366	6	2.3
NGC 1326A	…	…	…	0.006108	0.000003	1831	1713	5	1640	9	1725	8	86	2	72	1	109	2	23.0
NGC 1365	2012fr	03 33 35.9	-36 07 37	0.005457	0.000003	1639	1514	5	1499	9	1539	7	406	11	369	7	566	6	137.3
NGC 1425	…	…	…	0.005037	0.000010	1512	1397	5	1432	8	1411	8	369	10	353	7	401	6	53.0
NGC 1566	…	…	…	0.005017	0.000007	1503	1331	7	1286	13	1493	2	227	6	205	4	331	…	132.1
NGC 1808	1993af	05 08 00.8	-37 29 13	0.003319	0.000013	992	823	8	814	13	1017	4	320	9	267	5	283	5	66.9
NGC 2090	…	…	…	0.003072	0.000007	921	736	1	747	14	993	5	296	8	280	6	317	6	117.5
NGC 2227	1986O	06 25 57.9	-22 00 44	0.007532	0.000010	2257	2078	8	2095	14	2383	9	283	8	260	5	354	6	12.3
NGC 2487	…	…	…	0.016148	0.000010	4841	4777	5	4892	10	5043	14	276	7	260	5	…	…	6.1
NGC 2595	…	…	…	0.014443	0.000013	4330	4249	5	4380	13	4572	17	345	9	329	7	522	…	10.3
NGC 2713	1968E	08 57 21.1	02 54 58	0.013082	0.000020	3921	3775	8	3900	18	4226	22	631	17	604	12	650	15	10.1
NGC 2775	1993Z	09 10 19.6	07 01 40	0.004516	0.000017	1517	1217	6	1424	21	1660	22	418	11	406	8	678	…	4.7
NGC 2935	1996Z	09 36 44.8	-21 08 52	0.007575	0.000010	2272	2066	9	2208	23	2601	23	306	8	275	6	344	7	50.9
NGC 3351	…	…	…	0.002595	0.000013	779	677	1	610	10	1127	25	279	8	267	5	…	…	46.3
NGC 3367	1986A	10 46 36.5	13 45 01	0.010142	0.000024	3041	2948	8	3168	22	3385	25	292	8	231	5	…	…	19.6

Table 5.3: Continued

1	2	3	4	5	6	7	8	9	10	11	12	13	14	15	16	17	18	19	20
		SN Ia				Obs	GSR		Virgo infall		3K CMB		Parkes New Observations				Corrected		
GALAXY		J2000		Galaxy		21 cm	velocity		velocity		velocity		W_{20}		W_{50}		W_{50}^{i}		Jy
NAME		RA	DEC	z	σ	km s^{-1}	km s^{-1}	σ	km s^{-1}	σ	km s^{-1}	σ	km s^{-1}	σ	km s^{-1}	σ	km s^{-1}	σ	km s^{-1}
NGC 3368	1998bu	10 46 46.0	11 50 07	0.002992	0.000013	892	797	6	800	11	1246	25	362	10	337	7	445	6	78.0
NGC 3370	1994ae	10 47 01.9	17 16 31	0.004266	0.000013	1280	1198	5	1551	29	1615	24	289	8	271	5	318	6	31.2
NGC 3621	…	…	…	0.002435	0.000007	727	530	8	505	18	1064	23	279	8	261	5	299	5	479.8
NGC 3627	1989B	11 20 13.9	13 00 19	0.002425	0.000010	723	643	5	447	13	1075	25	385	10	347	7	440	7	43.6
NGC 3810	…	…	…	0.003309	0.000002	997	911	3	735	12	1341	24	268	7	243	5	343	5	48.4
NGC 4178	1963I	12 12 45.6	10 51 31	0.001248	0.000002	377	307	3	182	19	715	24	275	7	250	5	…	…	63.6
NGC 4321	…	…	…	0.005240	0.000003	1573	1525	2	957	37	1896	23	270	7	247	5	318	6	49.7
NGC 4462	1998bn	12 29 18.9	-23 09 49	0.005977	0.000013	1791	1639	7	1880	27	2129	24	398	11	383	8	409	7	7.7
NGC 4496A	1960F	12 31 42.0	03 56 48	0.005771	0.000010	1731	1650	4	957	45	2072	24	174	5	153	3	265	…	46.9
NGC 4501	1999cl	12 31 56.0	14 25 35	0.007609	0.000010	2280	2235	4	957	86	2605	23	530	14	505	10	574	9	28.8
NGC 4527	…	…	…	0.005791	0.000003	1735	1654	3	957	45	2079	24	377	10	356	7	367	7	98.8
NGC 4535	…	…	…	0.006551	0.000002	1963	1899	3	957	62	2299	23	288	8	269	5	333	5	73.2
NGC 4536	1981B	12 34 29.5	02 11 59	0.006031	0.000003	1804	1725	3	2110	33	2151	24	343	9	324	6	347	6	76.2
NGC 4548	…	…	…	0.001621	0.000013	482	442	4	255	12	808	23	242	7	228	5	304	5	10.1
NGC 4579	1989M	12 37 40.7	11 49 25	0.005060	0.000002	1520	1466	2	957	33	1843	23	375	10	359	7	520	7	9.0
NGC 4639	1990N	12 42 56.7	13 15 23	0.003395	0.000018	975	974	6	957	8	1338	23	295	8	276	6	396	6	16.6
NGC 4902	1991X	13 01 01.4	-14 30 28	0.008916	0.000017	2622	2557	7	2767	24	3001	24	279	8	225	5	…	…	29.1
NGC 4948	1994U	13 04 56.1	-07 56 52	0.003746	0.000021	1125	1027	7	1243	23	1451	24	172	5	157	3	…	…	12.0
NGC 5253	1972E	13 39 53.2	-31 40 15	0.001358	0.000010	407	274	6	204	13	681	19	102	3	64	1	80	1	36.7
NGC 5468	1999cp	14 06 31.3	-05 26 49	0.009480	0.000013	2842	2793	4	3003	20	3112	19	154	4	121	2	189	2	30.4
NGC 5668	…	…	…	0.005260	0.000003	1583	1575	1	1884	25	1880	16	115	3	95	2	…	…	43.7
NGC 6063	…	…	…	0.009500	0.000017	2850	2919	6	3098	15	2944	8	297	8	272	5	344	5	8.2
NGC 6384	1971L	17 32 26.1	07 04 02	0.005554	0.000004	1664	1784	5	1938	13	1627	3	380	10	362	7	476	6	74.5
NGC 6753	2000cj	19 11 27.6	-57 03 19	0.010570	0.000027	3177	3101	9	3064	10	3107	9	466	13	405	8	…	…	15.1

Table 5.3: End

1	2	3	4	5	6	7	8	9	10	11	12	13	14	15	16	17	18	19	20
GALAXY		SN Ia J2000		Galaxy		Obs 21 cm	GSR velocity		Virgo infall velocity		3K CMB velocity		Parkes New Observations W_{20}			W_{50}	Corrected W_{50}^{i}		Jy
NAME		RA	DEC	z	σ	km s^{-1}	km s^{-1}	σ	km s^{-1}	σ	km s^{-1}	σ	km s^{-1}	σ	km s^{-1}	σ	km s^{-1}	σ	km s^{-1}
NGC 6754	1998dq	19 11 23.8	50 38 26	0.010864	0.000033	3234	3213	10	3181	11	3176	11	416	11	385	8	398	7	8.6
NGC 6835	1962J	19 54 30.9	-12 34 28	0.005374	0.000030	1624	1720	10	1746	12	1387	18	177	5	95	2	…	…	16.5
NGC 7448	1997dt	23 00 02.9	15 58 51	0.007318	0.000003	2184	2370	7	2347	17	1828	26	295	8	269	5	301	5	35.5
NGC 7606	1987N	23 19 03.3	-08 28 37	0.007442	0.000017	2233	2331	6	2256	14	1874	26	521	14	503	10	538	9	24.8
NGC 7723	1975N	23 38 54.8	-12 57 09	0.006254	0.000027	1859	1951	9	1874	14	1529	26	329	9	316	6	423	6	7.9

Table 5.3: Column Description and References

Column 1. Galaxy name
Column 2. Type Ia Supernova (SN Ia) name
Column 3. SN Ia coordinates for right ascension
Column 4. SN Ia coordinates for declination
Column 5. Redshift z
Column 6. Redshift z uncertainty
Column 7. Observed 21 cm barycentric velocity in km s^{-1}
Column 8. Observed 21 cm barycentric velocity corrected to Galactic Standard of Rest in km s^{-1}
Column 9. 21 cm GSR corrected uncertainty in km s^{-1}
Column 10. 21 cm barycentric velocity corrected to the Virgo infall in km s^{-1}
Column 11. Virgo infall velocity uncertainty in km s^{-1}
Column 12. 3K CMB velocity in km s^{-1}
Column 13. 3K CMB velocity uncertainty in km s^{-1}
Column 14. W_{20} in km s^{-1} (Parkes New Observations)
Column 15. Velocity uncertainty in km s^{-1}
Column 16. W_{50} in km s^{-1} (Parkes New Observations)
Column 17. Velocity uncertainty in km s^{-1}
Column 18. W_{50} in km s^{-1} corrected to W_R^i
Column 19. W_{50} uncertainty
Column 20. Observed flux for the 21 cm measurements

Reference for columns 3 and 4. NED J2000 Epoch
Reference for columns 5 and 6. NED
Reference for columns 7 through 20. New observations

Table 5.4: SOFI - Absolute Magnitude, Apparent Magnitude and Distance Modulus for the Parkes / NTT Sub-Sample

1	2	3	4	5	6	7	8	9	10	11	12	13	14	15	16	17	18
GALAXY		Phillips Template SN Ia				Tully Template W_{20} B_T				Masters Template W_{50} - SOFI H^c				Masters Template W_{50} - SOFI K_s			
NAME		M_B	B	μ	σ	M_B	B_{tbik}	μ	σ	M_H	$H^{c\ bik}$	μ	σ	M_K	K_s^{bik}	μ	σ
ESO																	
269-G57	…	…	…	…	…	…	11.94	…	…	…	8.61	..	…	…	8.45	…	…
300-G09	1992bc	-19.62	14.57	33.93	…	…	…	…	…	…	…	…	…	…	…	…	…
576-G40	…	…	…	…	…	…	13.37	..	…	…	11.13	…	…	…	11.16	…	…
IC 5179	1999ee	-19.61	13.47	32.81	0.14	-21.85	11.48	33.33	0.15	-24.17	8.72	32.89	0.02	-24.42	8.47	32.89	0.02
MCG																	
+01-34-05	1959C	-19.67	9.81	29.22	0.12	-19.34	13.26	32.60	0.15	-19.74	12.52	32.26	0.16	-19.95	12.30	32.25	0.24
-01-04-44	1998dm	-19.68	…	…	…	…	…	…	…	…	…	…	…	…	…	…	…
NGC 1084	1963P	-19.59	13.61	32.94	0.14	-21.55	10.79	32.34	0.15	-23.36	8.03	31.39	0.02	-23.60	7.79	31.39	0.02
NGC 1320	1994aa	…	…	…	…	-21.16	12.19	33.35	0.15	-23.26	9.36	32.62	0.02	-23.50	9.18	32.68	0.03
NGC 1326	…	…	…	…	…	-17.66	13.66	31.32	0.14	-17.47	11.42	29.18	0.03	-17.67	11.38	29.33	0.03
NGC 1365	2012fr	-19.38	11.99	31.37	0.07	-22.75	9.70	32.45	0.15	-25.30	6.67	31.97	0.03	-25.56	6.37	31.93	0.04
NGC 1425	…	…	…	…	…	-21.48	10.94	32.42	0.15	-23.68	8.13	31.81	0.03	-23.93	8.03	31.96	0.04
NGC 1566	…	…	…	…	…	-21.05	13.25	34.30	0.16	-22.79	6.95	29.74	0.03	-23.03	6.88	30.00	0.03
NGC 1808	1993af	…	…	…	…	-20.80	9.87	30.67	0.14	-22.05	6.68	28.73	0.02	-22.28	6.53	28.81	0.02
NGC 2090	…	…	…	…	…	-20.76	10.98	31.74	0.14	-22.58	8.01	30.59	0.02	-22.82	7.85	30.67	0.02
NGC 2227	1986O	…	…	…	…	-21.21	12.73	33.94	0.15	-23.10	9.67	32.77	0.02	-23.34	9.41	32.75	0.06
NGC 2487	…	…	…	…	…	…	12.83	…	…	…	9.69	…	…	…	9.44	…	…
NGC 2595	…	…	…	…	…	-22.34	12.50	34.84	0.16	-24.93	9.32	34.30	0.03	-25.18	9.28	34.52	0.03
NGC 2713	1968E	-19.68	13.96	33.38	0.14	-23.02	11.55	34.57	0.16	-25.95	8.16	34.11	0.02	-26.21	8.09	34.30	0.02
NGC 2775	1993Z	-19.67	13.12	32.52	0.13	-23.11	10.59	33.70	0.15	-26.15	7.05	33.24	0.03	-26.41	6.91	33.37	0.03
NGC 2935	1996Z	-19.40	12.27	31.41	0.13	-21.19	11.16	32.35	0.15	-22.96	8.10	31.06	0.02	-23.20	8.02	31.22	0.02
NGC 3351	…	…	…	…	…	…	10.31	…	…	…	6.97	…	…	…	6.81	…	…

Table 5.4: SOFI - Continued

1	2	3	4	5	6	7	8	9	10	11	12	13	14	15	16	17	18
GALAXY		Phillips Template SN Ia				Tully Template W_{20} B_T				Masters Template W_{50} - SOFI H^c				Masters Template W_{50} - SOFI K_s			
NAME		M_B	B	μ	σ	M_B	B_{tbik}	μ	σ	M_H	$H^{c\ bik}$	μ	σ	M_K	K_s^{bik}	μ	σ
NGC 3367	1986A	-19.68	13.57	32.99	0.14	…	11.76	…	…	…	8.82	…	…	…	8.72	…	…
NGC 3368	1998bu	-19.52	10.43	29.68	0.12	-21.90	9.62	31.52	0.14	-24.18	6.39	30.57	0.02	-24.43	6.29	30.72	0.02
NGC 3370	1994ae	-19.36	12.73	31.82	0.13	-20.80	11.68	32.48	0.15	-22.60	9.40	32.09	0.03	-22.83	9.24	32.17	0.03
NGC 3621	…	…	…	…	…	-20.61	9.34	29.95	0.14	-22.30	6.70	29.00	0.02	-22.53	6.61	29.14	0.03
NGC 3627	1989B	-19.12	10.01	28.87	0.12	-21.97	9.07	31.04	0.14	-24.12	5.97	30.09	0.02	-24.37	5.86	30.23	0.02
NGC 3810	…	…	…	…	…	-21.15	10.88	32.03	0.14	-22.96	7.96	30.92	0.02	-23.20	7.85	31.05	0.03
NGC 4178	1963I	-19.39	12.64	31.76	0.13	0.00	10.87	30.70	0.14	…	8.75	…	…	…	8.70	…	…
NGC 4321	…	…	…	…	…	-20.88	9.59	30.47	0.14	-22.60	6.70	29.30	0.04	-22.84	6.54	29.47	0.03
NGC 4462	1998bn	-19.26	14.18	33.18	0.14	-21.53	11.53	33.06	0.15	-23.78	8.43	32.21	0.02	-24.03	8.32	32.35	0.02
NGC 4496	1960F	-19.70	10.75	30.18	0.12	-20.42	11.69	32.11	0.14	-21.74	9.29	31.03	0.02	-21.96	9.05	31.01	0.02
NGC 4501	1999cl	-19.36	9.82	28.92	0.12	-22.64	9.48	32.12	0.15	-25.37	6.28	31.65	0.02	-25.63	6.18	31.81	0.02
NGC 4527	…	…	…	…	…	-21.24	10.23	31.47	0.14	-23.27	6.85	30.12	0.02	-23.51	6.80	30.31	0.02
NGC 4535	…	…	…	…	…	-20.96	10.11	31.07	0.14	-22.81	7.44	30.25	0.04	-23.05	7.38	30.43	0.05
NGC 4536	1981B	-19.59	11.34	30.67	0.13	-21.06	10.31	31.37	0.14	-23.01	7.47	30.48	0.03	-23.25	7.34	30.59	0.03
NGC 4548	…	…	…	…	…	-20.64	10.51	31.15	0.14	-22.38	7.25	29.63	0.03	-22.61	7.19	29.80	0.03
NGC 4579	1989M	-19.26	11.29	30.29	0.13	-22.32	10.00	32.32	0.15	-24.91	6.66	31.57	0.03	-25.17	6.56	31.73	0.03
NGC 4639	1990N	-19.51	12.29	31.53	0.13	-21.51	11.85	33.36	0.15	-23.62	8.72	32.34	0.02	-23.87	8.61	32.48	0.02
NGC 4902	1991X	…	…	…	…	…	11.28	…	…	…	8.19	…	…	…	8.04	…	…
NGC 4948	1994U	…	…	…	…	…	…	…	…	…	10.14	…	…	…	10.04	…	…
NGC 5253	1972E	-19.25	7.984	26.97	0.11	…	10.81	…	…	…	8.38	…	…	…	8.18	…	…
NGC 5468	1999cp	…	…	…	…	-19.67	12.74	32.41	0.15	-20.13	9.69	29.82	0.03	-20.34	9.54	29.88	0.06
NGC 5668	…	…	…	…	…	…	11.98	…	…	…	9.48	…	…	…	9.41	…	…
NGC 6063	…	…	…	…	…	-21.12	13.18	34.30	0.16	-22.96	10.38	33.34	0.05	-23.20	10.32	33.52	0.08
NGC 6384	1971L	-19.58	11.38	30.70	0.13	-22.05	10.21	32.26	0.15	-24.50	7.56	32.06	0.03	-24.75	7.52	32.27	0.04
NGC 6753	2000cj	-19.68	14.05	33.47	0.14	…	11.32	…	…	…	7.62	…	…	…	7.45	…	…

Table 5.4: SOFI - End

1	2	3	4	5	6	7	8	9	10	11	12	13	14	15	16	17	18
GALAXY		Phillips Template SN Ia				Tully Template W_{20} B_T				Masters Template W_{50} - SOFI H^c				Masters Template W_{50} - SOFI K_s			
NAME		M_B	B	μ	σ	M_B	B_{tbik}	μ	σ	M_H	$H^{c\ bik}$	μ	σ	M_K	K_s^{bik}	μ	σ
NGC 6754	1998dq	-19.68	12.47	31.88	0.13	-21.56	11.50	33.06	0.15	-23.65	8.82	32.47	0.03	-23.89	8.71	32.60	0.04
NGC 6835	1962J	-19.67	12.14	31.54	0.13	…	12.13	…	…	…	9.20	…	…	…	8.80	…	…
NGC 7448	1997dt	-19.56	13.51	32.81	0.14	-20.71	11.40	32.11	0.15	-22.34	9.09	31.43	0.02	-22.57	8.90	31.47	0.03
NGC 7606	1987N	-19.68	10.47	29.89	0.12	-22.39	10.42	32.81	0.15	-25.06	7.71	32.77	0.02	-25.32	7.60	32.92	0.03
NGC 7723	1975N	-19.51	12.3	31.55	0.13	-21.64	11.46	33.10	0.15	-23.94	8.35	32.29	0.02	-24.19	8.09	32.28	0.03

Column 1. Galaxy Name

Column 2. Type Ia Supernova (SN Ia) name

Column 3. SN Ia absolute magnitude

Column 4. SN Ia apparent magnitude

Column 5. SN Ia distance modulus reduced by 0.27 for the Cepheid zero point

Column 6. SN Ia distance modulus uncertainty

Columns 7 through 18. W_R^i absolute magnitude, apparent magnitude, and distance modulus with uncertainty for bands B_T, H^c and K_s

Reference for columns 3 through 6. Calculations made using Phillips et al. (1999) $\Delta m_{15}(B)$ decline rate relation

Reference for columns 7 through 18. Calculations made using the calibration equations from § 2

Table 5.5: 2MASS - Absolute Magnitude, Apparent Magnitude and Distance Modulus for the Parkes / NTT Sub-Sample

1	2	3	4	5	6	7	8	9	10	11	12	13	14	15	16	17	18
GALAXY		Phillips Template SN Ia				Tully Template W_{20} B_T				Masters Template W_{50} - 2MASS H^c				Masters Template W_{50}- 2MASS K_s			
NAME		M_B	B	μ	σ	M_B	B_{tbik}	μ	σ	M_H	$H^{c\ bik}$	μ	σ	M_K	$K_s^{\ bik}$	μ	σ
ESO																	
269-G57	…	…	…	…	…	…	11.94	…	…	…	9.07	..	…	…	8.73	…	…
300-G09	1992bc	-19.62	14.57	33.93	…	…	…	…	…	…	…	…	…	…	…	…	…
576-G40	…	…	…	…	…	…	13.37	…	…	…	11.06	…	…	…	11.26	…	…
IC 5179	1999ee	-19.61	13.47	32.81	0.14	-21.85	11.48	33.33	0.15	-24.17	8.73	32.90	0.02	-24.42	8.51	32.93	0.02
MCG																	
+01-34-05	1959C	-19.67	9.81	29.22	0.12	-19.34	13.26	32.60	0.15	-19.74	13.52	33.26	0.16	-19.95	13.14	33.09	0.24
-01-04-44	1998dm	-19.68	…	…	…	…	…	…	…	…	…	…	…	…	…	…	…
NGC 1084	1963P	-19.59	13.61	32.94	0.14	-21.55	10.79	32.34	0.15	-23.36	8.09	31.45	0.02	-23.60	7.86	31.46	0.02
NGC 1320	1994aa	…	…	…	…	-21.16	12.19	33.35	0.15	-23.26	9.44	32.70	0.02	-23.50	9.22	32.72	0.03
NGC 1326	…	…	…	…	…	-17.66	13.66	30.68	0.15	-17.47	13.85	31.61	0.03	-17.67	13.54	31.49	0.03
NGC 1365	2012fr	-19.38	11.99	31.37	0.07	-22.75	9.70	32.45	0.15	-25.30	6.65	31.95	0.03	-25.56	6.33	31.89	0.04
NGC 1425	…	…	…	…	…	-21.48	10.94	32.42	0.15	-23.68	8.36	32.04	0.03	-23.93	8.22	32.15	0.04
NGC 1566	…	…	…	…	…	-21.05	13.25	34.30	0.16	-22.79	7.16	30.04	0.03	-23.03	6.85	29.97	0.03
NGC 1808	1993af	…	…	…	…	-20.80	9.87	30.67	0.14	-22.05	6.77	28.82	0.02	-22.28	6.53	28.81	0.02
NGC 2090	…	…	…	…	…	-20.76	10.98	31.74	0.14	-22.58	8.14	30.72	0.02	-22.82	7.96	30.78	0.02
NGC 2227	1986O	…	…	…	…	-21.21	12.73	33.94	0.15	-23.10	10.17	33.27	0.02	-23.34	9.60	32.94	0.06
NGC 2487	…	…	…	…	…	…	12.83	…	…	…	9.90	…	…	…	9.66	…	…
NGC 2595	…	…	…	…	…	-22.34	12.50	34.84	0.16	-24.93	9.85	34.83	0.03	-25.18	9.61	34.85	0.03
NGC 2713	1968E	-19.68	13.96	33.38	0.14	-23.02	11.55	34.57	0.16	-25.95	8.24	34.19	0.02	-26.21	8.16	34.37	0.02
NGC 2775	1993Z	-19.67	13.12	32.52	0.13	-23.11	10.59	33.70	0.15	-26.15	7.33	33.52	0.03	-26.41	6.99	33.45	0.03
NGC 2935	1996Z	-19.40	12.27	31.41	0.13	-21.19	11.16	32.35	0.15	-22.96	8.52	31.48	0.02	-23.20	8.23	31.43	0.02
NGC 3351	…	…	…	…	…	…	10.31	…	…	…	6.92	…	…	…	6.64	…	…

Table 5.5: 2MASS - Continued

1	2	3	4	5	6	7	8	9	10	11	12	13	14	15	16	17	18
GALAXY		Phillips Template SN Ia				Tully Template W_{20} B_T				Masters Template W_{50} - 2MASS H^c				Masters Template W_{50} - 2MASS K_s			
NAME		M_B	B	μ	σ	M_B	B_{tbik}	μ	σ	M_H	$H^{c\ bik}$	μ	σ	M_K	K_s^{bik}	μ	σ
NGC 3367	1986A	-19.68	13.57	32.99	0.14	…	11.76	…	…	…	9.08	…	…	…	8.72	…	…
NGC 3368	1998bu	-19.52	10.43	29.68	0.12	-21.90	9.62	31.52	0.14	-24.18	6.45	30.63	0.02	-24.43	6.26	30.69	0.02
NGC 3370	1994ae	-19.36	12.73	31.82	0.13	-20.80	11.68	32.48	0.15	-22.60	9.53	32.22	0.03	-22.83	9.35	32.28	0.03
NGC 3621	…	…	…	…	…	-20.61	9.34	29.95	0.14	-22.30	6.65	28.95	0.02	-22.53	6.50	29.03	0.03
NGC 3627	1989B	-19.12	10.01	28.87	0.12	-21.97	9.07	31.04	0.14	-24.12	6.01	30.13	0.02	-24.37	5.81	30.18	0.02
NGC 3810	…	…	…	…	…	-21.15	10.88	32.03	0.14	-22.96	8.21	31.17	0.02	-23.20	7.90	31.10	0.03
NGC 4178	1963I	-19.39	12.64	31.76	0.13	0.00	10.87	30.70	0.14	…	9.11	…	…	…	9.44	…	…
NGC 4321	…	…	…	…	…	-20.88	9.59	30.47	0.14	-22.60	6.72	29.32	0.04	-22.84	6.53	…	…
NGC 4462	1998bn	-19.26	14.18	33.18	0.14	-21.53	11.53	33.06	0.15	-23.78	8.48	32.26	0.02	-24.03	8.31	32.34	0.02
NGC 4496	1960F	-19.70	10.75	30.18	0.12	-20.42	11.69	32.11	0.14	-21.74	9.74	…	…	-21.96	9.53	…	…
NGC 4501	1999cl	-19.36	9.82	28.92	0.12	-22.64	9.48	32.12	0.15	-25.37	6.33	31.70	0.02	-25.63	6.15	31.78	0.02
NGC 4527	…	…	…	…	…	-21.24	10.23	31.47	0.14	-23.27	6.93	30.20	0.02	-23.51	6.78	30.29	0.02
NGC 4535	…	…	…	…	…	-20.96	10.11	31.07	0.14	-22.81	7.53	30.34	0.04	-23.05	7.32	30.37	0.05
NGC 4536	1981B	-19.59	11.34	30.67	0.13	-21.06	10.31	31.37	0.14	-23.01	7.65	30.66	0.03	-23.25	7.40	30.65	0.03
NGC 4548	…	…	…	…	…	-20.64	10.51	31.15	0.14	-22.38	7.29	29.67	0.03	-22.61	7.06	29.67	0.03
NGC 4579	1989M	-19.26	11.29	30.29	0.13	-22.32	10.00	32.32	0.15	-24.91	6.61	31.52	0.03	-25.17	6.43	31.60	0.03
NGC 4639	1990N	-19.51	12.29	31.53	0.13	-21.51	11.85	33.36	0.15	-23.62	8.95	32.57	0.02	-23.87	8.76	32.63	0.02
NGC 4902	1991X	…	…	…	…	…	11.28	…	…	…	8.53	…	…	…	8.29	…	…
NGC 4948	1994U	…	…	…	…	…	…	…	…	…	10.83	…	…	…	10.64	…	…
NGC 5253	1972E	-19.25	7.984	26.97	0.11	…	10.81	…	…	…	8.52	…	…	…	8.21	…	…
NGC 5468	1999cp	…	…	…	…	-19.67	12.74	32.41	0.15	-20.13	10.30	30.43	0.03	-20.34	10.37	30.71	0.06
NGC 5668	…	…	…	…	…	…	11.98	…	…	…	11.19	…	…	…	11.69	…	…
NGC 6063	…	…	…	…	…	-21.12	13.18	34.30	0.16	-22.96	10.66	33.62	0.05	-23.20	10.48	33.68	0.08
NGC 6384	1971L	-19.58	11.38	30.70	0.13	-22.05	10.21	32.26	0.15	-24.50	7.48	31.98	0.03	-24.75	7.43	32.18	0.04
NGC 6753	2000cj	-19.68	14.05	33.47	0.14	…	11.32	…	…	…	7.73	…	…	…	7.47	…	…

Table 5.5: 2MASS - End

1	2	3	4	5	6	7	8	9	10	11	12	13	14	15	16	17	18
GALAXY		Phillips Template SN Ia				Tully Template W_{20} B_T				Masters Template W_{50} - 2MASS H^c				Masters Template W_{50} - 2MASS K_s			
NAME		M_B	B	μ	σ	M_B	B_{tbik}	μ	σ	M_H	$H^{c\ bik}$	μ	σ	M_K	$K_s{}^{bik}$	μ	σ
NGC 6754	1998dq	-19.68	12.47	31.88	0.13	-21.56	11.50	33.06	0.15	-23.65	8.93	32.58	0.03	-23.89	8.68	32.57	0.04
NGC 6835	1962J	-19.67	12.14	31.54	0.13	…	12.13	…	…	…	…	…	…	…	…	…	…
NGC 7448	1997dt	-19.56	13.51	32.81	0.14	-20.71	11.40	32.11	0.15	-22.34	9.17	31.51	0.02	-22.57	8.92	31.49	0.03
NGC 7606	1987N	-19.68	10.47	29.89	0.12	-22.39	10.42	32.81	0.15	-25.06	7.40	32.46	0.02	-25.32	7.50	32.82	0.03
NGC 7723	1975N	-19.51	12.3	31.55	0.13	-21.64	11.46	33.10	0.15	-23.94	8.51	32.45	0.02	-24.19	8.22	32.41	0.03

Column 1. Galaxy Name

Column 2. Type Ia Supernova (SN Ia) name

Column 3. SN Ia absolute magnitude

Column 4. SN Ia apparent magnitude

Column 5. SN Ia distance modulus reduced by 0.27 for the Cepheid zero point

Column 6. SN Ia distance modulus uncertainty

Columns 7 through 18. $W_R{}^i$ absolute magnitude, apparent magnitude, and distance modulus with uncertainty for bands B_T, H^c and K_s

Reference for columns 3 through 6. Calculations made using Phillips et al. (1999) $\Delta m_{15}(B)$ decline rate relation

Reference for columns 7 through 18. Calculations made using the calibration equations from § 2

REFERENCES

Bonatto, C., Bica, E., Ortolani, S., & Barbuy, B. 2009 MNRAS, 397, 1032

Branch, D., & Miller, D. L. 1993, ApJ, 405, L5

CfA 2008, Supernova (Cambridge: Harvard University)

de Vaucouleurs, G., de Vaucouleurs, A., Corwin, H. G., Jr., Buta, R. J., Pautrel, G., & Fouqué, P. 1991, Third Reference Catalogue of Bright Galaxies (New York: Springer) (RC3)

Grosbøl, P. 2008, private communication (Garching: European Southern Observatory)

Grosbøl, P., Patsis, P. A., & Pompei, E. 2004, A&A, 423, 849

Klotz, A. & Childress, M. 2012, private communication (Toulouse: IRAP (Institut de Recherche en Astrophysique et Planetologie)

Lanoix, P. 1998, A&A, 331, 421

Madore, B. F., Freedman, W. L., Silbermann, N., Harding, P., Huchra, J., Mould, J. R., Graham, J. A., Ferrarese, L., Gibson, B. K., Mingsheng, H., Hoessel, J. G., Hughes, S. M., Illingworth, G. D., Phelps, R., Sakai, S., & Stetson, P. 1999 ApJ, 515, 29

NED – NASA/IPAC Extragalactic Database – http://ned.ipac.caltech.edu/

Petrosian, A., Navasardyan, H., Cappellaro, E., McLean, B., Allen, R., Panagia, N., Leitherer, C., MacKenty, J., & Turatto, M. 2005, AJ, 129, 1369

Phillips, M. M., Lira, P., Suntzeff, N. B., Schommer, R. A., Hamuy, M., & Maza, J. 1999, AJ, 118, 1766

Pierce-Price, D. 2008, ESO (La Silla: La Silla Observatory)

Reindl, B., Tammann, G. A., Sandage, A., & Saha, A. 2005, ApJ, 624, 532

Riess, A. G., Li, W., Stetson, P. B., Filippenko, A. V., Jha, S., Kirshner, R. P., Challis, P. M., Garnavich, P. M., & Chornock, R. 2005, ApJ, 627, 579

Sternberg Astronomical Institute (SAI) 2008, Supernova Catalogue (Moscow: Moscow University)

Tammann, G. A., & Leibundgut, B. 1990, A&A, 236, 9

2MASS – www.ipac.caltech.edu/2mass/releases/allsky/

CHAPTER 6
DISCUSSION OF THE THREE SAMPLE SETS

6.1 The Combined Data

In this chapter, the three observed samples are combined and their properties discussed. Firstly, Figures 6.1 and 6.2 show the comparison of velocity widths W_{20} and W_{50} uncorrected and corrected for inclination, respectively, for the three sample sets. There is in general a good correlation of the uncorrected values of W_{50} and W_{20} in Figures 6.1, but with the latter values being slightly higher, as they represent widths measured at a smaller percentage of the peak value. There are around 15 outliers, all from the Literature sample, with a scatter that implies discrepant observations, low signal-to-noise observations, or peculiar profiles. Seven have inconsistent and unphysical pairs of values ($W_{50} > W_{20}$). Even so, the inclination cut and the inclination corrections applied to velocity widths improve the correlation greatly, as shown in Figure 6.2. Whilst the TF template relations we use do not require equality, it is encouraging to note that there is physical meaning behind the resolution and dispersion corrections defined in Chapter 2.

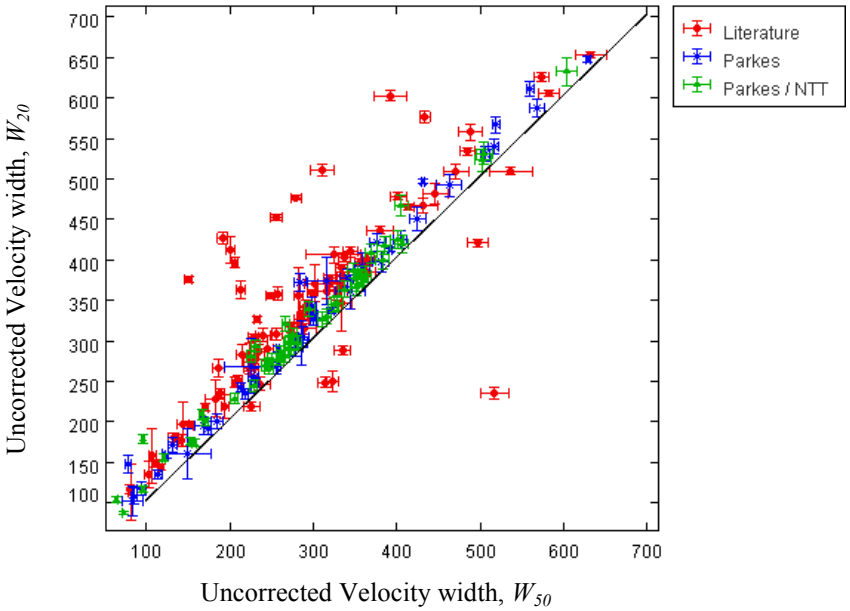

Figure 6.1: Comparison of 50% and 20% velocity widths W_{50} versus W_{20} for 180 galaxies from the combined sample sets. The mean difference is -36 km s^{-1} with an *rms* scatter of 51 km s^{-1}. The scatter and outliers are mainly due to inclination values that are beyond the range $35° < i < 80°$.

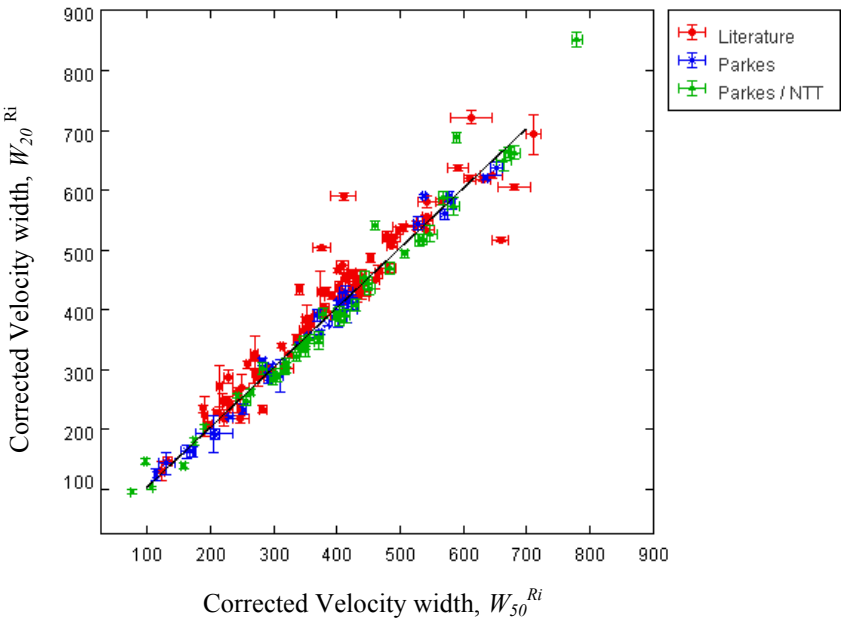

Figure 6.2: Comparison of 50% and 20% velocity widths W_{50}^{Ri} plotted against W_{20}^{Ri} for 134 galaxies from the combined sample sets after application of RC3 inclination corrections. The mean difference is -7 km s^{-1}, with an *rms* scatter of 26 km s^{-1}.

Included in Figure 6.2 is a correction for inclination, which being the same for W_{50} and W_{20}, makes no difference to the scatter. However, it greatly affects the accuracy of the line width measurement as defined in Chapter 2, and therefore the distance accuracy. It is one of the largest potential errors in the final result. The RC3 inclinations are based on the B_T -band, and are used for B_T -band 21 cm line width velocity corrections. For the *H* and *K* infrared data, the 2MASS co-added *JHK* bands were used to derive axis ratios and therefore inclinations. The new IR observations for the Parkes / NTT 51-galaxy sub-sample also provide more precise inclination data. These alternate measurements allow a comparison of the accuracy of different sources of inclination to be made. Figure 6.3 shows a comparison of 191 axis ratios from the RC3 B_T -band data with the 2MASS co-added IR bands of *JHK* for the three sample sets. An encouraging correlation is apparent with a small mean offset for the combined sample sets of 0.01 and an *rms* of 0.11. Figures 6.4 and 6.5 compare the calculated absolute magnitude K_s – band distance modulus to the NED and EDD (Extragalactic Distance Database) distance modulus respectively. Figure 6.6 compares of the log(cosec(*i*)) inclination corrections that are applied to velocity widths, for the RC3 B_T -band data and 2MASS co-added IR bands *JHK* data. In this space, the points are no longer symmetric about the straight line – values of the ratio *b/a*, which are close to

unity have larger corrections. The combined scatter of 0.05 dex, if equally divided in quadrature between RC3 and 2MASS, implies an intrinsic scatter of 0.035, or 8%, and a contribution to the final TF scatter of 0.35 mag. This is therefore one of the largest sources of error in the TF relation.

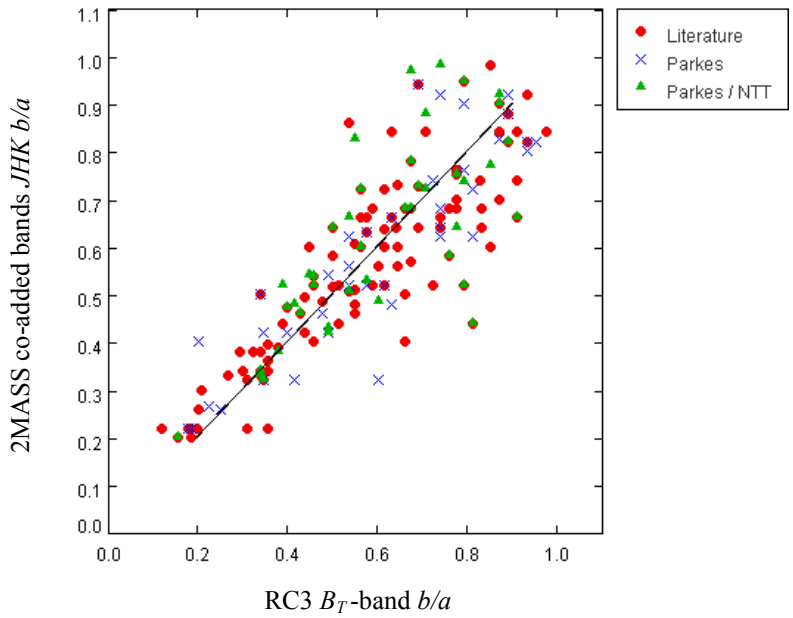

Figure 6.3: Axis ratio *b/a* comparison of the RC3 B_T-band data versus 2MASS co-added IR bands of *JHK*. The mean offset and *rms* scatter is 0.01±0.11, 0.01±0.11, and -0.01±0.14 for the Literature, Parkes, and Parkes / NTT samples, respectively. For all samples, the mean offset and *rms* scatter is 0.01±0.11.

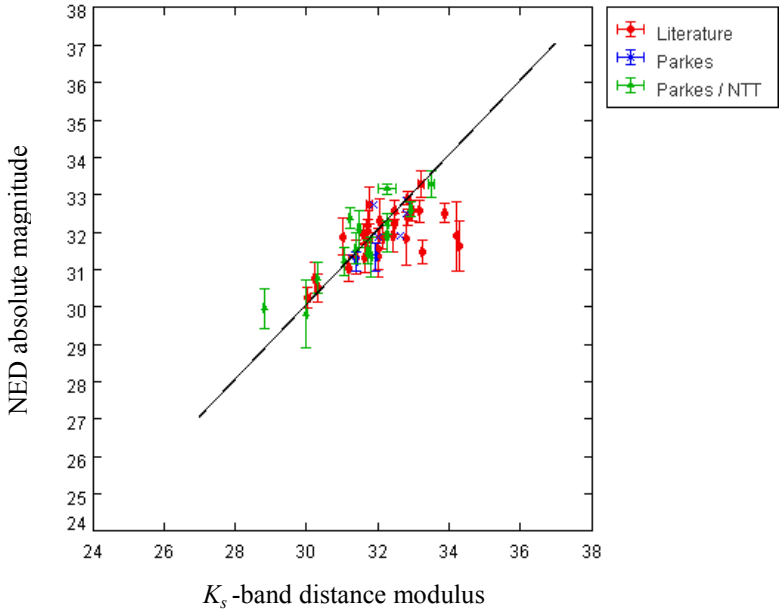

Figure 6.4: K_s -band distance modulus versus NED distance modulus for the three sample sets combined total of 52 galaxies. The reference line is through the origin with a slope = 1.000. The distance moduli have a mean offset of 0.17 mag, with an *rms* scatter of 0.76 mag.

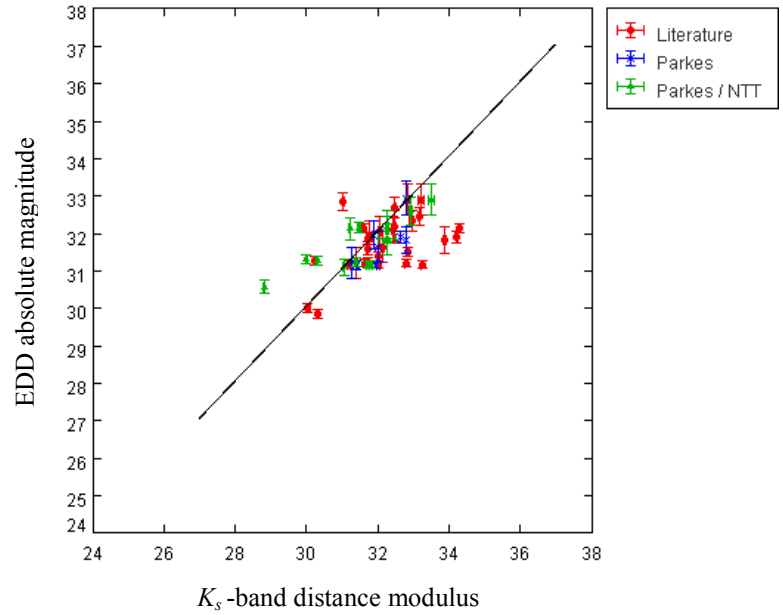

Figure 6.5: K_s -band distance modulus versus EDD distance modulus for the three sample sets combined total of 52 galaxies. The reference line is through the origin with a slope = 1.000. The distance moduli have a mean offset of 0.29 mag, with an *rms* scatter of 0.91 mag.

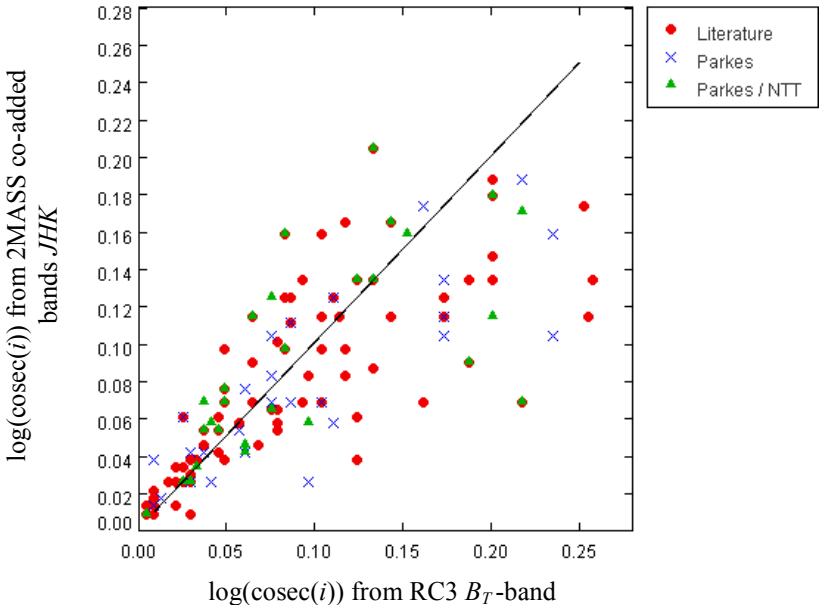

Figure 6.6: Comparison of log(cosec(inclination)) values for the RC3 B_T-band data and the 2MASS co-added *JHK* bands. The mean offset and *rms* scatter is 0.01±0.04, 0.01±0.04, 0.01±0.06 for the Literature, Parkes, and Parkes / NTT samples, respectively. For all samples, the mean offset and *rms* scatter is 0.01±0.05.

Moving on to the TF relations themselves, Figures 6.7 through 6.9 show the three pairwise relationships between the TF distance moduli derived from all three bands B_T, H^c, and K_s and for all galaxy samples. The results show an excellent correlation with the scatter, varying from 0.15 to 0.68 mag, with the correlation between the H^c and K_s TF relations being the tightest. When absolute magnitude, calculated from apparent magnitude and redshift (with extinction corrections applied), is plotted against corrected velocity width, the scatter is higher. This may be partly due to increased scatter from cosmic peculiar velocities, but mainly to reduced correlation between the variables plotted. Figure 6.10 shows such a plot (the Tully-Fisher or TF relation), where log 21cm line width velocity corrected for broadening, inclination, random and rotation motion is plotted against the mean (SOFI and 2MASS) absolute H^c and K_s -band magnitudes calculated from recession velocity. This has a larger spread of around 1.13 mag. In light of the excellent quality of both the SOFI and 2MASS data, and the H^c and K_s data, we choose to take the overall mean distance modulus across both sets of data and both wavebands in order to minimize sources of random and systematic scatter, as in Figure 6.10.

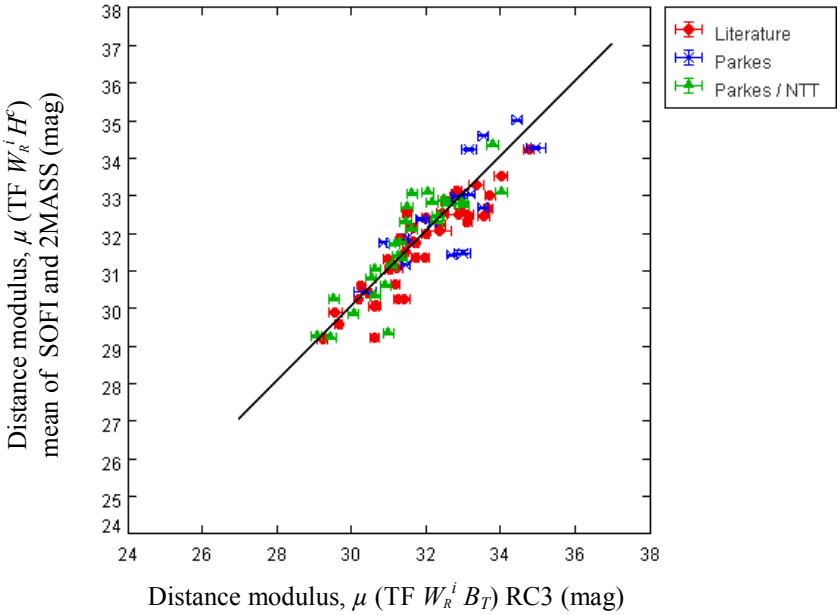

Figure 6.7: Comparison of the RC3 B_T -band based distance moduli and the mean of SOFI and 2MASS H^c -band based TF distance moduli for the three galaxy samples (120 galaxies total). The reference line goes through the origin with a slope of unity. The mean difference is 0.20 mag, with an *rms* scatter of 0.64 mag.

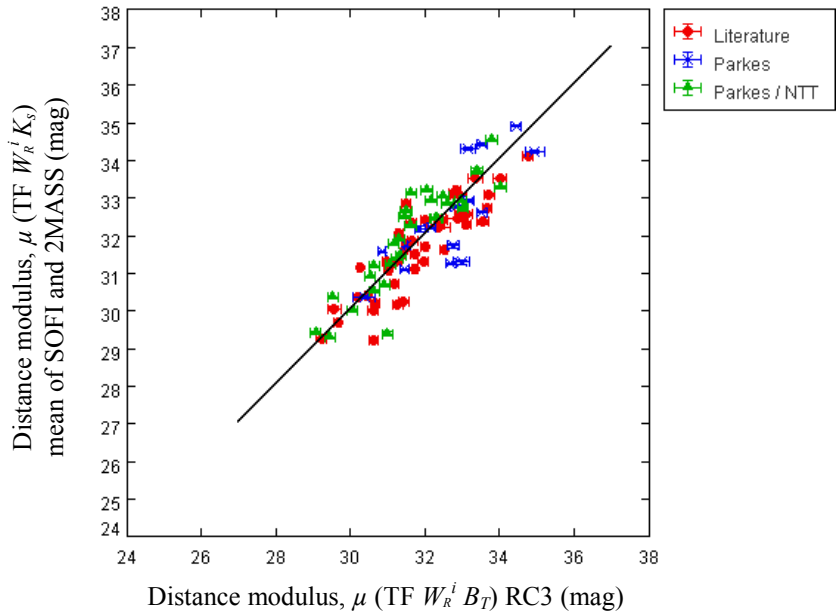

Figure 6.8: Comparison of the RC3 B_T -band based distance moduli and the mean of SOFI and 2MASS K_s -band based TF distance moduli for the three galaxy samples (120 galaxies total). The reference line goes through the origin with a slope of unity. The mean difference is 0.26 mag, with an *rms* scatter of 0.68 mag.

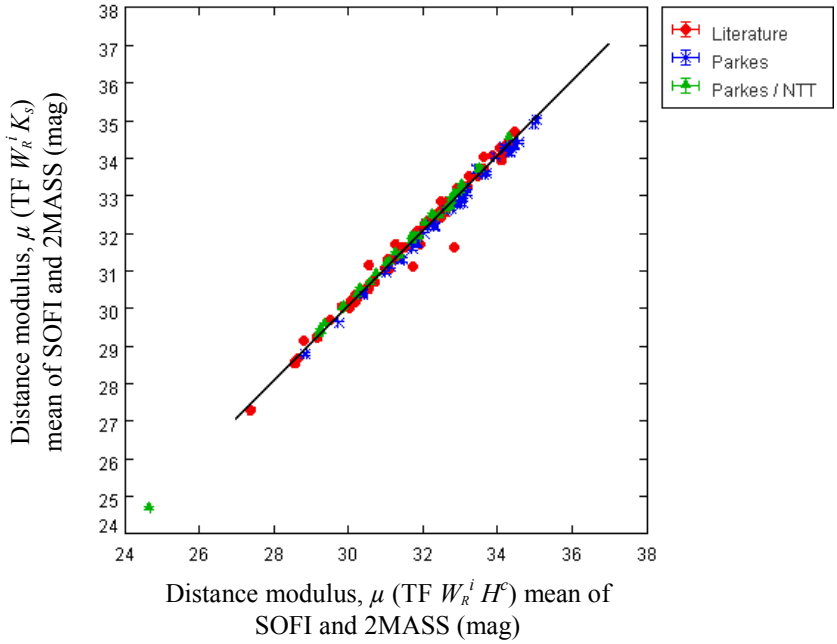

Figure 6.9: Comparison of the mean of SOFI and 2MASS H^c -band and the mean of SOFI and 2MASS K_s -band TF distance moduli for the three galaxy samples (183 galaxies total). The reference line goes through the origin with a slope of unity. The mean difference is 0.03 mag, with an *rms* scatter of 0.15 mag.

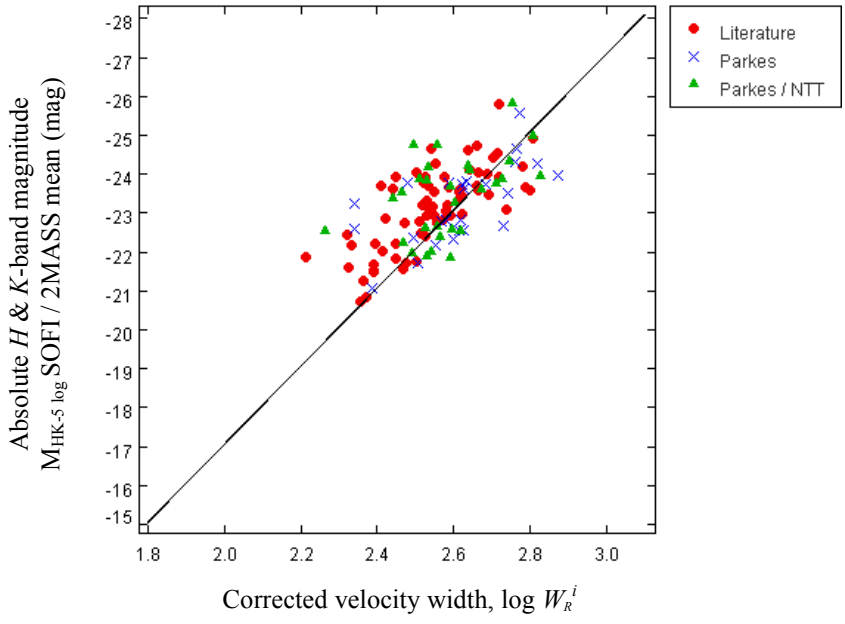

Figure 6.10: Absolute magnitude, calculated from CMB redshift and the' mean' of the SOFI and 2MASS H^c and K_s -band measurements, plotted against corrected velocity width for the combined sample of 103 galaxies. The offset and *rms* scatter is 0.24±1.03, 0.10±1.20, and 0.19±1.17 mag for the Literature, Parkes, and Parkes / NTT samples, respectively. The combined offset is 0.18 mag, with an *rms* scatter of 1.13 mag.

Figures 6.11, 6.12, and 6.13 plot the calculated distance moduli against redshift in the CMB frame, or the Hubble diagram. The mean *rms* scatter for TF B_T and *H/K* distance moduli plotted in Figures 6.11 and 6.12 is 0.93 and 1.19 mag, respectively. The latter is similar to the scatter in Figure 6.11, by definition. For SNe Ia distance moduli in Figure 6.13, the scatter is around 1.28 mag. Therefore, although CMB velocity is only an approximate indicator of distance, it does appear that the TF scatter is 20% smaller than for SNe Ia. The higher SNe Ia scatter may be due to the incomplete and inhomogeneous nature of the literature. Peculiar velocities may be another factor influencing the scatter (of both relations), as discussed latter in this chapter.

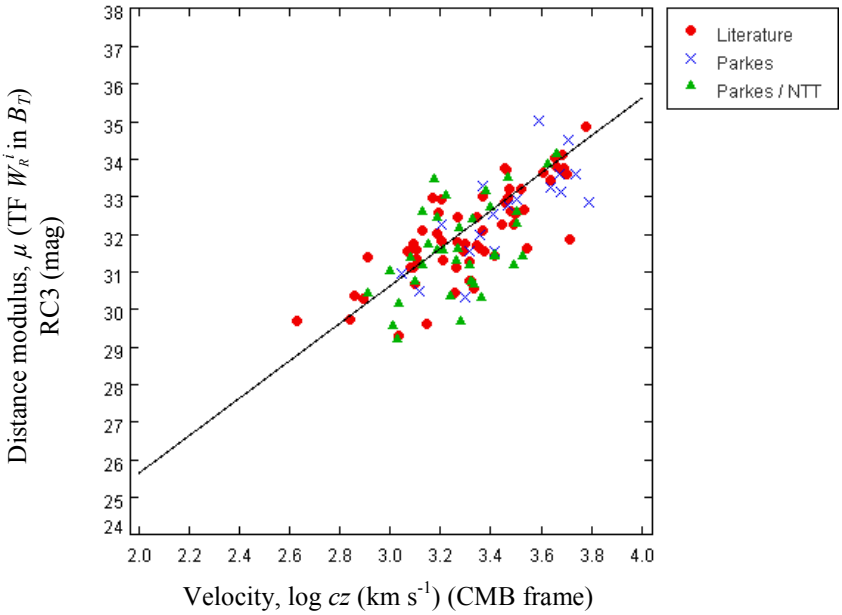

Figure 6.11: The Hubble diagram (TF distance modulus versus log *cz*, CMB frame) for 119 galaxies. The TF distance moduli are from the RC3 B_T -band based values. The offset and *rms* scatter is -0.40±0.91, -0.24±0.83, and -0.19±1.05 mag for the Literature, Parkes, and Parkes / NTT samples, respectively. For all samples, the offset and *rms* scatter is -0.28±0.93 mag.

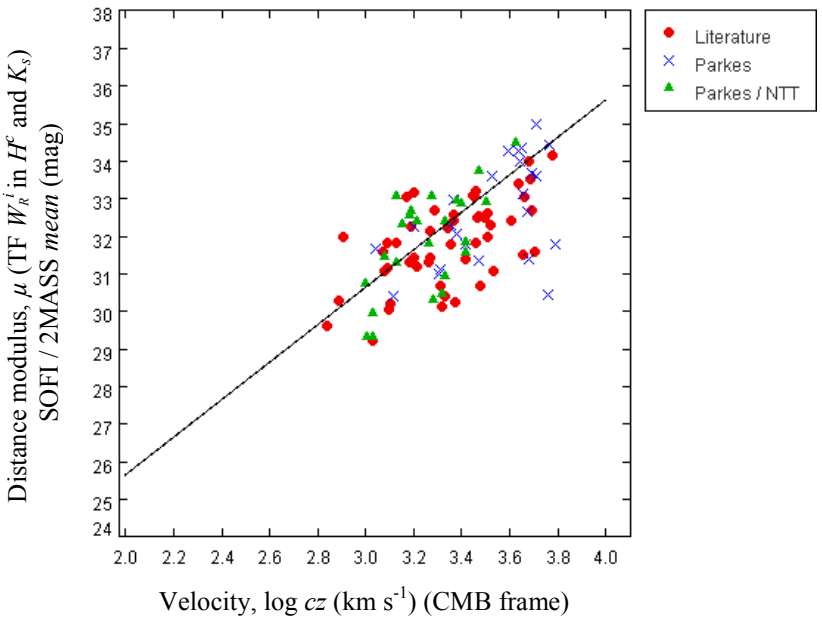

Figure 6.12: The Hubble diagram (TF distance modulus versus log *cz*, CMB frame) for 118 galaxies. The TF modulus is the mean of the SOFI and 2MASS H^c and K_s values. The offset and *rms* scatter is -0.43±1.19, -0.28±1.17, and -0.28±1.22 mag for the Literature, Parkes, and Parkes / NTT samples, respectively. For all samples, the offset and *rms* scatter is -0.33±1.19 mag.

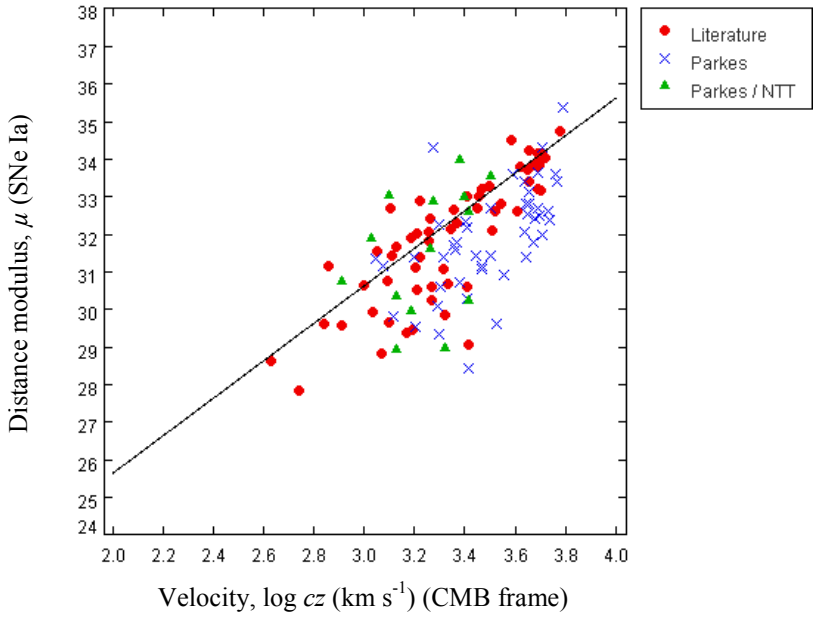

Figure 6.13: The Hubble diagram (SN Ia distance modulus versus log *cz*, CMB frame) for 118 galaxies. The offset and *rms* scatter is -0.54±0.98, -0.62±1.31, and -0.26±1.55 for the Literature, Parkes, and Parkes / NTT samples, respectively. For all samples, the offset and *rms* scatter is -0.47±1.28 mag.

For the subset of 67 galaxies with both TF and SN distance moduli, we plot in Figures 6.14 to 6.16 a comparison for the B_T, H^c, and K_s TF relations, respectively. Table 6.1 quantifies the comparison by listing the mean difference and scatter of the distance moduli calculated via the TF and SNe Ia methods for all three photometric bands (as previously listed in Tables 3.3, 4.8 and 5.4) and all three samples (Literature, Parkes, and the Parkes / NTT) for bands B_T, H^c, and K_s. The mean difference $\mu_{\rm TF}$-$\mu_{\rm SN1A}$, is generally within a few tenths of a magnitude, except for the B_T and K_s band TF distances from the Parkes sample. But the *rms* deviations $\sigma(\mu_{\rm TF}$-$\mu_{\rm SN1A})$, are all surprisingly high – over 1 mag. This is substantially higher than expected, and much higher than the *best* accuracies of ~0.4 mag and ~0.2 mag quoted for these two distance indicators by Freedman and Madore (2010). More typically, we find that a given spiral galaxy containing a Type Ia Supernova will have a TF distance and a SN Ia distance that differ by a factor of *two*. The TF and SNe Ia distances differ largely to a combination of observational errors and intrinsic variance in the distance indicators. The incomplete SNe Ia data in particular is much less accurate than will be the case with future SkyMapper surveys of the local Universe.

$\Delta\mu$ TF colour bands	B_T		H^c		K_s		MAD		
versus SNe Ia μ	mean	*rms*	mean	*rms*	mean	*rms*	B_T - H^c	B_T - K_s	H^c - K_s
$\Delta\mu$ Literature (mag)	0.54	1.34	-0.6	1.5	-0.67	1.42	0.27	0.25	0.03
$\Delta\mu$ Parkes (mag)	0.79	1.61	-0.78	1.84	-0.68	1.81	0.31	0.39	0.02
$\Delta\mu$ Parkes / NTT (mag)	0.56	1.13	0.76	1.43	0.87	1.51	0.18	0.18	0.01
$\Delta\mu$ Combined (mag)	0.63	1.36	-0.21	1.58	-0.16	1.58	0.25	0.27	0.02

Table 6.1: The difference in TF distance modulus in bands B_T, H^c, and K_s and the distance modulus of the SNe Ia (μ_{TF}-μ_{SN1A}), the corresponding *rms* about the mean difference, and MAD for bands B_T, H^c, and K_s.

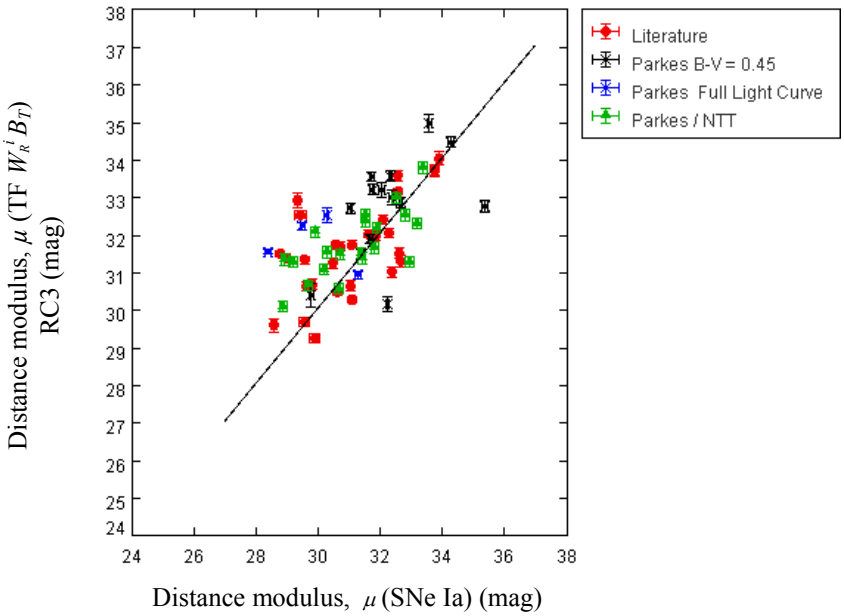

Figure 6.14: Comparison of the SN Ia distance moduli with the TF RC3 B_T -band based distance moduli for 67 galaxies in the combined samples. The reference line goes through the origin with a slope of unity. The mean difference is 0.63 mag, with an *rms* scatter of 1.36 mag.

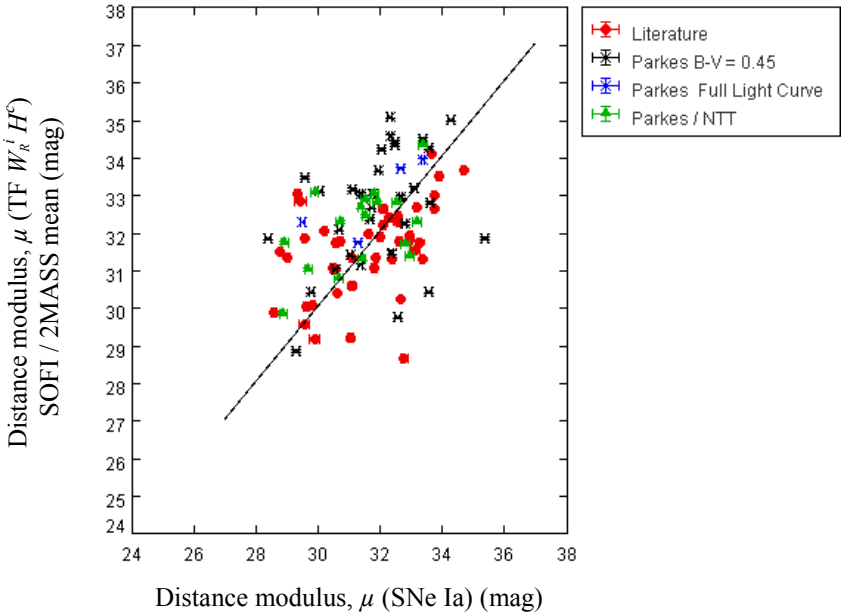

Figure 6.15: Comparison of the SN Ia distance moduli with the mean of SOFI / 2MASS TF IR H^c -band based distance moduli for 78 galaxies in the combined samples. The reference line goes through the origin with a slope of unity. The mean difference is -0.01 mag, with an *rms* scatter of 1.47 mag.

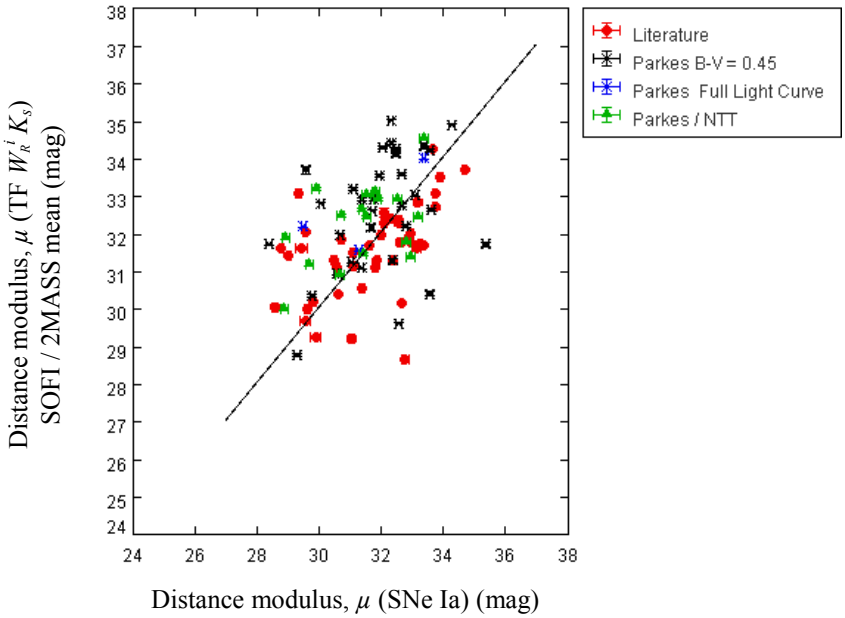

Figure 6.16: Comparison of the SN Ia distance moduli with the mean of SOFI / 2MASS TF IR K_s -band based distance moduli for 96 galaxies in the combined samples. The reference line goes through the origin with a slope of unity. The mean difference is -0.06 mag, with an *rms* scatter of 1.43 mag.

6.2 The Hubble Constant

Our initial TF distance moduli in the B_T -band (Tully et al. 2008) were based on nearby galaxies corrected to the Cepheid zero point, implicitly using $H_0 = 74$ km s^{-1} Mpc^{-1}. The IR (H and K) TF zero point was based on the Masters et al. (2008, Erratum 2014) value of $H_0 = 72$ km s^{-1} Mpc^{-1}. The Phillips et al. (1999) SNe Ia calibration implicitly uses $H_0 = 65$ km s^{-1} Mpc^{-1}, but was adjusted based on the Riess et al. (2005) maximum of $M_V^0(t_0) = -19.44$ mag and a correction of 0.27 mag to the Cepheid zero point, to the value of $H_0 = 73 \pm 4$ (statistical) ± 5 (systematic) km s^{-1} Mpc^{-1}. All input values are formally very similar, and all in reasonable agreement with the recent 'concordance' value of 69.6 km s^{-1} Mpc^{-1} (Bennett et al. 2014) which includes BAO and CMB determinations. However, any offset between our TF and SNe Ia distances implies an inconsistency between the calibrations adopted for the two distance estimators. Furthermore, any inconsistencies with redshift-based distances (cz/H_0) could imply an incorrect Hubble constant or an erroneous template relation. Conversely, any zero-point offset in the comparison of predicted TF or SN Ia distance moduli with redshift-based distance moduli can be used to re-calibrate the Hubble constant, or modify the coefficients of the template relations in order that a self-consistent Hubble constant is obtained.

For the galaxy samples presented in this thesis, Figures 6.11 to 6.13 compare the distance moduli, μ predicted by the TF and SN Ia template relation with logarithmic redshift. Any deviation from the predicted straight line defined by μ = 25 + 5 log(cz/H_0) is a measure of the zero-point offset. Figure 6.10 is similar to Figure 6.11 for the mean of the H and K TF relations, where redshift has instead been used to measure distance modulus and absolute magnitude and therefore appears in the vertical axis instead of the horizontal axis.

Substantial offsets, ranging from -0.11 mag to -0.47 mag are immediately apparent. If solely attributed to the Hubble constant, upward corrections of 16 ± 5% (B_T -band TF), 5 ± 5% (H^c and K_s -band TF) and 24 ± 7% (SN Ia) (12 ± 4 km s^{-1} Mpc^{-1}, 4 ± 4 km s^{-1} Mpc^{-1} and 17 ± 5 km s^{-1} Mpc^{-1}, respectively) would be required. However, several factors need to be considered before attributing to the Hubble constant or the template relations, namely: galaxy selection (does the appearance of a SN Ia bias the type of galaxy selected?); Malmquist bias (does the SN Ia selection eliminate usual

problems with Malmquist bias?); and bulk flow/peculiar velocities/redshift reference frame (do bulk flows, peculiar velocities, and mean sample redshift affect the results?). In doing so, there should be consistency between the *internal* comparison of distances between the various indicators. The numbers of galaxies available for the internal comparisons (Table 6.1 and Figures 6.14 to 6.16) is less than for comparisons with redshift distance (Figures 6.11 to 6.13) because of the effect of combined selection cuts. This needs to be taken into account in case biases arise. However, the importance of internal (SN Ia versus TF) comparisons, and part of the motivation for this thesis, is that effects such as bulk flow and peculiar velocity, and possible Malmquist bias, may disappear when comparing individual galaxies.

Measurements	Velocity km s^{-1} Mpc^{-1}	Reference
TF B_T	86 ± 4	This thesis
TF H & K	76 ± 4	This thesis
SNe Ia	90 ± 5	This thesis
Thesis mean data	84 ± 4	This thesis

Table 6.2: A compilation of recent measurements of H_o from the values derived in this thesis.

Measurements	Velocity km s^{-1} Mpc^{-1}	Reference
SNe Ia	72 ± 6	Wang et al. 2006
6dFGS	67 ± 3.2	Beutler et al. 2011
WFC3	73.8 ± 2.4	Riess et al. 2011
Key Project	74.3 ± 1.5	Freedman et al. 2012
WMAP9+ACT+SPT+BAO	69.32 ± 0.08	Bennett et al. 2013
ΛCDM	67.3 ± 1.2	Planck XVI 2013
Cosmicflows-2	74.4 ± 3.0	Tully et al. 2013
CMB-BAO	69.6 ± 0.7	Bennett et al. 2014

Table 6.3: A compilation of recent measurements of H_0 from the literature.

The formal results for H_0 are given in Table 6.2 with a comparison of other recent high-accuracy values listed in Table 6.3. No attempt has been made to correct for Malmquist bias, which is doubtless the cause of the high values (by 3σ to 4σ) measured compared with the literature.

6.3 Galaxy Morphology and Bars

In order to investigate possible sources of scatter and offsets, Table 6.4 and 6.5 explore the variation of the scatter $\sigma(\mu_{TF}-\mu_{SN1A})$, as a function of morphological type of the (host) galaxy, and the presence or absence of a bar. For morphological type, it is known that both the TF relation (Masters et al. 2008, Erratum 2014) and SNe Ia properties (Foley et al. 2012) are dependent on (host) galaxy morphology, although variations in the former are explicitly corrected for via the template relations.

Table 6.4 shows that there is a tendency for early type galaxies (S0/a-Sb) to have a smaller distance modulus measured via the TF relation than via the SN Ia calibration by ~0.2 mag. However, the scatter is large. Table 6.5 compares distance measurements for barred and unbarred galaxies. The scatter is again large, but barred galaxies (type SB) also tend to have a smaller distance modulus by 0.2-0.3 mag when compared with unbarred (type S) or mixed (type SAB) host galaxies. Translated to a Hubble constant, these correspond to potential variances of ~10%.

	Literature			Parkes			Parkes / NTT Sample		
Morphology	mean	$\Delta\mu$ *rms*	Fraction	mean	$\Delta\mu$ *rms*	Fraction	mean	$\Delta\mu$ *rms*	Fraction
S0/a-Sb	-0.15	1.36	32%	-0.89	1.34	48%	-0.68	0.98	57%
Sbc-Sd	0.25	1.10	68%	-0.50	0.96	52%	-0.78	1.24	43%

Table 6.4: The mean difference $(\mu_{TF}-\mu_{SN1A})$ and *rms* scatter $\sigma(\mu_{TF}-\mu_{SN1A})$, of the TF and SNe Ia distance moduli, broken down as a function of morphological type for the three sample sets: Literature, Parkes, and Parkes / NTT. The TF distance modulus is the mean of the H^c, and K_s values. The fraction of galaxies in each category is listed.

Galaxy	Literature			Parkes			Parkes / NTT Sample		
Type	mean	$\Delta\mu$ *rms*	Fraction	mean	$\Delta\mu$ *rms*	Fraction	mean	$\Delta\mu$ *rms*	Fraction
S	-0.30	1.22	39%	-0.32	0.99	40%	-0.82	0.94	14%
SAB	0.15	1.19	37%	-1.03	1.24	28%	-0.75	1.17	57%
SB	0.76	1.14	24%	-0.85	1.28	32%	-0.61	1.01	29%

Table 6.5: The mean difference $(\mu_{TF}-\mu_{SN1A})$ and *rms* scatter $\sigma(\mu_{TF}-\mu_{SN1A})$, of the TF and SNe Ia distance moduli, broken down as a function of bar parameter for the three sample sets: Literature, Parkes, and Parkes / NTT. The TF distance modulus is the mean of the H^c, and K_s values. The fraction of galaxies in each category is listed. Bar type 'S' is unbarred; type 'SAB' is weakly barred; and type 'SB' is strongly barred.

6.4 Malmquist Bias

The term 'Malmquist bias' has several definitions but, in general, the term refers to the tendency for only bright galaxies to be observable at large distances. This

can unfortunately result in biased distance estimates. For example, if all the faint objects from a sample of standard candles are eliminated, Malmquist (1925) showed that the mean absolute magnitude of the remaining candles would be $1.382\sigma^2$ mag brighter than the true mean, for a homogenous sample of Gaussian dispersion σ mag. Therefore the mean distance modulus of the candles will be $1.382\sigma^2$ mag more distant than the actual mean distance modulus, and the deduced Hubble constant will be correspondingly greater. The bias is thus very sensitive to the quality of the distance indicator.

Different manifestations of Malmquist bias and different methodologies of correction are widely available in the literature (see for example Strauss & Willick 1995; Teerikorpi, P. 2015). In general, the bias can be minimised if: (a) the sample is complete to an absolute magnitude much fainter than the objects being observed; (b) the indicators are statistically similar to the objects in question; and (c) the quality of the observations are similar. Alternatively, the bias can be corrected if: (a) the selection function for objects is known; (b) the form of the luminosity function is known; and (c) the density distribution of objects is known. Observations of standard candles in clusters are widely favoured because all galaxies are at almost the same distance, and it often easier to ascertain the completeness limit. A potential concern for the TF relation is that spiral galaxies in the centres of clusters will not be representative of the galaxies in the field owing to different evolution. Although stripping of the HI gas by the intracluster medium and rapid morphological evolution tends to result in few central cluster galaxies being useful application of the TF relation.

The current study has the distinct advantage that host galaxy selection is based on the appearance of a supernova. Thus the TF distance estimates are potentially devoid of direct luminosity bias. However, biases can still result from other means, for example:

1. A statistical dependence on supernova rate on host galaxy luminosity will tend to automatically select high-luminosity galaxies. On the other hand, Type Ia Supernovae rate is dependent on stellar mass and star-formation history that, for a given second parameter (rotation velocity) may not be well-correlated with luminosity.
2. An observational bias may arise if supernova monitoring has only been conducted towards luminous galaxies. For some of the historical SN used here, this will unfortunately be the case. This is somewhat mitigated against

in the current study because we only consider relatively local galaxies due to the difficulty of obtaining TF distances.

In order to further quantify the likely level of contamination by Malmquist bias, we plot SN Ia and TF distance modulus residuals in Figures 6.17 and 6.18 and plot host galaxy velocity width residuals in Figure 6.19. Residuals are plotted against *cz* in all cases. Smaller distance modulus residuals correspond to overly bright SNe Ia or galaxies. Large linewidth residuals correspond to more massive host galaxies.

Galaxies at 6000 km s^{-1} have TF distance modulus that are 1.3 mag smaller compared with those at 1000 km s^{-1} (Figure 6.17). However, a smaller bias (0.5 mag) is apparent for SNe Ia (Figure 6.18) and for velocity width residuals (Figure 6.19). Galaxies at 6000 km s^{-1} have velocity widths only 11% greater than at 1000 km s^{-1}. This corresponds to an average luminosity difference of 0.4 mag. However, the difference is less than the scatter. The slope of the line indicates the potential trend in the bias.

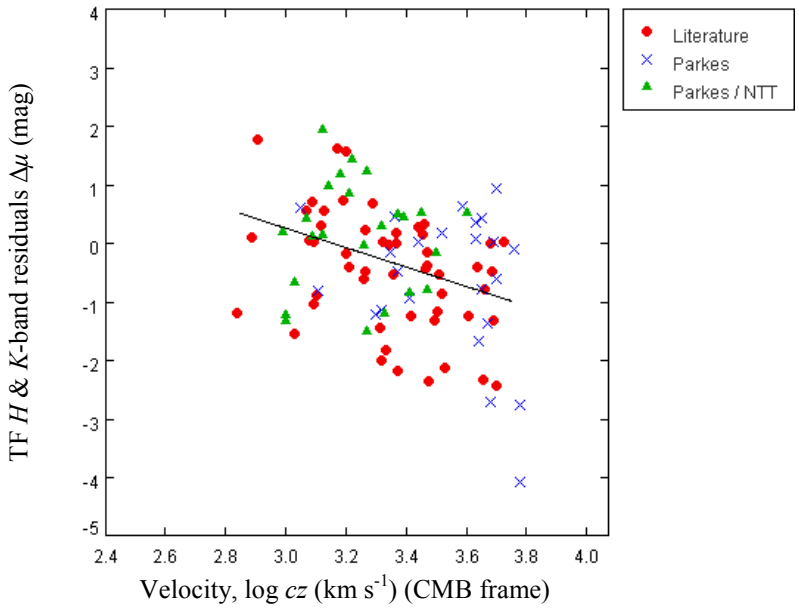

Figure 6.17: Residuals $\Delta\mu$ about the TF relation (see Figure 6.11) plotted as a function of velocity (*cz*) in the CMB frame log V_{CMB} for 103 galaxies comprised of the Literature, Parkes, and Parkes / NTT samples. Malmquist bias is evident in all samples – for a given velocity width, galaxies are brighter at higher redshift, therefore their predicted distance moduli are lower. The linear regression line for the combined three sample sets has a slope of -1.64 mag dex^{-1}, and the rms scatter is 1.03 mag.

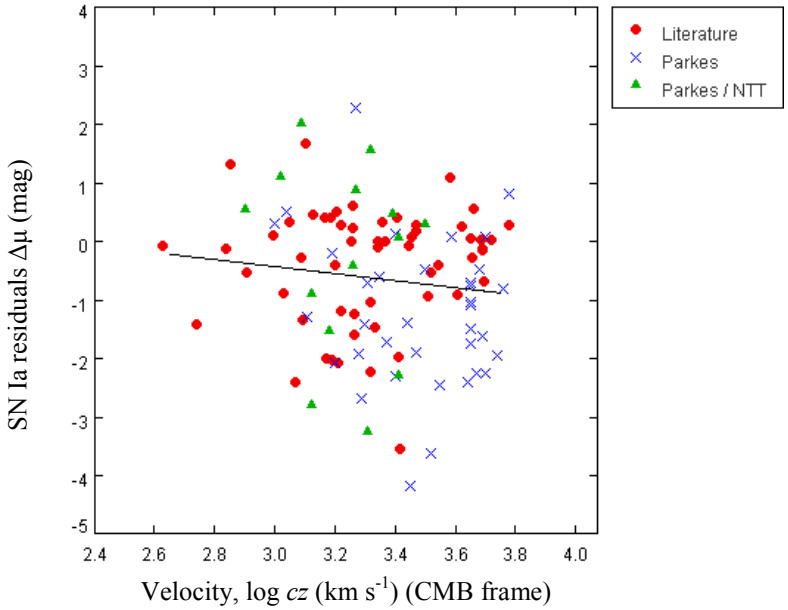

Figure 6.18: Supernova distance modulus residuals $\Delta\mu$ (see Figure 6.12) plotted as a function of velocity (cz) in the CMB frame for 119 galaxies in the Literature, Parkes, and Parkes / NTT samples. Less Malmquist bias appears present. The linear regression line for the combined three sample sets has a slope of -0.59 mag dex^{-1}, and the rms scatter is 1.44 mag.

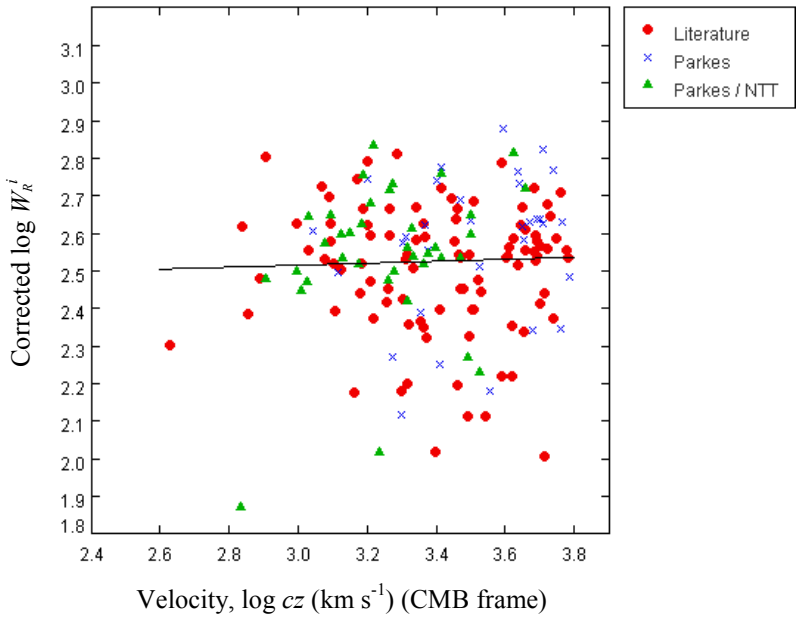

Figure 6.19: Linewidth $\log W_R^i$ plotted as a function of velocity (cz) in the CMB frame log $V_{\rm CMB}$ for 184 galaxies in the Literature, Parkes, and Parkes / NTT samples. There is some evidence for the mean velocity width tending to increase with redshift, implying that higher-mass galaxies are preferentially detected at larger distances. The linear regression line for the combined three sample sets has a slope of 0.06, with an *rms* scatter of 0.12 dex.

6.5 Peculiar Velocities

We have already seen that the ability to measure redshift-independent distances is useful for measuring the Hubble constant. Our deeper TF and SNe Ia measurements offer the advantage of better access to distances outside the local volume, where peculiar velocities may have a large component of redshift, and with perhaps less Malmquist bias.

There are two additional cosmological measurements for which the current data is well suited. Both of these rely on the measurement of peculiar velocity v_p, that is defined as the difference between redshift-distance cz and redshift-independent distance D expressed in units of velocity:

$$v_p = \frac{cz - H_0 D}{1+z} \tag{6.1}$$

(see Davis & Scrimgeour 2014 for a more accurate form). Peculiar velocities represent deviations from uniform Hubble flow due to gravitational perturbations from mass concentrations and are responsible for part of the scatter around the Hubble diagram (e.g., Figures 6.11 – 6.13). The first measurement is that of bulk flow in that the dipole anisotropy in the distribution of peculiar velocities can be used to measure the mean motion of the local Universe with respect to the CMB. This flow is very sensitive to the large-scale matter distribution and homogeneity, and therefore the cosmological model (Nusser & Davis 2011; Li et al. 2012; Hong et al. 2014). The bulk flow is an integral quantity; even very distant structures may have a significant influence if massive enough. The second measurement is the comparison of the individual peculiar velocities with those expected from the visible matter distribution. This is sensitive to cosmological parameters, in particular the matter density, and is a test of gravitational theory (Koda et al. 2014).

6.5.1 Bulk Flow

Recent bulk flow results from galaxy (e.g., Hong et al. 2014) and SNe Ia surveys (e.g., Turnbull et al. 2012) within 100 Mpc show good agreement in direction (towards Galactic coordinates l=290^o, b=15^o), though some variation in amplitude (see Table 6.7). The size of the amplitude has led to some debate (Feldman, Watkins & Hudson 2010; Nusser, Davis & Branchini 2014), as to whether ΛCDM is compatible with the observations.

Peculiar velocities are measured using Equation 6.1, with redshift (z) measured in the CMB frame. Bulk flow is modelled as a dipole anisotropy of v_p, assuming that all galaxies in the sample participate in the same flow. Therefore the expected value of v_p for a given galaxy is:

$$v_{p,i} = v_o(\cos l_i \cos l_o \cos b_i \cos b_o + \sin l_i \sin l_o \cos b_i \cos b_o + \sin b_i \sin b_o) \quad (6.2)$$

where v_o is the amplitude of the bulk flow towards Galactic coordinates (l_o, b_o) and the coordinates of the i'th object are (l_i, b_i).

The amplitude and direction of the bulk flow are computed using the log-normal minimum-χ^2 technique of Hong et al. (2014). This technique was derived from Aaronson et al. (1982) and Staveley-Smith & Davies (1989). The advantage of this over traditional maximum likelihood or minimum variance techniques (e.g., Scrimgeour et al. 2016) is that the non-normal nature of the peculiar velocity errors, which are substantial for the current sample, is correctly accounted for using the form:

$$\chi^2 = \frac{\sum_i w_i(\log(H_0 D_i) - \log(cz_i - (1+z_i)v_{0.}i))^2}{\sum_i w_i} \quad (6.3)$$

where the w_i are weight factors (proportional to inverse variance) and $v_{0.}i$ is the projection of the bulk flow in the direction of the i'th object.

The distribution of objects across the sky is shown in Figure 6.20. There is good all-sky coverage, with the Parkes samples providing the bulk of the southern TF measurements. A comparison of TF and SNe Ia-derived 'raw' peculiar velocities (i.e., monopole terms due to calibration differences are not removed) is shown in Figure 6.21. As expected there is a large scatter (~1100 km s^{-1}), consistent with the scatter around the Hubble diagrams of Figures 6.12 and 6.13.

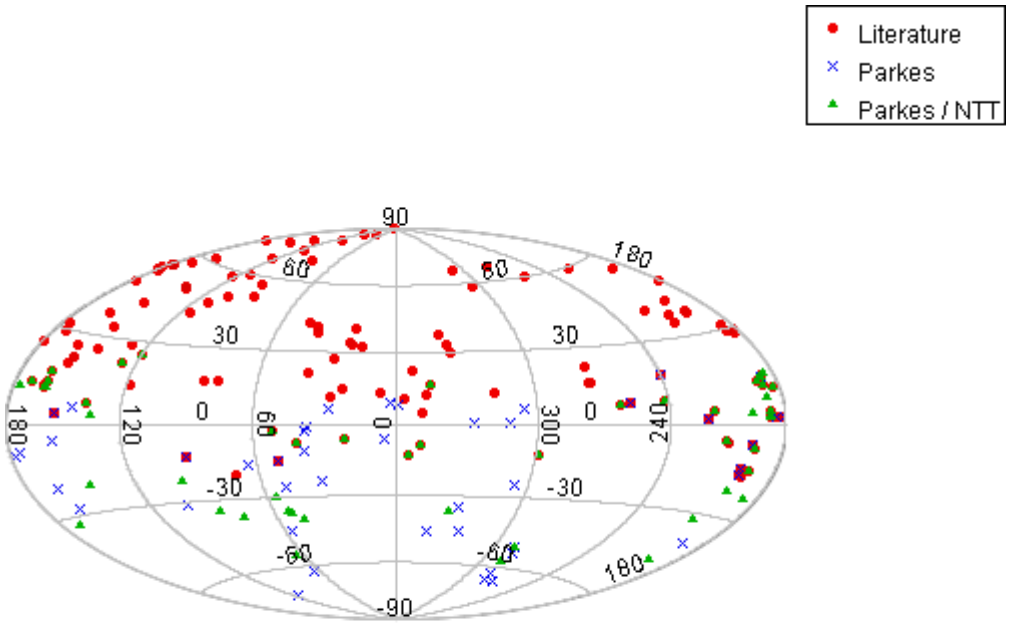

Figure 6.20: Sky coverage of the three sample sets, 227 galaxies, in Galactic coordinates with an Aitoff projection.

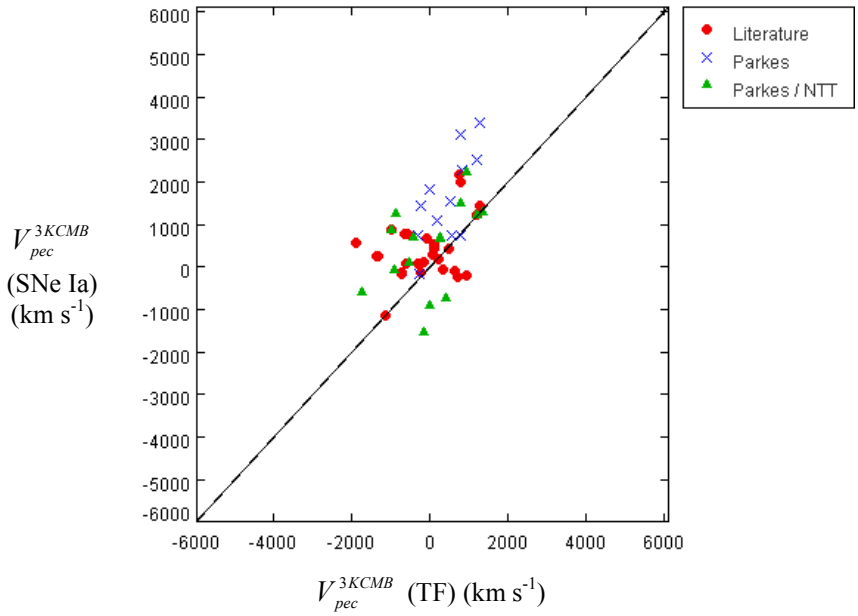

Figure 6.21: Comparison of TF and SNe Ia peculiar velocities for 54 galaxies. The error *rms* is: Literature = 991 km s^{-1}, Parkes = 1359 km s^{-1}, Parkes / NTT = 1081 km s^{-1}, and the three sample sets combined mean is 645 km s^{-1}, with an *rms* scatter of 1108 km s^{-1}.

Applying equation (6.3) to the data yields the bulk flow amplitudes shown in Table 6.6. A plot of peculiar velocity as a function of the cosine of the derive apex angle with respect to the direction of the bulk flow is shown in Figure 6.22 for the combined sample. Unfortunately, the number of galaxies is too small to be competitive with other recent studies summarised in Table 6.7. However, there are no systematic differences between the TF and SNe Ia bulk flows. Moreover, the combined result listed in Table 6.6 (208 km s^{-1}) is in excellent agreement with ΛCDM predictions for the mean distance (26 h^{-1} Mpc) of the sample (see Hong et al. 2014).

Data	Bulk flow components			Amplitude & direction			Monopole	Number objects
	V_x km s^{-1}	V_y km s^{-1}	V_z km s^{-1}	V_o km s^{-1}	l (deg)	b (deg)	V_z km s^{-1}	n
TF (H & K)	598 ± 198	-652 ± 167	-30 ± 120	885	313°	-2°	-68 ± 106	95
SNe Ia	208 ± 291	-206 ± 269	-314 ± 134	430	315°	-47°	165 ± 117	82
Combined	198 ± 161	62 ± 178	-1 ± 55	208	17°	0°	-71 ± 65	177

Table 6.6: Results of a bulk flow analysis for the TF and SNe Ia data sets. The Galactic components of bulk flow and the corresponding amplitude and direction are shown. The bulk flow is with respect to a CMB rest frame. The monopole amplitude (overall expansion or contraction relative to the fiducial Hubble constant) and the number of objects are listed.

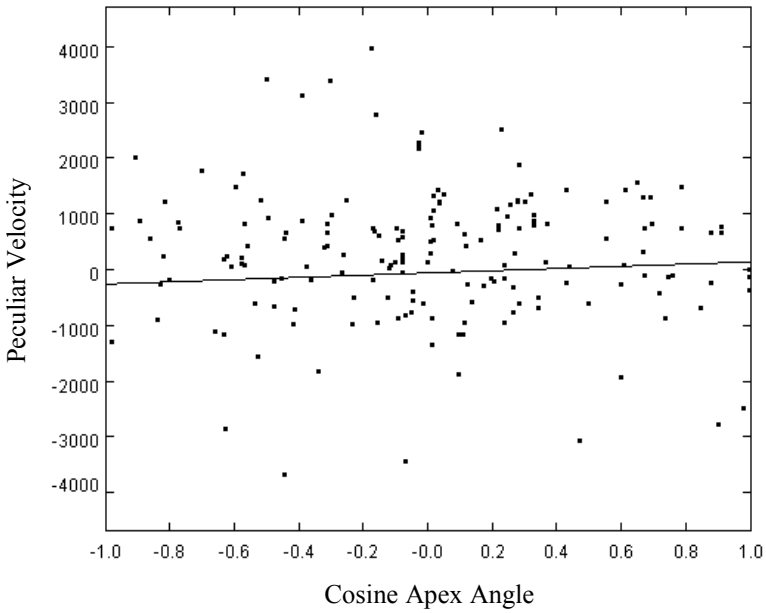

Figure 6.22: A plot of peculiar velocity as a function of the cosine of the apex angle listed in Table 6.6 for the combined sample of 177 TF and SNe Ia distance measurements. The bulk flow amplitude is small (208 km s^{-1}), implying the sample is at rest with respect to the CMB.

Measurements	Velocity km s^{-1}	Depths	l	b	Reference
Composite	407 ± 81	50 h^{-1} Mpc	287° ± 9°	8° ± 6°	Watkins et al. 2009
SFII++	333 ± 38	20 h^{-1} Mpc	276° ± 3°	14° ± 3°	Nusser & Davis 2011
Type Ia SNe	249 ± 76	…	319° ± 18°	7° ± 14°	Turnbull et al. 2012
6dFGS	337 ± 66	…	313° ± 9°	15° ± 10°	Magoulas 2012
6dFGS	272 ± 45	…	326° ± 9°	37° ± 14°	Springob et al. 2013
SN, ENEAR SFI++, A1SN	310	50 h^{-1} Mpc	280° ± 8°	5° ± 6°	Ma & Scott 2013
2MTF IV	280.8 ± 25.0	30 h^{-1} Mpc	296.4° ± 16.1°	19.3° ± 6.3°	Hong et al. 2014
ENEAR, SFI++, A1SN, SC	290 ± 30	…	281° ± 7°	8° ± 6°	Ma & Pan 2014
Thesis - combined data	208 ± 160	…	17° ± 40°	0° ± 15°	This thesis

Table 6.7: Bulk Flow measurements of the local Universe from the literature and this thesis.

6.5.2 Matter Density

Peculiar velocities can also be used to trace the mass distribution on more local scales. If light traces mass, then our peculiar velocity measurements will reflect the distribution of light in the nearby Universe. In linear perturbation theory (e.g., Strauss & Willick 1995), the (vector) peculiar velocity is proportional to gravitation acceleration, summed over the matter density field $\delta_m(r)$:

$$v(r) = \frac{H_0}{4\pi} f(\Omega\Lambda) \int d^3r' \frac{\delta_m(r')(r'-r)}{|r'-r|^3} \tag{6.4}$$

which, for a spherical region of mean matter overdensity δ(r) reduces to:

$$v(r) = \frac{H_0}{3} f(\Omega,\Lambda) r\delta(r) \tag{6.5}$$

For ΛCDM cosmology, a good approximation to the growth history is given by:

$$f(\Omega,\Lambda) = \Omega_{m,o'}^{\gamma} \tag{6.6}$$

where γ = 0.55 (Linder 2004). Therefore, it is possible to use the peculiar velocities derived above to measure the matter density parameter $\Omega_{m,o}$, but only if the overall shape of the density field is already known. Assuming linear bias theory, where the matter density field is related to the light distribution by $\delta_m(r) = \delta_L(r)/b$ (Kaiser & Lahav 1989), then the parameter $\beta = \Omega_{m,o}^{0.55}/b$ can be measured.

The three-dimension distribution of 'light' is best traced by all-sky redshift and photometric surveys such as the IRAS PSCz (Saunders et al. 2000) and 2MASS 2MRS (Huchra et al. 2012) surveys. These light distributions themselves require careful

corrections for selection effects, missing data (e.g., the Zone of Avoidance), and redshift-space distortion. Fortunately, some excellent models exist in the literature:

1. Lavaux et al. (2010) apply the Lagrangian Monge-Ampère-Kantorovich (MAK) technique to the 2MASS Redshift Survey (2MRS). Their MAK velocity predictions are provided in the Extragalactic Distance Database (EDD).
2. Erdoğdu et al. (2006, 2015) use a Wiener filter to suppress shot noise in their real-space density field, employing deconvolution to remove redshift-space distortions. They also use the 2MRS survey. Their updated 2014 predictions were interpolated to the positions of our galaxies by Christina Magoulas (2014 priv. comm.).
3. Branchini et al. (1999) apply a self-consistent, non-parametric model to the IRAS PSCz redshift survey (Saunders et al. 2000). Their predictions were again interpolated to the positions of our galaxies by Christina Magoulas (2014 priv. comm.).

We compare our TF and SNe Ia peculiar velocities with MAK, Erdoğdu and PSCz model velocities. The predicted peculiar velocities are derived from a velocity field calculated from the density field based from the above redshift surveys. Most of the scatter is due to measurement errors in our velocities. However, there are significant differences between the three model velocities as shown in Figure 6.23.

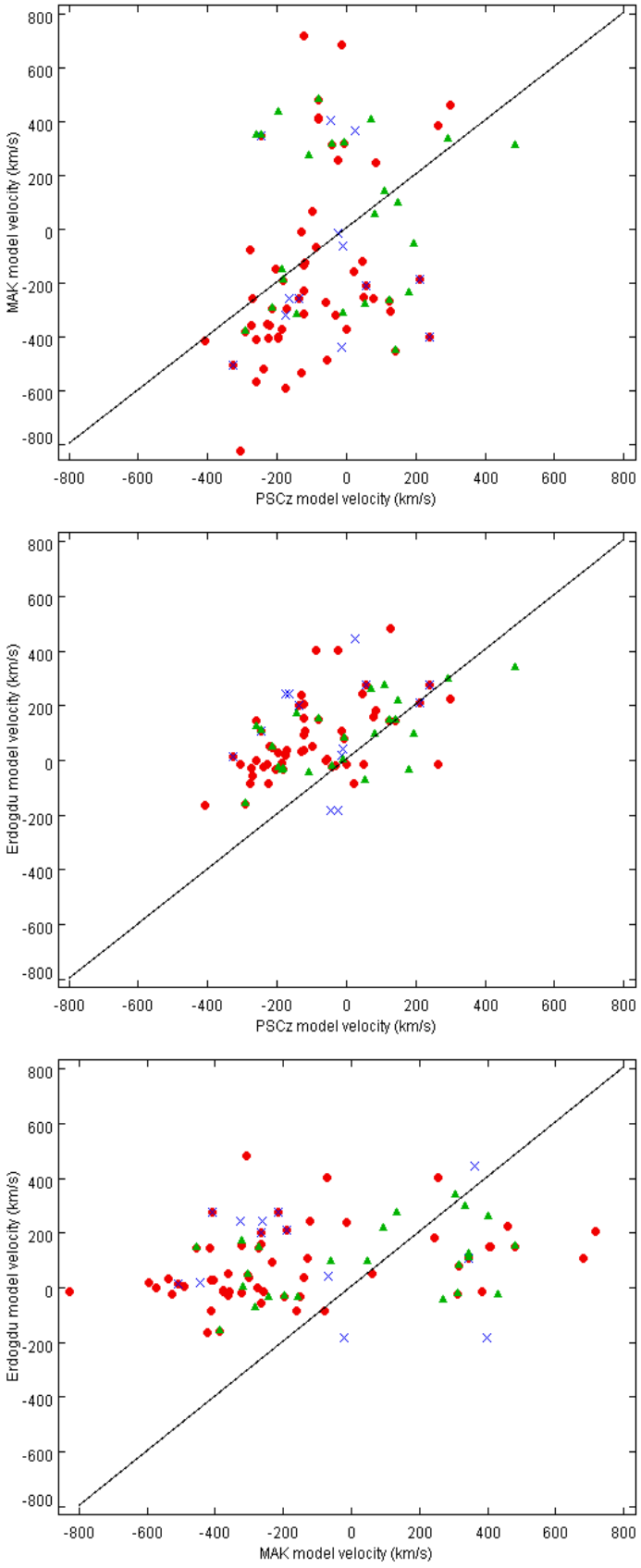

Figure 6.23: PSCz versus MAK and Erdoğdu model velocities, respectively, and MAK versus Erdoğdu velocities. The reference line is at a 45° angle through the origin.

These differences arise due to the differing input data sets and the differing ways in which the models were computed. There are some unusual systematic differences apparent between the models. However, analysis of these models is beyond the scope of this thesis. The model velocities are based on different fiducial values of β (β_o = 0.52 for MAK; β_o = 0.40 for Erdoğdu; and β_o = 0.50 for PSCz). However, we can deduce the actual value of β by treating it as a free parameter that best matches the data, in this case the TF and SNe Ia velocities. We do this using a minimisation procedure, which linearly re-scales the predictions and finds the minimum of the sum of the weighted squared differences, χ^2 between the model and the measured velocities in the CMB frame as follows:

$$\chi^2 = \sum_i \frac{\left(\frac{\beta}{\beta_o} v_i^{pred} - v_i^{mass}\right)^2}{\left(0.2 \log_{10} e \Delta\mu cz_{i,CMB}\right)^2} \tag{6.7}$$

where V^{pred} and V^{meas} are the predicted (MAK, PSCz or Erdoğdu) and measured (TF or SNe Ia) peculiar velocities, respectively, $\Delta\mu$ is the corresponding distance modulus error of the measurement, and z_{CMB} is the redshift.

Plots of χ^2 against β for MAK, Erdoğdu, and PSCz are shown in Figures 6.24 and 6.25. The minimum values represent the best-fit value for β that are listed in Table 6.8. Values range from β=0.25 to 0.80 with typical errors of 0.2. Combined values are also given for all the data presented in this thesis. The overall mean value is β=0.37±0.08. Table 6.9 shows that there is excellent agreement with values of β derived from other recent galaxy surveys, that range from 0.21 to 0.40.

As shown previously, the matter density of the Universe, $\Omega_{m,o}$ is related to β and the bias parameter as follows: $\Omega_{m,o} = (b\beta)^{1.82}$. Assuming a value of $b \approx 1$, which is appropriate for the gas-rich galaxies (Martin et al. 2012), the corresponding value for the matter density is $\Omega_{m,o} = 0.16 \pm 0.06$. This is within the combined errors of the WMAP value (0.27±0.04) shown in Table 6.10, but significantly lower than the high-accuracy Planck value (0.315±0.017). The difference may indicate that the galaxies chosen in this thesis have bias values significantly greater than unity. However, the Planck value also contains a significant number of assumptions that are absent from our value.

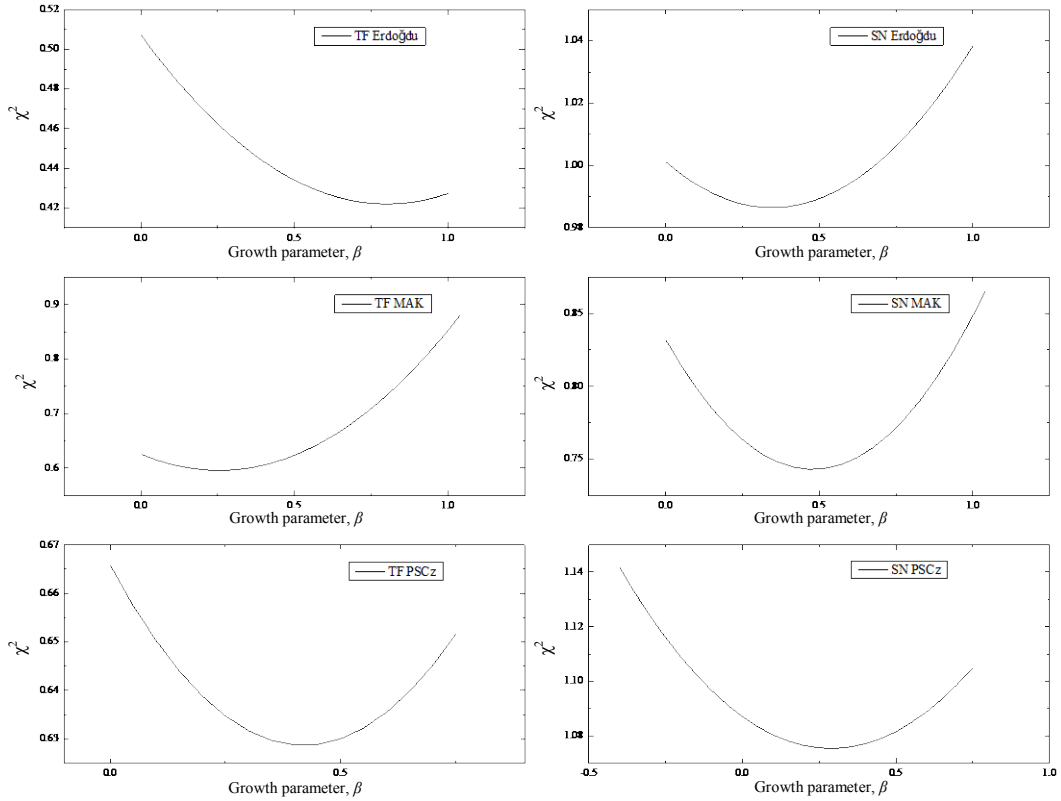

Figure 6.24: Plots of reduced-χ^2 against the growth parameter, β for TF and SNe Ia distance estimates for three different flow models of galaxies in the local Universe: Erdoğdu (Erdoğdu et al. 2015), MAK (Lauvaux et al. 2010) and PSCz (Branchini et al. 1999). The minimum value of χ^2 corresponds to the best fit value for β.

Model	TF	SN	Reference
	β	β	
Erdoğdu	0.80 ± 0.19	0.35 ± 0.31	Erdoğdu et al. 2006
MAK	0.25 ± 0.12	0.48 ± 0.17	Lavaux et al. 2010
PSCz	0.42 ± 0.18	0.29 ± 0.35	Magoulas 2014
Erdoğdu TF & SN	0.59 ± 0.18		Erdoğdu et al. 2006
MAK TF & SN	0.34 ± 0.10		Lavaux et al. 2010
PSCz TF&-SN	0.38 ± 0.17		Magoulas 2014
All Combined	0.37 ± 0.08		As above

Table 6.8: Values for β results obtained by comparing the observed TF and SN peculiar velocities with the Erdoğdu, MAK and PSCz flow models.

Measurements	β	Reference
2MASS	0.43 ± 0.03	Bilicki et al. 2013
2M++	0.43 ± 0.02	Carrick et al. 2015
6dFGS	0.29 ± 0.06	Magoulas et al. 2012
2MASS	0.49 ± 0.04	Pike & Hudson 2005
IRAS PSCz	0.48 ± 0.06	Radburn-Smith et al. 2004

Table 6.9: Values for low-redshift measurements of β from the literature, for a comparison with the results derived from the measured TF and SNe Ia peculiar velocities.

Measurements	Ω_m	Reference
Planck	0.315 ± 0.017	Planck 2013
WMAP	0.27 ± 0.04	Larson et al. 2011
Combined thesis data	0.16 ± 0.06	This thesis

Table 6.10: Values for Ω_m from Planck (2013), WMAP and this thesis.

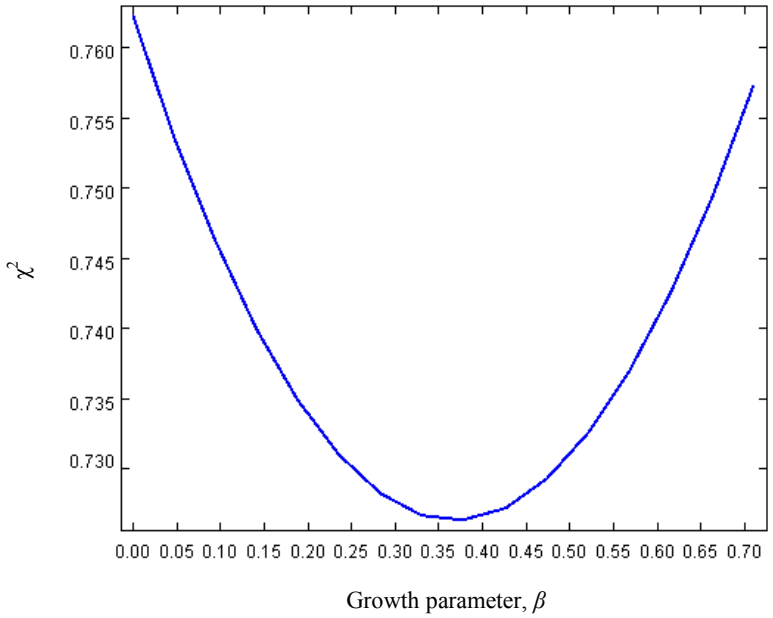

Figure 6.25: χ^2 as a function of the growth parameter β from a comparison of TF and SNe Ia peculiar velocities with the combined Erdoğdu, MAK, and PSCz models.

REFERENCES

Aaronson, M., Huchra, J., Mould, J. R., Tully, R. B., Fisher, J. R., van Woerden, H., Goss, W.M., Charmaraux, P., Mebold, U., Siegman, B., Berriman, G., & Persson, S. E. 1982, ApJS, 50, 241

Bennett, C. L., Larson, D., Weiland, J. L., Jarosik, N., Hinshaw, G., Odegard, N., Smith, K. M., Hill, R. S., Gold, B., Halpern, M., Komatsu, E., Nolta, M. R., Page, L., Spergel, D. N., Wollack, E., Dunkley, J., Kogut, A., Limon, M., Meyer, S. S., Tucker, G. S., Wright, E. L. 2013, ApJS, 208, 20

Bennett, C. L., Larson, D., Weiland, J. L., & Hinshaw 2014, ApJ, 794, 135

Beutler, F., Blake, C., Colless, M., Jones, D. H., Staveley-Smith, L., Campbell, L., Parker, Q., Saunders, W., & Watson, F. 2011, MNRAS, 416, 3017

Bilicki, M., Chodorowski, M. L., Hellwing, W., Jarrett, T., & Mamon, G. 2015, arXiv:1211.1246 [astro-ph.60]

Branchini, E., Teodoro, L., Frenk, C. S., Schmoldt, I., Efstathiou, G., White, S. D. M., Saunders, W., Sutherland, W., Rowan-Robinson, M., Keeble, O., Tadros, H., Maddox, S., & Oliver, S. 1999, MNRAS, 308, 1

Carrick, J., Turnbull, S. J., Guilhem, L. & Hudson, M. J. 2015, arXiv:1504.04627 [astro-ph.60]

Davis, T. M., & Scrimgeour, M. I. 2014, arXiv:1405.0105 [astro-ph.60]

Erdoğdu, P., Lahav, O., Huchra, J. P., Colless, M., Cutri, R. M., Falco, E., George T., Jarrett, T., Jones, D. H., Macri, L. M., Mader, J., Martimbeau, N., Pahre, M. A., Parker, Q. A., Rassat, A., & Saunders, W. 2006, MNRAS, 373, 45

Erdoğdu, P. et al. 2015, in preparation

Feldman, H. A., Watkins, R., & Hudson, M. J. 2010, MNRAS, 407, 2328

Foley, R. J., Simon, J. D., Burns, C. R., Gal-Yam, A., Hamuy, M., Kirshner, R. P., Morrell, N. I., Phillips, M. M., Shields, G. A., & Sternberg, A. 2012, ApJ, 752, 101

Freedman, W. L. & Madore, B. F. 2010 Annual Reviews, AA

Freedman, W. L., Madore, B. F., Scowcroft, V., Burns, C., Monson, A., Persson, S. E., Seibert, M., & Rigby, J. 2012, ApJ, 758, 24

Hong, Tao., Springob, C. M., Staveley-Smith, L., Scromgeour, M. I. Masters, K. L., Macri, L. M., Koribalski, B. S., Jones, D. H., & Jarrett, T. H. 2014, MNRAS, 445, 402

Huchra, J. P., Macri, L. M., Masters, K. L., Jarrett, T. H., Berlind, P., Calkins, M., Crook, A. C., Cutri, R., Erdoğdu, P., Falco, E., & 10 coauthors 2012, ApJS, 199, 26

Kaiser, N., & Lahav, O, 1989, MNRAS, 237, 129

Koda, J., Blake, C., Davis, T., Magoulas, C., Springob, C. M., Scrimgeour, M., Johnson, A., Poole, G. B., & Staveley-Smith, L. 2014, MNRAS, 445, 4267

Larson, D., Dinkley, J., Hinshaw, G., Komatsu, E., Nolta, M. R., Bennett, C. L., Gold, B., Halpern, M, Hill, R. S., Jarosik, N., Kogut, A., Limon, M., Meyer, S. S., Odegard, N., Page. L., Smith, K. M., Spergel, D. N., Tucker, G. S., Weiand,

J. L., Wollack, E., & Wright, E. L. 2011, ApJS, 192, 16

Lavaux, G., Tully, R. B., Mohayaee, R., & Colombi, S. 2010, ApJ, 709, 483

Li, M., Pan, J., Gao, L., Jing, Y., Yang, X., Chi, X., Feng, L., Kang, X., Lin, W., Shan, G., Wang, L., Zhao, D., & Zhang, P. 2012, ApJ, 761, 151

Linder, E. V. 2004, PhRvD, 70b3511

Ma. Y. –Z., Scott, D. 2013, MNRAS, 428, 2017

Ma. Y. –Z., & Pan, J. 2014, MNRAS, 437, 1996

Magoulas, C., Springob, C. M., Colless, M., Jones, D. H., Campbell, L. A., Lycey, J. R., Mould, J., Jarrett, T., Merson, A., & Brough, S. 2012, MNRAS, 427, 245

Magoulas, C. 2012, private communication, (Cape Town: University of Cape Twon)

Magoulas, C. 2014, private communication, (Cape Town: University of Cape Town)

Malmquist, K. G. 1925, Obs., 48, 142

Martin, A. M., Giovanelli, R., Haynes, M. P., & Guzzo, L 2012, ApJ, 750, 38

Masters, K. L., Springob, C. M., & Huchra, J. P. 2008, Erratum 2014, AJ, 135, 1738

Nusser, A., & Davis, M. 2011 ApJ, 736, 93

Phillips, M. M., Lira, P., Suntzeff, N. B., Schommer, R. A., Hamuy, M., & Maza, J. 1999, AJ, 118, 1766

Pike, R. W. & Hudson, M. J. 2005, ApJ, 635, 11

Planck 2013, arXiv:1303.5076 [astro-ph.60]

Radburn-Smith, D. J., Lucey, J. R., & Hudson, M. J. 2004, MNRAS, 355, 1378

Riess, A. G., Li, W., Stetson, P. B., Filippenko, A. V., Jha, S., Kirshner, R. P., Challis, P. M., Garnavich, P. M., & Chornock, R. 2005, ApJ, 627, 579

Riess, A. G., Macri, L., Casertano, S., Lampeitl, H., Ferguson, H. C., Filippenko, A. V., Jha, S. W., Li, W., & Chornock, R. 2011, ApJ, 730, 119

Saunders, W., Sutherland, W. J., Maddox, S. J., Keeble, O., Oliver, S. J., Rowan-Robinson, M., McMahon, R. G., Efstathiou, G. P., Tadros, H., White, S. D. M., Frenk, C. S., Carramiñana, A., & Hawkins, M. R. S. 2000 MNRAS, 317, 55

Scrimgeour, M. I., Davis, T. M., Blake, C., Staveley-Smith, L., Magoulas, C., Springob, C. M., Beutler, F., Colless, M., Johnson, A., Jones, D. H., Koda, J., Lucey, J. R., Ma, Y. Z., Mould, J., & Poole, G. B. 2016, MNRAS, 455, 386

Springob, C. M., Magoulas, C., Colless, M., Jones, D. H., Cambell, L., Lucey, J., Mould, J., & Erdoğdu, P. 2013, AUS, 289, 269

Staveley-Smith, L., & Davies, R. D. 1989, ASSL, 151, 439

Strauss, M., & Willick, J. A. 1995, PhR, 261, 271

2MASS – www.ipac.caltech.edu/2mass/releases/allsky/

Teerikorpi, P. 2015, A&A, 576, 75

Tully, R. B., Courtois, H. M., Dolphin, A. E., Fisher, J. R., Héraudeau, P., Jacobs, B. A., Karachentsev, I. D., Makarov, D., Makarova, L., Mitronova, S., Rizzi, L., Shaya, E. J., Sorce, J. G., Wu, P.-F. 2013, AJ, 146, 86

Tully, R. B., Shaya, E. J., Karachentsev, I. D., Courtis, H. M., Kocekski, D. D., Rizzi. L., & Peel, A. 2008, ApJ, 676, 184

Turnbull, S. J., Hudson, M. J., Feldman, H. A., Hicken, M., Kirshner, R. P., & Watkins, R. 2012, MNRAS, 420, 447

Wang, X., Wang, L., Pain, R., Zhou, X., & Li, Z 2006, ApJ, 645, 488
87

Watkins, R., Feldman, H. A., Hudson, M. J. 2009, MNRAS, 392, 743

CHAPTER 7
CONCLUSIONS

This thesis provides a comprehensive new set of distance measurements of nearby (cz < 6000 km s^{-1}) galaxies based on two of the best available distance indicators: the Tully-Fisher (TF) relation, and Type Ia Supernovae (SNe Ia). This thesis provides the combination of both approaches by providing Tully-Fisher data for and associated SN Ia host galaxies, thereby allowing the best possible calibration of the former relation and allowing the secure measurement of distances to much larger samples than provided by SNe Ia distances alone.

The TF relation is based on the good relationship between galaxy luminosity and rotation velocity. Near-IR observations in the H^c and K_s bands appear to produce the most accurate results. Due to the steepness of the relation, an important source of error is the 21 cm velocity width and the inclination correction. Fortunately, we have been able to use the 2MASS co-added *JHK* bands to decrease the dispersion.

SNe Ia distances are based on peak luminosity, colour and decline rate. One of the most systematic difficulties of using the indicator is the completeness of luminosity data. The most accurate distance determinations are only possible with complete light curve and photometric data.

The analysis presented in this thesis is based on three samples. The 'Literature' sample is compiled from data from the literature, including historical observations where accurate photometry is available. The second 'Parkes' sample contains new 21 cm observations, but again with photometry extracted from the literature. The final 'Parkes / NTT' 51-galaxy sample yields the most precise determinations from the new IR and 21 cm observations presented here.

There are important limitations, which arise from the data available for the above samples. The HI data from the literature may contain observations of limited S/N ratio or velocity resolution, and may be affected by confusion. There are even more important limitations which arise from the definition of the SNe Ia sample. For example, until more recent systematic surveys, SNe Ia discoveries were heavily biased towards luminous nearby galaxies. Furthermore, as already noted, only limited temporal and photometric coverage was previously available. For example, only eight

galaxies of the Parkes sample have full SNe Ia data for the host galaxy. The others are mostly missing $B_{max} - V_{max}$ photometry.

Nevertheless, we have been able to use our new IR and HI data, in combination with other available data to systematically compare SNe Ia and TF distance scales. We find no major differences, with residual offsets probably being due to the differing selection effects (Malmquist bias) in the SNe Ia and TF samples. The overall mean value is $H_0 = 84 \pm 4$ km s^{-1} Mpc^{-1} which is somewhat higher than the value of Riess et al. (2011) who obtained $H_0 = 73.8 \pm 2.4$ km s^{-1} Mpc^{-1} using the HST Wide Field Camera (WFC3) for observations of Cepheid variables. However, both these values remain in tension with the CMB and 6 degree Field Galaxy Survey (6dFGS) Baryon Acoustic Oscillation (BAO) measurement of $H_0 = 67.0 \pm 3.4$ km s^{-1} Mpc^{-1} (Beutler et al. 2011) and the Planck 2013 XVI result of $H_0 = 67.3 \pm 1.2$ km s^{-1} Mpc^{-1} (Planck Collaboration: et al. 2013).

As well as allowing us to measure the Hubble flow, our distance measurements also allow us to measure the non-Hubble flow. On large scales, these are generated by density inhomogeneities. Since the power spectrum of overdensities is a prediction of ΛCDM, non-Hubble velocities, or peculiar velocities, can be used as a test of ΛCDM (Johnson et al. 2014). On small scales, peculiar velocities also encode information on cosmology, but are in the non-linear regime, making theoretical prediction harder (Kwan, Lewis & Linder 2012).

The dipole moment of the peculiar velocity field contains information about the amplitude and direction of bulk flow. This is due to the vector sum of the gravitational pull of nearby and distant overdensities. The bulk flow measured at radius < R is caused by overdensities located outside R. Whether contributed by a single massive object (e.g., the 'Great Attractor'; Lynden-Bell et al. 1988) or a larger number of overdensities, the bulk flow amplitude nevertheless remains a prediction of cosmological theory. Values that are too high may be in direct contradiction with ΛCDM (Watkins, Feldman and Hudson 2009). An analysis using the peculiar velocities in our combined sample of 177 SNe Ia and Tully-Fisher measurements shows that the nearby Universe is substantially at rest with respect to the rest frame defined by the Cosmic Microwave Background. The residual bulk flow of 208 ± 160 km s^{-1} appears in agreement with the predictions of ΛCDM for the mean sample depth of 40 Mpc.

Higher order moments of the velocity field are difficult to extract from the current data set due to its small size, but it is possible to make a straightforward comparison with predicted velocities based on the distribution of luminous galaxies. Such comparisons not only allow tests of ΛCDM, but also tests whether light follows gravity, tests linear biasing assumptions and tests basic predictions of General Relativity (Crook, Silvestri & Zukin 2010). Since such predictions may themselves be subject to sample selection effects (wavelength, sky coverage etc), we have used predictions from three different sources: (1) the Lavaux et al. (2010) MAK predictions based on the 2MASS Redshift Survey (2MRS) as listed in the Extragalactic Distance Database (EDD) (Tully et al. 2009); (2) The Erdoğdu et al. (2006, 2015) Weiner filtered density, also from the 2MRS survey; and (3) the Branchini et al. (1999) model of the IRAS PSCz redshift survey (Saunders et al. 2000). For SNe Ia, we were able to make the best match between observations and theory by assuming $\beta=\Omega_{m,o'}^{0.55}/b=0.37$; for TF velocities, the best-match was β=0.49. By comparison, Radburn-Smith, Lucey and Hudson (2004) measured 0.55±0.06 for 98 local SNe Ia, and Pike and Hudson (2004) measured β=0.55±0.05 from the large SFI TF sample. Our combined estimate of β=0.37±0.08 implies a matter density parameter of $\Omega_{m,o'}=0.16\pm0.06$.

Finally, the results in this thesis can be considered a pilot study of what will be possible with surveys in the near future with SkyMapper and ASKAP, and surveys in the more distant future with LSST and the Square Kilometre Array (SKA). The SkyMapper supernova survey has just begun, with an early supernova detection by Scalzo et al. (2013). It is expected to measure around 100 nearby ($0.03 < z < 0.09$) SNe Ia light curves per year. Similarly, the ASKAP WALLABY survey is expected to detect HI in around 500,000 galaxies, with around 10% available for TF studies (Duffy et al. 2012). For studies of redshift-space distortions, the WALLABY survey is expected to improve on the 6dFGS measurements of the growth factor by a factor of 3-4 (Beutler et al. 2012). Similar improvements in the growth parameter can be expected from direct distance measurements.

REFERENCES

Beutler, F., Blake, C., Colless, M., Jones, D. H., Staveley-Smith, L., Campbell, L., Parker, Q., Saunders, W. 2011, MNRAS, 416, 3017

Beutler, F. 2012, University of Queensland, Cosmic Flows: In The Rainforest Conference

Branchini, E., Teodoro, L., Frenk, C. S., Schmoldt, I., Efstathiou, G., White, S. D. M., Saunders, W., Sutherland, W., Rowan-Robinson, M., Keeble, O., Tadros, H., Maddox, S., & Oliver, S. 1999, MNRAS, 308, 1

Crook, A. C., Silvestri, A., & Zukin, P. 2010, MNRAS, 401, 1219

Duffy, A. R., Meyer, M. J., Staveley-Smith, L., Bernyk, M., Croto, D. J., Koribalski, B. S., Gerstmann, D., & Westerlund, S. 2012, MNRAS, 426, 3385

Erdoğdu, P., Lahav, O., Huchra, J. P., Colless, M., Cutri, R. M., Falco, E., George T., Jarrett, T., Jones, D. H., Macri, L. M., Mader, J., Martimbeau, N., Pahre, M. A., Parker, Q. A., Rassat, A., & Saunders, W. 2006, MNRAS, 373, 45

Erdoğdu, P. et al. 2015, in preparation

Johnson, A., Blake, C., Koda, J., Ma, Y. Z., Colless, M., Crocce, M., Davis, T. M., Jones, H., Magoulas, C., Lucey, J. R., Mould, J., Scrimgeour, M. I., & Springob, C. M. 2014, MNRAS, 444, 3926

Kwan, J., Lewis, G., & Linder, E. V. 2012, ApJ, 748, 78

Lavaux, G., Tully, R. B., Mohayaee, R., & Colombi, S. 2010, ApJ, 709, 483

Lynden-Bell, D., Faber, S. M., Burstein, D., Davies, R. L., Dressler, A., Terlevich, R. J., & Wegner, G. 1988, ApJ, 326, 19

Pike, R. W. & Hudson, M. J. 2005, ApJ, 635, 11

Planck Collaboration; Abergel, A., Ade, P. A. R., Aghanim, N., Alina, D., Alves, M. I. R., Aniano, G., Armitage-Caplan, C., Arnaud, M.; Ashdown, M., and 238 co-authors 2013, arXiv:1303.5076P [astro-ph.60]

Radburn-Smith, D. J., Lucey, J. R., & Hudson, M. J. 2004, MNRAS, 355, 1378

Riess, A. G., Macri, L., Casertano, S., Lampeitl, H., Ferguson, H. C., Filippenko, A. G., Jha, S., Li, W., & Chornock, R. 2011, ApJ, 730, 119

Saunders, W., Sutherland, W. J., Maddox, S. J., Keeble, O., Oliver, S. J., Rowan-Robinson, M., McMahon, R. G., Efstathiou, G. P., Tadros, H., White, S. D. M., Frenk, C. S., Carramiñana, A., & Hawkins, M. R. S. 2000 MNRAS, 317, 55

Scalzo, R., Yuan, F., Childress, M., Tucker, B., & Schmidt, B. 2013, ATel, 5480

Tully, R. B., Rizi, L., Shaya, E. J., Courtis, H. M., Makarov, D., & Jacobs, B. A. 2009, AJ, 138, 323

Watkins, R., Feldman, H. A., Hudson, M. J. 2009, MNRAS, 392, 743

Appendix

Definitions

A_g − Amplitude of galaxy clustering

A_B^b − Galactic extinction correction for *B*-band

A_B^{i-0} − Inclination correction to face-on for *B*-band

A_B^k − k-correction for *B*-band

A_K^b − Galactic extinction correction for *K*-band

A_K^{i-0} − Inclination correction to face-on for *K*-band

A_K^k − k-correction for *K*-band

ACS – Advanced Camera for Surveys used in Cepheid observations

Arcmin − Arc minute − 1/60 of a degree

Arcsec − Arc second − 1/3600 of a degree

ATNF – Australia Telescope National Facility

Axis ratio − Semi minor axis to semi major axis ratio of the galaxy $r = b/a$

(b) − Galactic extinction

β − Redshift distortion parameter − Beta

B-band – Blue band of the optical spectrum with a central wavelength of 0.44 μm

$B-V$ − Blue band to visual band colour evolution

$B_{\max}-V_{\max}$ − Blue band to visual band at maximum luminosity used in supernova light curve analyses

B_T -band − Blue band total isophote apparent magnitude

$B_T^{b,i,k}$ − Blue total isophote apparent magnitude corrected for galactic extinction, inclination correction to face-on and k-correction

$B_T^{b,i,k} = B_T - A_B^b - A_B^{i-0} - A_B^k$ − The galactic extinction correction is A_B^b, A_B^{i-0} is the inclination correction to face-on and A_B^k is the *k*-correction

Barycentric – Reference to the centre of mass of the solar system

Baryon – Ordinary matter that are elements in the standard model of particle physics

Cepheid – Luminous yellow supergiant stars pulsating caused by expansion and contraction of the star's surface resulting in the capability to measure the pulsation period to determine the distance to the Cepheid

CMB − Cosmic Microwave Background radiation observable between 20 and 100 gigahertz is the relic background radiation produced by the collisions of particles where the radiation has been travelling freely in space approximately 379,000 years after the Big Bang

Cold Dark Matter – is a form of matter referenced to account for gravitational effects that cannot be accounted for by the quantity of observed matter

CSIRO – Commonwealth Science and Industrial Research Organisation

$\Delta m_{15}(B)$ − Delta 15-day index is the difference of the luminosity at maximum light and 15 days after maximum light in the *B*-band used in a supernova light curve study

ΔV − Delta for the *V*-band

ESO VII / 115 – European Southern Observatory VII / 115 catalogue

FWHP – Full Width Half Peak − Full width at the level of half of the peak for a neutral hydrogen radio observation

Gamma – Γ − Uppercase for Gamma − Scale of the break in the Cold Dark Matter (CDM) cosmic power spectrum

Gamma – γ – Lowercase for Gamma – luminosity function

GSR – Galactic Standard of Rest – the barycentric velocity of the solar system corrected to the Galactic Standard of Rest is $V_{GSR}^{O} = 219 \pm 12$ km s^{-1} about the centre of mass of the Milky Way galaxy

H-band – NIR band normally observed with an *H* filter $(1.50 - 1.80 \mu m)$ with a central wavelength $1.653 \mu m$

H^c -band – *H* band corrected for galactic extinction and *k*-correction

HI − Neutral hydrogen

H_0 – Hubble constant defining the cosmological expansion of space using the recession velocity in km s^{-1} and the distance in Mpc

Heliocentric – Reference to the Sun as the centre of the solar system

HST Key Project – Hubble Space Telescope Key Project studying Cepheid variables and Supernova

(i) – Inclination correction for inclination-dependent internal extinction

IRAS PSCz – Infrared Astronomical Satellite Point Source Catalogue Redshift Survey

Isophotal magnitudes – The isophotal measurements are set at the 20 mag per arcsec^2 isophote at the passband apparent magnitude measured to the isophotes

Jy – One Jansky = 10^{-26} W / m^2 / Hz

Jy km s^{-1} – Measurement of flux measured in Jansky's km s^{-1} for radio observations

J-band – NIR band normally observed with a filter J $(1.11-1.36\mu m)$ with a central wavelength $1.247\mu m$

(k) – *k*-correction is a correction to an astronomical object's magnitude (flux) that allows a measurement of a quantity of light from an object at a redshift *z* to be converted to an equivalent measurement in the rest frame of the object.

km s^{-1} – Kilometre per second

kpc – Kilo parsec

K-band – NIR band normally observed with a *K* filter (2.00 – 2.50 μm) with a central wavelength 2.20 μm

K'-band (*K*-prime) – NIR in *K*-band observed with a *K* filter with a cut-off of 2.32 μm and a central wavelength of 2.11 μm, eliminating the thermal background beyond 2.50 μm thereby reducing the sensitivity to the atmospheric absorption and the temperature-dependent background thermal emission

K_s -band (*K*-short) – NIR in *K*-band observed with a K_s filter (2.00 – 2.32 μm) central wavelength 2.15 μm, further reducing the sensitivity to the atmospheric absorption and the temperature-dependent background thermal emission

$K_s^{b,i,k}$ − NIR *K*-band apparent magnitude corrected for galactic extinction, inclination correction to face-on and *k*-correction

ΛCDM – Lambda-Cold Dark Matter – model is a parametrization of the Big Bang cosmological model in which the universe contains a cosmological constant, denoted by Lambda (Λ), associated with dark energy, and cold dark matter. The model uses the premise that the Universe is comprised of: (1) ordinary matter (baryons); (2) dark matter (that has mass and interaction with gravity); (3) dark energy (that accelerates the expansion of the Universe).

$L \propto V^4$ − Fourth order power law relation of the galaxy luminosity and neutral hydrogen line width velocity

LMC – Large Magellanic Cloud

log − Logarithm

m – Apparent magnitude

μm – Micron − Defining the wavelength – 10^{-6} m

μ − Distance modulus

M – Absolute magnitude

$M_B^{b,i,k}$ – Blue band absolute magnitude corrected for galactic extinction, inclination correction to face-on and *k*-correction

$M_H^{b,i,k}$ – *H*-band absolute magnitude corrected for galactic extinction, inclination correction to face-on and *k*-correction

$M_K^{b,i,k}$ – *K*-band absolute magnitude corrected for galactic extinction, inclination correction to face-on and *k*-correction

MAD – Median absolute deviation

mag – Magnitude

MAK – Monge-Ampere-Kantorovich technique applied to 2MRS for galactic and equatorial coordinates

MHz – Megahertz

MLCS – Multi Colour Light Curve Shape

MLCS2k2 – Multi Colour Light Curve Shape 2002 – analyses to determine the light curve shapes of supernova

Mpc – Mega parsec

M_{Sun} – One solar mass

n_{SFR} – Number of star-forming rate systems

NED – NASA / IPAC Extragalactic Database – http://ned.ipac.caltech.edu/

NGC – New General Catalogue

NIR – Near infrared

NRAO – National Radio Astronomy Observatory

NTT – New Technology Telescope

Neutral hydrogen – Neutral hydrogen consists of atoms, which themselves consist of a proton and an electron each. The nuclear and electronic spins transition within the ground state of HI between the two hyperfine-structure levels with total spin: $F = 1$ with the nuclear and electronic spins parallel and $F = 0$ with the nuclear and electronic spins anti-parallel. The parallel spins are of a higher energy than if the spins were anti-parallel. The energy difference of $6 \cdot 10^{-6} eV$ corresponds to a vacuum wavelength of $\sim \lambda_0 = 21.1$ cm that is equivalent to a frequency $\sim \nu_0 = 1420.406$ MHz.

Parsec – Parallax second – Pc is a measure of distance. It is the distance at which an object has a parallax as viewed from Earth of one second of arc. The semi major axis of the Earth's orbit subtends an angle of one arc second = 3.2616 light-years.

PSCz – Point Source Catalogue Redshift

Ω_m – Omega − Matter density parameter – total matter

Ω_b – Omega − Baryon content

Ω_{DE} – Omega − Dark Energy content

RC3 – Third Reference Catalogue of Bright Galaxies

S to Sdm, SA to SAdm – Galaxy classification: (S) defines a spiral galaxy, the subsequent sub-letters denote morphology of the galaxy and the letter (m) refers to the LMC as a prototype

SB to SBdm – Galaxy classification; the (SB) denotes a barred spiral galaxy

Sa – Spiral galaxy with tightly wound arms

Sb – Spiral galaxy with loosely wound arms

Sc – Spiral galaxy with very loosely wound arms

Note: – The + or – superscript designations further define the proximity of the arms

SDFITS files – Single Dish Flexible Image Transport System files

S/N – Signal to noise ratio indicating the potential quality of the neutral hydrogen observation integration and is closely related to the level of flux in Jy

SN Ia – Type Ia Supernova is the result of a white dwarf in a binary star system reaching the Chandrasekhar 1.38 M_{sun} limit resulting in a thermonuclear runaway

SNe Ia – Plural of SN Ia

SOFI – Son of Isaac infrared spectrograph and imaging camera on the 3.5m NTT at ESO La Silla, Chile

2MASS – Two Micron All Sky Survey of galaxies in the NIR *J*, *H* and K_s bands

2MRS – 2MASS Redshift Survey

2MTF – 2MASS TF survey

2M++ − 2MASS composite all-sky new redshift survey

TAROT – Télescope à Action Rapide pour les Objets Transitoires

TCS – Telescope Control Software controlling the Parkes 64 m Radio Telescope

3K CMB – Cosmic Microwave Background radiation referencing the radiation temperature rounded to 3 Kelvin; the WMAP determined an average temperature 2.725 K with a total temperature variance of 0.0004 K

TopHat – Algorithm used to process and display 21 cm observations and the plot represents the shape of a TopHat

Total magnitude – The 'total' aperture consists of the isophotal aperture plus the integration of the surface brightness profile that extends from the isophotal aperture out to ~ 4 disk scale lengths

21 cm – Neutral hydrogen at rest has a wavelength of 21 cm and a frequency 1420.405800 MHz

UGC – Uppsala General Catalogue

$V < 6000$ km s^{-1} – galaxy recession velocities to < 6000 km s^{-1}

V_{50} − Recession velocity measured at the 50% level of peak intensity of the neutral hydrogen line width

W_{20} − 21 cm line width velocity measurement at 20% of peak intensity

W_{40} − 21 cm line width velocity measurement at 40% of peak intensity

W_{50} − 21 cm line width velocity at 50% of peak intensity

W_R^i − 21 cm line width velocity corrected for broadening, inclination, random and rotation motion

WISE − Wide-Field Infrared Survey Explorer

WMAP9 − Wilkinson Microwave Anisotropy Probe 9 year – observing the Cosmic Microwave Background radiation temperature